Master's thesis

NTNU
Norwegian University of Science and Technology
Faculty of Natural Sciences
Department of Physics

Svein Åmdal

Phase perturbative calculations of diffuse light scattering on randomly rough surfaces in and out of plane

Master's thesis in Physics
Supervisor: Ingve Simonsen
July 2021

NTNU
Norwegian University of
Science and Technology

Svein Åmdal

Phase perturbative calculations of diffuse light scattering on randomly rough surfaces in and out of plane

Master's thesis in Physics
Supervisor: Ingve Simonsen
July 2021

Norwegian University of Science and Technology
Faculty of Natural Sciences
Department of Physics

NTNU
Norwegian University of
Science and Technology

English abstract

Phase perturbative calculations of diffuse light scattering on randomly rough surfaces in and out of plane

At some length scale or another, all surfaces show a degree of roughness, and it is imperative to understand the physical implications of it. This work tackles reflection of electromagnetic waves in the optical wavelength regime on randomly rough surfaces, described by statistical autocorrelation functions of Gaussian form. The incoherent mean differential reflection coefficient is calculated for such surfaces using the approximate method of phase perturbation theory, whose numerical computation is further simplified by performing some analytical integrals. The simplified governing equation is solved numerically, and the calculated reflection amplitudes are compared to previous experimental measurements and direct numerical solutions. In this way, the accuracy of the theory is assessed, and some of the general features of rough surface scattering is observed and discussed.

Overall, the present implementation of phase perturbation theory largely reproduce the general shape and features that is expected in rough surface scattering, and seems to be a better approximation than the closely related small-amplitude perturbation theory. However, there is still a difference between its result and those obtained previously. The main reason is believed to be that the involved roughness topography is too severe for the chosen approximation to be valid.

Norsk sammendrag

Fase-perturbative utregninger av diffus lysspredning på rue overflater, i og utenfor spredningsplanet

Ved en eller annen lendgdeskala viser alle overflater en grad av ruhet, og det er viktig å forstå de fysiske konsekvensene av det. Denne oppgaven handler om refleksjon av elekromagnetiske bølger i det optiske bølgelengderegimet på tilfeldige rue overflater, som beskrives av statistiske autokorrelasjonsfunksjoner på Gaussisk form. Den inkoherente midlere differensielle refleksjonskoeffesienten for slike overflater beregnes ved hjelp av faseperturbasjonsteori, som er en approkismasjonsmetode. Den numeriske utregningen forenkles videre ved å utføre noen integraler analytisk, og den gjenstående styrende ligningen løses numerisk. De beregnede refleksjonsamplitudene sammenlignes med tidligere anskaffede eksperimentelle målinger og direkte numeriske løsninger. På denne måten vurderes teoriens nøyaktighet, og noen generelle trekk ved spredning på rue overflater blir observert og diskutert.

Totalt sett reproduserer den nåværende implementasjonen de generelle fasongene og trekkene som forventes innen spredning på rue overflater, og teorien later til å være en bedre approksimasjon enn den nært relaterte liten-amplitude-perturbasjonsteorien. Men, det er likevel en viss forskjell mellom de nåværende og tidligere anskaffede resultatene. Hovedårsaken til dette antas å være at den aktuelle ruhetstopografien er for stor til at approksimasjonen er gyldig.

Preface

This Master's thesis is written in fulfilment of a Master of Science (M.Sc.) degree in physics (course code FY3900) from the Norwegian University of Science and Technology (Norges Teknisk-Naturvitenskapelige Universitet – NTNU), and concludes a two year masters study programme. The project was supervised by Prof. Ingve Simonsen at the Department of Physics at NTNU.

The work contains colourful contour plots, and other colour-coded graphs. To appreciate them, it is recommended that this thesis is read in a format that support colour, especially if printed out.

This year has been challenging for all students, due to restrictions set in place to fight the Coronavirus pandemic. The prospect of writing a thesis has been more difficult than usual, but after a few months of delay it is finally here.

My sincerest gratitude is owed to Ingve Simonsen for excellent supervision. Your patience and enthusiasm has enabled the completion of this thesis. Thanks also to my friends who eased the journey, especially the reading hall crew — you know who you are. Finally, thanks to my family for ever lasting love and support.

Kristiansand, July 29, 2021

Svein Åmdal

Table of Contents

English abstract **i**

Norsk sammendrag **iii**

Preface **v**

Table of Contents **vii**

List of Tables **ix**

List of Figures **xi**

1 Introduction **1**
1.1 Motivation 1
1.2 Aim of work 2
1.3 Thesis structure 2

2 Theory of random, rough surfaces **3**
2.1 A description of roughness 3
2.2 The surface profile and autocorrelation functions 4
2.3 Power spectrum and Fourier representations 6

3 Electromagnetic theory **9**
3.1 Maxwell's equations and related quantities 9
3.2 The Helmholtz equation and its solution 11
3.3 Boundary conditions 16

4 Scattering theory **17**
4.1 Scattering geometry 17
4.2 Description of the scattered field 19

4.3 The Rayleigh criterion 19
4.4 The reduced Rayleigh equation 20
4.5 Mean differential reflection coefficient 21
4.6 Reciprocity and the scattering matrix 23

5 Perturbation theory 25
5.1 Small amplitude perturbation theory 25
5.2 Phase perturbation theory 28
5.3 Included and non-included terms in the scattering matrix expansion 31
5.4 Analytic computation of angular integrals 33

6 Numerical Implementation and Considerations 35
6.1 Programming language and packages 35
6.2 Numerical considerations 36
6.3 Numerical justification of upper integral limits 36
6.4 An approach to calculating highly oscillating integrals 38

7 Results and Discussion 43
7.1 Comparison with previous numerical systems 43
7.2 Comparison with experimental systems 47
7.3 Off-diagonal calculation and comparison 58
7.4 Origin of discrepancies 82

8 Conclusion 87

A Derivation of the general form of the mean differential reflection coefficient 89

B Symmetric expansion of the second order scattering matrix 95

C Proof of expansion of the power spectrum 97

D Detailed calculation of the exponent factor of MDRC 101
D.1 List of analytical angular integrals 101
D.2 Calculation of the pp-component 105
D.3 Calculation of the ps-component 108
D.4 Calculation of the sp-component 111
D.5 Calculation of the ss-component 113

E Extra figures 117

References 125

List of Tables

7.1 Statistical parameters of the numerical test systems. 44
7.2 Statistical parameters of the experimental test systems. 48
7.3 Statistical parameters of some of the off-diagonal test systems. 60

List of Figures

2.1 Schematic one-dimensional randomly rough surface 5

3.1 The p- and s polarisation states in the scattering system 15

4.1 Scattering geometry 18

6.1 Integrand of the Bessel function integral 37
6.2 Integrand of the exponent integral 39

7.1 In-plane incoherent MDRC of ”system 1” with 0° incidence. 44
7.2 In-plane incoherent MDRC of ”system 1” with 40° incidence. 45
7.3 In-plane incoherent MDRC of ”system 2” with 4.56° incidence. 46
7.4 In-plane incoherent MDRC of ”system 2” with 30° incidence. 46
7.5 In-plane incoherent MDRC of ”system 3” with 0° incidence. 47
7.6 In-plane incoherent MDRC of ”sample 0061” with 5° incidence. 49
7.7 In-plane incoherent MDRC of ”sample 0061” with 15° incidence. 49
7.8 In-plane incoherent MDRC of ”sample 0061” with 30° incidence. 50
7.9 In-plane incoherent MDRC of ”sample 0061” with 50° incidence. 51
7.10 In-plane incoherent MDRC of ”sample 7047” with 5° incidence. 52
7.11 In-plane incoherent MDRC of ”sample 7047” with 30° incidence. 52
7.12 In-plane incoherent MDRC of ”sample 7047” with 60° incidence. 53
7.13 In-plane incoherent MDRC of ”sample 8053” with 5° incidence. 54
7.14 In-plane incoherent MDRC of ”sample 8053” with 15° incidence. 55
7.15 In-plane incoherent MDRC of ”sample 8053” with 30° incidence. 56
7.16 In-plane incoherent MDRC of ”sample 5122” with 5° incidence. 56
7.17 In-plane incoherent MDRC of ”sample 5122” with 15° incidence. 57
7.18 In-plane incoherent MDRC of ”sample 5122” with 30° incidence. 57
7.19 In-plane incoherent MDRC of ”sample 9032” with 5° incidence. 58
7.20 In-plane incoherent MDRC of ”sample 9032” with 15° incidence. 59

7.21 In-plane incoherent MDRC of ”sample 9032” with 30° incidence. 59
7.22 Out-of-plane incoherent MDRC from a rough dielectric surface at normal incidence. 61
7.23 Out-of-plane incoherent MDRC from a rough dielectric surface at 67° incidence. 63
7.24 Polarisation-ignorant out-of-plane incoherent MDRC from a rough dielectric surface at normal incidence. 64
7.25 Polarisation-ignorant out-of-plane incoherent MDRC from a rough dielectric surface at 67° incidence. 66
7.26 Out-of-plane incoherent MDRC from a rougher dielectric surface at normal incidence. 67
7.27 Out-of-plane incoherent MDRC from a rougher dielectric surface at 67° incidence. 68
7.28 Polarisation-ignorant out-of-plane incoherent MDRC from a rougher dielectric surface at normal incidence. 69
7.29 Polarisation-ignorant out-of-plane incoherent MDRC from a rougher dielectric surface at 67° incidence. 70
7.30 Out-of-plane incoherent MDRC from a rough gold surface at normal incidence. 72
7.31 Out-of-plane incoherent MDRC from a rough gold surface at 67° incidence. 73
7.32 Polarisation-ignorant out-of-plane incoherent MDRC from a rough gold surface at normal incidence. 74
7.33 Polarisation-ignorant out-of-plane incoherent MDRC from a rough gold surface at 67° incidence. 75
7.34 Planar cut taken at 0° azimuth scattering angle of the incoherent MDRC from a rough dielectric surface at normal incidence. 76
7.35 Planar cut taken at 0° azimuth scattering angle of the incoherent MDRC from a rougher dielectric surface at normal incidence. 77
7.36 Planar cut taken at 90° azimuth scattering angle of the incoherent MDRC from a rough dielectric surface at normal incidence. 78
7.37 Planar cut taken at 90° azimuth scattering angle of the incoherent MDRC from a rougher dielectric surface at normal incidence. 78
7.38 Planar cut taken at 0° azimuth scattering angle of the incoherent MDRC from a rough dielectric surface at 67° incidence. 79
7.39 Planar cut taken at 0° azimuth scattering angle of the incoherent MDRC from a rougher dielectric surface at 67° incidence. 80
7.40 Planar cut taken at 90° azimuth scattering angle of the incoherent MDRC from a rough dielectric surface at 67°. 80
7.41 Planar cut taken at 90° azimuth scattering angle of the incoherent MDRC from a rougher dielectric surface at 67° incidence. 81
7.42 Planar cut taken at 90° azimuth scattering angle of the incoherent MDRC from a rough gold surface at normal incidence. 82

7.43 Planar cut taken at 30° azimuth scattering angle of the incoherent MDRC from a rough gold surface at 67° incidence. 83
7.44 Planar cut taken at 60° azimuth scattering angle of the incoherent MDRC from a rough gold surface at 67° incidence. 83
7.45 Planar cut taken at 90° azimuth scattering angle of the incoherent MDRC from a rough gold surface at 67° incidence. 84

E.1 Planar cut taken at 30° azimuth scattering angle of the incoherent MDRC from a rough dielectric surface at normal incidence. 118
E.2 Planar cut taken at 60° azimuth scattering angle of the incoherent MDRC from a rough dielectric surface at normal incidence. 118
E.3 Planar cut taken at 30° azimuth scattering angle of the incoherent MDRC from a rougher dielectric surface at normal incidence. 119
E.4 Planar cut taken at 60° azimuth scattering angle of the incoherent MDRC from a rougher dielectric surface at normal incidence. 119
E.5 Planar cut taken at 30° azimuth scattering angle of the incoherent MDRC from a rough dielectric surface at 67° incidence. 120
E.6 Planar cut taken at 60° azimuth scattering angle of the incoherent MDRC from a rough dielectric surface at 67° incidence. 120
E.7 Planar cut taken at 30° azimuth scattering angle of the incoherent MDRC from a rougher dielectric surface at 67° incidence. 121
E.8 Planar cut taken at 60° azimuth scattering angle of the incoherent MDRC from a rougher dielectric surface at 67° incidence. 121
E.9 Planar cut taken at 0° azimuth scattering angle of the incoherent MDRC from a rough gold surface at normal incidence. 122
E.10 Planar cut taken at 0° azimuth scattering angle of the incoherent MDRC from a rough gold surface at 67° incidence. 122
E.11 Planar cut taken at 30° azimuth scattering angle of the incoherent MDRC from a rough gold surface at normal incidence. 123
E.12 Planar cut taken at 60° azimuth scattering angle of the incoherent MDRC from a rough gold surface at normal incidence. 123

Chapter 1

Introduction

1.1 Motivation

This work concerns itself with electromagnetic wave scattering from rough surfaces.

Rough surfaces accounts for *every* surface, at some length scale. This is sufficient motivation to study its fundamental properties, such as scattering properties. Electromagnetic wave scattering is a common tool for sample analysis, as it is often precise and non-destructive. Therefore, the random surface interaction with electromagnetic wave scattering is particularly interesting.

Surface roughness has traditionally been seen as a nuisance, whose imperfectness challenges exact theory. However, many recent applications have accounted for surface roughness, and some applications desire specific surface roughness to make use of its physical properties. Random surface scattering is also known to exhibit weak localisation effects, and gives rise to physical features that are interesting in their own right, such as the enhanced backscattering phenomenon (see for instance Ref. 1).

There is a wide range of applications where rough surface scattering is important, and here we will mention some examples. Electromagnetic scattering from rough surfaces has been utilised in research of remote sensing of layered media [2] or land surfaces such as soil or snow [3]. The scattering on rough-surfaced atmospheric dust particles [4, 5] or the randomly rough assembly of ice crystals on the surface of cirrus clouds [6] are relevant to atmospheric and climate science. Radar echoes of randomly rough interfaces is of use in geological surveying, and has been used to search for water on the surface of Mars [7, 8]. Rough scattering surfaces on the substrate of solar cells is one of the ways to increase their efficiency, by incoherent scattering angles possibly being conducive to total internal reflection within the optically active layer [9, 10]. Considerations of surface roughness has been used to study tyre grip on road surfaces [11].

Surface-specific parameters determine the structure of the surface, and in turn the scattering properties involved. Recently, the inverse problem has been considered [12–14], which implies that surface parameters are found from measurements of scattered waves. Inversion techniques would be of service to all the aforementioned applications. Rigorous solution of the governing equations of electromagnetism is computationally costly, which necessitates approximate solutions. Quick calculation of inversion methods might enable in situ microscopy of the parameters that define a rough surface.

1.2 Aim of work

This work uses *phase perturbation theory* (see Sec. 5.2), an approximate method of obtaining the incoherent *mean differential reflection coefficient* (see Chapter 4) - which is an experimentally accessible quantity that essentially gives the amplitude of scattered light in a certain direction. The aim is to formulate the theory in a similar way to Navarrete Alcalá et al. [15], but attempt to reduce the computational load by using an analytical mathematical expansion inspired by Simonsen, Kryvi and Maradudin [12]. The viability of the technique is discussed, after scrutinising the accuracy of a numerical implementation in comparison to previous implementations and experimental results [12, 15, 16]. Scattering both in and out of plane is considered, and both metal and dielectric surfaces are targets of the numerical analysis. No detailed discussion of computational complexity is provided, but some of the numerical challenges of such a problem has been addressed and discussed.

1.3 Thesis structure

Chapters 2–4 provide theoretical background in three distinct branches of physics. Firstly, the theory of random surfaces in Chapter 2 introduces some concepts of statistics and stochastic processes, which is used to describe the random surface parametrically. Chapter 3 gives a basic introduction to electromagnetic theory starting at Maxwell's equations, and points at all the underlying assumptions that often pass unmentioned. Chapter 4 gives some introduction to the theory of scattering, and gives an approximate coupling of the electromagnetic boundary conditions at a rough surface.

Chapter 5 describes the main approximation, the phase perturbation theories, and discusses the specific formulation and the order of errors that may be introduced. Chapter 6 discusses the specific numerical implementation, and some of the potential challenges.

Chapter 7 both present the result of the numerical analysis, compare it with previous results, and discusses some general features of random surface scattering and phase perturbation theory as they show up. A summary of the error-inducing approximations is given, and is discussed in light of the comparisons. Finally, the concluding statement of the thesis is given in Chapter 8.

Chapter 2

Theory of random, rough surfaces

This chapter aims to introduce the concept of surface roughness, and how to describe them statistically.

2.1 A description of roughness

At some length scale or another, any surface exhibits non-flat texture or *roughness*. Roughness describes the topographic relief on a surface, and is comprised of two parts; the heights of the topographic features (above and below) the mean level, and the in-plane distance between these features, sometimes called the *surface spatial wavelength* [17].

The ensuing discussion regards surface roughness that causes optical light scattering, and the surface spatial wavelength on such a surface is in the range from $\sim 0.1\ \mu\mathrm{m}$ to $\sim 1\ \mathrm{mm}$ [17, 18]. Such roughness may for instance appear due to the presence of scratches or polishing marks, machining marks or grooves, or the presence or particles on top of the surface. Determination of surface roughness may be measured experimentally, by for example atomic force microscopy or scanning near-field optical microscopy [19].

However, roughness also manifests itself on the nanometer scale as surface height differences, being in the range between $\sim 0.01\ \mathrm{nm}$ to more than $1\ \mu\mathrm{m}$. This range of roughness contains features of less distance than the inter-atomic spacing. Due to this wide range of roughness with relatively comparable relations between features, many surfaces can be well described by fractal theory, wherein, the *fractal dimension* is a measure of the roughness independent of the length scale [20]. The fractal dimension has been reported to be well defined and approximately constant over a significant range of length scales for a selection of materials [21]. The description of a surface in terms of fractal parameters is an alternative approach to the description in terms of statistical parameters that will be presented here.

The typical ratio between surface spatial wavelength and surface heights is in the range between $\sim$10 000 and $\sim$10 [18]. The roughest of these come from synthetically crafted surfaces, while the smoother end of the spectrum is a very close approximation to a flat surface. Therefore, typical surfaces of interest lend themselves to perturbations around the flat surface case, which is important for all the approximations to be introduced.

2.2 The surface profile and autocorrelation functions

Consider two materials connected by a perfectly flat interface at the $x_3 = 0$ -plane. Let the material in the region $x_3 > 0$ be labelled '$+$', and the material in the region $x_3 < 0$ is labelled '$-$'. A modestly rough interface is well described as a perturbation to this system. The plane of the interface is no longer perfectly flat, but described by the *surface profile function* $\zeta(\mathbf{x}_\parallel)$. The notation $\mathbf{x}_\parallel$ refers to the in-plane triplet of coordinates, $(x_1, x_2, 0)$.

For simplicity, we assume that the function $\zeta(\mathbf{x}_\parallel)$ is single-valued, i.e. we limit the roughness to a modest level. The Rayleigh hypothesis, to be discussed later, demands further restrictions on the roughness, so this simplification is inconsequential with respect to the final result. The single-valued property makes averaging the surface profile function into a well defined operation - it is the continuous sum of the displacement from the mean. We are free to choose the appropriate coordinate system for the x_3-coordinate, such that the spatial mean of the surface profile function vanishes;

$$\left\langle \zeta(\mathbf{x}_\parallel) \right\rangle = 0. \tag{2.1}$$

The notion of *random* roughness implies an absence of repeating topographical patterns, such as one would find in a grating. Therefore, we will assert that $\zeta(\mathbf{x}_\parallel)$ is a *stochastic process*. A one-dimensional schematic illustration of such a surface is depicted in Fig. 2.1, which also illustrates how intricately the scattering directions may depend on the specific surface topography. In Eq. (2.1), a *stationary* property has been assumed, which means that the mean of $\zeta(\mathbf{x}_\parallel)$ does not depend on $\mathbf{x}_\parallel$. The mean value may therefore be calculated at any point by averaging over a sufficiently large neighbourhood around $\mathbf{x}_\parallel$, instead of taking into account the entire (possibly infinite) surface. This manifests itself as translational symmetry of statistical properties [22]. From now on we will also assume that the surface is *ergodic*, meaning that the spatial average described above is the same as an average over any ensemble of realisations of ζ [22–24]. The ergodic property relates the height average over any particular realisation of the surface, to the true statistical ensemble average that depends on the statistical parameters that generated the surface in the first place.

In practice, it simplifies the process of calculating or measuring quantities relating to the surface. The process of spatially averaging over the surface may require very precise knowledge of ζ. Ensemble averaging, instead requires a new realisation of the surface for each data point. The statistical significance stems from the number of realisations, which is infinitely expandable. Experimentally, this can be achieved by measuring different parts of a single surface sample (abusing the stationarity which always follows from ergodicity).

However, not all manufactured surfaces are equally ergodic [25]. This represents a limit of the validity of the theory. Assuming the surface is stationary and ergodic anyway,

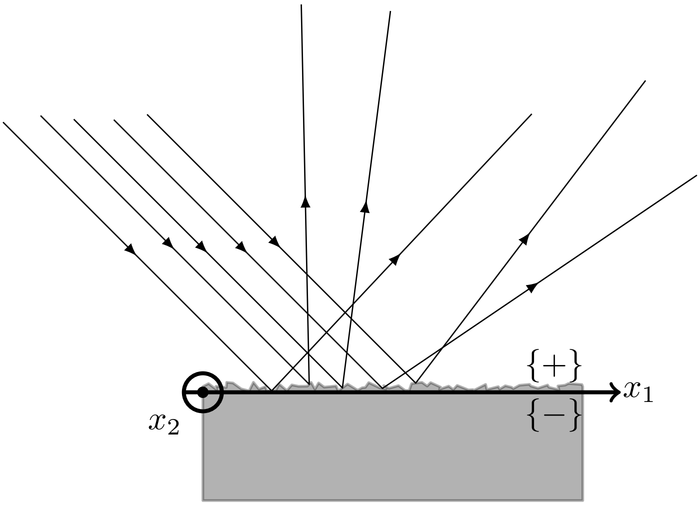

Figure 2.1: A schematic illustration of a one-dimensional randomly rough surface and some light reflected upon it. The scattering direction depends intricately on the specific surface topography. With respect to the described coordinate system, the x_3-axis is vertical, and the x_1-x_2 plane is the horizontal plane. The x_2-unit vector is pointing into the plane.

one may define the surface *autocorrelation* function by [1, 22]

$$\langle \zeta(\mathbf{x}_\parallel)\zeta(\mathbf{x}'_\parallel)\rangle = \delta^2 W(|\mathbf{x}_\parallel - \mathbf{x}'_\parallel|). \tag{2.2}$$

In the above equation, $\delta = \sqrt{\langle \zeta^2(\mathbf{x}_\parallel)\rangle}$ is the root mean square height of ζ, and W is the height autocorrelation function between the height of the points $\mathbf{x}'_\parallel$ and $\mathbf{x}_\parallel$. The autocorrelation is the surfaces statistical correlation between different realisations of itself. The average $\langle\cdot\rangle$ must therefore be the ensemble average, though as mentioned previously it makes no difference for ergodic surfaces. The dependence on the absolute difference stems from the stationary property. The case $W(|\mathbf{x}_\parallel|) = 1$ is known as perfect correlation. Obviously, any point is perfectly correlated with itself, meaning $W(\mathbf{0}) = 1$.

Inserting this final expression into Eq. (2.2), leaves the equation for δ, which is also known as the *variance* of ζ (also known as the second statistical moment, or the closely related cumulant). If the height distribution of ζ follows a Gaussian form, then Eqs. (2.1) and (2.2) uniquely determine the statistical properties of the surface, as all higher order cumulants vanish [22, 24].

2.3 Power spectrum and Fourier representations

Quantities that appear in random surface scattering theory is often given in terms of the *surface power spectrum* defined by

$$g(|\mathbf{k}_\parallel|) := \int d^2x_\parallel W(|\mathbf{x}_\parallel|)\exp\left[-i\mathbf{k}_\parallel\cdot\mathbf{x}_\parallel\right], \tag{2.3}$$

recognised as the Fourier transform[1] of the correlation function. Similarly, it is often convenient to define a spatial Fourier integral representation of the surface profile function ζ, i.e.

$$\zeta(\mathbf{x}_\parallel) = \int \frac{d^2k_\parallel}{(2\pi)^2}\hat{\zeta}(\mathbf{k}_\parallel)\exp\left[i\mathbf{k}_\parallel\cdot\mathbf{x}_\parallel\right]. \tag{2.4}$$

Here, $\hat{\zeta}(\mathbf{k}_\parallel)$ is a Fourier coefficient of $\zeta(\mathbf{x}_\parallel)$ given by

$$\hat{\zeta}(\mathbf{k}_\parallel) = \int d^2x_\parallel \zeta(\mathbf{x}_\parallel)\exp\left[-i\mathbf{k}_\parallel\cdot\mathbf{x}_\parallel\right]. \tag{2.5}$$

Therefore, the Fourier space equivalents of Eqs. (2.1) and (2.2) may be written down as [26]

$$\left\langle \hat{\zeta}(\mathbf{k}_\parallel)\right\rangle = 0, \tag{2.6}$$

$$\left\langle \hat{\zeta}(\mathbf{k}_\parallel)\hat{\zeta}(\mathbf{k}'_\parallel)\right\rangle = (2\pi)^2\delta(\mathbf{k}_\parallel - \mathbf{k}'_\parallel)\delta^2 g(|\mathbf{k}_\parallel|), \tag{2.7}$$

---

[1] We define the forward Fourier transform in space to have a minus sign in the exponential in its definition, which is not a unique or ubiquitous definition across all disciplines. The present definition is $\hat{f}(\mathbf{k}) := \int_{-\infty}^{\infty} d^3x f(\mathbf{x})\exp\left[-i\mathbf{k}\cdot\mathbf{x}\right]$.

where $\delta(\mathbf{k}_{\|})$ is the two-dimensional Dirac-delta function, not to be confused with the mean square height δ^2. Equations (2.6) and (2.7) also determine the complete statistical properties of the surface if applied to a Gaussian distribution.

For the numerical work, we assume the correlation function is Gaussian [22];

$$W(|\mathbf{x}_{\|}|) = \exp\left[-x_{\|}^2/a^2\right], \tag{2.8}$$

where a is the surface correlation length. By assuming a to be a direction-independent scalar, we have further assumed an *isotropic* surface. This simply means that the statistics are independent of the orientation of the surface, and it represents a significant simplification of the theory. The power spectrum associated with Eq. (2.8) is

$$g(|\mathbf{k}_{\|}|) = \pi a^2 \exp\left[-a^2 k_{\|}^2/4\right]. \tag{2.9}$$

Chapter 3

Electromagnetic theory

This chapter aims to introduce general concepts from electromagnetism. Then by selectively ignoring some concepts, the scope and validity of the work of the thesis is limited.

3.1 Maxwell's equations and related quantities

The fundamental equations that define the subject of electromagnetism are Maxwell's equations (MEs). In SI-units, on differential form, they read [1, 27, 28]

$$\nabla \cdot \mathbf{D}(\mathbf{x};t) = \rho(\mathbf{x};t) \tag{3.1a}$$

$$\nabla \times \mathbf{H}(\mathbf{x};t) - \frac{\partial \mathbf{D}(\mathbf{x};t)}{\partial t} = \mathbf{J}(\mathbf{x};t) \tag{3.1b}$$

$$\nabla \times \mathbf{E}(\mathbf{x};t) + \frac{\partial \mathbf{B}(\mathbf{x};t)}{\partial t} = 0 \tag{3.1c}$$

$$\nabla \cdot \mathbf{B}(\mathbf{x};t) = 0, \tag{3.1d}$$

where $\mathbf{E}$ and $\mathbf{H}$ are electric and magnetic fields, $\mathbf{D}$ and $\mathbf{B}$ are electric displacement and magnetic flux density, and ρ and $\mathbf{J}$ are (free) charge and current densities. Taking the divergence of Eq. (3.1b), inserting Eq. (3.1a) and using that divergence of curl is zero, one arrives at the continuity equation

$$\frac{\partial \rho}{\partial t}(\mathbf{x};t) + \nabla \cdot \mathbf{J}(\mathbf{x};t) = 0. \tag{3.2}$$

The charge and current densities exist due to charge-bearing particles that are present in the medium underlying the field in question. Conducting media is characterised by a subset of the charge-bearing particles being (nearly) unrestrained from the material internal electrical potential, and as such is free to align in a manner that counteracts external fields in the interior. Therefore, in conducting media, ρ and $\mathbf{J}$ can only manifest themselves on the medium surface. In vacuum they vanish completely, and for many materials they can be safely neglected.

The relations between $\mathbf{D}$ and $\mathbf{E}$, and between $\mathbf{H}$ and $\mathbf{B}$ depend on the medium the fields exists in. Generally, we have *constitutive relations* given by [27–29]

$$\mathbf{D} = \varepsilon_0 \mathbf{E} + \mathbf{P} \tag{3.3a}$$

$$\mathbf{B} = \mu_0 \mathbf{H} + \mu_0 \mathbf{M}, \tag{3.3b}$$

where ε_0 is the *vacuum permittivity* and μ_0 is the *vacuum permeability*. These are known to have the numerical values of $\varepsilon_0 \approx 8.854 \times 10^{-12}\,\mathrm{F/m}$ and $\mu_0 := 4\pi \times 10^{-7}\,\mathrm{H/m}$. We have also introduced $\mathbf{P}$, being the electric polarisation, and $\mathbf{M}$, the magnetic polarisation (magnetisation). They correspond to the response of bound (electric or magnetic) moments contained in the medium upon application of an external field, either $\mathbf{E}$ or $\mathbf{H}$ respectively.

The notation in Eqs. (3.3) is purposefully sloppy, as it does not denote dependence on $\mathbf{x}$ or t. We will now investigate the correct dependency of these quantities. The quantities $\mathbf{P}$ and $\mathbf{M}$ are the result of material *response*, which we will presently assume to be *linear*. The value of, say, $\mathbf{P}$ could in principle depend on the value of the applied field (in this case $\mathbf{E}$) at all points of the space of the parametrising variables. Those parameters are three spatial coordinates and one temporal, which we may now denote by primed symbols. Then, the i-th component of the electric polarisation could be written in terms of the general linear response function χ_E like

$$P_i(\mathbf{x};t) = \varepsilon_0 \int_{-\infty}^{\infty} dt' \int d^3x' \chi_{E,ij}(\mathbf{x},\mathbf{x}';t,t') E_j(\mathbf{x}';t'), \tag{3.4}$$

where the ij-indices denote the tensorial components of χ_E and summation over j is implied. The response function χ_E in the case of electric polarisation is specifically known as *electric susceptibility*. The factor ε_0 has been included for later convenience. The response from $\mathbf{x}' \neq \mathbf{x}$ is *spatial non-locality*, and we will ignore such contributions to all relevant response functions. In fact, we will assume that the medium response is isotropically constant through space, and no longer denote spatial dependence. We do *not* in principle assume that $t' = t$, but we *will* assume that all response functions have time translation symmetry. In which case, we may write $\chi_E(t,t') \to \chi_E(t-t')$ by a variable transformation [30], and write the general susceptibility response as

$$D_i(\mathbf{x};t) = \varepsilon_0 \int_{-\infty}^{\infty} dt' \chi_{E,ij}(t-t') E_j(\mathbf{x};t') = \epsilon_0 (\chi_{E,ij} * E_j)(\mathbf{x};t), \tag{3.5}$$

where $*$ denotes convolution in t.[1] By making use of the Fourier convolution theorem [31], one arrives at the conclusion that the linear response

$$\mathbf{P}(\mathbf{x};\omega) = \varepsilon_0 \chi_E(\omega) \mathbf{E}(\mathbf{x};\omega) \tag{3.6}$$

---

[1] Considerations of causality demands that $\chi(t-t') = 0$ for $t' > t$. Therefore, one could replace the upper integral boundary by t.

generally only holds in frequency domain. The same reasoning applies to all linear response functions we will encounter, and therefore it seems pertinent to develop the remaining theory in temporal frequency space. This is achieved by applying an appropriate Fourier transformation over time to Eqs. (3.1), where $\partial/\partial t \rightarrow -i\omega$.[2]

We quickly make a note of the fact that if the electric polarisation response is *not* linear, then it should be expressed as an expansion in powers of the external $\mathbf{E}$-field, namely

$$\mathbf{P}(\mathbf{x};\omega) = \varepsilon_0 \sum_{n=1}^{\infty} \chi_E^{(n)}(\omega)\mathbf{E}^n(\mathbf{x};\omega). \tag{3.7}$$

In Eq. (3.7), $\chi_E^{(n)}$ is known as the n-th order electric susceptibility, a tensor of rank $n+1$ which is typically highly dependent on symmetries in the material structure [32]. The presence of any non-zero term of order n is referred to as n-th order non-linear response, but for many applications the high order terms may be neglected [27, 33]. An exact analogy to the discussions of electric response and non-linearity exists for the magnetic response with magnetic susceptibility denoted χ_H. From here, we will always assume *linear* electromagnetic theory, which means that Eqs. (3.3) take on the linear form

$$\mathbf{D}(\mathbf{x};\omega) = \varepsilon_0\varepsilon(\omega)\mathbf{E}(\mathbf{x};\omega) \tag{3.8a}$$

$$\mathbf{B}(\mathbf{x};\omega) = \mu_0\mu(\omega)\mathbf{H}(\mathbf{x};\omega), \tag{3.8b}$$

where the *relative permittivity* tensor, $\varepsilon(\omega) = 1 + \chi_E^{(1)}(\omega)$, and the *relative permeability* tensor, $\mu(\omega) = 1 + \chi_H^{(1)}(\omega)$ have been defined. We note that $\varepsilon(\omega)$ is another linear response function, being the frequency and material dependent amount of induced electric $\mathbf{D}$-field that is produced after the external electric field $\mathbf{E}$ is applied.

3.2 The Helmholtz equation and its solution

3.2.1 The Helmholtz equation

We now limit our attention to the case where there is no free charge or current, i.e. $\rho(\mathbf{x};\omega) = \mathbf{J}(\mathbf{x};\omega) = 0$. By Fourier transforming the Maxwell equations in Eqs. (3.1) and using the result of Eqs. (3.8) we find that

$$\varepsilon_0\varepsilon(\omega)\nabla\cdot\mathbf{E}(\mathbf{x};\omega) = 0 \tag{3.9a}$$

$$\nabla\times\mathbf{H}(\mathbf{x};\omega) + i\omega\varepsilon_0\varepsilon(\omega)\mathbf{E}(\mathbf{x};\omega) = 0 \tag{3.9b}$$

$$\nabla\times\mathbf{E}(\mathbf{x};\omega) - i\omega\mu_0\mu(\omega)\mathbf{H}(\mathbf{x};\omega) = 0 \tag{3.9c}$$

$$\mu_0\mu(\omega)\nabla\cdot\mathbf{H}(\mathbf{x};\omega) = 0. \tag{3.9d}$$

---

[2] This transformation holds when the forward *temporal* Fourier transformation is defined by $\hat{f}(\omega) := \int_{-\infty}^{\infty} dt f(t)\exp[i\omega t]$. This is the *opposite* convention to the spatial Fourier transformation that defined Eqs. (2.3)–(2.5). The chosen conventions are standard in physics, but their mutual inconsistency is sometimes confusing.

By operating on Eq. (3.9c) with the curl operator we obtain

$$\nabla \times \nabla \times \mathbf{E}(\mathbf{x};\omega) - i\omega\mu_0\mu(\omega)\nabla \times \mathbf{H}(\mathbf{x};\omega) = 0. \tag{3.10}$$

Now, we insert $\nabla \times \mathbf{H}$ from Eq. (3.9b) and make use of the vector identity $\nabla \times [\nabla \times \mathbf{a}] = \nabla [\nabla \cdot \mathbf{a}] - \nabla^2 \mathbf{a}$ to find that

$$\nabla [\nabla \cdot \mathbf{E}(\mathbf{x};\omega)] - \nabla^2 \mathbf{E}(\mathbf{x};\omega) - \omega^2 \varepsilon_0 \varepsilon(\omega)\mu_0\mu(\omega)\mathbf{E}(\mathbf{x};\omega) = 0. \tag{3.11}$$

Finally, we insert Eq. (3.9a) to eliminate the first term, end up with

$$\left[\nabla^2 + \omega^2 \varepsilon_0 \varepsilon(\omega)\mu_0\mu(\omega)\right] \mathbf{E}(\mathbf{x};\omega) = 0, \tag{3.12}$$

which is recognised as the general vectorial Helmholtz (wave) equation [27, 34] with corresponding propagation velocity

$$v(\omega) = \frac{1}{\sqrt{\varepsilon_0 \varepsilon(\omega)\mu_0\mu(\omega)}}. \tag{3.13}$$

In vacuum, where $\varepsilon(\omega) = \mu(\omega) = 1$, one can relate electrostatic quantities to the velocity of light in vacuum[3];

$$c = \frac{1}{\sqrt{\varepsilon_0 \mu_0}} := 299\,792\,458\,\mathrm{m/s}. \tag{3.14}$$

A similar process, starting with the curl of Eq. (3.9b) yields that the magnetic field $\mathbf{H}(\mathbf{x};\omega)$ also solves Eq. (3.12) in exact analogy with $\mathbf{E}(\mathbf{x};\omega)$.

3.2.2 Dispersion

We make the ansatz that the solution to Eq. (3.12) is on the form[4]

$$\mathbf{E}(\mathbf{x};\omega) = \widetilde{\mathbf{E}}_0 \exp[-i\omega t] \exp[i\mathbf{k}\cdot\mathbf{x}] := \mathbf{E}_0(\omega) \exp[i\mathbf{k}\cdot\mathbf{x}], \tag{3.15}$$

where the harmonic time dependence has been included in the quantity $\mathbf{E}_0(\omega)$. The spatial dependence is also assumed to be harmonically oscillating with the spatial frequency k_i in the Cartesian x_i-direction. The form of the solution is known as a plane wave[5] with the *wave vector* $\mathbf{k}$ pointing in the direction of propagation. Equation (3.12) is *linear*, meaning any solution is a linear combination of solutions for specific $\mathbf{k}$, which also happen to constitute a complete set of solutions [36]. Therefore, it presently suffices to consider a single wave vector. There are two conditions on Eq. (3.15) to be a valid solution. The first is found by inserting Eq. (3.15) into Eq. (3.12) and using combinations of Eqs. (3.13) and (3.14), which yields

---

[3] This value defines the meter in the SI system [35].

[4] The implied form is made in conjunction with our previous definition of spatial and temporal Fourier transforms. The spatial and temporal components have different sign conventions.

[5] Strictly speaking, this is a plane wave only if we also have $\nabla \cdot \mathbf{E} = 0$. This was already implicitly assumed during the derivation of Eq. (3.12).

$$\exp\left[i\mathbf{k}\cdot\mathbf{x}\right]\left[-k^2+\varepsilon(\omega)\mu(\omega)\left(\frac{\omega}{c}\right)^2\right]\mathbf{E}_0(\omega)=0, \tag{3.16}$$

where $k^2 := |\mathbf{k}|^2$. The quantity $\exp\left[i\mathbf{k}\cdot\mathbf{x}\right]$ is never zero, so the condition in Eq. (3.16) must be fulfilled by the expression

$$k(\omega)^2=\varepsilon(\omega)\mu(\omega)\left(\frac{\omega}{c}\right)^2. \tag{3.17}$$

This is the light *dispersion relation* of electromagnetic waves. It relates the temporal (ω) and spatial ($\mathbf{k}$) frequencies of the light wave. By considering Eqs. (3.13) and (3.17), we note that propagation velocity depend on k (unless the varying quantities turn out to be constants, but in general they are not), which turn depend on the wavelength λ according to $k = 2\pi/\lambda$. This gives the physical interpretation of dispersion. A monochromatic wave will have its propagation velocity depend on the medium through which it traverses, which explains the phenomenon of refraction. A medium where $\varepsilon(\omega)$ and/or $\mu(\omega)$ are not constant is known as a dispersive medium. A wave composed of a linear combination of multiple plane waves will have its shape distorted when propagating through a dispersive medium, as each of the plane wave components will propagate with a different velocity.

Typically, we disregard the magnetic dispersion in optical application as few materials have significant classical magnetisation. Then, the dispersion relation gains its more familiar form

$$k(\omega)=n(\omega)\frac{\omega}{c}, \tag{3.18}$$

where $n(\omega) := \sqrt{\varepsilon(\omega)}$ is the *refractive index.*

3.2.3 Polarisation

The second condition on Eq. (3.15) is that is is a valid solution of Maxwell's equations. Demanding Eq. (3.9a) to be satisfied by insertion of Eq. (3.15) gives the constraint

$$\varepsilon_0\varepsilon(\omega)\exp\left[i\mathbf{k}\cdot\mathbf{x}\right]i\mathbf{k}\cdot\mathbf{E}_0(\omega)=0, \tag{3.19}$$

which in fact is already assumed in the derivation of Eq. (3.12). The only non-trivial case satisfying Eq. (3.19) is when $\mathbf{k}\perp\mathbf{E}_0(\omega)$. The exactly analogous derivation for the field $\mathbf{H}(\mathbf{x};\omega)$ gives the condition $\mathbf{k}\perp\mathbf{H}_0(\omega)$. We see that the waves of both electric and magnetic fields are transversal.

If we instead demand Eq. (3.9c) to be satsified by insertion of Eq. (3.15), we find the constraint

$$\begin{aligned}
i\hat{\mathbf{x}}_1\left[k_2E_{03}(\omega)-k_3E_{02}(\omega)\right]\exp\left[i\mathbf{k}\cdot\mathbf{x}\right]&=i\hat{\mathbf{x}}_1\omega\mu_0\mu(\omega)H_{01}(\omega)\exp\left[i\mathbf{k}\cdot\mathbf{x}\right]\\
i\hat{\mathbf{x}}_2\left[k_3E_{01}(\omega)-k_1E_{03}(\omega)\right]\exp\left[i\mathbf{k}\cdot\mathbf{x}\right]&=i\hat{\mathbf{x}}_2\omega\mu_0\mu(\omega)H_{02}(\omega)\exp\left[i\mathbf{k}\cdot\mathbf{x}\right]\\
i\hat{\mathbf{x}}_3\left[k_1E_{02}(\omega)-k_2E_{03}(\omega)\right]\exp\left[i\mathbf{k}\cdot\mathbf{x}\right]&=i\hat{\mathbf{x}}_3\omega\mu_0\mu(\omega)H_{03}(\omega)\exp\left[i\mathbf{k}\cdot\mathbf{x}\right].
\end{aligned} \tag{3.20}$$

After cancellation of the common $i \exp[i\mathbf{k} \cdot \mathbf{x}]$-terms, the remains may be recognised as the components of the equation $\mathbf{k} \times \mathbf{E}_0(\omega) = \omega\mu_0\mu(\omega)\mathbf{H}_0(\omega)$. Therefore, $\mathbf{E} \perp \mathbf{H} \perp \mathbf{k}$. Their relative directions respect a right-hand rule of $\{\mathbf{k}, \mathbf{E}, \mathbf{H}\}$, or equivalently $\{\mathbf{E}, \mathbf{H}, \mathbf{k}\}$.

Knowledge of $\mathbf{k}$ does not uniquely specify the direction of $\mathbf{E}$ (or $\mathbf{H}$). Therefore, we define *polarisation* as the direction of $\mathbf{E}$ in the plane perpendicular to $\mathbf{k}$. Invoking a coordinate system where $\mathbf{k} = [0, 0, k]^t$, the direction of $\mathbf{E}$ may be described by the coordinates x_1 and x_2, and the direction of $\mathbf{H}$ is then uniquely determined by $\mathbf{k}$ and $\mathbf{E}$. There may indeed still be a spatial phase difference between the x_1- and x_2-components of $\mathbf{E}$, previously given in the relation between k_1 and k_2. Upon the appropriate coordinate transformation to have $\mathbf{k} = [0, 0, k]^t$, we must encounter the relative phase difference in one of the components. We henceforth define the relative phase difference ξ to be an amendment to the x_2-component with respect to the x_1-component. Then, the general polarisation state is

$$\mathbf{E}(x_3; \omega) = \exp[ikx_3] \begin{bmatrix} E_{01}(\omega) \\ E_{02}(\omega) \exp[i\xi] \end{bmatrix}. \tag{3.21}$$

The in-plane vector $\mathbf{E}$ traces out an ellipse when propagated in either space or time. This is most easily seen when $\xi = (2m + 1)\pi/2$ for $m \in \mathbb{Z}$, as the phase factor becomes $\exp[i\pi/2 + im\pi] = \pm i$; a quarter-circle rotation in the complex plane. The extrema of the two components must be a quarter rotation apart, so the principal axes of the ellipse must coincide with x_1 and x_2 - having the principal values E_{01} and E_{02}. The quarter ellipse rotation in the polarisation description corresponds to the maxima in the directions x_1 and x_2 being physically separated by a quarter wavelength in the x_3-direction, and by a quarter period in time. Other choices for ξ means the angle between the extrema is different, which in general leads to a polarisation ellipse rotated by some angle.

If $\xi = (2m + 1)\pi/2$ for $m \in \mathbb{Z}$ and also $E_{01} = E_{02}$, the ellipse degenerates to a circle. This polarisation state is called *circular polarisation*. If instead $\xi = m\pi$ for $m \in \mathbb{Z}$, then E_1 and E_2 reach their zeros and extrema at the same time, which is to say the ellipse degenerates to a line. This is called *linear polarisation*.

From Eq. (3.21) we may write any polarisation state with relative phase ξ as a linear combination of orthogonal linear polarisation states, by noting that

$$\mathbf{E}(x_3; \omega) = \exp[ikx_3] \begin{bmatrix} E_{01}(\omega) \\ 0 \end{bmatrix} + \exp[ikx_3] \exp[i\xi] \begin{bmatrix} 0 \\ \pm E_{02}(\omega) \end{bmatrix}. \tag{3.22}$$

In a wave scattering problem, the incoming and scattered waves may each be described by such a linear combination. The normal choice of decomposition vectors are parallel to, and perpendicular to the plane of incidence, which is illustrated in Fig. 3.1. This is referred to as p-*polarisation* and s-*polarisation* respectively, and any polarisation state is a linear combination of its p- and s-components. The incoming and scattered wave may have its p- and s-components of polarisation be defined in different coordinate systems, unless the scattering azimuthal angle equals the incident azimuthal angle.

In linear electromagnetic theory, any relation between the incoming and scattered waves may be regarded as a linear operator on the incoming wave, as a consequence of the

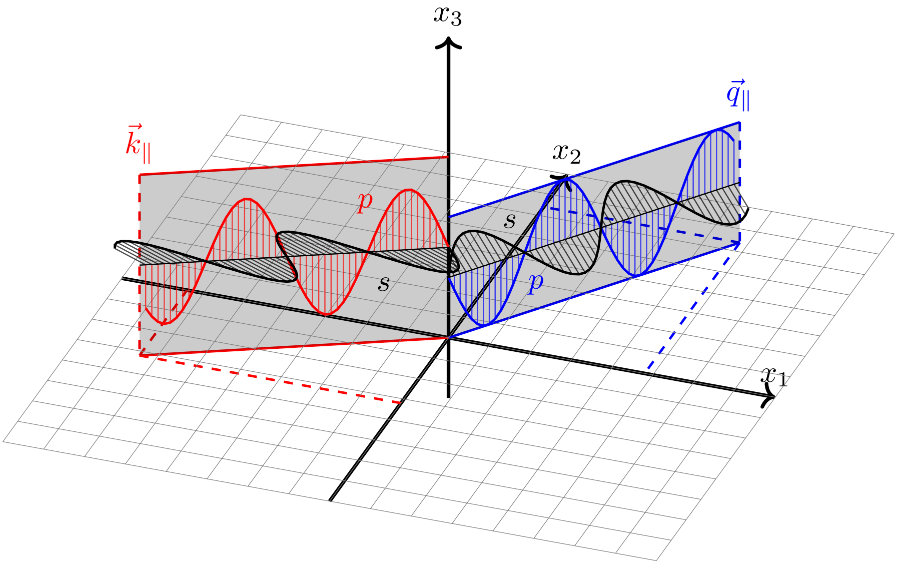

Figure 3.1: The p- and s polarisation states in the scattering system. In the incoming wave vector, $\mathbf{k}_{||}$, the in-plane component, marked in red, is p-polarised. The out-of-plane component, marked in black is s-polarised. Similarly, in the scattered wave vector, $\mathbf{q}_{||}$; the in-plane scattered component, marked in blue, is p-polarised, while the out-of-plane scattered component, also marked in black, is s-polarised. The scattering depends on the four possible interactions between any two components.

material response being linear too. Therefore, any scattering centre has four components, each describing the interaction between the incoming and scattered p- and s- components of polarisation. In order to completely describe the impact on the scattering centre on any polarisation state, *it suffices to describe the four pp-, ps-, sp- and ss-components*. They are arranged into a matrix called the *scattering matrix*, or the *reflection matrix* in the specific case of reflection. The reflection and scattering matrices will be discussed in Chapter 4.

3.3 Boundary conditions

One might write Maxwell's equations on integral form, rather than the form presented in Eqs. (3.1) or Eqs. (3.9). This is achieved by integrating the equations over either closed volumes or closed surfaces, and using the divergence theorem and Stokes' theorem where applicable. The integral forms of Maxwell's equations are particularly useful for calculating boundary conditions between materials with differing electromagnetic properties. The integration volumes are chosen to conveniently give correspondences between the two media without loss of generality. Denoting the media with '$+$' and '$-$' and subscripting their corresponding fields as such, one eventually finds that [1, 27, 28]

$$[\mathbf{D}_-(\mathbf{x};\omega) - \mathbf{D}_+(\mathbf{x};\omega)] \cdot \hat{\mathbf{n}} = \rho_\mathrm{s}(\mathbf{x};\omega) \tag{3.23a}$$

$$[\mathbf{B}_-(\mathbf{x};\omega) - \mathbf{B}_+(\mathbf{x};\omega)] \cdot \hat{\mathbf{n}} = 0 \tag{3.23b}$$

$$\hat{\mathbf{n}} \times [\mathbf{E}_-(\mathbf{x};\omega) - \mathbf{E}_+(\mathbf{x};\omega)] = 0 \tag{3.23c}$$

$$\hat{\mathbf{n}} \times [\mathbf{H}_-(\mathbf{x};\omega) - \mathbf{H}_+(\mathbf{x};\omega)] = \mathbf{J}_\mathrm{s}(\mathbf{x};\omega). \tag{3.23d}$$

Here, we have defined $\hat{\mathbf{n}}$ as the normal vector of the surface, with positive direction from $\{-\}$ to $\{+\}$. The quantities J_s and ρ_s denote the surface current density and surface charge density. In many optically relevant cases, these quantities are zero or may otherwise safely be neglected.

The scope of electromagnetic phenomena has now been limited to the linear case, with other restrictions on the (dielectric) response function of the materials involved in the scattering interface. None of the assumptions seem outrageously restrictive, but they nevertheless exist and should be remembered at appropriate moments.

Chapter 4

Scattering theory

This chapter aims to introduce some familiar quantities of scattering theory, and present the scattering system that will be subject to numerical calculations.

4.1 Scattering geometry

The scattering geometry of interest is depicted in Fig. 4.1. Two media are separated by an interface following a surface profile function $x_3 = \zeta(\mathbf{x}_{\|})$, with a coordinate system chosen such that $\langle\zeta(\mathbf{x}_{\|})\rangle = 0$. The surface topography is not shown explicitly in Fig. 4.1, but the actual surface should look akin to the one presented in Fig. 2.1. The media whose bulk satisfy $x_3 > 0$ may be labelled '$+$', and the other media '$-$'. An incoming plane wave may be represented by the wave vector $\mathbf{k}$, and scatter into some wave vector $\mathbf{q}$ upon interaction with the surface. Furthermore, we denote by $\mathbf{k}_{\|}$ and $\mathbf{q}_{\|}$ the wave vector components along the plane $x_3 = 0$. The polar and azimuthal angles of the wave vectors have also been denoted, with appropriate subscripts. For the waves propagating in the region '$+$', the value of the x_3-components of the wave vector is denoted by α_0. Therefore, we infer that $\mathbf{q}_+ = [q_1, q_2, \alpha_0(q_{\|})]^t$ and $\mathbf{k}_+ = [k_1, k_2, \alpha_0(k_{\|})]^t$. If instead the waves propagated in the region '$-$', we would write $\mathbf{q}_- = [q_1, q_2, \alpha(q_{\|})]^t$ and $\mathbf{k}_- = [k_1, k_2, \alpha(k_{\|})]^t$. By Eq. (3.17) with $\mu = 1$ and geometric considerations of Fig. 4.1, we must have the relations

$$\alpha_0(q_{\|}) = \alpha_0(q_{\|};\omega) := \begin{cases} \sqrt{\left(\frac{\omega}{c}\right)^2 - q_{\|}^2} & \text{if } q_{\|} \le \frac{\omega}{c} \\ i\sqrt{q_{\|}^2 - \left(\frac{\omega}{c}\right)^2} & \text{if } q_{\|} > \frac{\omega}{c} \end{cases} \tag{4.1a}$$

and

$$\alpha(q_{\|}) := \alpha(q_{\|};\omega) = \sqrt{\varepsilon(\omega)\left(\frac{\omega}{c}\right)^2 - q_{\|}^2} \qquad \Re\left(\alpha_0(q_{\|})\right) \ge 0, \Im\left(\alpha_0(q_{\|})\right) \ge 0. \tag{4.1b}$$

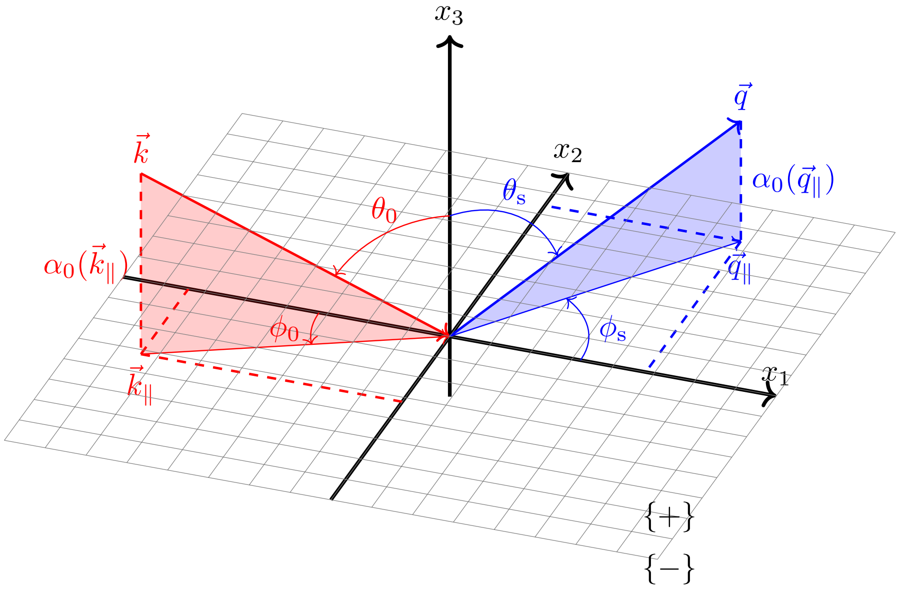
x_3
$\vec{q}$
$\vec{k}$
x_2
$\alpha_0(\vec{q}_\parallel)$
θ_s
θ_0
$\alpha_0(\vec{k}_\parallel)$
$\vec{q}_\parallel$
ϕ_s
ϕ_0
x_1
$\vec{k}_\parallel$
$\{+\}$
$\{-\}$

Figure 4.1: The scattering geometry of interest. The incoming wave vector **k** is scattered into the wave vector **q**. The surface topography is not drawn, but is responsible for the presence of non-specular scattering. The p-component of incoming light is contained in the shaded plane beneath **k**, while the incoming s-component is perpendicular to it. Similarly for the scattered wave vector **q**, it is noted that the two polarisations are not with respect to the same plane.

The symbol $\Re$ means real part, and the symbol $\Im$ means imaginary part. In Eqs. (4.1) and previously, we have used the quantities $q_{\|} = |\mathbf{q}_{\|}|$ and $k_{\|} = |\mathbf{k}_{\|}|$. For future reference, any quantity of the form $\mathbf{f}_{\|}$ is a vector in the $x_3 = 0$ plane, and $f_{\|}$ is its in-plane magnitude.

On a rough surface, the scattered wave vector depends intricately on the surface topography. The wave represented by $\mathbf{k}$ has a non-zero spatial extent, and does not typically scatter in only a single direction. Conversely, this means that the total amount of scattering in the direction $\mathbf{q}$ takes contributions from many parts of the surface. When considering the scattering into direction $\mathbf{q}$ from an incoming wave $\mathbf{k}$, one must indeed consider the interaction with a statistically representative region of the surface.

4.2 Description of the scattered field

Assuming the incoming field is a plane wave, by combining Eq. (3.15) and Eq. (4.1a) we may write for the incident electric field

$$\mathbf{E}_{\text{inc}}(\mathbf{x};\omega) = \mathbf{E}_i(\omega) \exp\left[i\mathbf{k}_{\|} \cdot \mathbf{x}_{\|} - i\alpha_0(k_{\|})x_3\right], \tag{4.2}$$

where ω-dependence has been suppressed. The minus sign in front of the third components is added because of the direction of $\mathbf{k}$ from Fig. 4.1. We may write for the reflected field

$$\mathbf{E}_{\text{refl}}(\mathbf{x};\omega) = \int \frac{d^2q_{\|}}{(2\pi)^2} \mathbf{E}_r(\mathbf{q}_{\|}|\mathbf{k}_{\|};\omega) \exp\left[i\mathbf{q}_{\|} \cdot \mathbf{x}_{\|} + i\alpha_0(q_{\|})x_3\right], \tag{4.3}$$

for a directionally dependent reflected amplitude $\mathbf{E}_r$. Equation (4.3) takes into account all the possible scattering processes from the point $\mathbf{x}_{\|}$. The asymptotic form of the field in the region '$+$' may be written

$$\mathbf{E}_{+}(\mathbf{x};\omega) = \mathbf{E}_{\text{inc}}(\mathbf{x};\omega) + \mathbf{E}_{\text{refl}}(\mathbf{x};\omega), \tag{4.4}$$

with the terms described by Eqs. (4.2) and (4.3). A similar story takes place for the asymptotic field in the region '$-$' which has been transmitted through the surface, namely

$$\mathbf{E}_{-}(\mathbf{x};\omega) = \int \frac{d^2q_{\|}}{(2\pi)^2} \mathbf{E}_t(\mathbf{q}_{\|}|\mathbf{k}_{\|};\omega) \exp\left[i\mathbf{q}_{\|} \cdot \mathbf{x}_{\|} - i\alpha_0(q_{\|})x_3\right], \tag{4.5}$$

where we note the absence of a incident wave term.

4.3 The Rayleigh criterion

Wave scattering is often described in terms of the waves asymptotic forms [37], as they are often experimentally obtainable and permits us to neglect the detailed structure of the scattering centre. However, the boundary conditions described in Sec. 3.3 relates the fields immediately adjacent to the surface. The specific surface topography influences the detailed nature of the fields, and makes the scattering problem hard to approach.

The *Rayleigh hypothesis* is the assumption that the asymptotic wave forms are valid in close proximity to the surface, to the extent that they are assumed to satisfy the boundary conditions [1, 38]. A flat surface is completely described by the asymptotic form, while a small perturbation to it is only approximately described.

It is theoretically known that for a one-dimensional periodic surface of the form $\zeta(x) = \zeta_0 \sin(\kappa x)$, the Rayleigh hypothesis is valid if $\kappa\zeta_0 < 0.448$, regardless of the relative material parameters involved [39, 40]. Numerical study has suggested that it may be valid for grating depths up to 15 times greater than this for a dielectric and a lossless metal [41]. A two-dimensional equivalent of the condition $\kappa\zeta_0 < 0.448$ has numerically been shown to hold for two-dimensional surfaces too [42]. Randomly rough surfaces are *not* periodic, but these examples place an upper bound on the permissible roughness. If the random surfaces roughness features are not weaker than the described periodic displacements, we should definitely not expect the Rayleigh hypothesis to be a valid approximation.

Few studies on the validity of the Rayleigh hypothesis for specifically rough surfaces have been carried out. But, for a two-dimensional surface profile of Gaussian height distribution with correlation length a and its rms-value δ bounded by 0.13λ it has been found that the Rayleigh hypothesis is valid if; $\delta/a \lesssim 0.2$ for a perfect conductor, and $\delta/a \lesssim 0.08$ for silver substrates [43]. These values were calculated using a wavelength of $457.9\,\mathrm{nm}$. Most of (but not all!) the samples, presented in Secs. 7.1.1 and 7.2.1, used for numerical calculation in this thesis fulfils the given criteria, albeit with substantially larger wavelength. The calculations in this thesis is carried out on the faith that the Rayleigh criterion holds, but we will acknowledge that it may be a source of error.

4.4 The reduced Rayleigh equation

By applying the Rayleigh hypothesis, we may demand that Eqs. (4.2) and (4.3) satisfy the boundary conditions in Eqs. (3.23). Then for the $\mathbf{E}$-field we have that [15]

$$\begin{aligned} \mathbf{E}_{\text{inc}}(\mathbf{x};\omega) = &\left\{ -\frac{c}{\omega}\left[\hat{\mathbf{k}}_{\|}\alpha_0(k_{\|}) + \hat{\mathbf{x}}_3 k_{\|}\right] E_{i;p}(\mathbf{k}_{\|}) + \left[\hat{\mathbf{x}}_3 \times \hat{\mathbf{k}}_{\|}\right] E_{i;s}(\mathbf{k}_{\|}) \right\} \\ &\times \exp\left[i\mathbf{k}_{\|}\cdot\mathbf{x}_{\|} - i\alpha_0(k_{\|})x_3\right] \exp\left[-i\omega t\right] \end{aligned} \tag{4.6}$$

and

$$\begin{aligned} \mathbf{E}_{\text{refl}}(\mathbf{x};\omega) = \int \frac{d^2 q_{\|}}{(2\pi)^2} &\left\{ \frac{c}{\omega}\left[\hat{\mathbf{q}}_{\|}\alpha_0(q_{\|}) - \hat{\mathbf{x}}_3 q_{\|}\right] E_{r;p}(\mathbf{q}_{\|}) + \left[\hat{\mathbf{x}}_3 \times \hat{\mathbf{q}}_{\|}\right] E_{r;s}(\mathbf{q}_{\|}) \right\} \\ &\times \exp\left[i\mathbf{q}_{\|}\cdot\mathbf{x}_{\|} + i\alpha_0(q_{\|})x_3\right] \exp\left[-i\omega t\right]. \end{aligned} \tag{4.7}$$

It is noted that the expressions inside square brackets in these two equations are, respectively, unit vectors parallel to and perpendicular to the plane of incidence, and both are perpendicular to the total wave vector. This fact may be seen upon careful consideration of Fig. 4.1 and its accompanying equations. The subscripts p and s refer to the respective components along each polarisation component. The amplitudes of the incoming (E_i) and reflected (E_r) fields must be related through the reflection coefficient by definition;

$$E_{r;\alpha}(\mathbf{q}_\parallel) = \sum_\beta R_{\alpha\beta}(\mathbf{q}_\parallel|\mathbf{k}_\parallel)E_{i;\beta}(\mathbf{k}_\parallel) \tag{4.8}$$

for $\alpha, \beta \in \{p, s\}$. Following Eq. (3.22), the four components of the matrix $\overline{\overline{\mathbf{R}}}$ is sufficient to deduce the reflection between any polarisation states. The component $R_{\alpha\beta}$ is the component relating incoming β-polarised light to scattered α-polarised light.

A similar relation holds between the incident and transmitted amplitudes. These are the *Rayleigh equations*, a set of coupled integral equations. Through a lengthy algebraic computation, it is possible to decouple them by eliminating the transmission coefficient $\overline{\overline{\mathbf{T}}}$ [15, 44, 45], which is the counterpart to $\overline{\overline{\mathbf{R}}}$ for the region $-$. The decoupled equation for the reflection coefficient is

$$\begin{aligned}\int \frac{d^2q_\parallel}{(2\pi)^2}\frac{I(\alpha(p_\parallel)-\alpha_0(q_\parallel)|\mathbf{p}_\parallel-\mathbf{q}_\parallel)}{\alpha(p_\parallel)-\alpha_0(q_\parallel)}&\overline{\overline{\mathbf{M}}}(\mathbf{p}_\parallel|\mathbf{q}_\parallel)\overline{\overline{\mathbf{R}}}(\mathbf{q}_\parallel|\mathbf{k}_\parallel)\\ = -\frac{I(\alpha(p_\parallel)+\alpha_0(k_\parallel)|\mathbf{p}_\parallel-\mathbf{k}_\parallel)}{\alpha(p_\parallel)+\alpha_0(k_\parallel)}&\overline{\overline{\mathbf{N}}}(\mathbf{p}_\parallel|\mathbf{k}_\parallel),\end{aligned} \tag{4.9}$$

where $\mathbf{p}_\parallel$ is a wave vector inserted to aid the computation. Equation (4.9) is the governing equation in theories of random surface wave scattering. The function $I(\gamma|\mathbf{Q}_\parallel)$ is defined by

$$I(\gamma|\mathbf{Q}_\parallel) := \int d^2x_\parallel \exp\left[-i\mathbf{Q}_\parallel\cdot\mathbf{x}_\parallel\right]\exp\left[-i\gamma\zeta(\mathbf{x}_\parallel)\right], \tag{4.10}$$

and the matrices $\overline{\overline{\mathbf{M}}}(\mathbf{p}_\parallel|\mathbf{q}_\parallel)$ and $\overline{\overline{\mathbf{N}}}(\mathbf{q}_\parallel|\mathbf{k}_\parallel)$ are defined by [15, 44, 45]

$$\overline{\overline{\mathbf{M}}}(\mathbf{p}_\parallel|\mathbf{q}_\parallel) := \begin{bmatrix} p_\parallel q_\parallel + \alpha(p_\parallel)[\hat{\mathbf{p}}_\parallel\cdot\hat{\mathbf{q}}_\parallel]\alpha_0(q_\parallel) & -\left(\frac{\omega}{c}\right)\alpha(p_\parallel)[\hat{\mathbf{p}}_\parallel\times\hat{\mathbf{q}}_\parallel]_3 \\ \left(\frac{\omega}{c}\right)[\hat{\mathbf{p}}_\parallel\times\hat{\mathbf{q}}_\parallel]_3\alpha_0(q_\parallel) & \left(\frac{\omega}{c}\right)^2[\hat{\mathbf{p}}_\parallel\cdot\hat{\mathbf{q}}_\parallel]\end{bmatrix}, \tag{4.11a}$$

$$\overline{\overline{\mathbf{N}}}(\mathbf{p}_\parallel|\mathbf{k}_\parallel) := \begin{bmatrix} p_\parallel k_\parallel - \alpha(p_\parallel)[\hat{\mathbf{p}}_\parallel\cdot\hat{\mathbf{k}}_\parallel]\alpha_0(k_\parallel) & -\left(\frac{\omega}{c}\right)\alpha(p_\parallel)[\hat{\mathbf{p}}_\parallel\times\hat{\mathbf{k}}_\parallel]_3 \\ -\left(\frac{\omega}{c}\right)[\hat{\mathbf{p}}_\parallel\times\hat{\mathbf{k}}_\parallel]_3\alpha_0(k_\parallel) & \left(\frac{\omega}{c}\right)^2[\hat{\mathbf{p}}_\parallel\cdot\hat{\mathbf{k}}_\parallel]\end{bmatrix}. \tag{4.11b}$$

4.5 Mean differential reflection coefficient

The $\alpha\beta$-component of the *mean differential reflection coefficient* (MDRC) is the fraction of the incident energy flux from β-polarised light that is reflected into α-polarised light in the solid angle element $d\Omega_\text{s}$. MDRC is of interest as it is an experimentally accessible quantity. It may for instance be measured by scanning different scattering angles with a polarimeter.

Appendix A reveals that the MDRC is given by

$$\left\langle\frac{\partial R_{\alpha\beta}}{\partial\Omega_\text{s}}\right\rangle = \frac{1}{A}\left(\frac{\omega}{2\pi c}\right)^2\frac{\cos^2(\theta_\text{s})}{\cos(\theta_0)}\left\langle\left|R_{\alpha\beta}(\mathbf{q}_\parallel|\mathbf{k}_\parallel)\right|^2\right\rangle, \tag{4.12}$$

where A is the area in the x_1x_2-plane covered by the scattering surface. The MDRC is denoted by the entire expression on the left hand side of Eq. (4.12), and the choice of notation is telling of its definition. After noting that

$$\begin{aligned}\left\langle\left|R_{\alpha\beta}(\mathbf{q}_\parallel|\mathbf{k}_\parallel)\right|^2\right\rangle &= \left\langle\left|R_{\alpha\beta}(\mathbf{q}_\parallel|\mathbf{k}_\parallel)\right|^2\right\rangle - \left|\left\langle R_{\alpha\beta}(\mathbf{q}_\parallel|\mathbf{k}_\parallel)\right\rangle\right|^2 + \left|\left\langle R_{\alpha\beta}(\mathbf{q}_\parallel|\mathbf{k}_\parallel)\right\rangle\right|^2 \\ &= \left|\left\langle R_{\alpha\beta}(\mathbf{q}_\parallel|\mathbf{k}_\parallel)\right\rangle\right|^2 + \mathrm{Var}\left[R_{\alpha\beta}(\mathbf{q}_\parallel|\mathbf{k}_\parallel)\right]\end{aligned}, \tag{4.13}$$

with Var[$\cdot$] denoting the statistical variance, it is pertinent to describe the MDRC as a sum of what is known as its coherent and incoherent contributions.

For I_1 and I_2 referring to the intensities measured at some fixed point by light which scattered at two different locations on the surface, the stationary part of the total measured intensity from both points has an interference term $2\sqrt{I_1}\sqrt{I_2}\cos(\delta)$ where $\delta = \frac{2\pi}{\lambda}\Delta$OPL is the accrued phase difference and ΔOPL is the difference in optical path length [34]. A flat surface only reflects specularly — in the direction where the incident and reflected angles are the same — meaning scattering from the two points will only be observed at a single point when the scattering points turn out to be the same point. Therefore ΔOPL is zero by default, and $\cos(\delta) = \cos(0) = 1$. A rough surface has a stochastic distribution of ΔOPL, which means that when every pair of points that may interact is summed over, the collective interference term is $\sim \langle\cos(\delta)\rangle = 0$; which is defined as complete incoherence [34].

The coherent contribution is captured by $\left|\left\langle R_{\alpha\beta}(\mathbf{q}_\parallel|\mathbf{k}_\parallel)\right\rangle\right|^2$, which is the same as $\left\langle\left|R_{\alpha\beta}(\mathbf{q}_\parallel|\mathbf{k}_\parallel)\right|^2\right\rangle$ in the case where the surface is perfectly flat. Recall the ergodic property, which leaves $\langle\cdot\rangle$ of a flat surface to be the same as the spatial average of a constant. Therefore it cannot matter if the averaging takes place inside or outside of $|\cdot|^2$.

The average non-specular scattering of a flat surface is zero. Therefore the variance of R, being the measure of the statistical deviation from the average, must equal the total scattering amplitude for that set of wave vectors. This scattering contribution is solely due to the surface topography, which is stochastic, and therefore we may state that it is the incoherent contribution. The incoherent contribution scatters into diffuse (non-specular) as well as specular directions.

In total, we may then write separately

$$\left\langle\frac{\partial R_{\alpha\beta}}{\partial\Omega_\mathrm{s}}\right\rangle_\mathrm{coh} = \frac{1}{A}\left(\frac{\omega}{2\pi c}\right)^2\frac{\cos^2(\theta_\mathrm{s})}{\cos(\theta_0)}\left|\left\langle R_{\alpha\beta}(\mathbf{q}_\parallel|\mathbf{k}_\parallel)\right\rangle\right|^2 \tag{4.14a}$$

and

$$\left\langle\frac{\partial R_{\alpha\beta}}{\partial\Omega_\mathrm{s}}\right\rangle_\mathrm{incoh} = \frac{1}{A}\left(\frac{\omega}{2\pi c}\right)^2\frac{\cos^2(\theta_\mathrm{s})}{\cos(\theta_0)}\left[\left\langle\left|R_{\alpha\beta}(\mathbf{q}_\parallel|\mathbf{k}_\parallel)\right|^2\right\rangle - \left|\left\langle R_{\alpha\beta}(\mathbf{q}_\parallel|\mathbf{k}_\parallel)\right\rangle\right|^2\right]. \tag{4.14b}$$

Proceeding from here, we will focus our attention on the unique contribution of a rough surface, being the incoherent Eq. (4.14b). Any mention of the MDRC should be assumed to be the incoherent contribution, unless otherwise specified.

4.6 Reciprocity and the scattering matrix

Scattering of electromagnetic waves is subject to Lorentz's reciprocity theorem, which implies that for some scattering centre represented by the matrix $\bar{\bar{\mathbf{S}}}$, we must have fulfilled the *reciprocal relation* [37]

$$\bar{\bar{\mathbf{S}}}(\mathbf{q}_{\|}|\mathbf{k}_{\|}) = \bar{\bar{\mathbf{S}}}^{t}(-\mathbf{k}_{\|}| - \mathbf{q}_{\|}). \tag{4.15}$$

Reciprocity means that the light source and the observation point can be freely interchanged without altering the result. This is always upheld if the *scattering matrix* is defined by [1, 15, 44, 45]

$$\bar{\bar{\mathbf{S}}}(\mathbf{q}_{\|}|\mathbf{k}_{\|}) := \sqrt{\frac{\alpha_0(q_{\|})}{\alpha_0(k_{\|})}}\,\bar{\bar{\mathbf{R}}}(\mathbf{q}_{\|}|\mathbf{k}_{\|}). \tag{4.16}$$

This definition implies that

$$\left|R_{\alpha\beta}(\mathbf{q}_{\|}|\mathbf{k}_{\|})\right|^2 = \left|\frac{\alpha_0(k_{\|})}{\alpha_0(q_{\|})}\right| \left|S_{\alpha\beta}(\mathbf{q}_{\|}|\mathbf{k}_{\|})\right|^2. \tag{4.17}$$

From Eq. (3.18), we find that in the region '$+$' of Fig. 4.1, the length of both wave vectors $\mathbf{k}$ and $\mathbf{q}$ is $\left(\frac{\omega}{c}\right)$. Then, we find geometrically that

$$\alpha_0(k_{\|}) = \left(\frac{\omega}{c}\right)\cos(\theta_0) \tag{4.18a}$$

$$\alpha_0(q_{\|}) = \left(\frac{\omega}{c}\right)\cos(\theta_{\mathrm{s}}), \tag{4.18b}$$

such that

$$\left|\frac{\alpha_0(k_{\|})}{\alpha_0(q_{\|})}\right| = \frac{\cos(\theta_0)}{\cos(\theta_{\mathrm{s}})}. \tag{4.19}$$

Obviously, the quantities in Eq. (4.19) are invariant with respect to applying the statistical mean. Therefore, it is straightforward to insert Eq. (4.17) and Eq. (4.19) into Eq. (4.14) to obtain the MDRC in terms of $S_{\alpha\beta}$ to be

$$\left\langle \frac{\partial R_{\alpha\beta}}{\partial\Omega_{\mathrm{s}}} \right\rangle_{\mathrm{coh}} = \frac{1}{A}\left(\frac{\omega}{2\pi c}\right)^2 \cos(\theta_{\mathrm{s}}) \left|\left\langle S_{\alpha\beta}(\mathbf{q}_{\|}|\mathbf{k}_{\|})\right\rangle\right|^2 \tag{4.20a}$$

and

$$\left\langle \frac{\partial R_{\alpha\beta}}{\partial\Omega_{\mathrm{s}}} \right\rangle_{\mathrm{incoh}} = \frac{1}{A}\left(\frac{\omega}{2\pi c}\right)^2 \cos(\theta_{\mathrm{s}}) \left[\left\langle \left|S_{\alpha\beta}(\mathbf{q}_{\|}|\mathbf{k}_{\|})\right|^2\right\rangle - \left|\left\langle S_{\alpha\beta}(\mathbf{q}_{\|}|\mathbf{k}_{\|})\right\rangle\right|^2\right]. \tag{4.20b}$$

In this thesis, Eq. (4.20b) is solved by perturbatively approximating S. The approximation is discussed in Chapter 5.

Chapter 5

Perturbation theory

This chapter aims to introduce the perturbation theory that the thesis is based upon, and introduce some simplifications that reduce the amount of numerical calculation.

5.1 Small amplitude perturbation theory

The result of the thesis is contained to *phase perturbation theory* described in Sec. 5.2, which builds upon the results of *small amplitude perturbation theory*. The main idea is to expand the functions contained in Eq. (4.9) into increasing integer powers of the surface profile function $\zeta(\mathbf{x}_\parallel)$, and to ignore terms above a certain order. The underlying assumption of the Rayleigh hypothesis being valid, substantially constrains the maximum achieved displacement of $\zeta(\mathbf{x}_\parallel)$. Therefore, $\max\{\left|\zeta(\mathbf{x}_\parallel)\right|\}$ can be assumed to be "small" in some sense, such that $\left[\max\{\left|\zeta(\mathbf{x}_\parallel)\right|\}\right]^n$ vanishes for increasing $n \in \mathbb{N}$. Obviously, the non-extreme values of ζ will subside even quicker. In this thesis, perturbation results containing terms including ζ^2 will be considered.

The expansion of Eq. (4.10) in terms of powers of the surface profile function is [1, 15, 45, 46]

$$
\begin{aligned}
I(\gamma|\mathbf{Q}_\parallel) &:= \int d^2x_\parallel \exp\left[-i\mathbf{Q}_\parallel \cdot \mathbf{x}_\parallel\right] \exp\left[-i\gamma\zeta(\mathbf{x}_\parallel)\right] = \sum_{n=0}^{\infty} \frac{(-i\gamma)^n}{n!}\hat{\zeta}^{(n)} \\
&= (2\pi)^2\delta(\mathbf{Q}_\parallel) + \frac{(-i)^1}{1!}\gamma^1\hat{\zeta}^{(1)}(\mathbf{Q}_\parallel) + \frac{(-i)^2}{2!}\gamma^2\hat{\zeta}^{(2)}(\mathbf{Q}_\parallel) + O(\zeta^{(3)}),
\end{aligned}
\tag{5.1}
$$

with $\hat{\zeta}^{(n)}(\mathbf{Q}_\parallel)$ being given by

$$
\hat{\zeta}^{(n)}(\mathbf{Q}_\parallel) := \int d^2x_\parallel \zeta^n(\mathbf{x}_\parallel) \exp\left[-i\mathbf{Q}_\parallel \cdot \mathbf{x}_\parallel\right], \tag{5.2}
$$

being the generalisation of Eq. (2.5) to the possibilities that $n \neq 1$. The expansion for $\overline{\overline{\mathbf{R}}}$ is performed in terms of expansion matrices $\overline{\overline{\mathbf{R}}}^{(n)}$ of the n-th order, and the first few terms are defined by

$$\begin{aligned}\overline{\overline{\mathbf{R}}}(\mathbf{q}_\parallel|\mathbf{k}_\parallel) := {}& (2\pi)^2\delta(\mathbf{q}_\parallel-\mathbf{k}_\parallel)\overline{\overline{\mathbf{R}}}^{(0)}(k_\parallel)+\overline{\overline{\mathbf{R}}}^{(1)}(\mathbf{q}_\parallel|\mathbf{k}_\parallel)\hat{\zeta}^{(1)}(\mathbf{q}_\parallel-\mathbf{k}_\parallel)\\ &+\int\frac{d^2p_\parallel}{(2\pi)^2}\overline{\overline{\mathbf{R}}}^{(2)}(\mathbf{q}_\parallel|\mathbf{p}_\parallel|\mathbf{k}_\parallel)\hat{\zeta}^{(1)}(\mathbf{q}_\parallel-\mathbf{p}_\parallel)\hat{\zeta}^{(1)}(\mathbf{p}_\parallel-\mathbf{k}_\parallel)+O([\hat{\zeta}^{(1)}]^3).\end{aligned} \tag{5.3}$$

Inserting Eq. (5.1) and Eq. (5.3) into Eq. (4.9) gives the reduced Rayleigh equation expanded in powers of ζ, and it is

$$\begin{aligned}\int\frac{d^2q_\parallel}{(2\pi)^2}&\frac{1}{\alpha(p_\parallel)-\alpha_0(q_\parallel)}\Bigg\{(2\pi)^2\delta(\mathbf{p}_\parallel-\mathbf{q}_\parallel)+\frac{(-i[\alpha(p_\parallel)-\alpha_0(q_\parallel)])^1}{1!}\gamma^1\hat{\zeta}^{(1)}(\mathbf{p}_\parallel-\mathbf{q}_\parallel)\\ &+\frac{(-i[\alpha(p_\parallel)-\alpha_0(q_\parallel)])^2}{2!}\gamma^2\hat{\zeta}^{(2)}(\mathbf{p}_\parallel-\mathbf{q}_\parallel)+\ldots\Bigg\}\overline{\overline{\mathbf{M}}}(\mathbf{p}_\parallel|\mathbf{q}_\parallel)\\ &\times\Bigg\{(2\pi)^2\delta(\mathbf{q}_\parallel-\mathbf{k}_\parallel)\overline{\overline{\mathbf{R}}}^{(0)}(\mathbf{k}_\parallel)+\overline{\overline{\mathbf{R}}}^{(1)}(\mathbf{q}_\parallel|\mathbf{k}_\parallel)\hat{\zeta}^{(1)}(\mathbf{q}_\parallel-\mathbf{k}_\parallel)\\ &+\int\frac{d^2r_\parallel}{(2\pi)^2}\overline{\overline{\mathbf{R}}}^{(2)}(\mathbf{q}_\parallel|\mathbf{r}_\parallel|\mathbf{k}_\parallel)\hat{\zeta}^{(1)}(\mathbf{q}_\parallel-\mathbf{r}_\parallel)\hat{\zeta}^{(1)}(\mathbf{r}_\parallel-\mathbf{k}_\parallel)+\ldots\Bigg\}\\ &=\frac{-1}{\alpha(p_\parallel)+\alpha_0(k_\parallel)}\Bigg\{(2\pi)^2\delta(\mathbf{p}_\parallel-\mathbf{k}_\parallel)+\frac{(-i[\alpha(p_\parallel)+\alpha_0(k_\parallel)])^1}{1!}\gamma^1\hat{\zeta}^{(1)}(\mathbf{p}_\parallel-\mathbf{k}_\parallel)\\ &+\frac{(-i[\alpha(p_\parallel)+\alpha_0(k_\parallel)])^2}{2!}\gamma^2\hat{\zeta}^{(2)}(\mathbf{p}_\parallel-\mathbf{k}_\parallel)+\ldots\Bigg\}\overline{\overline{\mathbf{N}}}(\mathbf{p}_\parallel|\mathbf{k}_\parallel),\end{aligned} \tag{5.4}$$

with $\overline{\overline{\mathbf{M}}}$ and $\overline{\overline{\mathbf{N}}}$ defined by Eqs. (4.11). Expressions for each of the $\overline{\overline{\mathbf{R}}}^{(n)}$-matrices that appear in Eq. (5.3) may now be found by equating terms of equal order in ζ. The ζ^0-terms give the equation satisfied by $\overline{\overline{\mathbf{R}}}^{(0)}$, the ζ^1-terms define $\overline{\overline{\mathbf{R}}}^{(1)}$ and ζ^2-terms define $\overline{\overline{\mathbf{R}}}^{(2)}$. The resulting equation for $\overline{\overline{\mathbf{R}}}^{(0)}$ is [15, 46]

$$\overline{\overline{\mathbf{R}}}^{(0)}(\mathbf{k}_\parallel)=\begin{bmatrix}\frac{\varepsilon\alpha_0(k_\parallel)-\alpha(k_\parallel)}{\varepsilon\alpha_0(k_\parallel)+\alpha(k_\parallel)} & 0\\ 0 & \frac{\alpha_0(k_\parallel)-\alpha(k_\parallel)}{\alpha_0(k_\parallel)+\alpha(k_\parallel)}\end{bmatrix}, \tag{5.5}$$

which is the Fresnel amplitudes describing the scattering on a flat surface. Unsurprisingly, the lowest order perturbation to a flat surface turns out to be the flat surface itself. We note that Eq. (5.5) only depends on the amplitude of the argument $\mathbf{k}_\parallel$, so we might have chosen to write $\overline{\overline{\mathbf{R}}}^{(0)}(k_\parallel)$ instead. We don't, as to keep consistent to the notation that reflection matrices have vector arguments, which is the case for higher order expansion terms. The corresponding equation for $\overline{\overline{\mathbf{R}}}^{(1)}$ is

$$R^{(1)}_{\alpha\beta}(\mathbf{q}_\parallel|\mathbf{k}_\parallel) = \frac{2i\alpha_0(k_\parallel)}{d_\alpha(q_\parallel)d_\beta(k_\parallel)}\nu_{\alpha\beta}(\mathbf{q}_\parallel|\mathbf{k}_\parallel), \tag{5.6}$$

with the definitions

$$\nu_{pp}(\mathbf{q}_\parallel|\mathbf{k}_\parallel) := \frac{\varepsilon-1}{\varepsilon^2}\left[\varepsilon q_\parallel k_\parallel - \alpha(q_\parallel)[\hat{\mathbf{q}}_\parallel\cdot\hat{\mathbf{k}}_\parallel]\alpha(k_\parallel)\right] \tag{5.7a}$$

$$\nu_{ps}(\mathbf{q}_\parallel|\mathbf{k}_\parallel) := -\frac{\varepsilon-1}{\varepsilon}\left(\frac{\omega}{c}\right)\alpha(q_\parallel)[\hat{\mathbf{q}}_\parallel\times\hat{\mathbf{k}}_\parallel]_3 \tag{5.7b}$$

$$\nu_{sp}(\mathbf{q}_\parallel|\mathbf{k}_\parallel) := -\frac{\varepsilon-1}{\varepsilon}\left(\frac{\omega}{c}\right)[\hat{\mathbf{q}}_\parallel\times\hat{\mathbf{k}}_\parallel]_3\alpha(k_\parallel) \tag{5.7c}$$

$$\nu_{ss}(\mathbf{q}_\parallel|\mathbf{k}_\parallel) := (\varepsilon-1)\left(\frac{\omega}{c}\right)^2[\hat{\mathbf{q}}_\parallel\cdot\hat{\mathbf{k}}_\parallel], \tag{5.7d}$$

and

$$d_p(q_\parallel) := \alpha_0(q_\parallel) + \frac{\alpha(q_\parallel)}{\varepsilon} \tag{5.8a}$$

$$d_s(q_\parallel) := \alpha_0(q_\parallel) + \alpha(q_\parallel). \tag{5.8b}$$

Finally, the equation for $\overline{\overline{\mathbf{R}}}^{(2)}$ is

$$R^{(2)}_{\alpha\beta}(\mathbf{q}_\parallel|\mathbf{p}_\parallel|\mathbf{k}_\parallel) = \frac{\alpha_0(k_\parallel)}{d_\alpha(q_\parallel)d_\beta(k_\parallel)}\left[w_{\alpha\beta}(\mathbf{q}_\parallel|\mathbf{p}_\parallel|\mathbf{k}_\parallel) - 2\sum_{\gamma\in\{p,s\}}\frac{\nu_{\alpha\gamma}(\mathbf{q}_\parallel|\mathbf{p}_\parallel)\nu_{\gamma\beta}(\mathbf{p}_\parallel|\mathbf{k}_\parallel)}{d_\gamma(p_\parallel)}\right] \tag{5.9}$$

whose compactness is facilitated by the definitions of

$$\begin{aligned} w_{pp}(\mathbf{q}_\parallel|\mathbf{p}_\parallel|\mathbf{k}_\parallel) :=\ & \frac{\varepsilon-1}{\varepsilon^2}\left[q_\parallel k_\parallel - \alpha(q_\parallel)[\hat{\mathbf{q}}_\parallel\cdot\hat{\mathbf{k}}_\parallel]\alpha(k_\parallel)\right]\left[\alpha(q_\parallel)+\alpha(k_\parallel)\right] \\ & + \frac{2}{\varepsilon}\left(\frac{\varepsilon-1}{\varepsilon}\right)^2\alpha(q_\parallel)[\hat{\mathbf{q}}_\parallel\cdot\hat{\mathbf{p}}_\parallel]\alpha(p_\parallel)[\hat{\mathbf{p}}_\parallel\cdot\hat{\mathbf{k}}_\parallel]\alpha(k_\parallel) \end{aligned} \tag{5.10a}$$

$$\begin{aligned} w_{ps}(\mathbf{q}_\parallel|\mathbf{p}_\parallel|\mathbf{k}_\parallel) :=\ & \nu_{ps}(\mathbf{q}_\parallel|\mathbf{k}_\parallel)\left[\alpha(q_\parallel)+\alpha(k_\parallel)\right] \\ & + 2\left(\frac{\varepsilon-1}{\varepsilon}\right)^2\left(\frac{\omega}{c}\right)\alpha(q_\parallel)[\hat{\mathbf{q}}_\parallel\cdot\hat{\mathbf{p}}_\parallel]\alpha(p_\parallel)[\hat{\mathbf{p}}_\parallel\times\hat{\mathbf{k}}_\parallel]_3 \end{aligned} \tag{5.10b}$$

$$\begin{aligned} w_{sp}(\mathbf{q}_\parallel|\mathbf{p}_\parallel|\mathbf{k}_\parallel) :=\ & \nu_{sp}(\mathbf{q}_\parallel|\mathbf{k}_\parallel)\left[\alpha(q_\parallel)+\alpha(k_\parallel)\right] \\ & + 2\left(\frac{\varepsilon-1}{\varepsilon}\right)^2\left(\frac{\omega}{c}\right)[\hat{\mathbf{q}}_\parallel\times\hat{\mathbf{p}}_\parallel]_3\alpha(p_\parallel)[\hat{\mathbf{p}}_\parallel\cdot\hat{\mathbf{k}}_\parallel]\alpha(k_\parallel) \end{aligned} \tag{5.10c}$$

$$\begin{aligned} w_{ss}(\mathbf{q}_\parallel|\mathbf{p}_\parallel|\mathbf{k}_\parallel) :=\ & \nu_{ss}(\mathbf{q}_\parallel|\mathbf{k}_\parallel)\left[\alpha(q_\parallel)+\alpha(k_\parallel)\right] \\ & + 2\left(\frac{\varepsilon-1}{\varepsilon}\right)^2\varepsilon\left(\frac{\omega}{c}\right)^2[\hat{\mathbf{q}}_\parallel\times\hat{\mathbf{p}}_\parallel]_3\alpha(p_\parallel)[\hat{\mathbf{p}}_\parallel\times\hat{\mathbf{k}}_\parallel]_3. \end{aligned} \tag{5.10d}$$

For Eqs. (5.10), expressions adapted from Ref. 46 have been used, which differ slightly from those in Ref. 15 from which the notation has been taken. The choice is motivated by Eq. 39 in Ref. 15 having inconsistent dimensions, and the choice is also well justified by later comparisons between calculated and experimentally gathered MDRC, which are given in Sec. 7.2. Calculations corresponding to the alternative expressions resulted in MDRC which differed greatly from the experimental values.

5.2 Phase perturbation theory

Phase perturbation theory [47] aims to formulate the expansion of the reflection amplitude in such a way that its terms correspond to a Taylor expansion of the exponential function with a complex argument. By (in approximation) equating the exponential function with a few terms of its expansion, the formulation is of the form $\exp[r]\exp[i\theta]$. This formulation aims to be similar to the complex formulation for $\mathbf{E}$, introduced in Sec. 3.2. There, the imaginary part of the argument is interpreted as a phase shift, which in turn explains the name of the method. Phase perturbation theory is preferred as it has been found to have a wider range of validity than small-amplitude perturbation theory [48], and be in better agreement with experimental results [15]. Especially, when compared to the small-amplitude method, it is useful when the correlation length of the surface isn't much smaller than the incident wavelength. The following presentation closely resembles the one given in Ref. 15.

As discussed in Sec. 4.6 any scattering theory should be reciprocal. This will now be explicitly enforced by formulating the theory in terms of the scattering matrix $\overline{\overline{\mathbf{S}}}$. By inserting its definition, Eq. (4.16), into Eq. (5.3) we find a similar expansion of $\overline{\overline{\mathbf{S}}}$ into expansion matrices $\overline{\overline{\mathbf{S}}}^{(n)}$ of order n as was found for $\overline{\overline{\mathbf{R}}}$. The first terms are

$$\begin{aligned}\overline{\overline{\mathbf{S}}}(\mathbf{q}_\parallel|\mathbf{k}_\parallel) &= (2\pi)^2\delta(\mathbf{q}_\parallel-\mathbf{k}_\parallel)\overline{\overline{\mathbf{S}}}^{(0)}(\mathbf{q}_\parallel|\mathbf{k}_\parallel) + \overline{\overline{\mathbf{S}}}^{(1)}(\mathbf{q}_\parallel|\mathbf{k}_\parallel)\hat{\zeta}^{(1)}(\mathbf{q}_\parallel-\mathbf{k}_\parallel) \\ &\quad + \int \frac{d^2p_\parallel}{(2\pi)^2}\overline{\overline{\mathbf{S}}}^{(2)}(\mathbf{q}_\parallel|\mathbf{p}_\parallel|\mathbf{k}_\parallel)\hat{\zeta}^{(1)}(\mathbf{q}_\parallel-\mathbf{p}_\parallel)\hat{\zeta}^{(1)}(\mathbf{p}_\parallel-\mathbf{k}_\parallel) + O\big([\hat{\zeta}^{(1)}]^3\big),\end{aligned} \tag{5.11}$$

with each expansion term $\overline{\overline{\mathbf{S}}}^{(n)}$ individually fulfilling Eq. (4.16). We are careful to point out that $\overline{\overline{\mathbf{S}}}^{(0)}(\mathbf{q}_\parallel|\mathbf{k}_\parallel)$ does not have a direct equivalent in $\overline{\overline{\mathbf{R}}}^{(0)}(\mathbf{k}_\parallel)$ as the latter only depends on a single argument. As long as it is paired with a δ-function, it remains inconsequential. However, we may then rewrite

$$\begin{aligned}S_{\alpha\beta}(\mathbf{q}_\parallel|\mathbf{k}_\parallel) = S^{(0)}_{\alpha\beta}(\mathbf{q}_\parallel|\mathbf{k}_\parallel)\Bigg\{&(2\pi)^2\delta(\mathbf{q}_\parallel-\mathbf{k}_\parallel) + \frac{S^{(1)}_{\alpha\beta}(\mathbf{q}_\parallel|\mathbf{k}_\parallel)}{S^{(0)}_{\alpha\beta}(\mathbf{q}_\parallel|\mathbf{k}_\parallel)}\hat{\zeta}^{(1)}(\mathbf{q}_\parallel-\mathbf{k}_\parallel) \\ &+ \int \frac{d^2p_\parallel}{(2\pi)^2}\frac{S^{(2)}_{\alpha\beta}(\mathbf{q}_\parallel|\mathbf{p}_\parallel|\mathbf{k}_\parallel)}{S^{(0)}_{\alpha\beta}(\mathbf{q}_\parallel|\mathbf{k}_\parallel)}\hat{\zeta}^{(1)}(\mathbf{q}_\parallel-\mathbf{p}_\parallel)\hat{\zeta}^{(1)}(\mathbf{p}_\parallel-\mathbf{k}_\parallel) + O\big([\hat{\zeta}^{(1)}]^3\big)\Bigg\},\end{aligned} \tag{5.12}$$

where $S^{(0)}_{\alpha\beta}(\mathbf{q}_\parallel|\mathbf{k}_\parallel)$ is defined as an amplitude of the perturbation. Following the relative relations between the coefficients given in Ref. 49 we find that the relative first order term must be

$$\frac{S^{(1)}_{\alpha\beta}(\mathbf{q}_\parallel|\mathbf{k}_\parallel)}{S^{(0)}_{\alpha\beta}(\mathbf{q}_\parallel|\mathbf{k}_\parallel)} = -2i\sqrt{\alpha_0(q_\parallel)\alpha_0(k_\parallel)}. \tag{5.13}$$

Then, by Eq. (4.16) we may utilise the result of Eq. (5.6) to solve for $S^{(0)}_{\alpha\beta}(\mathbf{q}_\parallel|\mathbf{k}_\parallel)$ in Eq. (5.13) to obtain

$$S^{(0)}_{\alpha\beta}(\mathbf{q}_\parallel|\mathbf{k}_\parallel) = -\frac{\nu_{\alpha\beta}(\mathbf{q}_\parallel|\mathbf{k}_\parallel)}{d_\alpha(\mathbf{q}_\parallel)d_\beta(\mathbf{k}_\parallel)}, \tag{5.14}$$

with the definitions of $\nu_{\alpha\beta}$ and d_γ given by Eqs. (5.7) and Eqs. (5.8). It is noted that through Eq. (5.14), the property $S^{(0)}_{\alpha\beta}(\mathbf{k}_\parallel|\mathbf{k}_\parallel) = R^{(0)}_{\alpha\beta}(\mathbf{k}_\parallel)$ is true.

By using the fact that

$$(2\pi)^2\delta(\mathbf{q}_\parallel - \mathbf{k}_\parallel) = \int d^2x_\parallel \exp\left[-i(\mathbf{q}_\parallel - \mathbf{k}_\parallel)\cdot\mathbf{x}_\parallel\right], \tag{5.15}$$

and keeping in mind the form of Eq. (5.2), we will try to collect the integration over $\mathbf{x}_\parallel$ outside the sum of the different order terms. In the context of the integral, the zeroth order term remains a constant; the same as the first term in the Taylor expansion of the exponential function, which we recall is the goal of our procedure. The corresponding integrals in the term containing $S^{(2)}_{\alpha\beta}$ are coupled to an intermediate integral over the variable $\mathbf{p}_\parallel$, but the coupling may be removed by a linear variable transformation. There are two possible such transformations, eliminating either of the integration variables in one of the $\hat{\zeta}^{(1)}$-expressions. We will follow the formulation of Ref. 15 being a symmetric sum of both transformations, each with weight $1/2$. The details is given in Appendix B leading to the second order term being given by Eq. (B.6). Then, we can rewrite Eq. (5.12) as

$$\begin{aligned} S_{\alpha\beta}(\mathbf{q}_\parallel|\mathbf{k}_\parallel) = S^{(0)}_{\alpha\beta}(\mathbf{q}_\parallel|\mathbf{k}_\parallel) &\int d^2x_\parallel \exp\left[-i(\mathbf{q}_\parallel - \mathbf{k}_\parallel)\cdot\mathbf{x}_\parallel\right] \\ &\times \left\{ 1 + -2i\sqrt{\alpha_0(q_\parallel)\alpha_0(k_\parallel)}\zeta(\mathbf{x}_\parallel) + \frac{1}{2}\int \frac{d^2p_\parallel}{(2\pi)^2} \frac{S^{(2)}_{\alpha\beta}(\mathbf{q}_\parallel|\mathbf{p}_\parallel|\mathbf{k}_\parallel)}{S^{(0)}_{\alpha\beta}(\mathbf{q}_\parallel|\mathbf{k}_\parallel)} \right. \\ &\quad \times \int d^2u_\parallel \left(\exp\left[i(\mathbf{q}_\parallel - \mathbf{p}_\parallel)\cdot\mathbf{u}_\parallel\right] + \exp\left[i(\mathbf{p}_\parallel - \mathbf{k}_\parallel)\cdot\mathbf{u}_\parallel\right]\right) \\ &\quad \left. \times\, \zeta(\mathbf{x}_\parallel)\zeta(\mathbf{x}_\parallel - \mathbf{u}_\parallel) + \ldots \right\}, \end{aligned} \tag{5.16}$$

which are the leading terms of an exponential function

$$S_{\alpha\beta}(\mathbf{q}_\parallel|\mathbf{k}_\parallel) = S^{(0)}_{\alpha\beta}(\mathbf{q}_\parallel|\mathbf{k}_\parallel) \int d^2x_\parallel \exp\left[-i(\mathbf{q}_\parallel - \mathbf{k}_\parallel)\cdot\mathbf{x}_\parallel\right] \left\{ 1 + G_{\alpha\beta} + \frac{1}{2}G^2_{\alpha\beta} \right\} \tag{5.17a}$$

$$\approx S^{(0)}_{\alpha\beta}(\mathbf{q}_\parallel|\mathbf{k}_\parallel) \int d^2x_\parallel \exp\left[-i(\mathbf{q}_\parallel - \mathbf{k}_\parallel)\cdot\mathbf{x}_\parallel\right] \exp\left[G_{\alpha\beta}(\mathbf{q}_\parallel|\mathbf{x}_\parallel|\mathbf{k}_\parallel)\right]. \tag{5.17b}$$

We need to take some precautions with how $G_{\alpha\beta}(\mathbf{q}_\parallel|\mathbf{x}_\parallel|\mathbf{k}_\parallel)$ is defined. The term $-2i\sqrt{\alpha_0(q_\parallel)\alpha_0(k_\parallel)}\zeta(\mathbf{x}_\parallel)$ of Eq. (5.16) must be supplied by the first order term of Eq. (5.17a) as it is linear in ζ. However, then $G^2_{\alpha\beta}$ contains a part that is $\sim \zeta^2$. This is precisely the square of the aforementioned linear term, and it should be counted in our second order theory. Unfortunately, the ζ^2-terms inside Eq. (5.16) do not have comparable prefactors to the ζ^1-terms, which makes it hard to distil which part of the ζ^2-terms that belong to $G_{\alpha\beta}$ and which belong to $G^2_{\alpha\beta}$. This apparent problem is circumvented by defining the function

$G_{\alpha\beta}$ to be

$$\begin{aligned} G_{\alpha\beta}(\mathbf{q}_\parallel|\mathbf{x}_\parallel|\mathbf{k}_\parallel) :=& -2i\sqrt{\alpha_0(q_\parallel)\alpha_0(k_\parallel)}\zeta(\mathbf{x}_\parallel) + \frac{1}{2}\int \frac{d^2p_\parallel}{(2\pi)^2}\frac{S^{(2)}_{\alpha\beta}(\mathbf{q}_\parallel|\mathbf{p}_\parallel|\mathbf{k}_\parallel)}{S^{(0)}_{\alpha\beta}(\mathbf{q}_\parallel|\mathbf{k}_\parallel)} \\ &\times \int d^2u_\parallel \left(\exp\left[i(\mathbf{q}_\parallel - \mathbf{p}_\parallel)\cdot\mathbf{u}_\parallel\right] + \exp\left[i(\mathbf{p}_\parallel - \mathbf{k}_\parallel)\cdot\mathbf{u}_\parallel\right]\right) \\ &\times \zeta(\mathbf{x}_\parallel)\zeta(\mathbf{x}_\parallel - \mathbf{u}_\parallel) + 2\alpha_0(q_\parallel)\alpha_0(k_\parallel)\zeta^2(\mathbf{x}_\parallel). \end{aligned} \tag{5.18}$$

Note the inclusion of the term $2\alpha_0(q_\parallel)\alpha_0(k_\parallel)\zeta^2(\mathbf{x}_\parallel)$, which was not present in Eq. (5.16). This term in $G_{\alpha\beta}$ exactly cancel out the ζ^2-term of $G^2_{\alpha\beta}$ by noting that

$$\frac{1}{2}\left[-2i\sqrt{\alpha_0(q_\parallel)\alpha_0(k_\parallel)}\zeta(\mathbf{x}_\parallel)\right]^2 = 2\alpha_0(q_\parallel)\alpha_0(k_\parallel)\zeta^2(\mathbf{x}_\parallel). \tag{5.19}$$

All other contributions of equal or higher orders of $G_{\alpha\beta}$ is also of order ζ^3 or higher, so we may ignore them in second order phase perturbation theory. The given approach to define $G_{\alpha\beta}(\mathbf{q}_\parallel|\mathbf{x}_\parallel|\mathbf{k}_\parallel)$ is a matter of keeping things simple. There is no straightforward physical interpretation of the function, so its definition is a matter of convenience.

Conveniently, all dependence on ζ in Eq. (5.17b) lies inside of $G_{\alpha\beta}(\mathbf{q}_\parallel|\mathbf{x}_\parallel|\mathbf{k}_\parallel)$, so the averaging taking place in Eq. (4.20) only interacts with the final part. The average up to second order in ζ is therefore given by

$$\begin{aligned} \left\langle S_{\alpha\beta}(\mathbf{q}_\parallel|\mathbf{k}_\parallel)\right\rangle = S^{(0)}_{\alpha\beta}(\mathbf{q}_\parallel|\mathbf{k}_\parallel)\int d^2x_\parallel \exp\left[-i(\mathbf{q}_\parallel - \mathbf{k}_\parallel)\cdot\mathbf{x}_\parallel\right] \\ \times \left\langle \exp\left[G_{\alpha\beta}(\mathbf{q}_\parallel|\mathbf{x}_\parallel|\mathbf{k}_\parallel)\right]\right\rangle. \end{aligned} \tag{5.20}$$

By inserting Eq. (5.20) into Eq. (4.20b) and expanding $|S|^2 = SS^*$ we may write down

$$\begin{aligned} &\left\langle\left|S_{\alpha\beta}(\mathbf{q}_\parallel|\mathbf{k}_\parallel)\right|^2\right\rangle - \left|\left\langle S_{\alpha\beta}(\mathbf{q}_\parallel|\mathbf{k}_\parallel)\right\rangle\right|^2 \\ &\quad= \left|S^{(0)}_{\alpha\beta}(\mathbf{q}_\parallel|\mathbf{k}_\parallel)\right|^2 \int d^2x_\parallel \int d^2x'_\parallel \exp\left[-i(\mathbf{q}_\parallel - \mathbf{k}_\parallel)\cdot(\mathbf{x}_\parallel - \mathbf{x}'_\parallel)\right] \\ &\quad\times \Bigg\{ \left\langle \exp\left[G_{\alpha\beta}(\mathbf{q}_\parallel|\mathbf{x}_\parallel|\mathbf{k}_\parallel) + G^*_{\alpha\beta}(\mathbf{q}_\parallel|\mathbf{x}'_\parallel|\mathbf{k}_\parallel)\right]\right\rangle \\ &\qquad - \left\langle \exp\left[G_{\alpha\beta}(\mathbf{q}_\parallel|\mathbf{x}_\parallel|\mathbf{k}_\parallel)\right]\right\rangle \left\langle \exp\left[G^*_{\alpha\beta}(\mathbf{q}_\parallel|\mathbf{x}'_\parallel|\mathbf{k}_\parallel)\right]\right\rangle \Bigg\}, \end{aligned} \tag{5.21}$$

where $\mathbf{x}_\parallel$ is the integration variable over the first term and $\mathbf{x}'_\parallel$ is the integration variable over the second term. Further evaluating Eq. (5.21) is non-trivial but by using cumulant methods [50] one may find that [15]

$$\begin{aligned} &\left\langle \exp\left[G_{\alpha\beta}(\mathbf{q}_\parallel|\mathbf{x}_\parallel|\mathbf{k}_\parallel) + G^*_{\alpha\beta}(\mathbf{q}_\parallel|\mathbf{x}'_\parallel|\mathbf{k}_\parallel)\right]\right\rangle \\ &- \left\langle \exp\left[G_{\alpha\beta}(\mathbf{q}_\parallel|\mathbf{x}_\parallel|\mathbf{k}_\parallel)\right]\right\rangle \left\langle \exp\left[G^*_{\alpha\beta}(\mathbf{q}_\parallel|\mathbf{x}'_\parallel|\mathbf{k}_\parallel)\right]\right\rangle \\ =& \exp\left[\delta^2\Re\int\frac{d^2p_\parallel}{(2\pi)^2}\left[g(|\mathbf{q}_\parallel - \mathbf{p}_\parallel|) + g(|\mathbf{p}_\parallel - \mathbf{k}_\parallel|)\right]\frac{S^{(2)}_{\alpha\beta}(\mathbf{q}_\parallel|\mathbf{p}_\parallel|\mathbf{k}_\parallel)}{S^{(0)}_{\alpha\beta}(\mathbf{q}_\parallel|\mathbf{k}_\parallel)}\right] \\ &\times \left\{\exp\left[4\delta^2\alpha_0(q_\parallel)\alpha_0(k_\parallel)W(|\mathbf{x}_\parallel - \mathbf{x}'_\parallel|)\right] - 1\right\}. \end{aligned} \tag{5.22}$$

The appearance of the surface autocorrelation function $W(|\mathbf{x}_{\|} - \mathbf{x}'_{\|}|)$ is due to Eq. (2.2), and the same goes for the appearance of the surface power spectrum defined by Eq. (2.3) which just happens to be contained in a Fourier integral. Some terms from Eq. (5.18) are absent due to Eq. (2.1). By substituting Eq. (5.22) into Eq. (5.21) and further into Eq. (4.20b) and using the substitution $\mathbf{u}_{\|} = \mathbf{x}_{\|} - \mathbf{x}'_{\|}$ one obtains

$$\begin{aligned}\left\langle \frac{\partial R_{\alpha\beta}}{\partial \Omega_{\mathrm{s}}} \right\rangle_{\text{incoh}} &= \left(\frac{\omega}{2\pi c}\right)^2 \cos(\theta_{\mathrm{s}}) \left| S^{(0)}_{\alpha\beta}(\mathbf{q}_{\|}|\mathbf{k}_{\|}) \right|^2 \\ &\times \exp\left[\delta^2 \Re \int \frac{d^2 p_{\|}}{(2\pi)^2} \left[g(|\mathbf{q}_{\|} - \mathbf{p}_{\|}|) + g(|\mathbf{p}_{\|} - \mathbf{k}_{\|}|)\right] \frac{S^{(2)}_{\alpha\beta}(\mathbf{q}_{\|}|\mathbf{p}_{\|}|\mathbf{k}_{\|})}{S^{(0)}_{\alpha\beta}(\mathbf{q}_{\|}|\mathbf{k}_{\|})}\right] \\ &\times \int d^2 u_{\|} \exp\left[-i(\mathbf{q}_{\|} - \mathbf{k}_{\|}) \cdot \mathbf{u}_{\|}\right] \left\{\exp\left[4\delta^2 \alpha_0(q_{\|})\alpha_0(k_{\|}) W(|\mathbf{u}_{\|}|)\right] - 1\right\}. \end{aligned} \tag{5.23}$$

In obtaining the result of Eq. (5.23), we have used that the integrand becomes independent of $\mathbf{x}_{\|}$ after performing the variable substitution, and that the integral over $\mathbf{x}_{\|}$ itself produces the scattering area in the x_1x_2-plane. Following the discussion after Eq. (A.22) this is the same as the quantity A in Eq. (4.20b), and those contributions cancel. Equation (5.23) gives the value of the incoherent MDRC through phase perturbation theory up to second order in the surface profile function, in a formulation that is symmetric in the couplings of $\mathbf{q}_{\|}$ and $\mathbf{k}_{\|}$ to the variable $\mathbf{p}_{\|}$.

5.3 Included and non-included terms in the scattering matrix expansion

Let us briefly return to considering how Eq. (5.11) interacts with Eqs. (4.20), which depends on $|S_{\alpha\beta}(\mathbf{q}_{\|}|\mathbf{k}_{\|})|^2$. If we follow the idea of Ref. 51 and define

$$A^{(0)}_{\alpha\beta} = S^{(0)}_{\alpha\beta}(\mathbf{k}_{\|})(2\pi)^2 \delta(\mathbf{q}_{\|} - \mathbf{k}_{\|}) \tag{5.24a}$$

$$A^{(1)}_{\alpha\beta} = S^{(1)}_{\alpha\beta}(\mathbf{q}_{\|}|\mathbf{k}_{\|}) \hat{\zeta}^{(1)}(\mathbf{q}_{\|} - \mathbf{k}_{\|}) \tag{5.24b}$$

$$A^{(2)}_{\alpha\beta} = \int \frac{d^2 p_{\|}}{(2\pi)^2} S^{(2)}_{\alpha\beta}(\mathbf{q}_{\|}|\mathbf{p}_{\|}|\mathbf{k}_{\|}) \hat{\zeta}^{(1)}(\mathbf{q}_{\|} - \mathbf{p}_{\|}) \hat{\zeta}^{(1)}(\mathbf{p}_{\|} - \mathbf{k}_{\|}), \tag{5.24c}$$

and so on, we may write down the expansion for $S_{\alpha\beta}$ to be

$$S_{\alpha\beta} = A^{(0)}_{\alpha\beta} + A^{(1)}_{\alpha\beta} + A^{(2)}_{\alpha\beta} + A^{(3)}_{\alpha\beta} + A^{(4)}_{\alpha\beta} + \ldots. \tag{5.25}$$

Each $A^{(n)}_{\alpha\beta}$ is of order ζ^n. Equation (5.11) includes terms up to $n = 2$ in the scattering amplitude. Let us calculate $|S_{\alpha\beta}|^2$ with the expansion of Eq. (5.25), resulting in

$$\begin{aligned}|S_{\alpha\beta}|^2 = &\left|A_{\alpha\beta}^{(0)}\right|^2 \\ &+ \left|A_{\alpha\beta}^{(1)}\right|^2 + 2\Re\left(A_{\alpha\beta}^{(0)}A_{\alpha\beta}^{(1)}\right) \\ &+ \left|A_{\alpha\beta}^{(2)}\right|^2 + 2\Re\left(A_{\alpha\beta}^{(0)}A_{\alpha\beta}^{(2)}\right) + 2\Re\left(A_{\alpha\beta}^{(1)}A_{\alpha\beta}^{(2)}\right) \\ &+ \left|A_{\alpha\beta}^{(3)}\right|^2 + 2\Re\left(A_{\alpha\beta}^{(0)}A_{\alpha\beta}^{(3)}\right) + 2\Re\left(A_{\alpha\beta}^{(1)}A_{\alpha\beta}^{(3)}\right) + 2\Re\left(A_{\alpha\beta}^{(2)}A_{\alpha\beta}^{(3)}\right) \\ &+ \left|A_{\alpha\beta}^{(4)}\right|^2 + 2\Re\left(A_{\alpha\beta}^{(0)}A_{\alpha\beta}^{(4)}\right) + \ldots .\end{aligned} \tag{5.26}$$

The terms accounted for in Eq. (5.11) inhabits the three top rows of Eq. (5.26), and contains terms up to ζ^4. The $\left|A_{\alpha\beta}^{(2)}\right|^2$-term is responsible for this, and is called the 2-2 term. We make note of the distinction between $\bar{\bar{\mathbf{S}}}$ which has been expanded to order ζ^2 through second order phase perturbation theory, and $\left|\bar{\bar{\mathbf{S}}}\right|^2$ which is of order ζ^4 by consequence. There are three other terms in Eq. (5.26) which is also of order ζ^4 or less, which has *not* been accounted for in the phase perturbation theory: The terms $\Re\left(A_{\alpha\beta}^{(0)}A_{\alpha\beta}^{(3)}\right)$ and $\Re\left(A_{\alpha\beta}^{(0)}A_{\alpha\beta}^{(4)}\right)$ are only non-zero if $\mathbf{q}_{\|} = \mathbf{k}_{\|}$, which only accounts for a single point in the parameter space. However, the term $\Re\left(A_{\alpha\beta}^{(1)}A_{\alpha\beta}^{(3)}\right)$ may in principle be different from zero for all $\mathbf{q}_{\|}$ and $\mathbf{k}_{\|}$, and is of order ζ^4. It is referred to as the 1-3 term.

The preceding discussion shows that it is impossible to capture all second order scattering phenomena through second order phase perturbation theory. Indeed the same argument holds for small-amplitude perturbation theory, and for all perturbation theories on a quantity S that produces a result depending on S^2. A third-order perturbation theory is required to determine the 1-3 term. By a similar argument, one could determine that fifth order perturbation theory is required to capture all third order scattering phenomena which requires a 1-5 type term to be of the same order as the presumed 3-3 term accounted for in the perturbation.

Indeed, the present second order phase perturbation theory does not depend simply on $|S_{\alpha\beta}|^2$, but on the difference $\langle|S_{\alpha\beta}|^2\rangle - |\langle S_{\alpha\beta}\rangle|^2$. However, this does not change the fact that the dependence on the 1-3 term is not accounted for in our theory. Introducing the averages leaves the 1-3 term to have the form

$$2\Re\left(\left\langle A_{\alpha\beta}^{(1)}A_{\alpha\beta}^{(3)}\right\rangle - \left\langle A_{\alpha\beta}^{(1)}\right\rangle\left\langle A_{\alpha\beta}^{(3)}\right\rangle\right) \tag{5.27}$$

which is recognised as being proportional to the statistical *covariance* [23, 24] between the 1 and 3 terms. In general, the covariance is different from zero.

The various formulations of phase perturbation theory have varying reliance on the 1-3 and 2-2 terms. A second order phase perturbation theory should ideally have little dependence on the 1-3 term, or have its contribution be counteracted by higher order effects. It is unclear which formulation most accurately reproduces experimental MDRC values, and it may very well depend on the media involved as well as the wavelength regime.

It may also be variable for different polarisation components, and/or out-of-plane angles. The comparisons made inside this thesis should therefore not be regarded to hold in all circumstances.

5.4 Analytic computation of angular integrals

We aim to reduce the numerical calculation by performing the angular integrals present in Eq. (5.23) analytically, starting with the integral over $\mathbf{u}_\parallel$ in Eq. (5.23). Writing it out in polar coordinates gives

$$\int d^2u_\parallel \cdots = \int_0^\infty du_\parallel u_\parallel f(u_\parallel) \int_{-\pi}^{\pi} d\phi \exp\left[-i\left|\mathbf{q}_\parallel - \mathbf{k}_\parallel\right| u_\parallel \cos(\phi)\right], \tag{5.28}$$

where $f(u_\parallel) := \exp\left[4\delta^2\alpha_0(q_\parallel)\alpha_0(k_\parallel)W(\left|\mathbf{u}_\parallel\right|)\right] - 1$. There is no angular dependence in f, so by using the fact that $\cos(\cdot)$ is symmetric around 0 we may instead integrate ϕ twice over the interval $[0, \pi]$. Coincidentally, this permits usage of a Bessel function identity [52, 53]

$$J_0(z) = \frac{1}{\pi}\int_0^\pi d\phi \exp\left[iz\cos(\phi)\right], \tag{5.29}$$

where $J_0(z)$ denotes the Bessel function of the first kind and order zero (and in general $J_n(z)$ of order n). Equation (5.28) therefore reduces to

$$\int d^2u_\parallel \cdots = \int_0^\infty du_\parallel u_\parallel f(u_\parallel) 2\pi J_0(-\left|\mathbf{q}_\parallel - \mathbf{k}_\parallel\right| u_\parallel). \tag{5.30}$$

Finally, we may also use the fact that $J_0(z)$ is symmetric around 0, to purge the first minus sign away from the argument of J_0 in Eq. (5.30).

Onto the "exponential" part of Eq. (5.23), being given by $\exp\left[\tau_{\alpha\beta}\right]$ for

$$\tau_{\alpha\beta}(\mathbf{q}_\parallel|\mathbf{k}_\parallel) := \delta^2\Re\int \frac{d^2p_\parallel}{(2\pi)^2}\left[g(\left|\mathbf{q}_\parallel - \mathbf{p}_\parallel\right|) + g(\left|\mathbf{p}_\parallel - \mathbf{k}_\parallel\right|)\right] \frac{S^{(2)}_{\alpha\beta}(\mathbf{q}_\parallel|\mathbf{p}_\parallel|\mathbf{k}_\parallel)}{S^{(0)}_{\alpha\beta}(\mathbf{q}_\parallel|\mathbf{k}_\parallel)}, \tag{5.31}$$

a definition motivated by convenience of notation. We will perform some simplifications to τ and exponentiate it at the end. The first approach is to split the integral over $\mathbf{p}_\parallel$ into its radial angular components, and perform the angular integral analytically. To extract the angular dependence of the power spectrum, we will make use of the identity

$$g(|\mathbf{p}_\parallel - \mathbf{k}_\parallel|) = 2\pi \sum_{n=-\infty}^{\infty} \exp\left[in(\phi_p - \phi_k)\right] L_n(p_\parallel|k_\parallel), \tag{5.32}$$

with the notation-compacting definitions of

$$L_n(s_\parallel|t_\parallel) := \int_0^\infty du_\parallel u_\parallel W(u_\parallel) J_n(s_\parallel u_\parallel) J_n(t_\parallel u_\parallel). \tag{5.33}$$

A proof of Eq. (5.32) is given in Appendix C. The usage of this expansion is inspired by Ref. 12, but we will subject the idea to the symmetric formulation of Ref. 15. This also happens to remove the only explicit reference to the power spectrum, so in practice there is no reason to calculate it in the first place. That may turn out to be useful for complicated surface profile functions which cannot be written down on closed form, making the calculation of $g(\mathbf{Q}_{\|})$ non-trivial.

We point out that there is no angular dependence inside Eq. (5.33). Meanwhile, all the angular dependence of the remaining integrand is inside $S^{(2)}_{\alpha\beta}$, but as may be seen from Eqs. (4.16), (5.7), (5.9) and (5.10), the angular dependence is only given by combinations of $[\hat{\mathbf{q}}_{\|} \cdot \hat{\mathbf{p}}_{\|}]$, $[\hat{\mathbf{p}}_{\|} \cdot \hat{\mathbf{k}}_{\|}]$, $[\hat{\mathbf{q}}_{\|} \times \hat{\mathbf{p}}_{\|}]_3$ and $[\hat{\mathbf{p}}_{\|} \times \hat{\mathbf{k}}_{\|}]_3$. These angular dependents only contribute combinations of sine and cosine functions in the in-plane angle differences between $\mathbf{q}_{\|}$ and $\mathbf{k}_{\|}$. The result of the analytic integrals is that only terms with $|n| \leq 2$ contributes to the sum in Eq. (5.32). The result of the analytic integrals as a function of n serves as weights for the different L_n. The specific dependence on either $\{\mathbf{q}_{\|}, \mathbf{p}_{\|}\}$ or $\{\mathbf{p}_{\|}, \mathbf{k}_{\|}\}$ pertains to the two contributions of g in Eq. (5.31). The detailed calculation of the exponent terms is given in Appendix D, and shows that $\tau_{\alpha\beta}(\mathbf{q}_{\|}|\mathbf{k}_{\|})$ is given by the somewhat involved expressions in Eqs. (D.8)–(D.11).

Collecting these expressions, the final expression that calculates the incoherent MDRC, which is implemented numerically, is given by

$$\left\langle \frac{\partial R_{\alpha\beta}}{\partial \Omega_{\mathrm{s}}} \right\rangle_{\mathrm{incoh}} = \frac{1}{2\pi} \left(\frac{\omega}{c}\right)^2 \cos(\theta_{\mathrm{s}}) \left| S^{(0)}_{\alpha\beta}(\mathbf{q}_{\|}|\mathbf{k}_{\|}) \right|^2 \exp\left[\tau_{\alpha\beta}(\mathbf{q}_{\|}|\mathbf{k}_{\|})\right] \\ \times \int_0^\infty du_{\|} u_{\|} J_0(\left|\mathbf{q}_{\|} - \mathbf{k}_{\|}\right| u_{\|}) \left\{\exp\left[4\delta^2 \alpha_0(q_{\|})\alpha_0(k_{\|}) W(u_{\|})\right] - 1\right\}. \tag{5.34}$$

Chapter 6

Numerical Implementation and Considerations

This chapter aims to discuss the numerical implementation, and some numerical pit-falls.

6.1 Programming language and packages

Equation (5.34) is solved numerically. The implementation is performed in python version 3.8.5, due to its versatility and the authors prior experience with it. A common objection against using python is its numerical inefficiency, due to the lack of compilation. However, the numerical heavy lifting — specifically the numerical integration — was performed by a pre-compiled function from the *SciPy* [54] library. The function emulates a low-level technique from the Fortran library QUADPACK. The semi-infinite integral of Eq. (5.30) is computed as a Fourier integral, while the semi-infinite integrals of Eq. (5.33) and Eqs. (D.8)–(D.11) are approximated with a finite upper boundary. An estimation of appropriate boundaries is given in Sec. 6.3. Once the integrals have been set to have a finite range, the integration function uses a Clenshaw-Curtis method which uses Chebyshev moments [55].

To further facilitate numerical efficiency, the calculation is performed on *NumPy* [56] arrays, which are memory-contiguous. As far as possible, native python-functions have been replaced by their NumPy-equivalents which are all pre-compiled in C. By making use of these packages, we suspect that the python implementation is only slightly slower than fully compiled code.

6.2 Numerical considerations

The expressions given by Eqs. (D.8)–(D.11) are complex quantities, but the integral solver requires real-valued functions. To facilitate this, the implementation interchanges the order of the integral and taking the real part. This operation is performed pointwise on all the evaluation points, which is unproblematic. However, if one were to initiate the operation on its functional form with the formula $\Re(\psi) = 1/2\,(\psi + \psi^*)$, some imaginary part might remain due to limited numerical precision.

The order of the operations might slightly alter the result, again due to limited numerical precision. If the equivalent of $S^{(0)}_{\alpha\beta}$ in Eq. (5.31) approaches zero for some input $(\mathbf{q}_\parallel, \mathbf{k}_\parallel)$, then $\tau_{\alpha\beta}$ may quickly diverge. To combat this, the numerator in all numerical expressions is always multiplied in first. That way, if the argument of the integral turns out to be some $0/0$ type of expression, it is multiplied by zero first. From experience, this usually prevents divergent behaviour. Even if the value of the expression is not completely accurate, it only accounts for a single point in parameter space, meaning the error upon integration is small.

6.3 Numerical justification of upper integral limits

Equation (5.31) contains a double integral, which in principle is evaluated over a semi-infinite plane in two dimensions of parameter space. As mentioned in Sec. 6.1, we seek to limit the integral domain to be finite by placing upper bounds on each of them. For clarity, let us define the integrands l_n and $I_{\alpha\beta}$ by the equations

$$L_n(\mathbf{s}_\parallel|\mathbf{t}_\parallel) := \int_0^\infty du_\parallel l_n(u_\parallel; s_\parallel, t_\parallel) \tag{6.1a}$$

$$\tau_{\alpha\beta(\mathbf{s}_\parallel|\mathbf{t}_\parallel)} := C_{\alpha\beta}(\mathbf{s}_\parallel|\mathbf{t}_\parallel) + \delta^2 \int_0^\infty dp_\parallel I_{\alpha\beta}(p_\parallel; \mathbf{s}_\parallel, \mathbf{t}_\parallel), \tag{6.1b}$$

where L_n is the quantity from Eq. (5.33) and it is contained inside $I_{\alpha\beta}$. Also, the constant C in Eq. (6.1b) just represents all the terms that are constant with respect to $p_\parallel$, and it is not considered further in this section. The detailed form of both $I_{\alpha\beta}$ and $C_{\alpha\beta}$ is provided by Eqs. (D.8)–(D.11).

In our case, the surface has a Gaussian height distribution, meaning l_n is contained inside an envelope function with the form of Eq. (2.8). An appropriate upper boundary may be deduced from considerations of the envelope function alone. Demanding that $W(x_\parallel^{\max}) \lesssim 10^{-7}$ for instance, corresponds to $x_\parallel^{\max} \lesssim 4a$. As shown by Fig. 6.1 for two example wave vectors and two sets of surface parameters from Ref. 15, the integrand has all but vanished for $x_\parallel = 4a$. The specific surface parameters and description of the samples is given in Sec. 7.2.1 and Table 7.2. The remaining integrand decreases in amplitude like a squared exponential function, and the integrand even oscillates, meaning any introduced error partially cancels out.

As long as the surface profile is Gaussian, this prescribed cut-off is seemingly innocuous. But for a general surface autocorrelation function, greater care might have to be

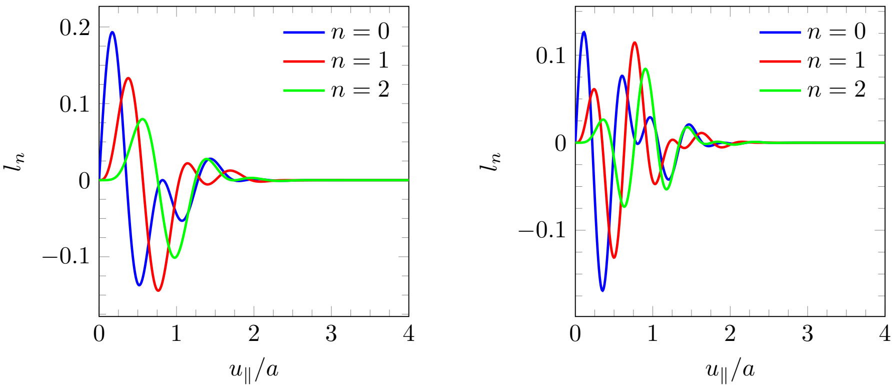

(a) The integrand $l_n(u_\parallel; s_\parallel t_\parallel)$ as a function of $u_\parallel$ with statistical parameters from sample 0061 of Ref. 15. The wave numbers $s_\parallel$ and $t_\parallel$ are taken from example wave vector 1.

(b) The integrand $l_n(u_\parallel; s_\parallel t_\parallel)$ as a function of $u_\parallel$ with statistical parameters from sample 0061 of Ref. 15. The wave numbers $s_\parallel$ and $t_\parallel$ are taken from example wave vector 2.

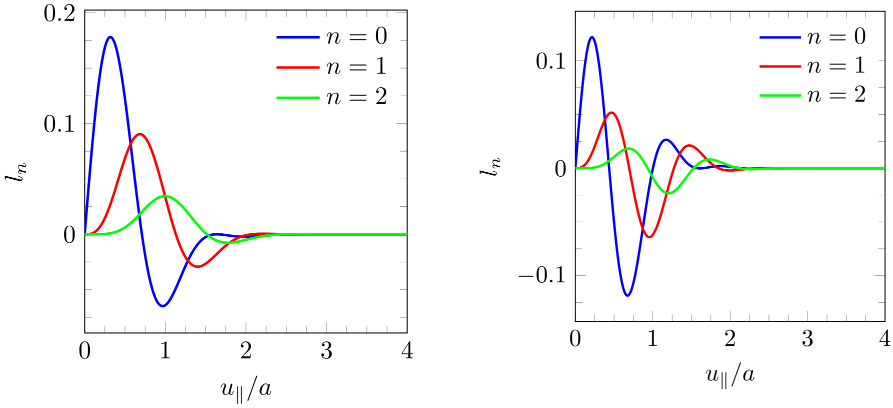

(c) The integrand $l_n(u_\parallel; s_\parallel t_\parallel)$ as a function of $u_\parallel$ with statistical parameters from sample 7047 of Ref. 15. The wave numbers $s_\parallel$ and $t_\parallel$ are taken from example wave vector 1.

(d) The integrand $l_n(u_\parallel; s_\parallel t_\parallel)$ as a function of $u_\parallel$ with statistical parameters from sample 7047 of Ref. 15. The wave numbers $s_\parallel$ and $t_\parallel$ are taken from example wave vector 1.

Figure 6.1: Representative behaviour for the integrands $l_n(u_\parallel; s_\parallel, t_\parallel)$ of Eq. (5.33) as functions of $u_\parallel$. All integrands are contained in an envelope which is dominated by a Gaussian surface auto-correlation function with mean correlation length a. All integrands are extremely close to zero for all $u_\parallel > 4a$. Wave vector 1 is defined by the parameters $\{\theta_0 = 15°, \phi_0 = 0°, \theta_\text{s} = 37°, \phi_\text{s} = 0°\}$. Wave vector 2 is defined by the parameters $\{\theta_0 = 78°, \phi_0 = 0°, \theta_\text{s} = -15°, \phi_\text{s} = 24°\}$.

taken. The integrand l_n is oscillatory with respect to $u_{\parallel}$. If the oscillation frequency is large compared to the size of the envelope function, the evaluation of L_n becomes increasingly challenging. One approach to solving it is discussed in Sec. 6.4.

After applying the cut-off for L_n, the behaviour of the integrands $I_{\alpha\beta}(p_{\parallel})$ remains immediately non-obvious. To produce an accurate approximation with a finite upper bound, the integrand ought to decrease quickly. We check numerically if this is the case for $I_{\alpha\beta}(p_{\parallel})$, and plot the results for two example wave vectors and two sets of surface parameters from Ref. 15 in Fig. 6.2. The result shows that $|I_{\alpha\beta}|$ decreases up to a certain $p_{\parallel}$, and thereafter it fluctuates erratically around a constant value.

The sudden shift in character of $I_{\alpha\beta}$ is suspicious, and the form of its tail is telling of numerical limitations dominating the form of the integrand. This form of graphic is common for expressions that are defined only through numeric computation. It does not justify a conclusion that the integral does not converge. In the end, we are calculating the MDRC, a measurable quantity that clearly is finite. Therefore, we look to the smooth parts of Fig. 6.2 to evaluate convergence on a part of $I_{\alpha\beta}$ that seems less tarnished by numerical limitations. Their analytical form were extracted from a curve fitting through the calculated points, with the fitting function of the form

$$f_{\text{fit}}(p_{\parallel}; f_1, f_2, f_3, f_4) = f_1 \exp\left[-(f_2 p_{\parallel})^{f_3}\right] + f_4. \tag{6.2}$$

The curve fitting was performed with a least-square method using the Levenberg-Marquardt algorithm [57]. The most relevant fitting parameter from Eq. (6.2) is f_3, and it was recorded for all the sets of scattering parameters studied in this thesis, and for both the example wave vectors used to create Figs. 6.1 and 6.2. In all cases, $f_3 \approx 6$, meaning the smooth form of the integrand decreases like $\exp\left[-p_{\parallel}^6\right]$. This supports the claim that $\tau_{\alpha\beta}$ is reasonably well approximated by any upper bound that exceeds the "critical point" of the integrand, which we take to be the point where the nature of the integrand changes from analytical to numerical.

In the implementation, the upper boundaries often exceed the "critical point" significantly. This is done to make sure the upper boundary is always large enough, even for all the wave vector combinations unaccounted for in the examples. There is no reason to believe the form of the integrands should vary massively within the constraints placed on $\mathbf{q}_{\parallel}$ and $\mathbf{k}_{\parallel}$. But there is also no reason to believe that the possible error of including the erratic part of I is significant. We note that the plots in Fig. 6.2 show the absolute value of $I_{\alpha\beta}$ instead of $I_{\alpha\beta}$ itself. Sans for a possible numerical bias, it seems unlikely that the integral of the tail end amounts to anything that matters.

6.4 An approach to calculating highly oscillating integrals

The integrand of Eq. (5.33) oscillates with frequencies equal to the functions arguments, as may be observed in Fig. 6.1. Equations (D.8)–(D.11) shows that these arguments are either $\{q_{\parallel}, p_{\parallel}\}$ or $\{p_{\parallel}, k_{\parallel}\}$. Any $q_{\parallel}$ or $k_{\parallel}$ is bounded by the interval $[-\omega/c, \omega/c]$ since these two wave vectors are related to the polar angles of scattering and incidence respectively, but

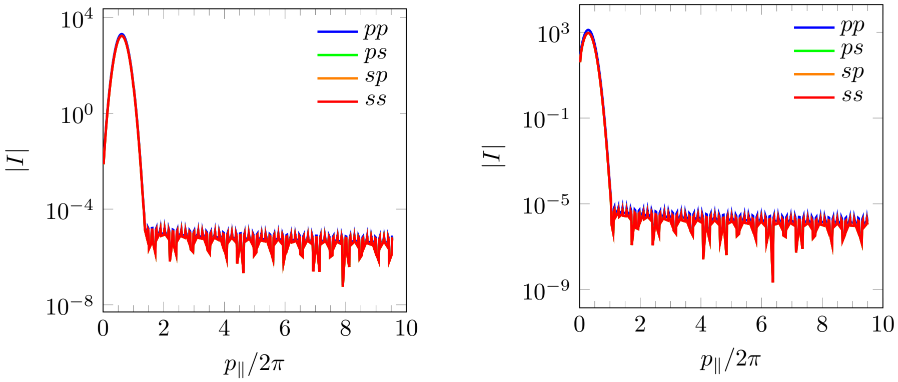

(a) The integrand $I_{\alpha\beta}(p_{\|}; s_{\|}t_{\|})$ as a function of $p_{\|}$ with statistical parameters from sample 0061 of Ref. 15. The wave numbers $s_{\|}$ and $t_{\|}$ are taken from example wave vector 1.

(b) The integrand $I_{\alpha\beta}(p_{\|}; s_{\|}t_{\|})$ as a function of $p_{\|}$ with statistical parameters from sample 0061 of Ref. 15. The wave numbers $s_{\|}$ and $t_{\|}$ are taken from example wave vector 2.

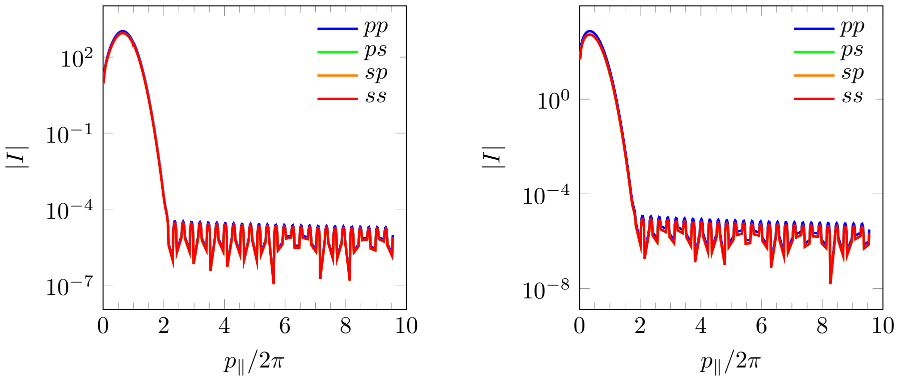

(c) The integrand $I_{\alpha\beta}(p_{\|}; s_{\|}t_{\|})$ as a function of $p_{\|}$ with statistical parameters from sample 7047 of Ref. 15. The wave numbers $s_{\|}$ and $t_{\|}$ are taken from example wave vector 1.

(d) The integrand $I_{\alpha\beta}(p_{\|}; s_{\|}t_{\|})$ as a function of $p_{\|}$ with statistical parameters from sample 7047 of Ref. 15. The wave numbers $s_{\|}$ and $t_{\|}$ are taken from example wave vector 2.

Figure 6.2: Representative behaviour for the absolute value of the integrands $I_{\alpha\beta}(p_{\|}; s_{\|}, t_{\|})$ of Eqs. (D.8)–(D.11) as functions of $p_{\|}$. All integrands have been calculated for a Gaussian surface autocorrelation function, with the upper boundaries of Eq. (5.33) set to $4a$. The smooth part of $I_{\alpha\beta}$ have been curve fitted to a function that decreases like $\exp\left[-p_{\|}^6\right]$. Wave vector 1 is defined by the parameters $\{\theta_0 = 15°, \phi_0 = 0°, \theta_\mathrm{s} = 37°, \phi_\mathrm{s} = 0°\}$. Wave vector 2 is defined by the parameters $\{\theta_0 = 78°, \phi_0 = 0°, \theta_\mathrm{s} = -15°, \phi_\mathrm{s} = 24°\}$.

the integral variable $p_{\|} \in [0, \infty)$ may provide extremely rapid oscillation. This is the main motivation of providing an upper limit of the integral over $p_{\|}$, and as discussed in Sec. 6.3 the integrand *does* in fact seem to vanish quickly as $p_{\|}$ increases. However, the argument is quite specific to the relatively narrow range of surface parameters presented, and not generally valid. It remains challenging to define a generally robust criterion for where to place the upper limit. In some parameter regimes, it may be required that the upper boundary is large compared to the other quantities in the integrand. There is in general no reason to suspect that the fluctuating effects have to remain as small as in Fig. 6.2.

Some of the numerical uncertainties comes down to evaluation of Eq. (5.33). The naïve approach presented until now fails to evaluate oscillations that are more frequent than the frequency of the interval subdivision points used for integral evaluation. One case where this may occur is on a surface with long range correlations, such that l_n oscillates many times within the confines of the correlation function envelope. Another case is if the amplitude of $I_{\alpha\beta}$ does not decrease quickly. At many test stages for the present code implementation, the evaluation of L_n for large frequencies ($p_{\|}$) was a cause of concern. This prompts the investigation of a more robust method for evaluating Eq. (5.33) for large frequencies.

The suggested approach is to convert the oscillating integral into a sequence of integrals between the alternating positive and negative contributions, and then evaluate the convergence of the sequence with Wynn's ϵ-method [58]. The method can determine the convergence of a oscillating series with only a few given terms. A python-specific implementation [59] was used in practice. A pseudo-coded overview of the method is given in Algorithm 1. The zeros of the integrand l_n is easily found in the Gaussian case, as they exactly coincide with frequency-scaled zeros of the n-th order Bessel function.

Algorithm 1 Alternative approach to the evaluation of Eq. (5.33).

```
lzeros ← the first K zeros of the integrand, which are scaled Bessel function zeros.
for $z$ in lzeros:
    $S_k \leftarrow \int_{z[k-1]}^{z[k]} du_{\|} l_n(u_{\|})$, evaluated with the regular method
if $S_K = S_{K-1}$ then
        return $S_K$ (The partial sums converged within $K$ terms)
else $L_n \approx$ Wynn-$\epsilon \left( \{S_k\}_{k=1}^{K} \right)$
```

Given the specifics of how Eq. (5.33) appears in Eqs. (D.8)–(D.11), only one of the frequencies in the Bessel functions has the possibility of becoming large. To capture the correct large-scale behaviour of the integrand, which is the oscillation of the low-frequency Bessel function as well as the high-frequency, a significant part of the integrand should be included. As shown by Fig. 6.1, the low frequency Bessel function also oscillates a few times within the confines of the enveloping autocorrelation function. A large frequency difference is a challenge, because a lot of terms needs to be evaluated in the Wynn-ϵ algorithm. So; while in principle Algorithm 1 accurately evaluates each term and their collective convergence, the large number of terms that is required for a single high frequency makes the method computationally challenging in practice. This method would probably benefit greatly for a formulation where the ”inner” integral of the exponent in MDRC only contains a single oscillating function.

Chapter 7

Results and Discussion

This chapter presents calculated MDRC for some example systems, compares the results to previous implementations and experiments, and comments on similarities and differences between them, as well as the physical origins of some of the observed phenomena. All calculation is performed using the phase perturbation theory culminating in the expression Eq. (5.34), with the implementation detailed in Chapter 6.

7.1 Comparison with previous numerical systems

In Ref. 12, a direct solution of the reduced Rayleigh equation, as well as a computation using a different formulation of phase perturbation theory was performed. Its authors introduced some systems for numerical testing, and we now compare the results of the present implementation in these systems. For the comparisons in this section and the next, we quickly mention that the cross-polarised components of MDRC are always zero for in-plane scattering. This may be seen by the multiplicative factor $\left|S^{(0)}_{\alpha\beta}(\mathbf{q}_{||}|\mathbf{k}_{||})\right|^2$ in Eq. (5.23) through its definition in Eq. (5.14) depends on the function $\nu_{\alpha\beta}(\mathbf{q}_{||}|\mathbf{k}_{||})$, which itself depends linearly on $[\hat{\mathbf{q}}_{||} \times \hat{\mathbf{p}}_{||}]_3$ if $\alpha \neq \beta$, as can be seen from Eqs. (5.7). So for $\alpha \neq \beta$ and $\hat{\mathbf{q}}_{||} \parallel \hat{\mathbf{k}}_{||}$, the MDRC must vanish as the cross product does. This is why the ps- and sp-components are absent from the MDRC plots shown in Secs. 7.1 and 7.2.

Both the results of the present calculation as well as the direct calculation performed in Ref. 12 are presented in Figs. 7.1–7.3 and Fig. 7.5. The calculations performed by Ref. 12 has been labelled ”external” (or ”Ext.”) to distinguish them from the results of the present implementation.

Table 7.1: Statistical parameters of the numerical test systems from Ref. 12.

System	λ[nm]	$\varepsilon(\omega)$	δ/λ	a/λ	δ/a
1	457.90	$-7.50 + i0.24$	0.05	1.0	0.05
2	457.90	$-7.50 + i0.24$	0.05	0.5	0.10
3	632.80	$-18.28 + i0.48$	0.025	0.25	0.10

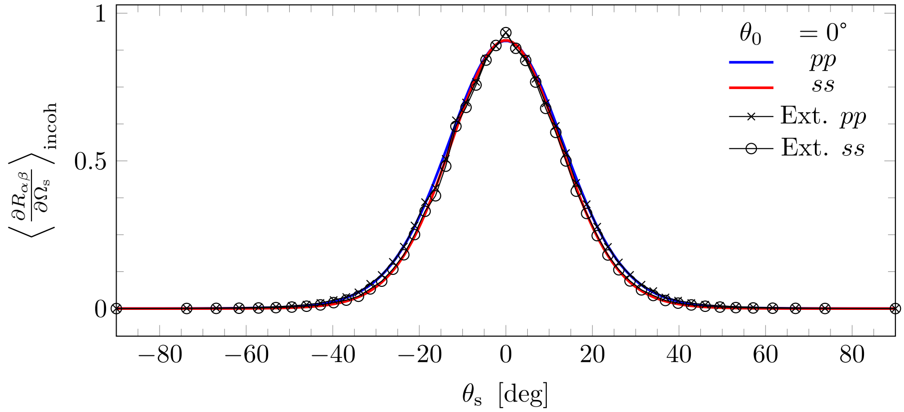

Figure 7.1: Calculated in-plane incoherent MDRC as a function of the polar scattering angle on a randomly rough silver surface, with an incidence angle of 0°. The surface height distribution is Gaussian, with statistical parameters $\delta = 0.05\lambda$ and $a = 1.0\lambda$ taken from "system 1" of Ref. 12, which is also the origin of the "external" data sets included for comparison.

7.1.1 Presentation of the systems

The scattering systems used for comparison is presented in Table 7.1. These all emulate a randomly rough silver surface with a Gaussian height distribution. The given dielectric functions are constants at the given wavelengths.

7.1.2 Presentation of the calculated MDRC

The calculated in-plane incoherent MDRC for system 1 in Table 7.1 is plotted in Figs. 7.1 and 7.2 for incidence angles of $0°$ and $40°$. When compared to the results presented in Ref. 12, both components compares favourably for both of the considered incidence angles. It is noted that in Fig. 7.2, the peak MDRC is slightly skewed towards reduced scattering angles with respect to the specular angle of $40°$. The tendency is most pronounced for the pp-component. The same effect is observed in Ref. 12.

The calculated in-plane MDRC for system 2 in Table 7.1 is plotted in Fig. 7.3 with incidence angle $4.56°$. There is good agreement between the results reported in Ref. 12

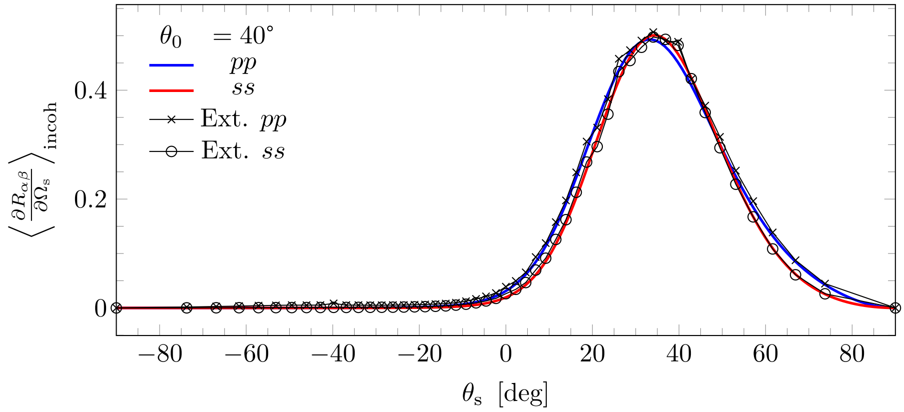

Figure 7.2: Calculated in-plane incoherent MDRC as a function of the polar scattering angle on a randomly rough silver surface, with an incidence angle of $40°$. The surface height distribution is Gaussian, with statistical parameters $\delta = 0.05\lambda$ and $a = 1.0\lambda$ taken from "system 1" of Ref. 12, which is also the origin of the "external" data sets included for comparison.

and the present calculation in terms of relative shape between the components, but the peak value deviates. The choice of incidence angle is slightly peculiar, but the MDRC is centered around the specular angle in any case. Such a small incidence angle leaves little room for a skewing of the peak that was present in Fig. 7.2 but not in Fig. 7.1.

In Fig. 7.4 the calculation for the system 2 has been given for an incidence angle of $30°$. There is no direct comparison of this case in Ref. 12, but it is included to point out the same tendency as above. The MDRC peak is skewed to a smaller angle than the specular, that being $30°$ in this case.

The calculated in-plane MDRC for system 3 in Table 7.1 is plotted in Fig. 7.5 with incidence angle $0°$. In both the pp- and ss-components the shape of the MDRC is in good agreement between the present calculation and the results reported in Ref. 12. However, again the peak amplitudes of the present implementation is less than the value reported by Ref. 12, whose solution also included a sharper peak around the origin. This is believed to be the enhanced backscattering peak, a feature which is evidently not picked up by the present perturbation theory. It was also not picked up by the perturbation theory based reconstruction performed in Ref. 12. The enhanced backscattering phenomenon is known to be the result of multiple scattering from surface waves known as surface plasmon polaritons [1, 12].

In both the cases where the present formulation reported a different MDRC from the external case, the present formulation reported a lower value. However, the differences are limited to the value of the MDRC peak, and their difference does not have a common ratio. Neither does there seem to be any pattern to where they appear. This does not point to a systemic issue. The phase perturbation calculation presented by Ref. 12 give a slightly

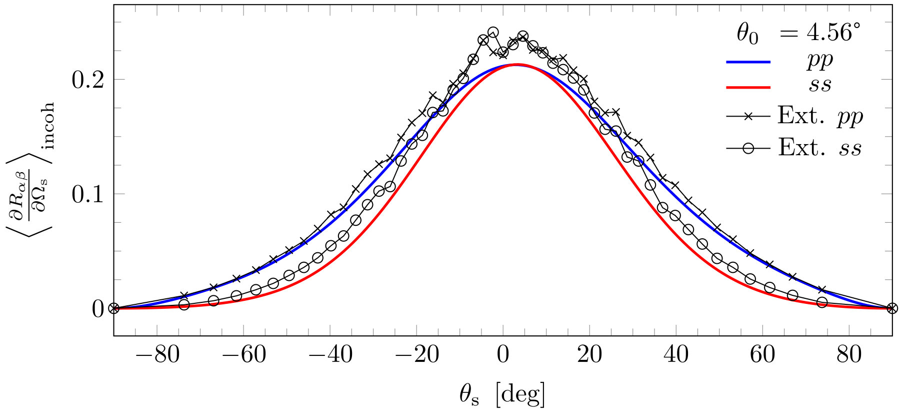

Figure 7.3: Calculated in-plane incoherent MDRC as a function of the polar scattering angle on a randomly rough silver surface, with an incidence angle of $4.56°$. The surface height distribution is Gaussian, with statistical parameters $\delta = 0.05\lambda$ and $a = 0.5\lambda$ taken from "system 2" of Ref. 12, which is also the origin of the "external" data sets included for comparison.

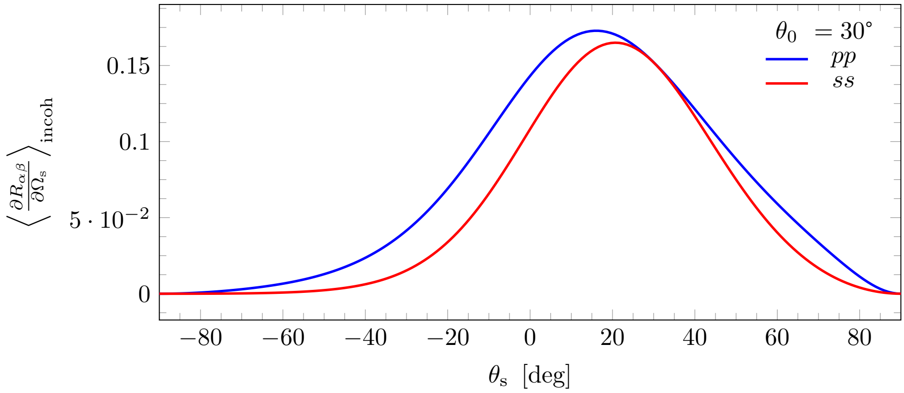

Figure 7.4: Calculated in-plane incoherent MDRC as a function of the polar scattering angle on a randomly rough silver surface, with an incidence angle of 30°. The surface height distribution is Gaussian, with statistical parameters $\delta = 0.05\lambda$ and $a = 0.5\lambda$ taken from "system 2" of Ref. 12.

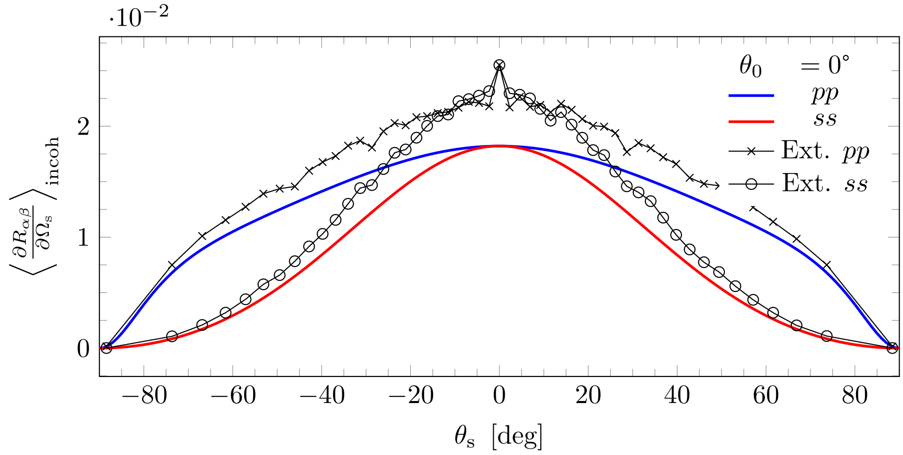

Figure 7.5: Calculated in-plane incoherent MDRC as a function of the polar scattering angle on a randomly rough silver surface, with an incidence angle of 0°. The surface height distribution is Gaussian, with statistical parameters $\delta = 0.025\lambda$ and $a = 0.25\lambda$ taken from ”system 3” of Ref. 12, which is also the origin of the ”external” data sets included for comparison.

better agreement. However, the formulations of the phase perturbation theories are not the same, so the difference may well be explained by varying reliance on the 2-2 and 1-3 terms in the two formulations, as discussed in Sec. 5.3. The indication is that the present formulation and/or implementation is inadequate to calculate the incoherent MDRC as accurately as the non-perturbative calculation.

The shift in the form of the incoherent MDRC from systems 1 and 2 to system 3, exhibits some of the physical intuitions about rough surface scattering. The rms-roughness δ in system 3 is halved compared to systems 1 and 2. This explains why the amplitude of the MDRC in Fig. 7.5 is much smaller than in Figs. 7.1–7.4; the surface more closely resembles a flat one, and a smaller fraction of the light is scattered incoherently as opposed to coherently. Also, the angular range of the pp-component of the MDRC in Fig. 7.5 is much larger than in the others. This might be due to the lower surface correlation length, a, and therefore larger rms slope of system 3 making the surface spatial wavelength closer to the light wavelength; which increase the possible interactions in different angles.

7.2 Comparison with experimental systems

A phase perturbation theory calculation was presented along experimentally gathered MDRC in Ref. 15. In this section we compare the results with the present implementation. Some (but not all) of the experimental data was available, and has been presented along corresponding plots of the calculated incoherent MDRC in Sec. 7.2.2. The experimental data is

Table 7.2: Statistical parameters of the experimental test systems from Ref. 15.

System	λ[µm]	$\varepsilon(\omega)$	δ/λ	a/λ	δ/a
0061	10.6	$-2489.77 + i2817.36$	0.047 ± 0.001	1.79 ± 0.160	0.026
5122	10.6	$-2489.77 + i2817.36$	0.040 ± 0.001	0.198 ± 0.019	0.20
7047	10.6	$-2489.77 + i2817.36$	0.151 ± 0.005	0.896 ± 0.123	0.17
8053	10.6	$-2489.77 + i2817.36$	0.071 ± 0.004	0.283 ± 0.160	0.25
9032	10.6	$-2489.77 + i2817.36$	0.071 ± 0.004	0.708 ± 0.066	0.10

the work of the authors of Ref. 15.

7.2.1 Presentation of the systems

The scattering parameters are given in Table 7.2. All the systems considered have the same wavelength originating from a CO_2 laser, and dielectric function originating from a gold substrate at the given wavelength. The naming scheme for the samples is also taken from Ref. 15, and the reasoning behind the names is not explained.

7.2.2 Presentation of the calculated MDRC

Sample 0061

Only plots for samples 0061, 7047 and 8053 have been included in Ref. 15. Here, we present the calculated MDRC for all the samples in Table 7.2, to point out their interesting features. Ordering them numerically, the first considered sample is 0061. Its calculated in-plane MDRC and corresponding available experimental data is plotted in Figs. 7.6–7.9 for incidence angles of $5°$, $15°$, $30°$ and $50°$, respectively. Note that in Fig. 7.9 only the pp-component is shown, to match the experimental data provided in Fig. 11 in Ref. 15. For the present calculations, the MDRC of the ss-component is indistinguishable from the pp, so the distinction hardly matters for the sake of comparison.

For the cases of $5°$ and $15°$ incidence, shown in Figs. 7.6 and 7.7, there is strong agreement between the presently calculated MDRC and both the phase-perturbative and experimental MDRC of Ref. 15, if one disregards the missing experimental MDRC in the region that is obscured by the light source.

For the case of $30°$ incidence in sample 0061, there is fair agreement between all calculations and experiments for the ss-component. However, the peak value of the pp-component of the MDRC in Fig. 7.8 is slightly lower than the phase perturbation theory in Ref. 15 reports. It remains impossible to discern the exact experimental value of the MDRC at the peak, given that the peak is close to the specular direction where the detector may become saturated. Neither the MDRC from the present calculation or the phase perturbation theory of Ref. 15 is obviously correct or incorrect near the specular direction, while both coincide well with the experimental values away from the specular direction. The fact that the experimental values for the pp-component has its specular peak (where

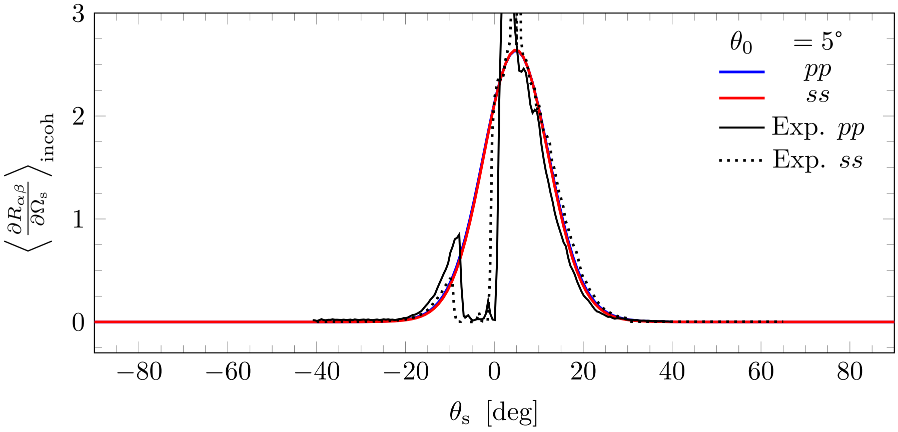

Figure 7.6: Calculated and experimental in-plane incoherent MDRC as a function of the polar scattering angle on a randomly rough gold surface, with an incidence angle of $5°$. The surface height distribution is Gaussian, with statistical parameters $\delta = 0.047\lambda$ and $a = 1.79\lambda$ and the corresponding experimental data all taken from "sample 0061" of Ref. 15.

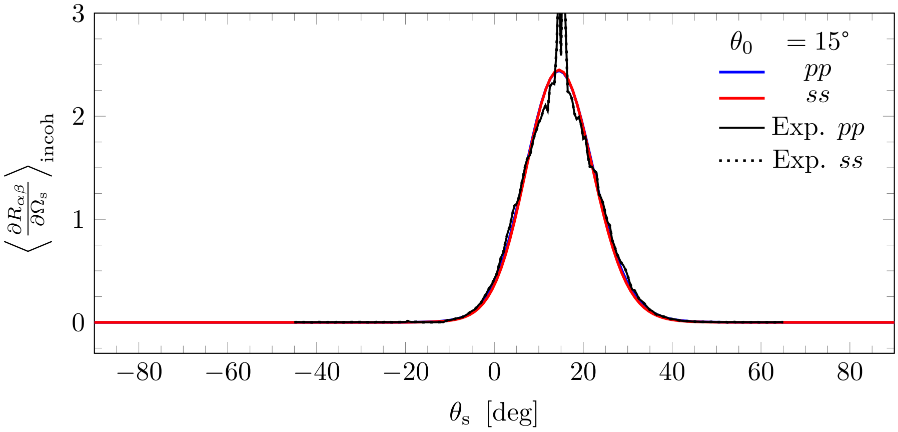

Figure 7.7: Calculated and experimental in-plane incoherent MDRC as a function of the polar scattering angle on a randomly rough gold surface, with an incidence angle of $15°$. The surface height distribution is Gaussian, with statistical parameters $\delta = 0.047\lambda$ and $a = 1.79\lambda$ and the corresponding experimental data all taken from "sample 0061" of Ref. 15.

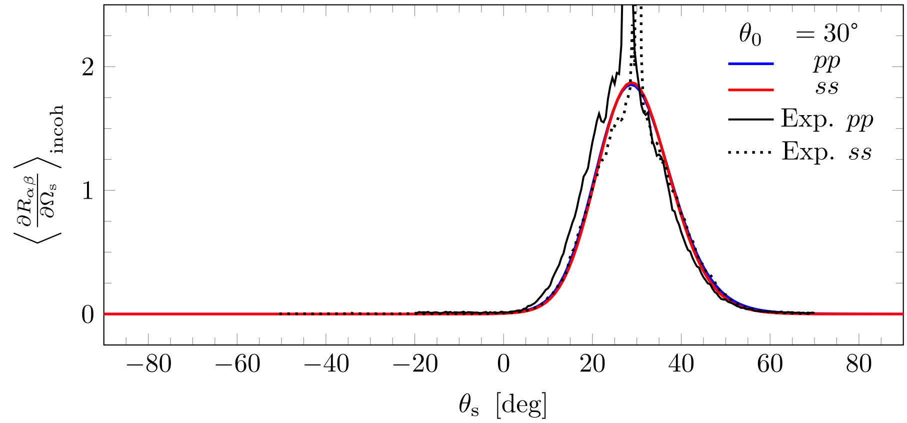

Figure 7.8: Calculated and experimental in-plane incoherent MDRC as a function of the polar scattering angle on a randomly rough gold surface, with an incidence angle of 30°. The surface height distribution is Gaussian, with statistical parameters $\delta = 0.047\lambda$ and $a = 1.79\lambda$ and the corresponding experimental data all taken from ”sample 0061” of Ref. 15.

also coherently scattered light contribute to the measured MDRC) at a scattering angle slightly lower than $30°$, suggests a small misalignment in the experiment or the corresponding dataset. Translating the experimental pp-component to have its peak at 30° gives even better alignment with calculated values.

The pp-component of the calculated incoherent MDRC in the case of $50°$ incidence is shown in Fig. 7.9, but the corresponding experimental data was not available for direct comparison. There is however excellent agreement between the two phase perturbation calculations, and good fit with experimental data from Fig. 11 in Ref. 15 away from the specular direction. Near the specular direction the measured MDRC is large, while in an intermediate region near the specular direction it fluctuates somewhat above the phase perturbation. The manner of the fluctuation does not suggest the discrepancy to be caused by detector saturation near the specular direction.

A feature obviously present in Fig. 7.9, and less obviously in Fig. 7.8, is the skewing of the incoherent MDRC peak to smaller scattering angles than the specular angle. This feature was also seen in the purely numeric examples shown in Figs. 7.2 and 7.4.

Sample 7047

The incoherent MDRC from sample 7047 is shown in Figs. 7.10–7.12, for incidence angles of $5°$, $30°$ and $60°$, respectively. For the case of $5°$ incidence, there is good agreement in the amplitude and position of the MDRC peak between the phase perturbation theories. However, the phase perturbation theory in Ref. 15 slightly undershoots the experimental MDRC for scattering angles below the specular angle for the ss-component, and above

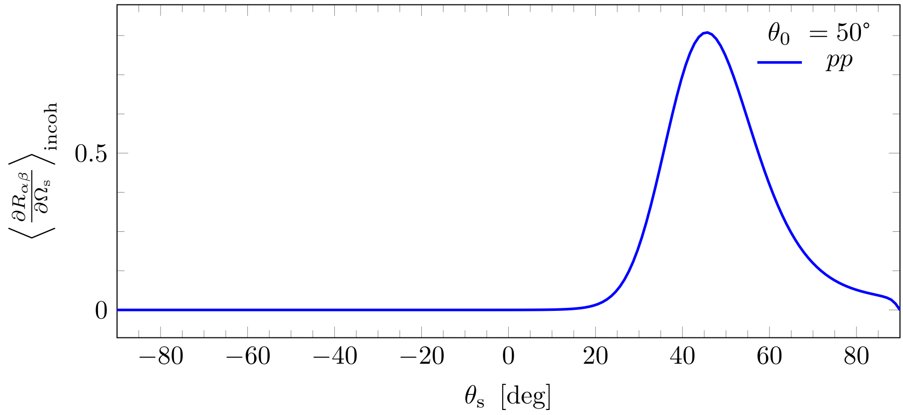

Figure 7.9: Calculated in-plane incoherent MDRC as a function of the polar scattering angle on a randomly rough gold surface, with an incidence angle of $50°$. The surface height distribution is Gaussian, with statistical parameters $\delta = 0.047\lambda$ and $a = 1.79\lambda$ taken from "sample 0061" of Ref. 15.

the specular angle for the pp-component. In the present implementation, the MDRC of which being shown in Fig. 7.10, the ss-component seems to compare well to the phase perturbation theory of Ref. 15. The MDRC of the present pp-component is noticeably wider than the corresponding phase perturbation calculation, and it seems to compare slightly more favourably with the experimental data.

For instance, by noting the scattering angles where the incoherent MDRC takes on the value 0.25, we report that the present implementations claim of $\theta_s = 47°$ is closer to the experimental value of $\theta_s = 45°$ than the phase perturbation theory of Ref. 15 which claims $\theta_s = 38°$. On the other side of the specular direction, the present implementation takes on the MDRC value of 0.25 at $\theta_s = -37°$, which is slightly lower than the experimental value of $\theta_s = -35°$ and the phase perturbation theory by Ref. 15 of $\theta_s = -32°$. This is one of the considered examples that most clearly favour the current implementation.

The calculated MDRC of sample 7047 with $30°$ incidence is given in Fig. 7.11. There is good agreement between the ss-components. The pp-components have good agreement in their peak values and placements, and their shapes for scattering angles smaller than the specular. However, the shape of the pp-component near $90°$ scattering angle in Fig. 7.11 is distorted compared to the experimental and phase perturbative results given by Ref. 15. The reason for this behaviour we are currently not able to explain, however we may suggest that the larger values of $q_{||}$ at large scattering angles gives more frequent oscillation in Eq. (5.33) as per the discussion in Sec. 6.4. It may be a contributing factor, but is unlikely to entirely account for all the observed difference.

For the case of $60°$ there is excellent agreement between the ss-component of MDRC between the phase perturbation theories shown in Fig. 7.12 and Ref. 15. Neither repli-

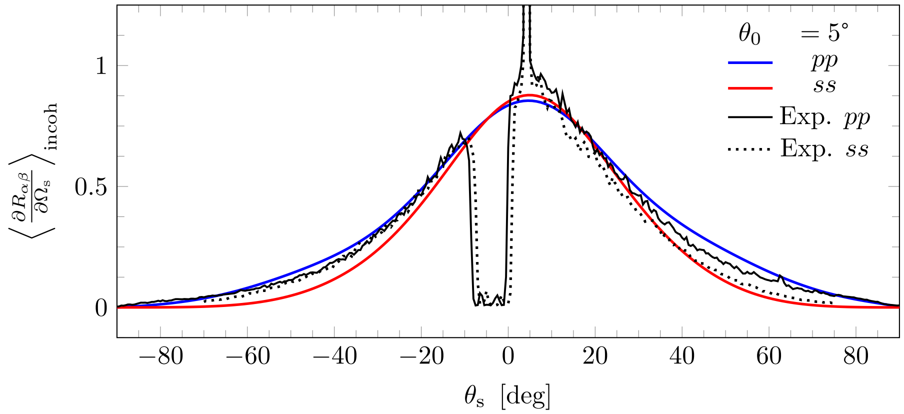

Figure 7.10: Calculated and experimental in-plane incoherent MDRC as a function of the polar scattering angle on a randomly rough gold surface, with an incidence angle of 5°. The surface height distribution is Gaussian, with statistical parameters $\delta = 0.151\lambda$ and $a = 0.896\lambda$ and the corresponding experimental data all taken from "sample 7047" of Ref. 15.

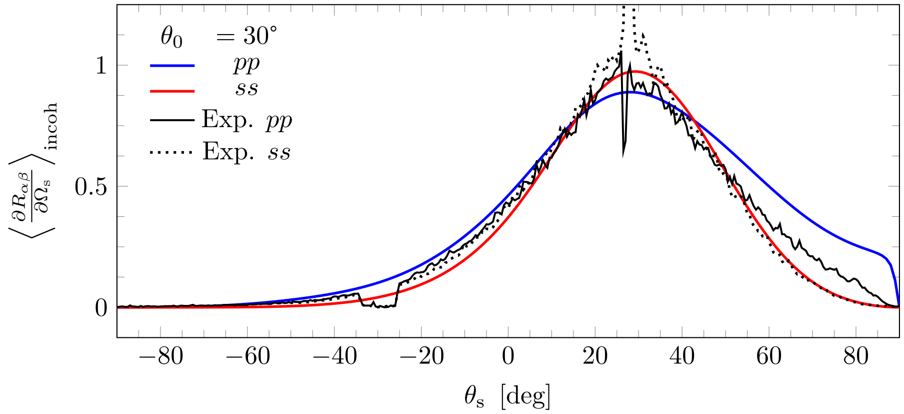

Figure 7.11: Calculated and experimental in-plane incoherent MDRC as a function of the polar scattering angle on a randomly rough gold surface, with an incidence angle of 30°. The surface height distribution is Gaussian, with statistical parameters $\delta = 0.151\lambda$ and $a = 0.896\lambda$ and the corresponding experimental data all taken from "sample 7047" of Ref. 15.

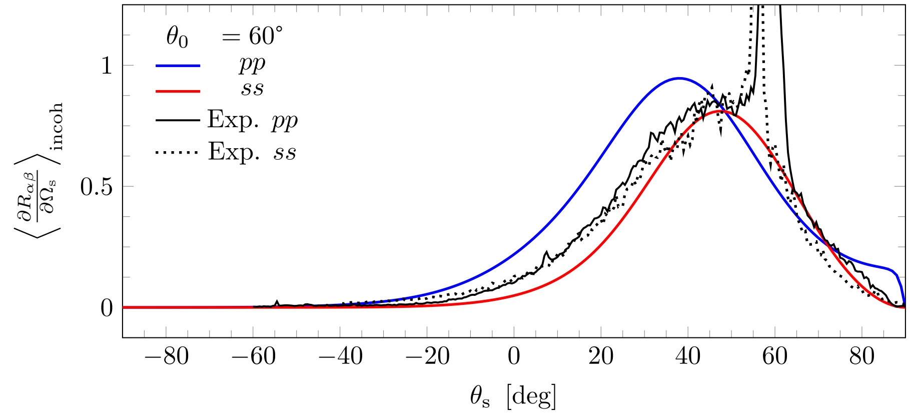

Figure 7.12: Calculated and experimental in-plane incoherent MDRC as a function of the polar scattering angle on a randomly rough gold surface, with an incidence angle of 60°. The surface height distribution is Gaussian, with statistical parameters $\delta = 0.151\lambda$ and $a = 0.896\lambda$ and the corresponding experimental data all taken from ”sample 7047” of Ref. 15.

cate the experimental data exactly in and around the region of $30°$ scattering angle. The present calculation of the pp-component shows fairly good agreement for scattering angles smaller than about $30°$, but overestimates the MDRC for larger angles compared to the phase perturbation theory and experimental data of Ref. 15. Although the values are different, the overall shape is maintained. It is uncertain whether the experimental data set for the ss-component in Fig. 7.12 is indeed taken at $60°$ incidence, as the specular peak of the experimental data is displaced with respect to this value. Internally, this dataset was labelled as being taken at $50°$ incidence, but at the same time presents itself as being the experimental data belonging to Fig. 8 of Ref. 15. Therefore, the labelling of the experimental ss-component results may be insincere. However, their inclusion still gives a good indication of the presumed correct result, and is a good basis for comparison.

The tendency for the pp-component to approach a non-zero value as the scattering angle approaches $90°$ is present in both implementations of the phase perturbation theory. In Figs. 7.11 and 7.12 it is far more pronounced than in their counterparts in Ref. 15. The present implementation seems to overestimate the MDRC for large scattering angles in this sample. It might be interesting to note, then, that sample 7047 has the largest rms-roughness parameter δ of all the studied samples, by a wide margin. While it does not have the most severe roughness to correlation length ratio (which is proportional to the rms slope), it may indeed be influenced by the present implementation depending on δ and a individually, and not just as a ratio.

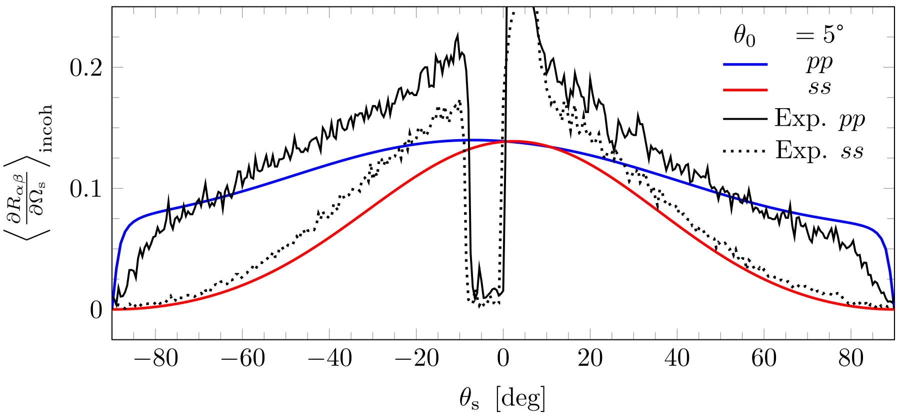

Figure 7.13: Calculated and experimental in-plane incoherent MDRC as a function of the polar scattering angle on a randomly rough gold surface, with an incidence angle of 5°. The surface height distribution is Gaussian, with statistical parameters $\delta = 0.071\lambda$ and $a = 0.283\lambda$ and the corresponding experimental data all taken from ”sample 8053” of Ref. 15.

Sample 8053

The incoherent MDRC calculated from sample 8053 is shown in Figs. 7.13–7.15, along with corresponding experimental data. This is the sample with the highest roughness to correlation length ratio, which presents the fiercest challenge to our underlying assumptions out of all the samples considered. This fact is also shown in that the incoherent MDRC spread out across a wider range of scattering angles than in the previous samples. Like with the other samples, there is very good agreement between the ss-components of the two phase perturbation theories in all the considered angles of incidence, however they underestimate the experimental value slightly near the specular direction. For the pp-component of Fig. 7.13 the peaks value of the MDRC is lower than both the experimental and phase-perturbative values reported in Ref. 15 by about 25%, and the form of the MDRC looks more like what was calculated with the Kirchhoff approximation. The shape and values of the MDRC close to the edges of the plot of Fig. 7.13 is a closer match between the phase perturbation theories and the experimental data. The authors of Ref. 15 propose that the sharp drop-off of the pp-component near the edges is due to the existence of surface plasmon polaritons. This feature seems to be somewhat captured by the phase perturbation theory, but its value near the origin is inadequate.

In Figs. 7.14 and 7.15 the underestimation is less severe, and the experimental values seem to lie somewhere in-between the peaks of the MDRC of the present theory and the phase perturbation theory of Ref. 15. Also in Figs. 7.14 and 7.15 the MDRC peak of the pp-component is slightly more backwards skewed than the phase perturbation theory in Ref. 15, approaching the backscattering angle; the angle where the reflected wave

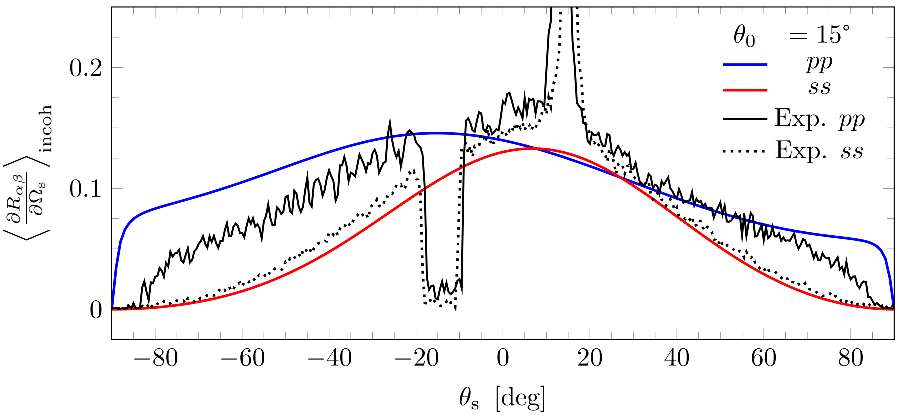

Figure 7.14: Calculated and experimental in-plane incoherent MDRC as a function of the polar scattering angle on a randomly rough gold surface, with an incidence angle of 15°. The surface height distribution is Gaussian, with statistical parameters $\delta = 0.071\lambda$ and $a = 0.283\lambda$ and the corresponding experimental data all taken from ”sample 8053” of Ref. 15.

vector is antiparallel to the incoming wave vector. It is unclear whether or not this is a departure from the experimental values, as the backscattering direction is obscured by the light source and is not conducive to producing accurate scattering data. There calculated pp-component in Fig. 7.15 dips below the experimental significantly around the specular direction, but it remains difficult to know how much the experimental values are influenced by the coherently scattered MDRC near the specular direction. However, at least the general shape of the MDRC is a much better fit at this incidence angle for the remaining scattering directions.

The pp-component does not approach zero close to $\pm 90°$ scattering angle in Figs. 7.13–7.15, but instead it seems to approach the value of 0.07, which is replicated by the phase perturbation theory of Ref. 15. The experimental data also show this tendency, but measurements are practically difficult to measure at extreme angles so we are careful to not conclude too much from it.

Samples 5122 and 9032

Sample 5122 was not considered in detail in Ref. 15, but its calculated in-plane MDRC is plotted in Figs. 7.16–7.18. The system has a rms-roughness to correlation length ratio that lies between samples 7047 and 8053, however the absolute size of its topographic features is much smaller than either of those samples. This explains that the range of relevant scattering angles is wide, especially for the pp-component, but also that the absolute magnitude of the incoherent MDRC is far smaller. Otherwise, the general form of the MDRC shows many similarities to sample 8053.

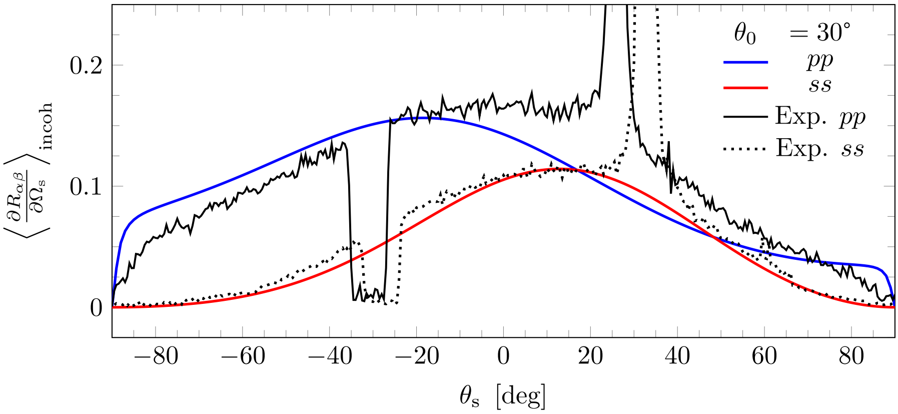

Figure 7.15: Calculated and experimental in-plane incoherent MDRC as a function of the polar scattering angle on a randomly rough gold surface, with an incidence angle of 30°. The surface height distribution is Gaussian, with statistical parameters $\delta = 0.071\lambda$ and $a = 0.283\lambda$ and the corresponding experimental data all taken from "sample 8053" of Ref. 15.

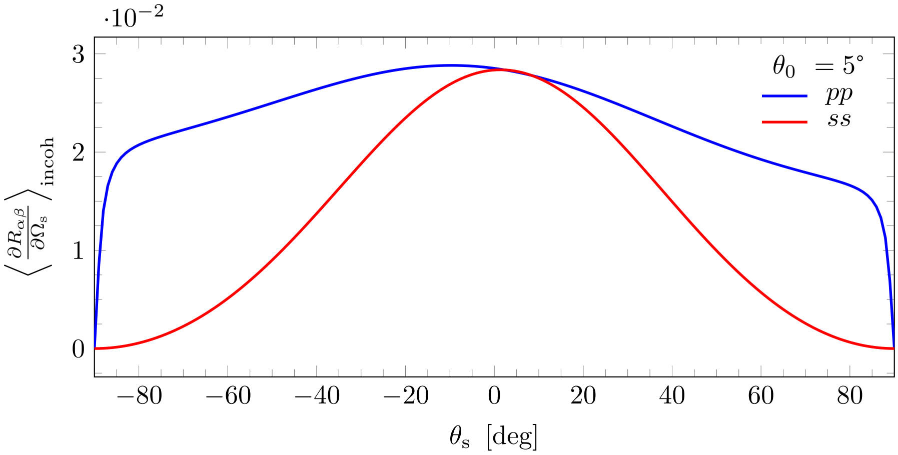

Figure 7.16: Calculated in-plane incoherent MDRC as a function of the polar scattering angle on a randomly rough gold surface, with an incidence angle of 5°. The surface height distribution is Gaussian, with statistical parameters $\delta = 0.040\lambda$ and $a = 0.198\lambda$ taken from "sample 5122" of Ref. 15.

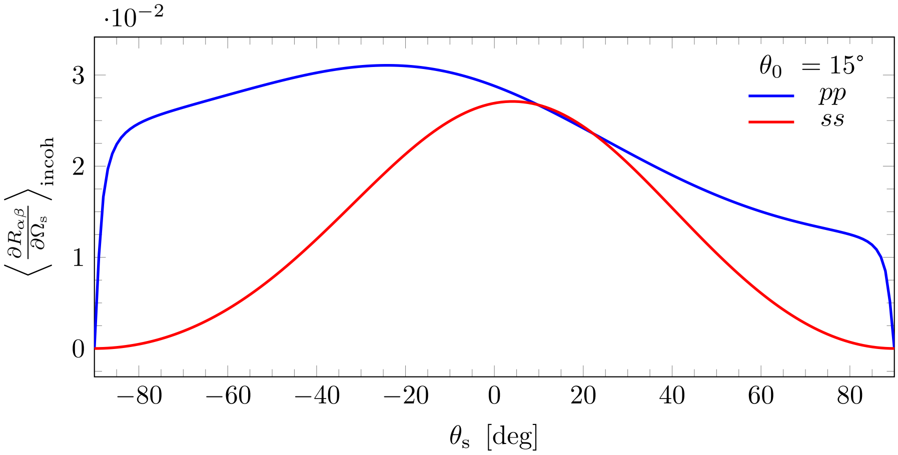

Figure 7.17: Calculated in-plane incoherent MDRC as a function of the polar scattering angle on a randomly rough gold surface, with an incidence angle of $15°$. The surface height distribution is Gaussian, with statistical parameters $\delta = 0.040\lambda$ and $a = 0.198\lambda$ taken from ”sample 5122” of Ref. 15.

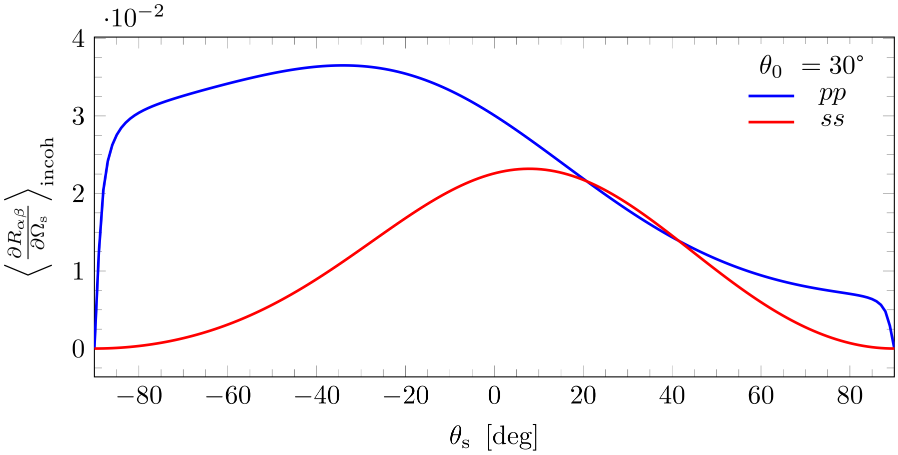

Figure 7.18: Calculated in-plane incoherent MDRC as a function of the polar scattering angle on a randomly rough gold surface, with an incidence angle of $30°$. The surface height distribution is Gaussian, with statistical parameters $\delta = 0.040\lambda$ and $a = 0.198\lambda$ taken from ”sample 5122” of Ref. 15.

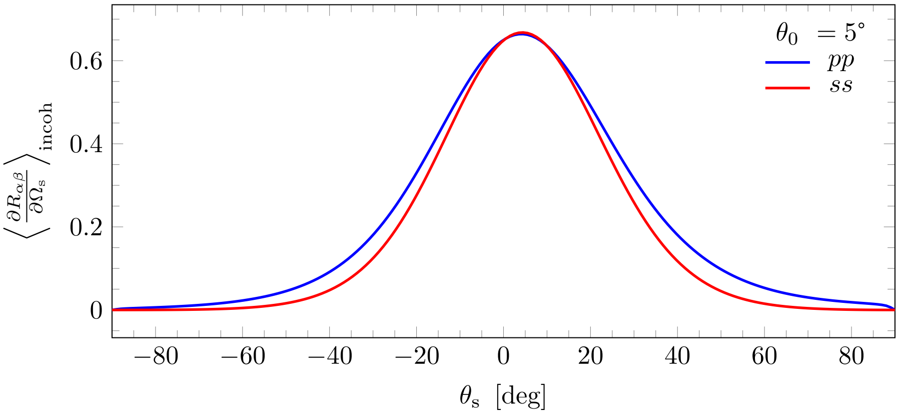

Figure 7.19: Calculated in-plane incoherent MDRC as a function of the scattering angle on a randomly rough gold surface, with an incidence angle of 5°. The surface height distribution is Gaussian, with statistical parameters $\delta = 0.071\lambda$ and $a = 0.708\lambda$ taken from "sample 9032" of Ref. 15.

Finally, we consider sample 9032 from Table 7.2 which also was not considered in detail in Ref. 15. Plots of the calculated in-plane incoherent MDRC is shown in Figs. 7.19–7.21. System 9032 has the same rms-roughness as system 8053, but much greater correlation length. As might be expected, the MDRC of system 9032 looks quite like system 7047 shape-wise, as it is the system with the most comparable rms-roughness to correlation length ratio. However, it is slightly lower than system 7047 and the absolute roughness is smaller too, which explains the comparatively reduced incoherent MDRC amplitude.

7.3 Off-diagonal calculation and comparison

We perform the out-of-plane calculation for the systems presented in Ref. 16, which solves the Reduced Rayleigh equation in a non-perturbative way. This was also performed in Ref. 60 on surfaces that were so rough that perturbation theory cannot be expected to be correct. Similar systems was also considered by Ref. 61 for an "inverse" case of a medium-to-vacuum interface, or a layered dielectric system in Ref. 62. We also perform a calculation for the sample 0061 from Ref. 15. The statistical parameters of the scattering situations adapted from Ref. 16 are presented in Table 7.3.

System 1

The out-of-plane incoherent MDRC calculation with phase perturbation theory for system 1 from Table 7.3 is shown in Figs. 7.22 and 7.23 for 0° and 67° incidence, respectively.

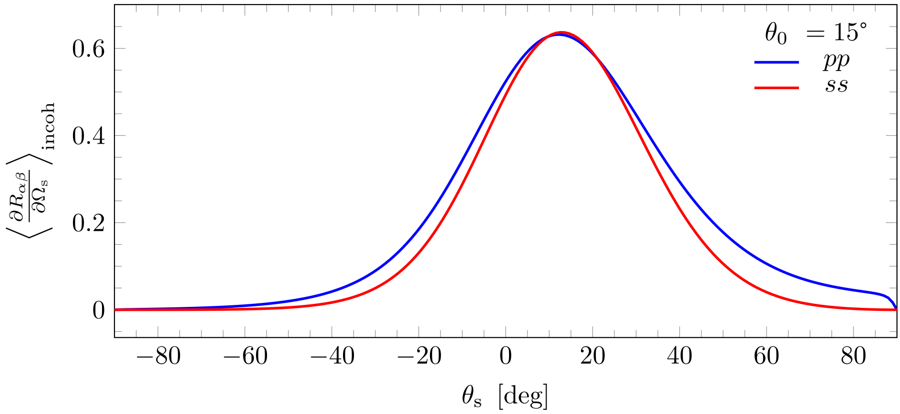

Figure 7.20: Calculated in-plane incoherent MDRC as a function of the polar scattering angle on a randomly rough gold surface, with an incidence angle of $15°$. The surface height distribution is Gaussian, with statistical parameters $\delta = 0.071\lambda$ and $a = 0.708\lambda$ taken from ”sample 9032” of Ref. 15.

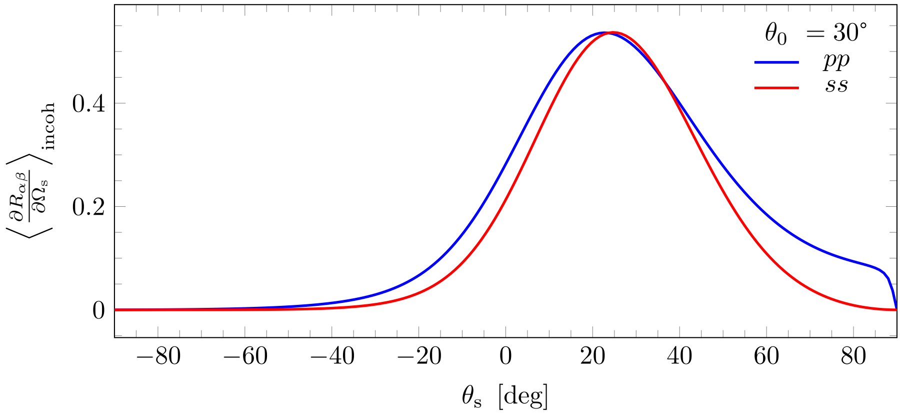

Figure 7.21: Calculated in-plane incoherent MDRC as a function of the polar scattering angle on a randomly rough gold surface, with an incidence angle of $30°$. The surface height distribution is Gaussian, with statistical parameters $\delta = 0.071\lambda$ and $a = 0.708\lambda$ taken from ”sample 9032” of Ref. 15.

Table 7.3: Statistical parameters of some of the off-diagonal test systems which are taken from Ref. 16. Another scattering sample used for off-diagonal calculation was sample 0061 from Table 7.2 and Ref. 15.

System	$\lambda[1]$	$\varepsilon(\omega)$	δ/λ	a/λ	δ/a
1	1	2.64	0.025	0.25	0.10
2	1	2.64	0.050	0.25	0.20

The incidence direction is defined by a zero degree incident azimuthal angle ϕ_0, meaning the plane of incidence is parallel to the q_1-axis. The result compares well to the result presented in Ref. 16 whose calculations solved the reduced Rayleigh equation directly, and echoes the fact that the amplitude of the s-component outweighs the p-component in the case of $67°$ incidence. The value of the MDRC at the point $(0, 0)$ in Figs. 7.22 and 7.23 is not well-defined, and seem to approach different values from different directions. The plots indicate that the in-plane MDRC has a local minimum there, which it does not. The value is a compromise of the colour gradient being interpolated by adjacent evaluation points. Here, as well as in the in-plane calculations, the MDRC at the origin is not evaluated explicitly. The scale of the interpolated MDRC value around the origin is slightly exaggerated due to the resolution of interpolation points being lower than ideal around this region. A refined distribution of calculation points should crowd the region around the origin more than was done in the calculations that produced Figs. 7.22, 7.23, 7.26, 7.27, 7.30 and 7.31.

The result of the contour plot in Fig. 7.22 is visually striking from the onset. A dipole-like pattern is produced, which is oriented along the plane of incidence for the co-polarised components, and perpendicular to the plane of incidence for the cross-polarised components. One explanation for this is that amplitude of the incoherent MDRC of modestly rough surfaces is dominated by single scattering, which describes light that has interacted exactly once with the surface. In the case of single scattering, the reflection of any one incoming wave vector is well approximated by specular scattering from the tangent plane at the specific interaction point of the surface profile function. But then, the reflected amplitude is subject to the regular Fresnel coefficients for the tangent plane interface, whose cross-polarised components are known to be zero. The Fresnel coefficients for co-polarised scattering is different from zero, and these factors explain the shape of the incoherent MDRC in Fig. 7.22 along the scattering plane. For the completely out-of-plane scattering wave vectors along the q_2-axis, the plane that defines the scattered polarisation components has been rotated $90°$ which corresponds to the p- and s-components being mutually relabelled. This fact may be understood by imagining the appearance of Fig. 3.1 with the depicted planes having an intermediate angle of $90°$. The previous argument, using the tangent plane Fresnel coefficients, explains the shape of the incoherent MDRC along the q_2-axis as well. The completely out-of-plane contribution to the sp-component of Fig. 7.22 is being calculated using the tangent plane Fresnel coefficients for p-polarised light, and vice versa. Any other point in Fig. 7.22 is a linear combination of tangent plane Fresnel coefficients, with liner coefficients proportional to the distance from the respective

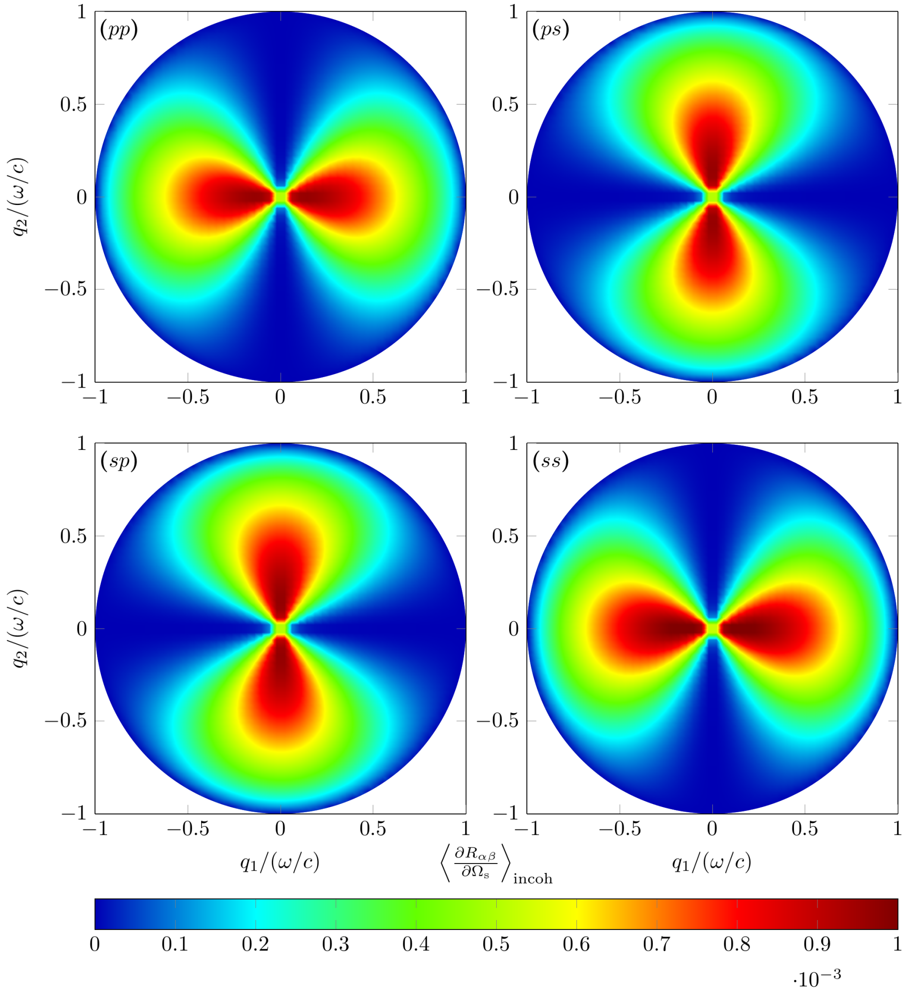

Figure 7.22: Calculated incoherent MDRC as a function of both parallel components of the scattering wave vector, after light scattering from a randomly rough dielectric surface at incidence angles $\theta_0 = 0°$ and $\phi_0 = 0°$. The surface height distribution is Gaussian, with statistical parameters $\delta = 0.025\lambda$ and $a = 0.25\lambda$ taken from Ref. 16 and system 1 in Table 7.3.

axes. This gives a good explanation for how the gradual slope of the incoherent MDRC.

The dipole-like pattern of the incoherent MDRC remains with non-normal incidence, as seen in Fig. 7.23, but the shape is comparatively elongated along the plane of incidence, and the amplitude is reduced. The pp-component is weaker than the ss-component near the specular direction, and this may be explained by the dielectric constant which is used to calculate Figs. 7.22 and 7.23. The dielectric constant $\varepsilon = 2.64$ is close to the value for glass, which is 2.25. Glass is known to have a Brewster angle of $56°$, at which no p-polarised light is reflected. The larger dielectric constant gives a slightly increased Brewster angle, which makes it close to the incident polar angle of $\theta_0 = 67°$ used to calculate the incoherent MDRC in Fig. 7.23. Because of the modest roughness, most tangent planes give reflection near the specular direction, the pp-component of which is suppressed. This explains why the amplitude of the ss-component is larger than the pp-component in the right half-plane of Fig. 7.23, but not why the amplitude of the pp-component is the largest in the left half-plane. The presence of incoherent MDRC completely out-of-plane in the pp-component of Fig. 7.23, is due to the incident angle providing some p-polarised component in the would-be p-direction out-of-plane. The remaining features of the incoherent MDRC can largely be explained by the various combinations of p- and s-components determining the Fresnel coefficients of various tangent planes. But this does not account for everything, as we recall the phase perturbation theory is of second order and includes some (presumed weak) second order contributions which are not explainable by such simple means.

The value of the incoherent MDRC at the origin is remedied by the results of Figs. 7.24 and 7.25. These figures show the calculated incoherent MDRC without polarisation sensitivity in the scattered waves after incoming p-polarised $(p \to *)$ and s-polarised $(s \to *)$ light onto system 1 from Table 7.3. They also show the calculated incoherent MDRC with the incoming light being unpolarised, and the scattered light being p-polarised $(\circ \to p)$ and s-polarised $(\circ \to s)$, for respective incidence angles of $0°$ and $67°$. The notation $*$ means that the polarisation is not recorded, and is therefore obtained by a direct (unscaled) sum of the p- and s-components. Note that this does not mean that the scattered wave is unpolarised. In certain directions it is more p-polarised than s-polarised and the ratio of these polarisations can vary strongly with the scattering direction. The notation $\circ$ on the other hand, represents unpolarised light which is an *equally weighted* linear combination of the p- and s-components. Therefore, the amplitude of the plots containing $\circ$ is only half of the ones containing $*$. We will refer to the collective of these types of plots as being polarisation-ignorant.

The plots in Figs. 7.24 and 7.25 are obtained by adding the pp- and sp-components of Figs. 7.22 and 7.23 to get $(p \to *)$, the ps- and ss-components to get $(s \to *)$, the pp- and ps-components to get $(\circ \to p)$ and the sp- and ss-components to get $(\circ \to s)$. If we wish to obtain the polarisation-ignorant incoherent MDRC-distribution for unpolarised incident light, we calculate the arithmetic average of the $(p \to *)$ and $(s \to *)$ components. The same general remarks for how Figs. 7.24 and 7.25 is constructed, also holds for Figs. 7.28, 7.29, 7.32 and 7.33.

If one considered the incoherent MDRC without polarisation sensitivity, the $(p \to *)$

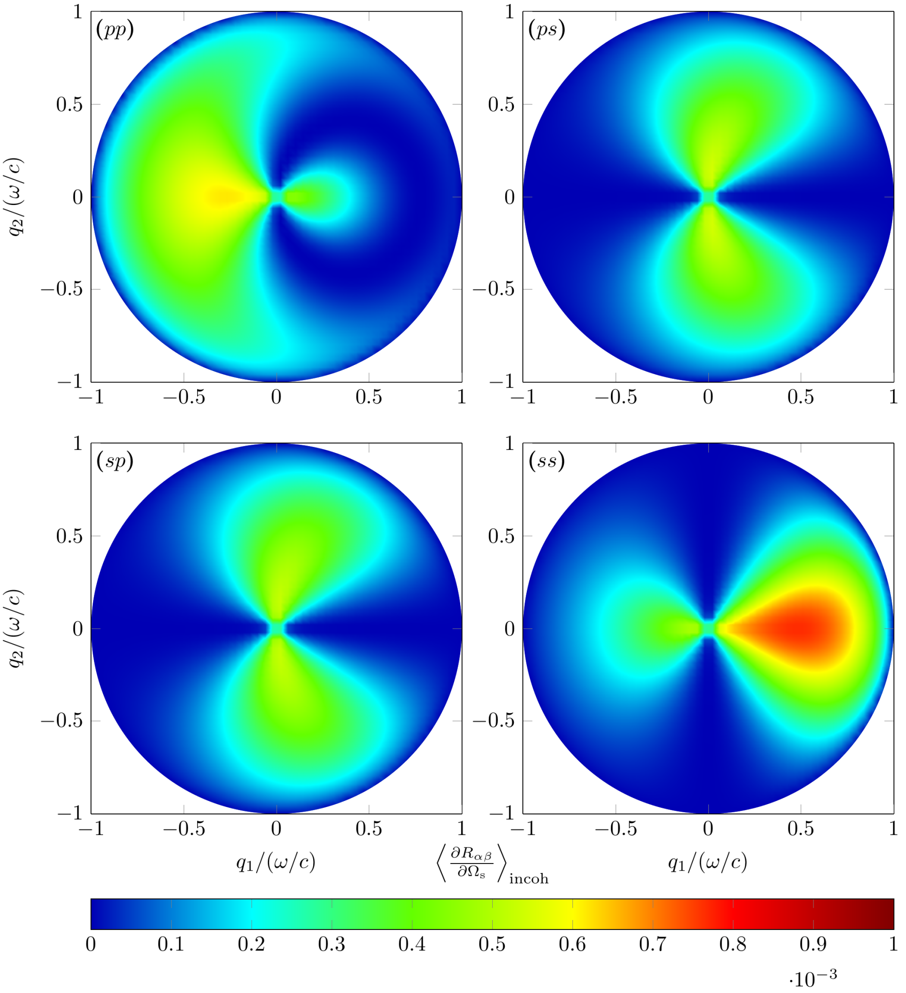

Figure 7.23: Calculated incoherent MDRC as a function of both parallel components of the scattering wave vector, after light scattering from a randomly rough dielectric surface at incidence angles $\theta_0 = 67^\circ$ and $\phi_0 = 0^\circ$. The surface height distribution is Gaussian, with statistical parameters $\delta = 0.025\lambda$ and $a = 0.25\lambda$ taken from Ref. 16 and system 1 in Table 7.3.

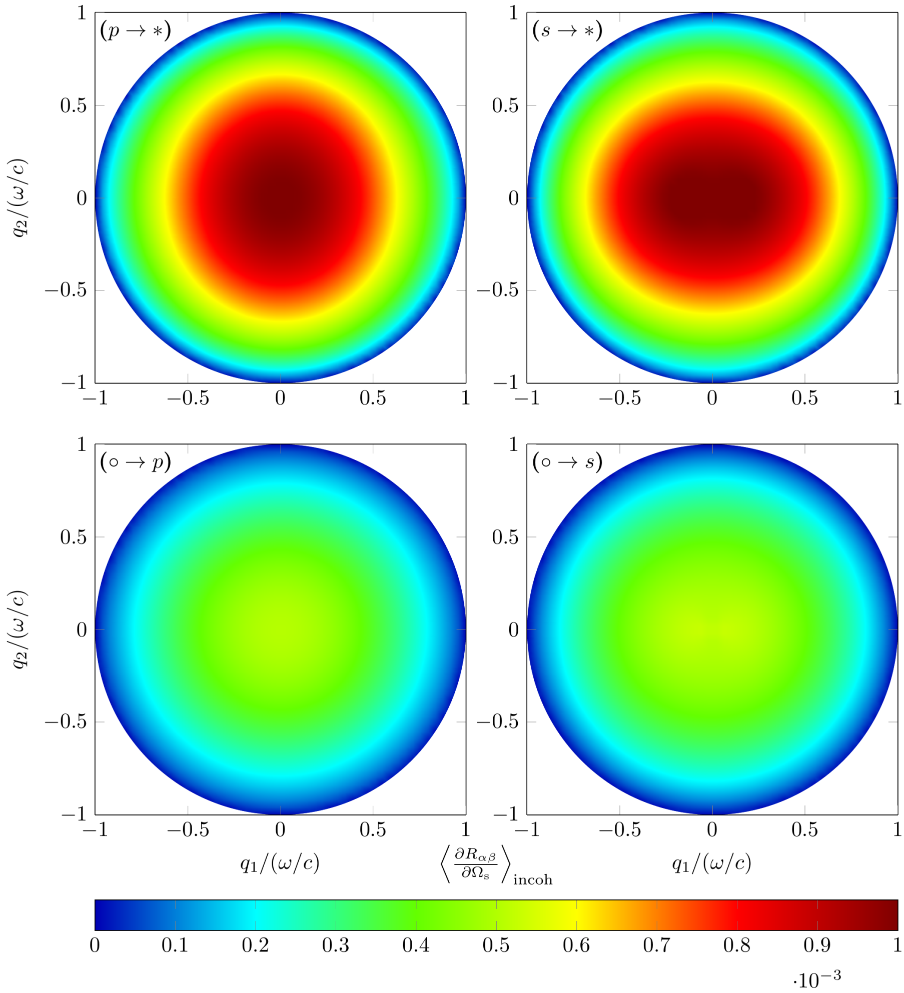

Figure 7.24: The polarisation-ignorant components of the calculated incoherent MDRC as a function of both parallel components of the scattering wave vector, after light scattering from a randomly rough dielectric surface at incidence angles $\theta_0 = 0°$ and $\phi_0 = 0°$. The surface height distribution is Gaussian, with statistical parameters $\delta = 0.025\lambda$ and $a = 0.25\lambda$ taken from Ref. 16 and system 1 in Table 7.3. The notation $*$ refers to the sum of p- and s-polarised light, and $\circ$ refers to unpolarised light which is a normalised sum of the p- and s-components.

and $(s \to *)$ components of Fig. 7.24 suggest that the MDRC nearly has circular symmetry. Similarly, if the wave source provides unpolarised incident light, the resulting p- and s-components of the incoherent MDRC appear to be more or less equal. The intricate dependence on the incoming polarisation is not picked up in these cases. The discrepancy between Fig. 7.24 and Fig. 7.22 or between Fig. 7.25 and Fig. 7.23 explains the need for polarisation sensitive detection systems in experimental measurements. Otherwise, the intricate nature of the MDRC may not be found.

The shapes and overall features of Figs. 7.24 and 7.25 also compares well to the corresponding figures of the same system presented in Ref. 16. As with Figs. 7.22 and 7.23, the overall correspondence contributes to verification of the present implementation.

System 2

For system 2 from Table 7.3, the rms-roughness is doubled compared to system 1. The calculated out-of-plane MDRC for this system is shown in Figs. 7.26 and 7.27 for $0°$ and $67°$ incidence, respectively. Especially note that the colour bar is scaled differently from Figs. 7.22 and 7.23, and the maximum recorded amplitude is approximately four times greater in Fig. 7.26. The increase in amplitude of the incoherent MDRC is not surprising, as the deviation from surface flatness is greater. Otherwise, the shape and features of the incoherent MDRC is predictably similar to system 1, with the only notable difference being that the magnitude of the ss-component of Fig. 7.26 slightly dominates the other components, even for normal incidence.

As with system 1, the polarisation-ignorant incoherent MDRC for this system are given in Figs. 7.28 and 7.29. They mainly differ from Figs. 7.24 and 7.25 in the fact that their overall amplitude is larger; we again draw notice to the scaling of the colour bars. The slight dominance of the ss-term of Fig. 7.26 at normal incidence remains. The increased amplitude of the s-components at normal incidence is not predicted by Ref. 16 for the rougher system. It may be that the roughness involved represents the boundary of validity of the phase perturbation theory.

Sample 0061

Finally, the out-of-plane incoherent MDRC for system 0061 of Ref. 15 and Table 7.3 is shown in Figs. 7.30 and 7.31 for incidence angles of $0°$ and $67°$, respectively. This specific sample was considered, due to the in-plane incoherent MDRC (Figs. 7.6–7.9) being deemed a good fit with experimental data. The most obvious feature is that the incoherent MDRC of this system is more centred around a small region. Keeping in mind that the colour bar is scaled differently, the amplitude itself is actually far greater than in Figs. 7.22–7.29.

The reason for the relatively narrow range of scattering angles contribution to the incoherent MDRC is the far lower rms-roughness to correlation length relationship for this sample than the previous, described in Table 7.3. The difference in amplitude is attributed to the vastly different dielectric functions at play, as sample 0061 is not a dielectric but a

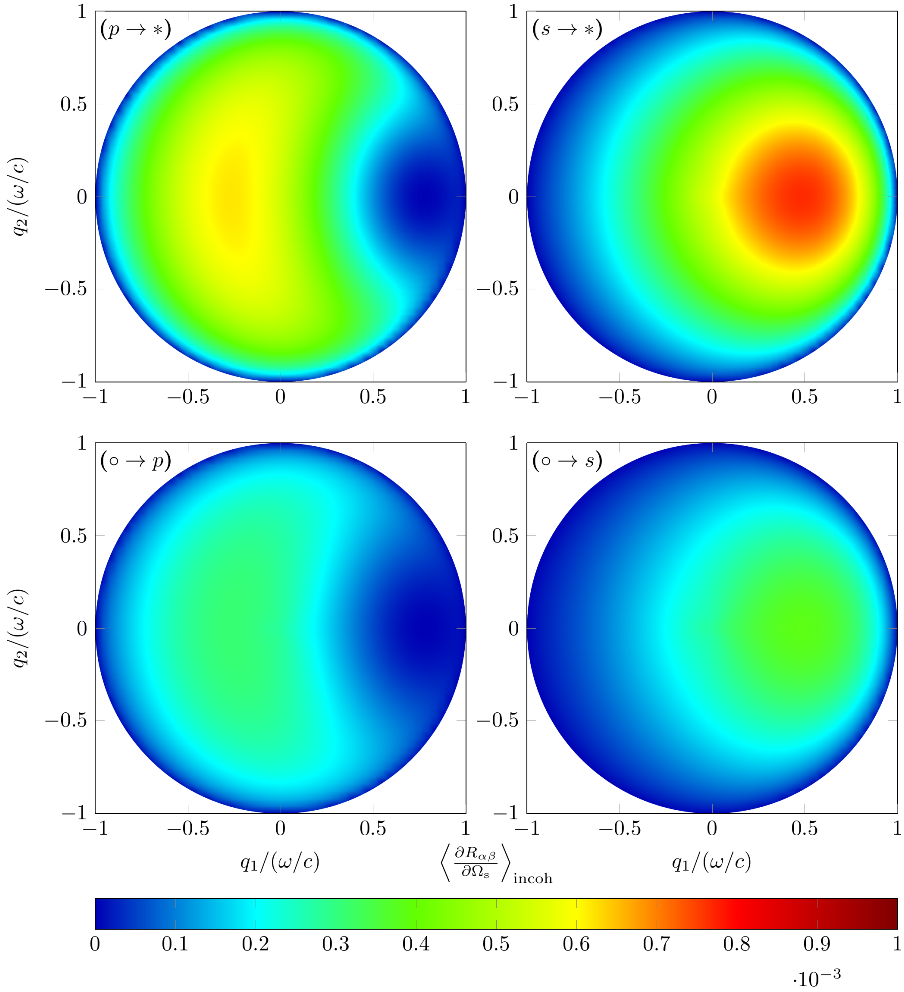

Figure 7.25: The polarisation-ignorant components of the calculated incoherent MDRC as a function of both parallel components of the scattering wave vector, after light scattering from a randomly rough dielectric surface at incidence angles $\theta_0 = 67°$ and $\phi_0 = 0°$. The surface height distribution is Gaussian, with statistical parameters $\delta = 0.025\lambda$ and $a = 0.25\lambda$ taken from Ref. 16 and system 1 in Table 7.3. The notation $*$ refers to the sum of p- and s-polarised light, and $\circ$ refers to unpolarised light which is a normalised sum of the p- and s-components.

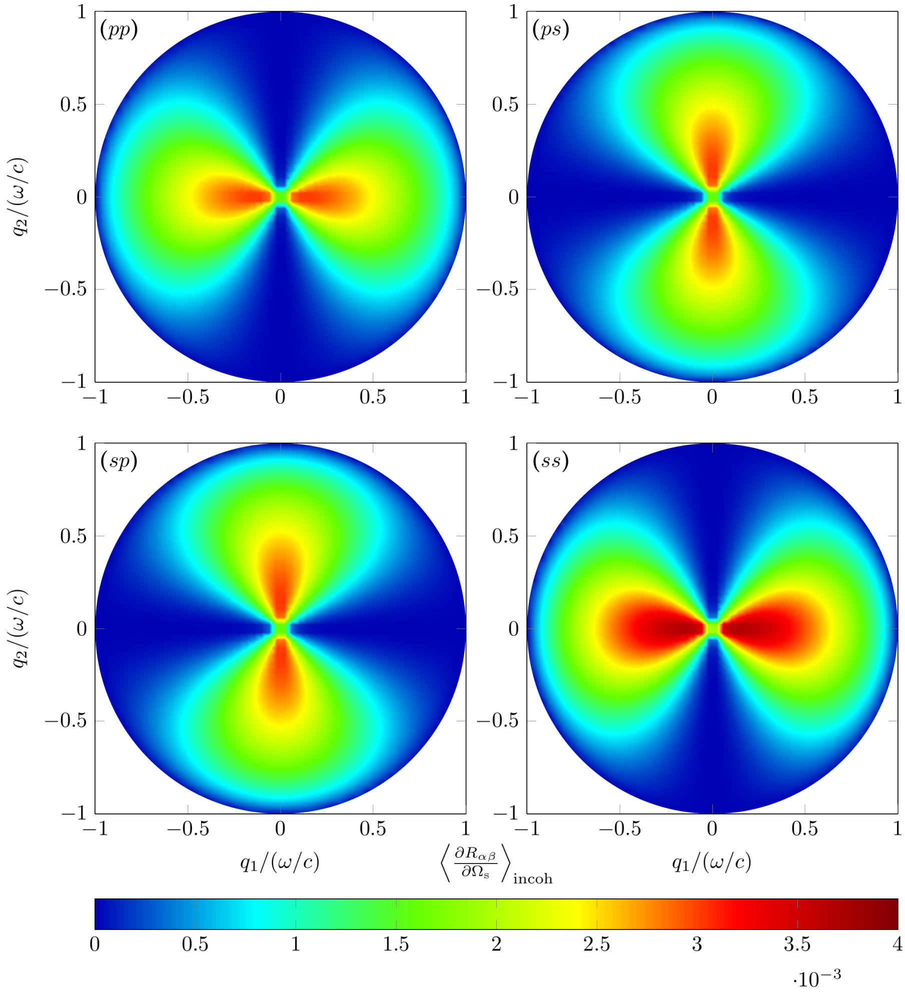

Figure 7.26: Calculated incoherent MDRC as a function of both parallel components of the scattering wave vector, after light scattering from a randomly rough dielectric surface at incidence angles $\theta_0 = 0°$ and $\phi_0 = 0°$. The surface height distribution is Gaussian, with statistical parameters $\delta = 0.050\lambda$ and $a = 0.25\lambda$ taken from Ref. 16 and system 2 in Table 7.3. Note that the colour bar is scaled differently from Figs. 7.22–7.25.

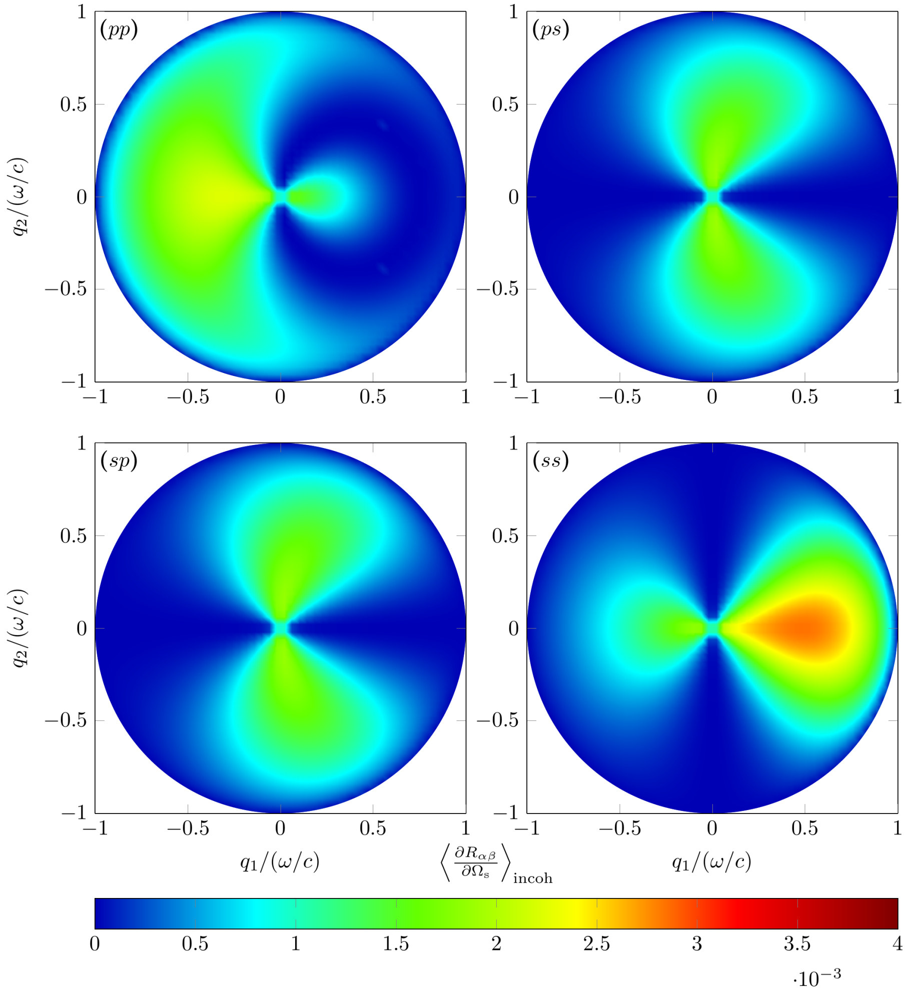

Figure 7.27: Calculated incoherent MDRC as a function of both parallel components of the scattering wave vector, after light scattering from a randomly rough dielectric surface at incidence angles $\theta_0 = 67°$ and $\phi_0 = 0°$. The surface height distribution is Gaussian, with statistical parameters $\delta = 0.050\lambda$ and $a = 0.25\lambda$ taken from Ref. 16 and system 2 in Table 7.3. Note that the colour bar is scaled differently from Figs. 7.22 and 7.23.

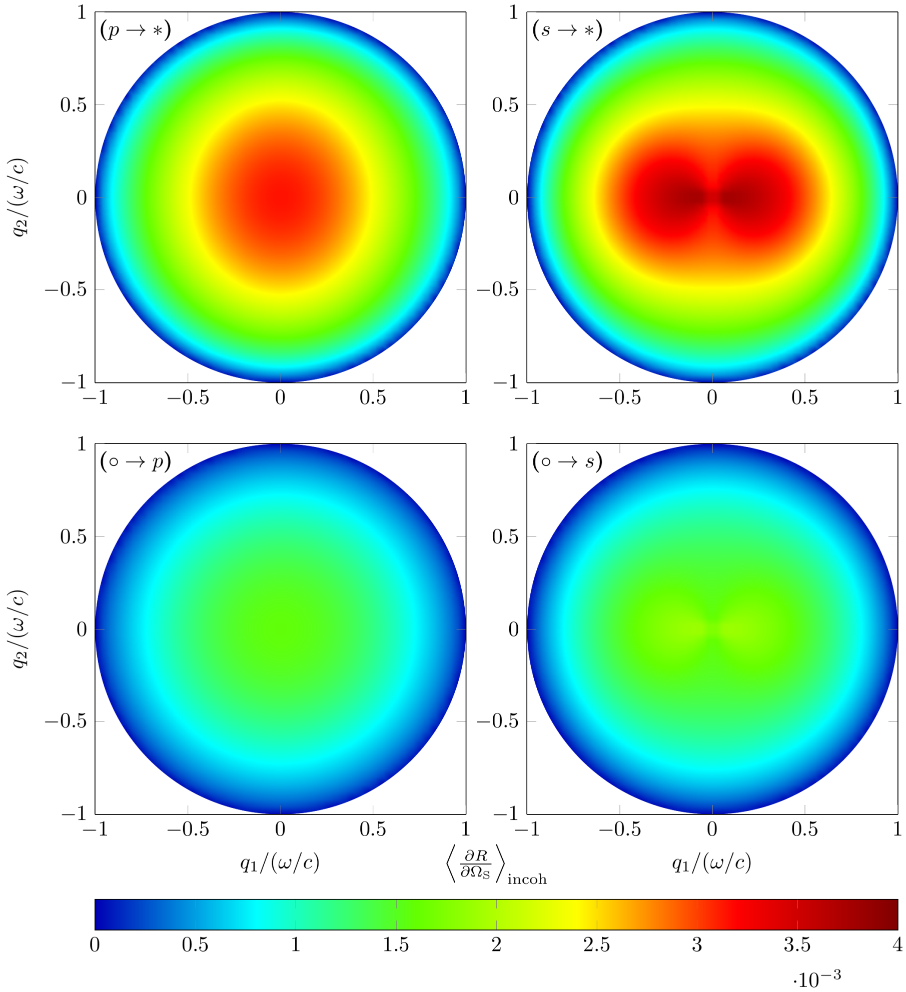

Figure 7.28: The polarisation-ignorant components of the calculated incoherent MDRC as a function of both parallel components of the scattering wave vector, after light scattering from a randomly rough dielectric surface at incidence angles $\theta_0 = 0°$ and $\phi_0 = 0°$. The surface height distribution is Gaussian, with statistical parameters $\delta = 0.050\lambda$ and $a = 0.25\lambda$ taken from Ref. 16 and system 2 in Table 7.3. The notation $*$ refers to the sum of p- and s-polarised light, and $\circ$ refers to unpolarised light which is a normalised sum of the p- and s-components. Note that the colour bar is scaled the same way as in Figs. 7.26 and 7.27.

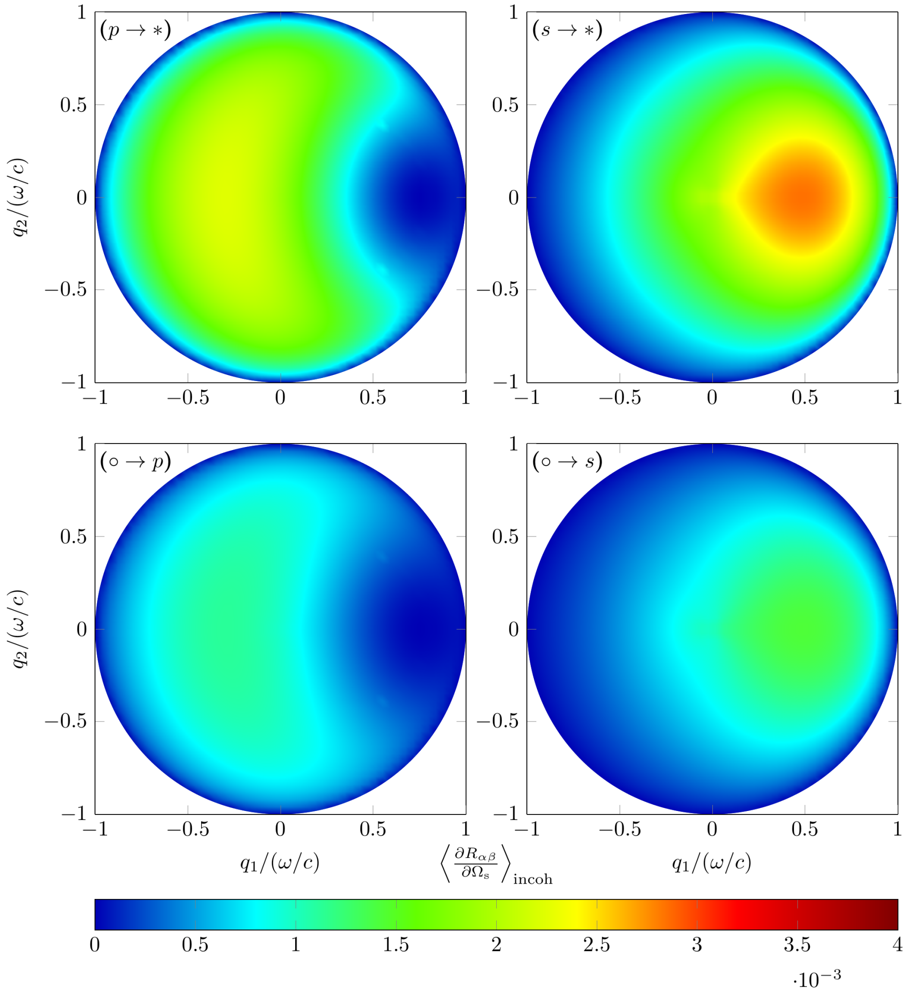

Figure 7.29: The polarisation-ignorant components of the calculated incoherent MDRC as a function of both parallel components of the scattering wave vector, after light scattering from a randomly rough dielectric surface at incidence angles $\theta_0 = 67°$ and $\phi_0 = 0°$. The surface height distribution is Gaussian, with statistical parameters $\delta = 0.050\lambda$ and $a = 0.25\lambda$ taken from Ref. 16 and system 2 in Table 7.3. The notation $*$ refers to the sum of p- and s-polarised light, and $\circ$ refers to unpolarised light which is a normalised sum of the p- and s-components. Note that the colour bar is scaled the same way as in Figs. 7.26 and 7.27.

metal, which is known to have generally much higher reflectivity of light at optical wavelengths.

Another notable feature in Fig. 7.31 is the absence of the dipole-like shape of the incoherent MDRC which was present in Figs. 7.22, 7.23, 7.26, 7.27 and 7.30. The general trend of the MDRC with $67°$ incidence, has been that the cross-polarisation components have been weaker than the co-polarised. A possible explanation for the missing dipole shape is therefore a lack of colour bar range, which makes it impossible to discern small amplitudes. It is also possible that the co-polarised components have their shape compromised by the limited density of numerical evaluation points, or its features too small to reasonably be picked up by a plot of this scale. This slight curiosity was not investigated further.

We have also included the polarisation-ignorant calculations for this system in Figs. 7.32 and 7.33. No surprising behaviour emerges from it, given the form of Figs. 7.30 and 7.31.

It is suspected that a different kind of surface autocorrelation function could drastically alter the behaviour of the incoherent MDRC. A few tests calculating the MDRC corresponding to a so-called Gaussian-cosine correlation function, $W(\mathbf{x}_{\parallel}) = \exp\left[-x_{\parallel}^2/a^2\right]\cos(bx_{\parallel})$, was performed. The dipole-like shape was retained for modest cosine frequencies, while the range of the MDRC seemed to be extended when the correlation function was permitted to oscillate a few times within the Gaussian envelope. Further time and resources could be spent on studying the detailed dependence of the incoherent MDRC on the choice of different correlation functions, and it would be a natural next step after the contents of the current work.

Planar cuts of the out-of-plane incoherent MDRC

To better compare the exact values of the incoherent MDRC, some higher resolution planar cuts of the off-diagonal plots are provided. It is worth noting that due to the assumed isotropy of the surface, the cuts in positive and negative azimuthal scattering angles should be equal, and inspections of Figs. 7.22, 7.23, 7.26, 7.27, 7.30 and 7.31, as well as test calculations not included in the thesis all reinforce this assumption.

Figure 7.34 shows the calculated in-plane incoherent MDRC from the system labelled 1 in Table 7.3 with normal incidence, and has an exact equivalent in Ref. 16. Comparatively, the values in Fig. 7.34 more closely resembles values found by a direct solution of the reduced Rayleigh equation, than values found using simple small-amplitude perturbation theory. Particularly, the pp-component of Fig. 7.34 is well approximated by the direct solution. The shape of the MDRC found directly is usually quite jagged around the origin, while the presently found data is smooth. Some of the jaggedness around the origin is due to the enhanced backscattering phenomenon; the effect of which seems to generally not be picked up by our phase perturbation theory, as commented on previously.

Similarly, Fig. 7.35 shows the same situation as Fig. 7.34 but with the statistical parameters of system 2 from Table 7.3. The discrepancy between the direct solution of the reduced Rayleigh equation and the small-amplitude perturbation theory reported in Ref. 16 is notable, while the MDRC presented in Fig. 7.35 aligns itself much more with the direct solution. As was the case for system 1, the pp-component aligns itself very well with the

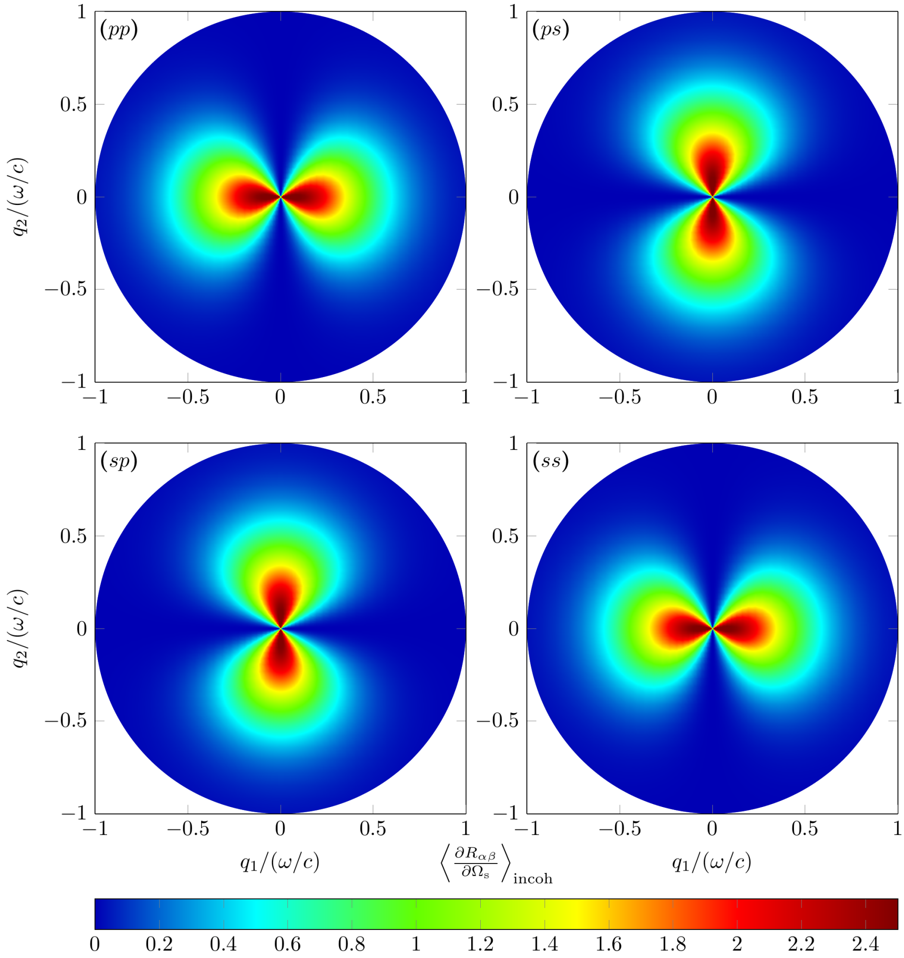

Figure 7.30: Calculated incoherent MDRC as a function of both parallel components of the scattering wave vector, after light scattering from a randomly rough gold surface at incidence angles $\theta_0 = 0°$ and $\phi_0 = 0°$. The surface height distribution is Gaussian, with statistical parameters $\delta = 0.047\lambda$ and $a = 1.79\lambda$ taken from Ref. 15 and sample 0061 in Table 7.2. Note that the colour bar is scaled differently from both Figs. 7.22–7.25 and Figs. 7.26–7.29.

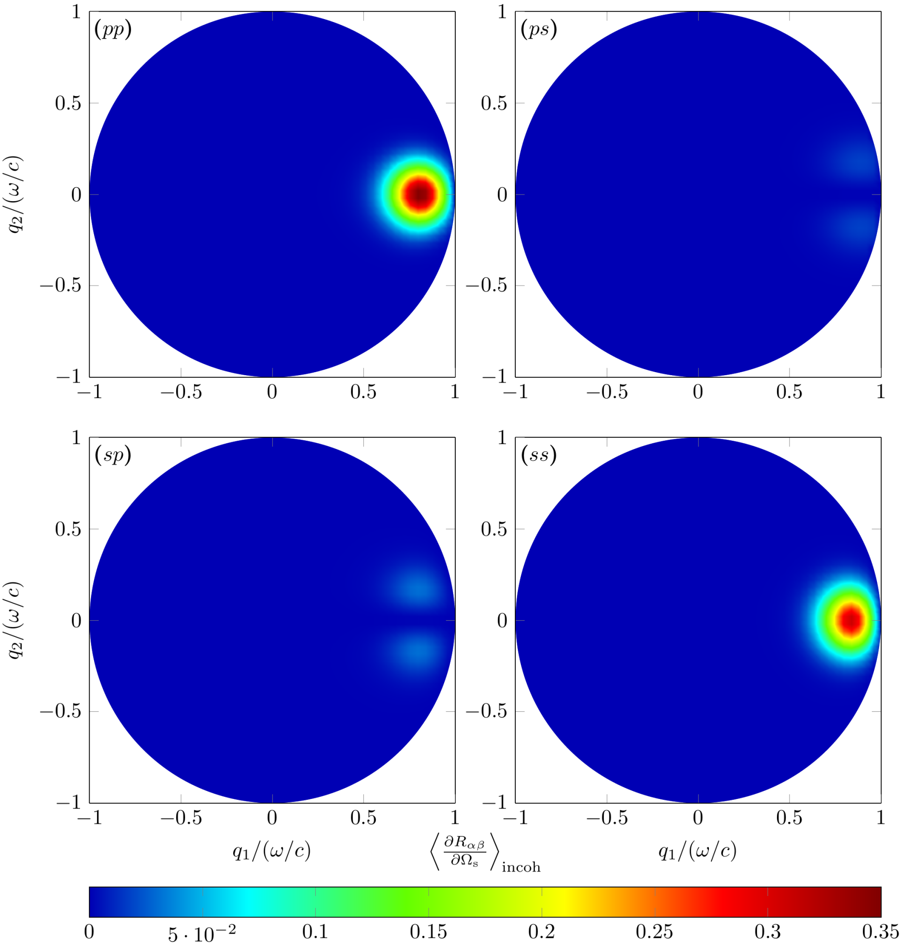

Figure 7.31: Calculated incoherent MDRC as a function of both parallel components of the scattering wave vector, after light scattering from a randomly rough gold surface at incidence angles $\theta_0 = 67°$ and $\phi_0 = 0°$. The surface height distribution is Gaussian, with statistical parameters $\delta = 0.047\lambda$ and $a = 1.79\lambda$ taken from Ref. 15 and sample 0061 in Table 7.2. Note that the colour bar is scaled differently from all the previous figures, including Fig. 7.30.

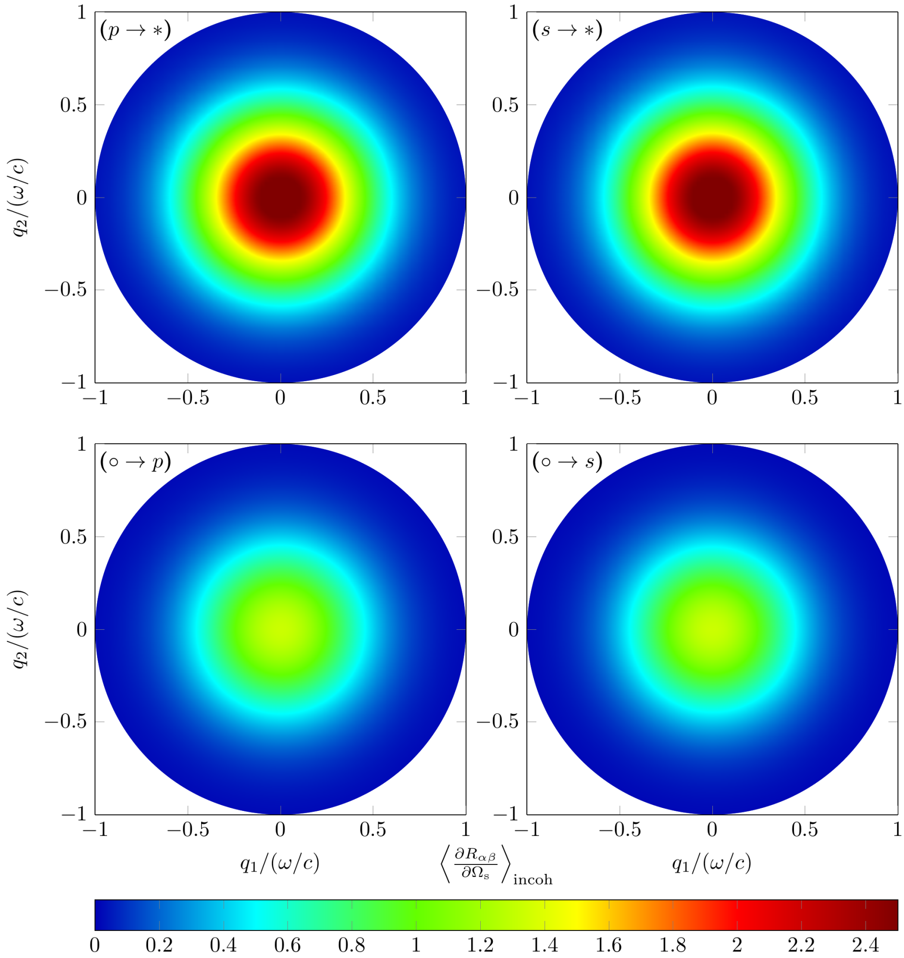

Figure 7.32: The polarisation-ignorant components of the calculated incoherent MDRC as a function of both parallel components of the scattering wave vector, after light scattering from a randomly rough gold surface at incidence angles $\theta_0 = 0°$ and $\phi_0 = 0°$. The surface height distribution is Gaussian, with statistical parameters $\delta = 0.047\lambda$ and $a = 1.79\lambda$ taken from Ref. 15 and sample 0061 in Table 7.2. The notation $*$ refers to the sum of p- and s-polarised light, and $\circ$ refers to unpolarised light which is a normalised sum of the p- and s-components. Note that the colour bar is scaled the same way as in Fig. 7.30.

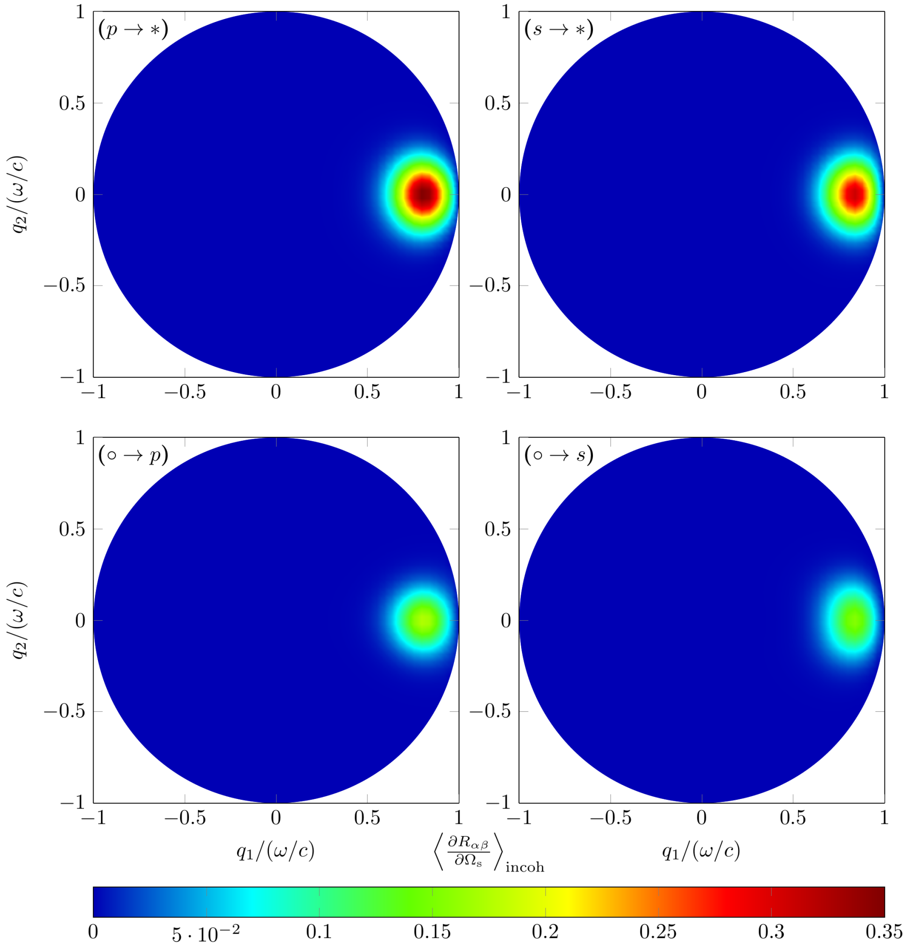

Figure 7.33: The polarisation-ignorant components of the calculated incoherent MDRC as a function of both parallel components of the scattering wave vector, after light scattering from a randomly rough gold surface at incidence angles $\theta_0 = 67°$ and $\phi_0 = 0°$. The surface height distribution is Gaussian, with statistical parameters $\delta = 0.047\lambda$ and $a = 1.79\lambda$ taken from Ref. 15 and sample 0061 in Table 7.2. The notation $*$ refers to the sum of p- and s-polarised light, and $\circ$ refers to unpolarised light which is a normalised sum of the p- and s-components. Note that the colour bar is scaled the same way as in Fig. 7.31.

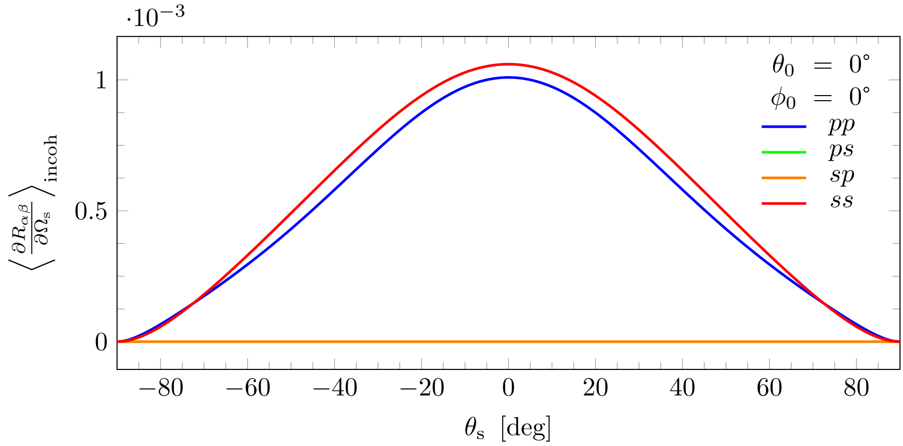

Figure 7.34: Planar cut of the calculated incoherent MDRC as a function of the polar scattering angle, after light scattering from a randomly rough dielectric surface with incidence angles $\theta_0 = 0°$ and $\phi_0 = 0°$, and the azimuthal scattering angle $\phi_S = 0°$. The surface height distribution is Gaussian, with statistical parameters $\delta = 0.025\lambda$ and $a = 0.25\lambda$ taken from Ref. 16.

direct solution, while the ss-component is slightly more rogue. The authors of Ref. 16 suggest that the small-amplitude perturbation theory is inadequate for this level of surface roughness; if that is the case, the result of Fig. 7.35 shows that phase perturbation theory is better equipped to produce correct results for this level of surface roughness (based on the assumption that non-perturbative results are more accurate).

The fact that the pp- and ss-components are different from one another in Figs. 7.34 and 7.35 is unexpected. The almost equivalent in-plane incoherent MDRC of sample 0061 for a very low incidence angle given in Fig. 7.6 shows that the pp- and ss-components coincide for that sample. Due to the isotropy of the surfaces, we do not expect polarisation dependence at normal incidence. Evaluating Eq. (5.23) with $\mathbf{q}_{\|} = \mathbf{k}_{\|} = 0$, as an example, the difference between the pp- and ss-components must stem from Eqs. (D.8) and (D.11), but the form of the expressions does not make it clear whether the difference in inherently built into the formulation or not. We dare not speculate too much as to the reason why the components are unequal, but we may instead describe one of its consequences; it explains the dipole-like patterns that remain in the $(s \to *)$-components of Figs. 7.24 and 7.28, the former of which is just barely noticeable. The relatively larger amplitude of the ss-component gives more weight to the amplitude along the scattering plane, resulting in the observed shapes.

Figures 7.36 and 7.37 show the complete out-of-plane cuts (i.e. with the scattering azimuth angle ϕ_s of $(\pm)90°$) of the incoherent MDRC after normal incidence scattering from systems 1 and 2 from Table 7.3. The resemblance between the shapes of Figs. 7.34

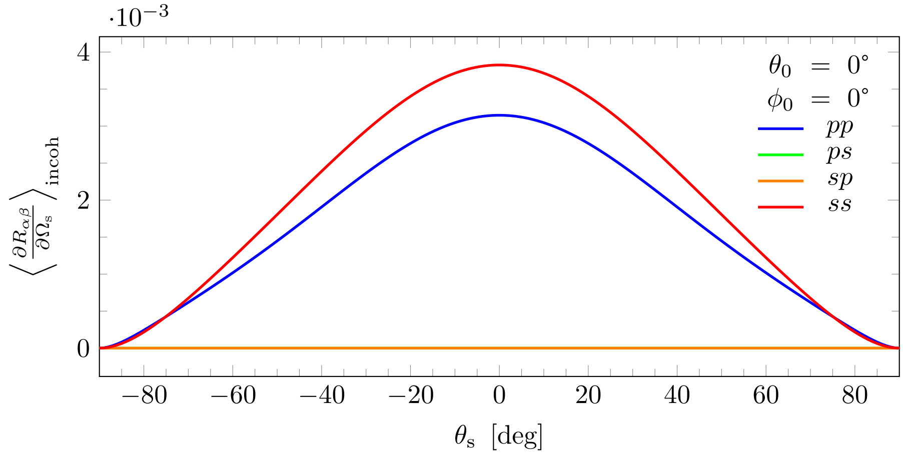

Figure 7.35: Planar cut of the calculated incoherent MDRC as a function of the polar scattering angle, after light scattering from a randomly rough dielectric surface with incidence angles $\theta_0 = 0°$ and $\phi_0 = 0°$, and the azimuthal scattering angle $\phi_S = 0°$. The surface height distribution is Gaussian, with statistical parameters $\delta = 0.050\lambda$ and $a = 0.25\lambda$ taken from Ref. 16.

and 7.36 and between Figs. 7.35 and 7.37 is striking, especially in the pp-components of the former. But this similarity is completely expected; by rotating the scattering plane by $90°$ the p-polarisation turns into s, and vice versa, as was discussed during the consideration of Fig. 7.22.

The underlying reason why this symmetry may be expected in the first place, is the assumption of the surfaces being isotropic. In fact, the discrepancy between the pp- and ss-components in Fig. 7.35 might suggest an internal inconsistency in the implementation, or it might be that the roughness sensitivity is not equal among all components.

The incoherent MDRC is also provided for cuts of intermediate azimuthal scattering angles for the two situations discussed until now, and they turn out to be nothing more than stages of intermediate amplitude between the end stages of each component; their behaviour is as expected from inspection of Figs. 7.22 and 7.26. Therefore, these plots have been relegated to Appendix E, and are given in Figs. E.1–E.4.

The calculated in-plane incoherent MDRC of system 1 of Table 7.3 and $67°$ incidence is provided in Fig. 7.38. The overall shape and amplitude of the incoherent MDRC compares well to the equivalent data reported in Ref. 16. The pp-component has its peak skewed towards low scattering angles, as was observed in Secs. 7.1 and 7.2, while the ss-components larger amplitude for non-normal incidence was a common amplitude for the dielectric systems, as shown in Figs. 7.23 and 7.27.

Similarly, for the rougher dielectric system 2 from Table 7.3, its calculated in-plane

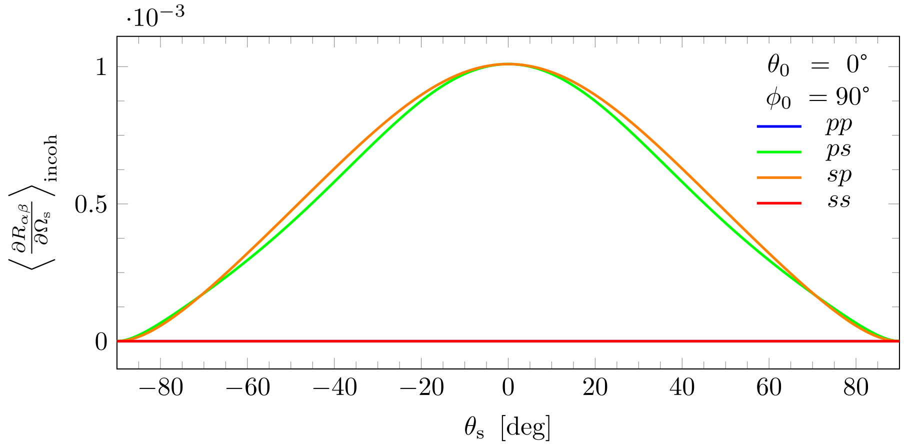

Figure 7.36: Planar cut of the calculated incoherent MDRC as a function of the polar scattering angle, after light scattering from a randomly rough dielectric surface with incidence angles $\theta_0 = 0°$ and $\phi_0 = 0°$, and the azimuthal scattering angle $\phi_S = 90°$. The surface height distribution is Gaussian, with statistical parameters $\delta = 0.025\lambda$ and $a = 0.25\lambda$ taken from Ref. 16.

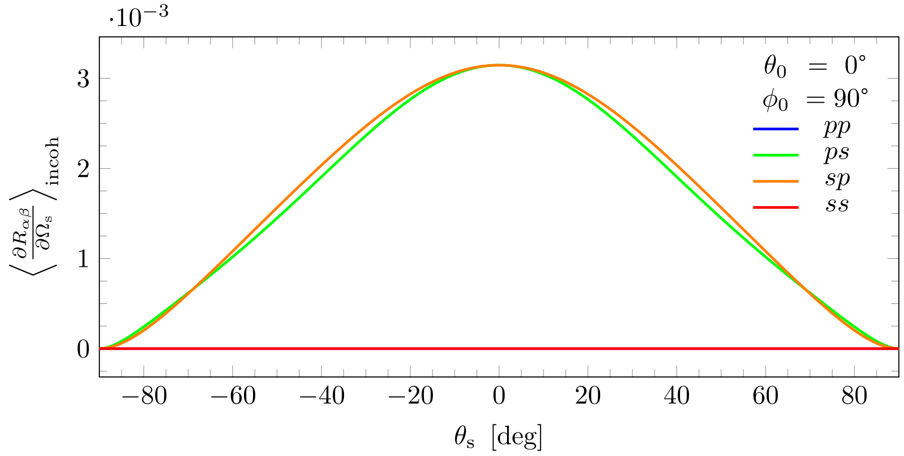

Figure 7.37: Planar cut of the calculated incoherent MDRC as a function of the polar scattering angle, after light scattering from a randomly rough dielectric surface with incidence angles $\theta_0 = 0°$ and $\phi_0 = 0°$, and the azimuthal scattering angle $\phi_S = 90°$. The surface height distribution is Gaussian, with statistical parameters $\delta = 0.050\lambda$ and $a = 0.25\lambda$ taken from Ref. 16.

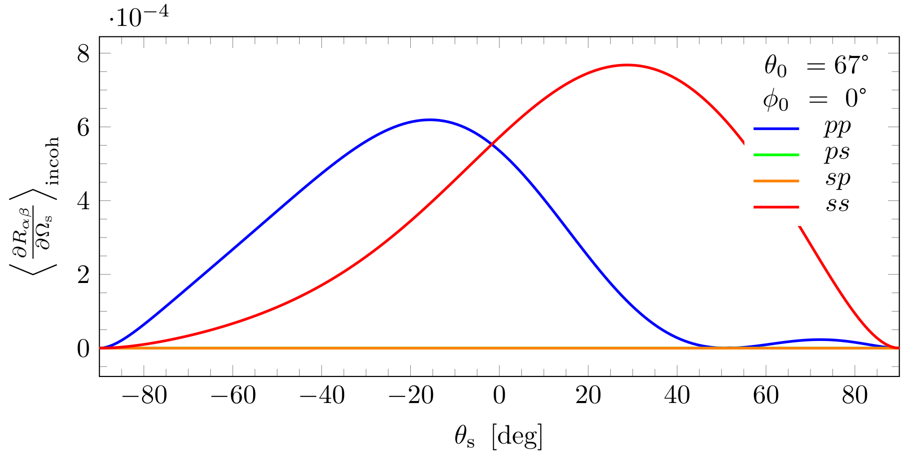

Figure 7.38: Planar cut of the calculated incoherent MDRC as a function of the polar scattering angle, after light scattering from a randomly rough dielectric surface with incidence angles $\theta_0 = 67°$ and $\phi_0 = 0°$, and the azimuthal scattering angle $\phi_S = 0°$. The surface height distribution is Gaussian, with statistical parameters $\delta = 0.025\lambda$ and $a = 0.25\lambda$ taken from Ref. 16.

incoherent MDRC at $67°$ incidence is shown in Fig. 7.39. This results reinforces the previously observed fact that the currently implemented phase perturbation theory gives a closer approximation to the direct solution of the reduced Rayleigh equation than the small-amplitude perturbation theory, both presented in Ref. 16. Apart from the scale of the involved amplitude, the general shapes and features of Figs. 7.38 and 7.39 are predictably comparable.

The completely out-of-plane cut-through of the calculated incoherent MDRC with $67°$ incidence is given in Figs. 7.40 and 7.41 for systems 1 and 2 from Table 7.3, respectively. Yet again, the phase perturbation theory is superior to the small-amplitude perturbation theory in terms of replicating the direct solution of the reduced Rayleigh equation, especially for the rougher system. Again, the shapes and features of the two systems are quite comparable. The cross-polarised components of Figs. 7.40 and 7.41 exist mainly as a consequence of the rotation of the observation plane making the p- and s-directions of the rotated and non-rotated planes coincide, which in turn makes the tangent plane Fresnel coefficients different from zero, as was suggested during the discussion of Fig. 7.22. The fact that the amplitudes of the cross-polarisation components of Figs. 7.40 and 7.41 is respectively slightly smaller than the co-polarised components of Figs. 7.38 and 7.39 may suggest that this effect is limited to the component of direct downwards ($-\hat{x}_3$) propagating incident light. The appearance of the pp-component away from the origin is predicted from the pp-components of Figs. 7.23 and 7.27.

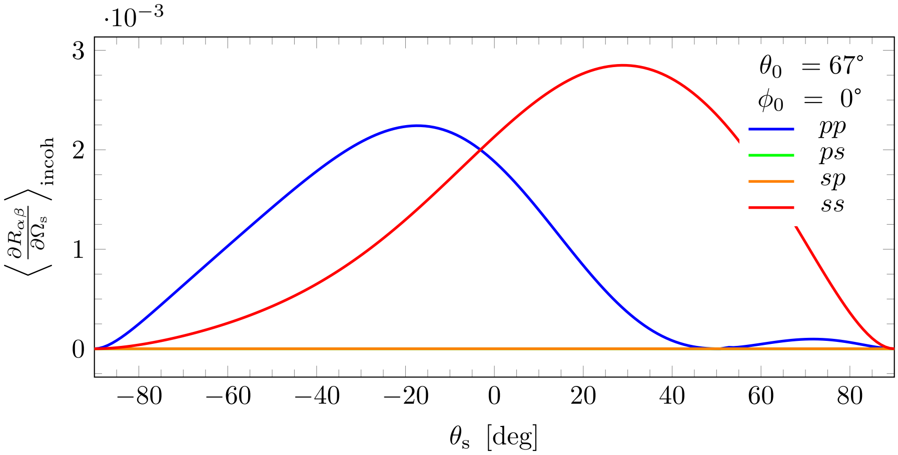

Figure 7.39: Planar cut of the calculated incoherent MDRC as a function of the polar scattering angle, after light scattering from a randomly rough dielectric surface with incidence angles $\theta_0 = 67°$ and $\phi_0 = 0°$, and the azimuthal scattering angle $\phi_S = 0°$. The surface height distribution is Gaussian, with statistical parameters $\delta = 0.050\lambda$ and $a = 0.25\lambda$ taken from Ref. 16.

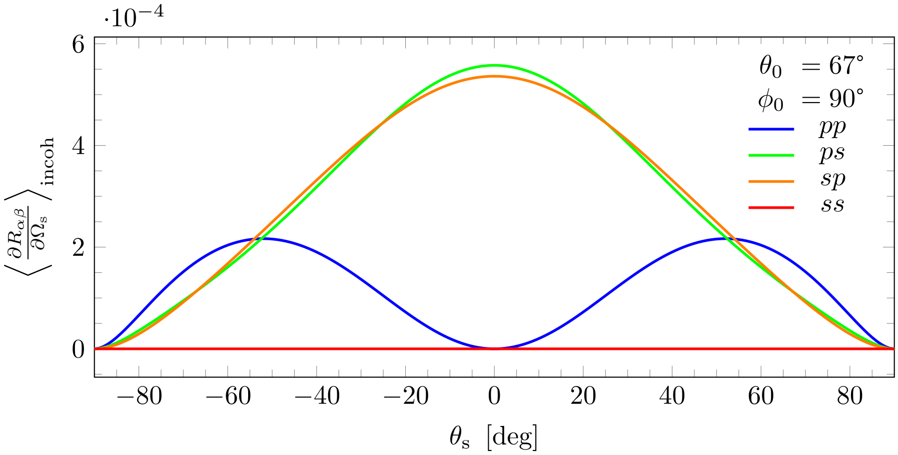

Figure 7.40: Planar cut of the calculated incoherent MDRC as a function of the polar scattering angle, after light scattering from a randomly rough dielectric surface with incidence angles $\theta_0 = 67°$ and $\phi_0 = 0°$, and the azimuthal scattering angle $\phi_S = 90°$. The surface height distribution is Gaussian, with statistical parameters $\delta = 0.025\lambda$ and $a = 0.25\lambda$ taken from Ref. 16.

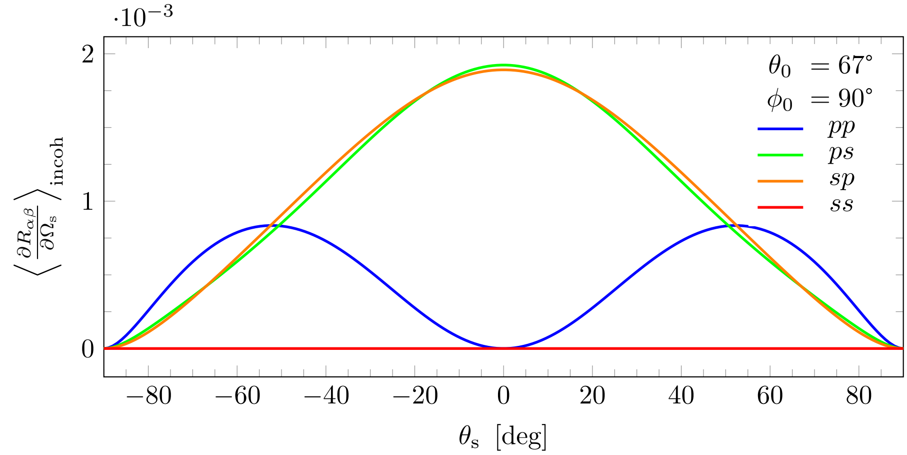

Figure 7.41: Planar cut of the calculated incoherent MDRC as a function of the polar scattering angle, after light scattering from a randomly rough dielectric surface with incidence angles $\theta_0 = 67°$ and $\phi_0 = 0°$, and the azimuthal scattering angle $\phi_S = 90°$. The surface height distribution is Gaussian, with statistical parameters $\delta = 0.050\lambda$ and $a = 0.25\lambda$ taken from Ref. 16.

Like in the case of normal incidence, some intermediate stages between the $0°$ and $90°$ azimuthal scattering angles have been provided by Figs. E.5–E.8 in Appendix E. Their behaviour is predictable from Figs. 7.23 and 7.27. A notable aspect is that the cross-polarised components are centred around larger polar scattering angles for cuts at lower azimuthal scattering angles, which is due to the skewed dipole shape of the cross-polarised components of said figures. The origin of this feature also seems non-trivial.

Finally, planar cuts of the incoherent MDRC of the experimental sample 0061 from Ref. 15 has also been calculated. The in-plane cases closely resemble Figs. 7.6 and 7.9, where the incident angles are close to the cases considered in Figs. 7.30 and 7.31. These calculated incoherent MDRC plane cuts is given in Figs. E.9 and E.10 in Appendix E.

The cross-plane calculation of the incoherent MDRC of sample 0061 at normal incidence is given by Fig. 7.42. The ps- and sp-components are more or less indistinguishable, just like the pp- and ss-components in Fig. 7.6, and have the same general shape as their in-plane co-polarised counterparts. This is a result of the p↔s-relabelling discussed during the comments on Figs. 7.22, 7.36 and 7.37. The planar cuts along intermediate azimuthal scattering angles, only provide intermediate stages for the calculated MDRC, which is shown in Figs. E.11 and E.12 in Appendix E.

For $67°$ incidence, the evolution of the calculated incoherent MDRC of sample 0061 from increasingly rotated scattering planes is given in Figs. 7.43–7.45. They show a gradual decline of the co-polarised components, which was not observed in Fig. 7.31. In addi-

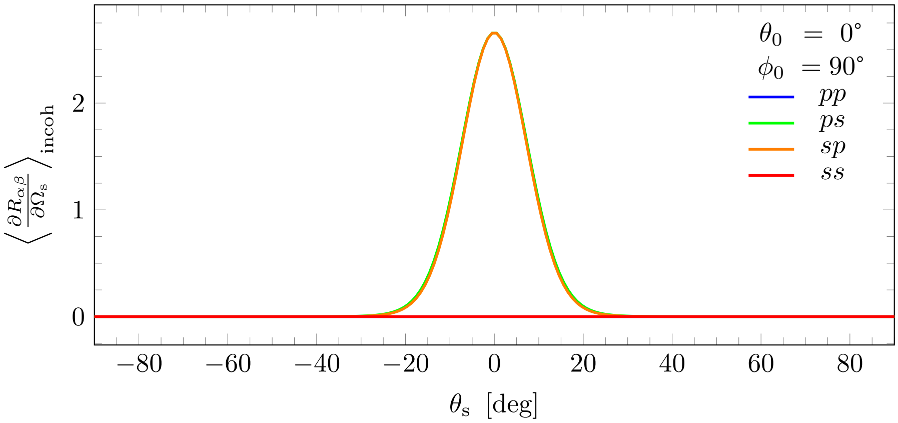

Figure 7.42: Planar cut of the calculated incoherent MDRC as a function of the polar scattering angle, after light scattering from a randomly rough gold surface with incidence angles $\theta_0 = 0°$ and $\phi_0 = 0°$, and the azimuthal scattering angle $\phi_S = 90°$. The surface height distribution is Gaussian, with statistical parameters $\delta = 0.047\lambda$ and $a = 1.79\lambda$ taken from Ref. 15.

tion, there seems to be a certain dominance of the sp-component which is interesting. The most striking fact is that the amplitude of Figs. 7.43–7.45 is far smaller than the colour bar of Fig. 7.31 indicates.

All these observations supports the previous hypothesis that Fig. 7.31 is an inaccurate image of the incoherent MDRC, possibly due to excessive interpolation between points that are spaced too far apart. Close inspection of Fig. 7.45 reveals some dependence on the pp-component away from the origin, which is the same general shape that was observed in Figs. 7.36 and 7.37. This may suggest that the out-of-plane incoherent MDRC distribution at 67° incidence for sample 0061 really looks more like the slanted dipole shape of the dielectric systems. The eminence of the sp-component challenges this view, but for such low absolute amplitudes the discrepancy is more likely than not a result of numerical instability or the approximation of perturbation.

7.4 Origin of discrepancies

The comparison between the present implementation, earlier experiments [15] and numerical analysis [12, 15, 16] is mostly convincing, but not entirely. In this section, we summarise and speculate on the origins of the difference.

Firstly, we recall that the calculations have been performed used second order phase perturbation theory. In itself, that may introduce errors of order $[\zeta^3]^2 = \zeta^6$. Additionally, only the the 2-2 term is accounted for, while the 3-1 term may introduce errors of order ζ^4. In cases where the incoherent MDRC is small but the relative roughness of the

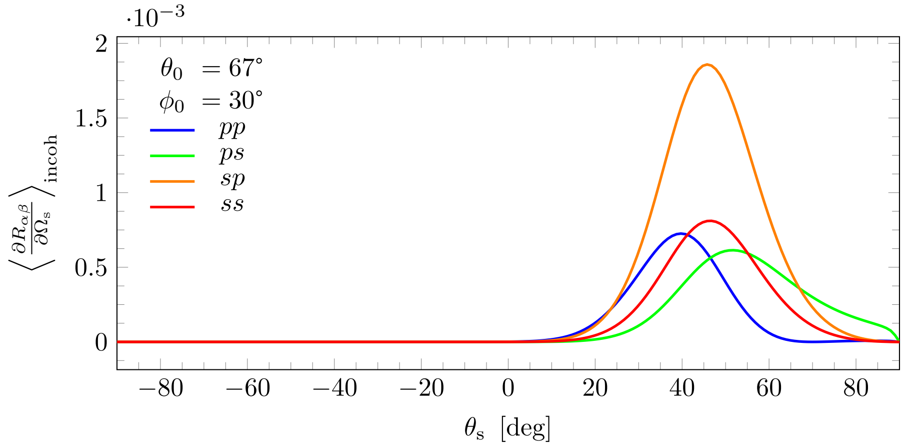

Figure 7.43: Planar cut of the calculated incoherent MDRC as a function of the polar scattering angle, after light scattering from a randomly rough gold surface with incidence angles $\theta_0 = 67°$ and $\phi_0 = 0°$, and the azimuthal scattering angle $\phi_S = 30°$. The surface height distribution is Gaussian, with statistical parameters $\delta = 0.047\lambda$ and $a = 1.79\lambda$ taken from Ref. 15.

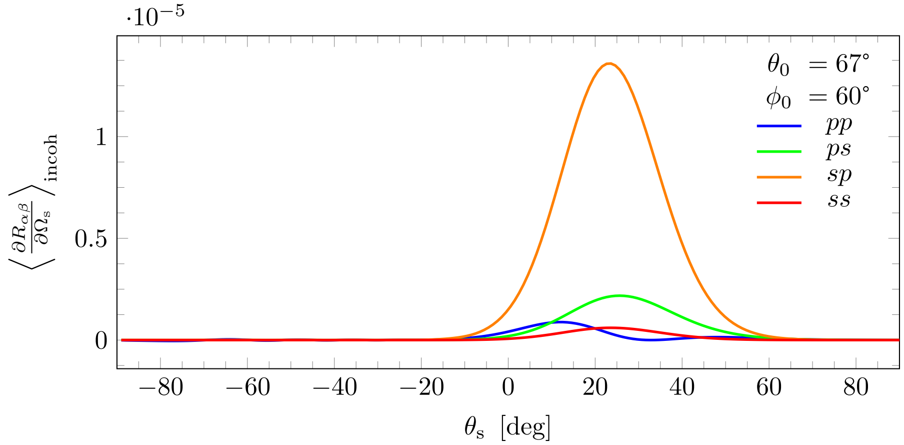

Figure 7.44: Planar cut of the calculated incoherent MDRC as a function of the polar scattering angle, after light scattering from a randomly rough gold surface with incidence angles $\theta_0 = 67°$ and $\phi_0 = 0°$, and the azimuthal scattering angle $\phi_S = 60°$. The surface height distribution is Gaussian, with statistical parameters $\delta = 0.047\lambda$ and $a = 1.79\lambda$ taken from Ref. 15.

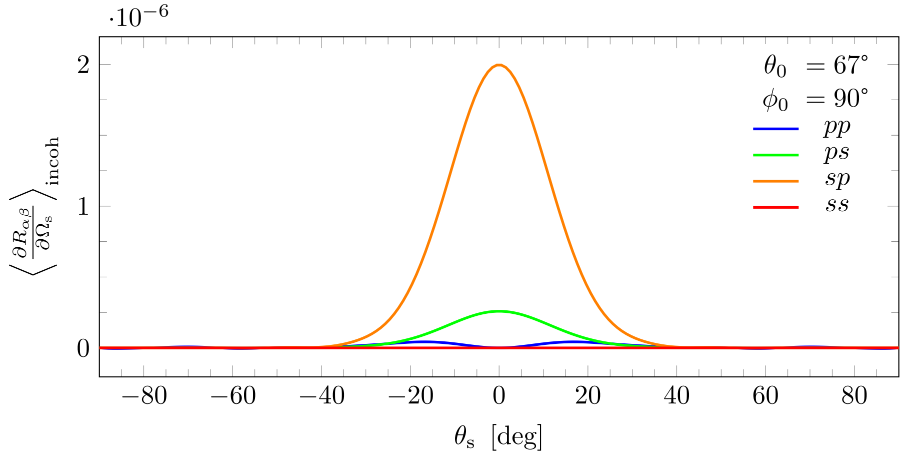

Figure 7.45: Planar cut of the calculated incoherent MDRC as a function of the polar scattering angle, after light scattering from a randomly rough gold surface with incidence angles $\theta_0 = 67°$ and $\phi_0 = 0°$, and the azimuthal scattering angle $\phi_S = 90°$. The surface height distribution is Gaussian, with statistical parameters $\delta = 0.047\lambda$ and $a = 1.79\lambda$ taken from Ref. 15.

surface is large, such errors may be significant. This is exemplified by sample 8053 (Table 7.2 and Figs. 7.13–7.15) whose modest roughness compared to light wavelength left the amplitude of the incoherent MDRC to remain small, while its large roughness compared to the surface spatial wavelength means that the assumptions of modest roughness (made in perturbation theory or due to the Rayleigh hypothesis) is not necessarily correct. The quantity δ/a for sample 8053 is 0.25, which is not guaranteed to fulfil the Rayleigh criterion, as per the discussion in Sec. 4.3. And while the parameters of the present implementation and the ones used to study the Rayleigh criterion for rough surfaces [43] are different, this fact presents the possibility that the samples currently considered does not fulfil the Rayleigh criterion, causing the theory to fail.

Errors due to numerical precision may also be present. The numerical error in evaluation of Eq. (5.33) should not exceed 10^{-7} following the discussion in Sec. 6.3. Each of these may be applied to a range of evaluation of Eq. (6.1b) between 0 and 10 appropriate units, meaning the error scales to a maximum of 10^{-6}, plus the numerical error in the remaining evaluation of Eq. (6.1b) which according to Fig. 6.2 should be limited to around $10 \times 10^{-5} = 10^{-4}$. Some of this is likely due to error in evaluating Eq. (5.33), so the real numerical error is likely to be less, as we in this estimate is compounding two errors where one might be the result of the other. This level of numerical error could still give some impact on the incoherent MDRC in the dielectric systems considered in Sec. 7.3, as the amplitude of the incoherent MDRC there is comparable to 10^{-4}. Overall, we deem it to be unlikely that the accuracy of the calculation is ultimately contingent on the numerics involved more than other factors.

Results in Ref. 12 indicate that small changes in the statistical parameters (which were measured experimentally) may explain some of the differences in the maximum achieved amplitude. It may be the case that the incoherent MDRC is sensitive to variation in the measured surface parameters within their experimental uncertainty, meaning exact calculation beyond the MDRC variation within the uncertainty is unreasonable.

Overall, the present implementation of phase perturbation theory captures most of the features present in the results with which they are compared. However, in a few places the specific values involved differ slightly. Some of the systems considered possess statistical parameters that makes them potentially challenge the Rayleigh criterion, or other criteria for modest roughness approximation. This may result in the values of the calculated incoherent MDRC being more uncertain, and specific to the implementation. But it is also acknowledged that the implementation itself may possibly be responsible for some of the odd results.

Chapter 8

Conclusion

The comparison between experimentally acquired data and data calculated using phase perturbation theory, both in Sec. 7.2 and elsewhere, show that phase perturbation theory is a method that quite well approximates the incoherent MDRC for light scattered on randomly rough metal surfaces with modest amplitudes. The specific implementation performed in this thesis was compared to a previous calculation using a different formulation of the phase perturbation theory, and was largely able to reproduce its features. It is currently not possible to conclude that one formulation is better than another, and the ability to reproduce experimental values likely depends on the regime of the wavelength, material parameters and roughness parameters involved. The present implementation of the phase perturbation theory was also compared to a previous calculation of the distribution of the incoherent MDRC outside the incident plane after scattering on a randomly rough dielectric surface, where the reduced Rayleigh equation was solved directly. Also in this instance, the phase perturbation theory reproduces the main features.

The present formulation makes use of a mathematical identity based on the Jacobi-Anger expansion to simplify the result of the phase perturbation theory further. The expansion introduces some integrals that oscillate rapidly under some circumstances, and challenges accuracy and performance. Practical compromises was made to accommodate the calculation.

In the cases where the present implementation does not coincide with other results, the surfaces in question may be inadequately rough for phase perturbation theory to be correct, or the specific set of parameters involved may present numerical difficulty or shortcomings inherent in the implementation itself.

Appendix A

Derivation of the general form of the mean differential reflection coefficient

This derivation is based on Ref. 63 which is again based on Ref. 34. We begin by considering the scalar wave equation

$$\nabla^2\psi(\mathbf{x};t) - \frac{1}{c^2}\frac{\partial^2}{\partial t^2}\psi(\mathbf{x};t) = 0. \tag{A.1}$$

Note that

$$\frac{\partial\psi}{\partial t}\nabla^2\psi = \nabla\cdot\left(\frac{\partial\psi}{\partial t}\nabla\psi\right) - \frac{1}{2}\frac{\partial}{\partial t}[\nabla\psi]^2, \tag{A.2}$$

which may be verified by using the chain rule of differentiation on the first term on the right hand side, allowing for the order of ∇ and $\frac{\partial}{\partial t}$ to be interchanged. Note also that

$$\frac{\partial\psi}{\partial t}\frac{\partial^2\psi}{\partial t^2} = \frac{1}{2}\frac{\partial}{\partial t}\left[\frac{\partial\psi}{\partial t}\right]^2, \tag{A.3}$$

which may again be verified by using the chain rule. Upon multiplying both sides of Eq. (A.1) by $\frac{\partial\psi}{\partial t}$ and inserting Eqs. (A.2) and (A.3) appropriately, we arrive at the relation

$$\nabla\cdot\left[\frac{\partial\psi}{\partial t}\nabla\psi\right] - \frac{1}{2}\frac{\partial}{\partial t}[\nabla\psi]^2 - \frac{1}{2c^2}\frac{\partial}{\partial t}\left[\frac{\partial\psi}{\partial t}\right]^2 = 0. \tag{A.4}$$

By introducing the functions

$$\mathbf{S}(\mathbf{x};t) := -a\left[\frac{\partial}{\partial t}\psi(\mathbf{x};t)\right]\nabla\psi(\mathbf{x};t) \tag{A.5}$$

and

$$W(\mathbf{x};t) := \frac{a}{2}\left([\nabla\psi(\mathbf{x};t)]^2 + \frac{1}{c^2}\left[\frac{\partial}{\partial t}\psi(\mathbf{x},t)\right]^2\right), \tag{A.6}$$

where a is an arbitrary positive constant, Eq. (A.4) may instead be written

$$\nabla\cdot\mathbf{S}(\mathbf{x};t) + \frac{\partial}{\partial t}W(\mathbf{x};t) = 0. \tag{A.7}$$

Equation (A.7) has the form of a continuity equation (compare for instance to Eq. (3.2)) with $\mathbf{S}$ representing the energy flux of the field ψ and W representing the energy density. As discussed in Sec. 3.2.2, any solution ψ of Eq. (A.1) is a linear combination of monochromatic waves, so we may limit our focus to a single monochromatic component and write

$$\psi = \Re\left\{\psi(\mathbf{x};\omega)\exp\left[-i\omega t\right]\right\} = \frac{1}{2}\left[\psi(\mathbf{x};\omega)\exp\left[-i\omega t\right] + \psi^*(\mathbf{x};\omega)\exp\left[i\omega t\right]\right], \tag{A.8}$$

where ψ^* denotes the complex conjugate of ψ. Therefore, as $\frac{\partial}{\partial t}\to -i\omega$,

$$\mathbf{S}\to -i\omega\frac{a}{4}\left[\psi^*\nabla\psi - \psi\nabla\psi^* + \psi^*\nabla\psi^*\exp\left[2i\omega t\right] - \psi\nabla\psi\exp\left[-2i\omega t\right]\right], \tag{A.9}$$

and

$$\begin{aligned} W \to &\frac{a}{8}\Big[2\nabla\psi\cdot\nabla\psi^* + (\nabla\psi)^2\exp\left[-2i\omega t\right] + (\nabla\psi^*)^2\exp\left[2i\omega t\right] \\ &- \left(\frac{\omega}{c}\right)^2\left[-2\psi^*\psi + \psi^2\exp\left[-2i\omega t\right] + (\psi^*)^2\exp\left[2i\omega t\right]\right]\Big]. \end{aligned} \tag{A.10}$$

In scattering problems we are interested in the stationary situation, so only solutions of ψ which have been averaged over a time $T \gg \frac{2\pi}{\omega}$ are of relevance. Then, by denoting $\langle\cdot\rangle_t$ as time average, it follows that the oscillations cancel out and we have

$$\left\langle\exp\left[\pm 2i\omega t\right]\right\rangle_t \to 0. \tag{A.11}$$

Then,

$$\langle\mathbf{S}\rangle_t = \frac{i\omega a}{4}\left[\psi^*\nabla\psi - \psi\nabla\psi^*\right] = \frac{\omega a}{2}\Im\left\{\psi^*\nabla\psi\right\}, \tag{A.12}$$

where $\Im$ denotes the imaginary part of its argument, and

$$\langle W\rangle_t = \frac{a}{4}\left[\nabla\psi^*\cdot\nabla\psi + \left(\frac{\omega}{c}\right)^2\psi^*\psi\right]. \tag{A.13}$$

In consideration of a scattering process on a surface, the relevant flux component of either incident or scattered waves is the component that is orthogonal to the average of the surface. This constraint arises from the continuity equation. By selecting the same coordinate system as in Sec. 4.1 we may limit our attention to the x_3-component of $\mathbf{S}$, and let $\nabla\to\frac{\partial}{\partial x_3}$. Then

$$\langle\mathbf{S}\rangle_t \to \langle S_3\rangle_t = \frac{\omega a}{2}\Im\left\{\psi^*\frac{\partial}{\partial x_3}\psi\right\}. \tag{A.14}$$

The total incoming energy flux in the region $x_1 \in \left[-\frac{L_1}{2}, \frac{L_1}{2}\right], x_2 \in \left[-\frac{L_2}{2}, \frac{L_2}{2}\right]$ is then given by

$$\begin{aligned} P_{\text{inc}} &= \int dx_1 \int dx_2 \left\langle -S_3 \right\rangle_{t;\text{ inc}} \\ &= -\frac{\omega a}{2} \Im \int_{-L_1/2}^{L_1/2} dx_1 \int_{-L_2/2}^{L_2/2} dx_2 \psi_{\text{inc}}^* \frac{\partial}{\partial x_3} \psi_{\text{inc}}. \end{aligned} \tag{A.15}$$

The incident energy flux in the x_3-direction is directed *towards* the surface from above, resulting in $\left\langle S_3 \right\rangle_{t;\text{ inc}} < 0$. To recognise that the energy carried by the wave is in fact positive, the minus sign is included above. If ψ_{inc} is β-polarised and the coordinate system is chosen to have the x_1-axis aligned with the parallel component of ψ_{inc}[1], then from Eq. (4.2) we have that

$$\psi_{\text{inc}} = \psi_{(\beta)} \exp\left[ik_{\|}x_1 - i\alpha_0(k_{\|})x_3\right] \exp\left[-i\omega t\right], \tag{A.16}$$

where $[k_{\|}, 0, \alpha_0(k_{\|})]$ is the wave propagation vector. Inserting this into Eq. (A.15) yields

$$\begin{aligned} P_{\text{inc}} = &-\frac{\omega a}{2} \Im \int_{-L_1/2}^{L_1/2} dx_1 \int_{-L_2/2}^{L_2/2} dx_2 \psi_{(\beta)}^* \exp\left[-ik_{\|}x_1 + i\alpha_0(k_{\|})x_3\right] \exp\left[i\omega t\right] \\ &(-i\alpha_0(k_{\|})) \exp\left[ik_{\|}x_1\right] \psi_{(\beta)} \exp\left[-i\alpha_0(k_{\|})x_3\right] \exp\left[-i\omega t\right] \\ = &\frac{\omega a \alpha_0(k_{\|})}{2} \Im i \int_{-L_1/2}^{L_1/2} dx_1 \int_{-L_2/2}^{L_2/2} dx_2 \underbrace{\psi_{(\beta)}^* \psi_{(\beta)}}_{=|\psi_{(\beta)}|^2} = \frac{1}{2} a\omega \left(\frac{\omega}{c}\right) L_1 L_2 \left|\psi_{(\beta)}\right|^2, \end{aligned} \tag{A.17}$$

where we note that $\psi_{(\beta)}$ denotes the wave amplitude which does not depend on $\mathbf{x}$ while ψ_{inc} *does*. In the last step above, we have replaced $\alpha_0(k_{\|})$ with ω/c in line with its definition in Eq. (4.1a) with only the wave vector component in the x_3-direction different from zero. Similarly, the total *reflected* energy flux in the same region is

$$\begin{aligned} P_{\text{refl}} &= \int dx_1 \int dx_2 \left\langle S_3 \right\rangle_{t;\text{ refl}} \\ &= \frac{\omega a}{2} \int_{-L_1/2}^{L_1/2} dx_1 \int_{-L_2/2}^{L_2/2} dx_2 \psi_{\text{refl}}^* \frac{\partial}{\partial x_3} \psi_{\text{refl}}, \end{aligned} \tag{A.18}$$

while the solution of the reflected wave is given by a continuous linear combination over the parallel component of the scattering wave vector $\mathbf{q}_{\|} = [q_{\|} \cos(\theta_s), q_{\|} \sin(\theta_s)]$ by

$$\psi_{\text{refl}} = \int \frac{dq_{\|}^2}{(2\pi)^2} R_{\alpha\beta}(\mathbf{q}_{\|}|\mathbf{k}_{\|}) \psi_{(\beta)} \exp\left[i\mathbf{q}_{\|} \cdot \mathbf{x}_{\|} + i\alpha_0(q_{\|})x_3\right] \exp\left[-i\omega t\right], \tag{A.19}$$

if we assume the scattered wave to be α-polarised with respect to the reflected plane of incidence. Inserted into Eq. (A.18), this reveals the reflected energy flux to be

---

[1] There is no loss of generality in making this choice of coordinates.

$$
\begin{aligned}
P_{\text{refl}} = {} & \frac{\omega a}{2}\Im \int_{-L_1/2}^{L_1/2} dx_1 \int_{-L_2/2}^{L_2/2} dx_2 \Bigg[\int \frac{d^2 q_\parallel}{(2\pi)^2} R^*_{\alpha\beta}(\mathbf{q}_\parallel|\mathbf{k}_\parallel)\psi^*_{(\beta)} \exp\left[-i\mathbf{q}_\parallel \cdot \mathbf{x}_\parallel - i\alpha_0(q_\parallel)x_3\right] \exp\left[i\omega t\right] \\
& \times \int \frac{d^2 q_\parallel'}{(2\pi)^2} (i\alpha_0(q_\parallel')) R_{\alpha\beta}(\mathbf{q}_\parallel'|\mathbf{k}_\parallel)\psi_{(\beta)} \exp\left[i\mathbf{q}_\parallel' \cdot \mathbf{x}_\parallel + i\alpha_0(q_\parallel')x_3\right] \exp\left[-i\omega t\right] \Bigg] \\
= {} & \frac{\omega a}{2}\Im \int \frac{d^2 q_\parallel}{(2\pi)^2} R^*_{\alpha\beta}(\mathbf{q}_\parallel|\mathbf{k}_\parallel)\psi^*_{(\beta)} \int \frac{d^2 q_\parallel'}{(2\pi)^2} (i\alpha_0(q_\parallel')) R_{\alpha\beta}(\mathbf{q}_\parallel'|\mathbf{k}_\parallel)\psi_{(\beta)} \\
& \times i\alpha_0(q_\parallel') \exp\left[i[\alpha_0(q_\parallel') - \alpha_0(q_\parallel)]x_3\right] \underbrace{\int d^2 x_\parallel \exp\left[i\mathbf{x}_\parallel \cdot [\mathbf{q}_\parallel - \mathbf{q}_\parallel']\right]}_{=(2\pi)^2\delta(\mathbf{q}_\parallel - \mathbf{q}_\parallel')},
\end{aligned}
\tag{A.20}
$$

which disposes of the integral over $q_\parallel'$ and finally leaves the expression

$$
\begin{aligned}
P_{\text{refl}} &= \frac{\omega a}{2}\Im \int \frac{d^2 q_\parallel}{(2\pi)^2} R^*_{\alpha\beta}(\mathbf{q}_\parallel|\mathbf{k}_\parallel) R_{\alpha\beta}(\mathbf{q}_\parallel|\mathbf{k}_\parallel)\psi^*_{(\beta)}\psi_{(\beta)} \times i\alpha_0(q_\parallel) \\
&= \frac{\omega a}{2}|\psi_{(\beta)}|^2 \int \frac{d^2 q_\parallel}{(2\pi)^2} \alpha_0(q_\parallel) \left|R_{\alpha\beta}(\mathbf{q}_\parallel|\mathbf{k}_\parallel)\right|^2 .
\end{aligned}
\tag{A.21}
$$

It is of interest to note that the final integral term of Eq. (A.20) requires $\mathbf{q}_\parallel = \mathbf{q}_\parallel'$, which if inserted leaves only an integral of a constant over a square region with area L_1L_2. Therefore, we have

$$
L_1L_2 = (2\pi)^2\delta(\mathbf{q}_\parallel - \mathbf{q}_\parallel'). \tag{A.22}
$$

If the area in question is not square, one could apply an appropriate integral measure, and replace L_1L_2 with a more general area A.

It is in our interest to express this as the sum of all solid scattering angle contributions, i.e. to write

$$
P_{\text{refl}} = \int d\Omega_{\text{s}} P_{\text{refl}}(\Omega_{\text{s}}). \tag{A.23}
$$

From the scattering geometry, we have that

$$
\mathbf{q}_\parallel = \left(\frac{\omega}{c}\right)\sin(\theta_{\text{s}})[\cos(\phi_{\text{s}}), \sin(\phi_{\text{s}})], \tag{A.24}
$$

implying that $\left(\frac{\omega}{c}\right)\sin(\theta_{\text{s}})$ is the in-plane vector magnitude, let's label it ρ, in the differential element $d^2 q_\parallel = \rho \cdot d\rho d\phi_{\text{s}}$ which means that

$$
d^2 q_\parallel = \left(\frac{\omega}{c}\right)^2 \cos(\theta_{\text{s}}) d\Omega_{\text{s}}, \tag{A.25}
$$

where $d\Omega_{\text{s}} = \sin(\theta_{\text{s}})d\theta_{\text{s}}d\phi_{\text{s}}$. Replacing the appropriate quantity in Eq. (A.21) with Eq. (A.25) leaves

$$
P_{\text{refl}}(\Omega_{\text{s}}) = \frac{\omega a}{2}|\psi_{(\beta)}|^2 \left(\frac{\omega}{c}\right)\left(\frac{\omega}{2\pi c}\right)^2 \cos^2(\theta_{\text{s}}) \left|R_{\alpha\beta}(\mathbf{q}_\parallel|\mathbf{k}_\parallel)\right|^2, \tag{A.26}
$$

to be the quantity defined by Eq. (A.23). In Eq. (A.26) we have replaced $\alpha_0(q_\parallel)$ with ω/c for the same reason as before.

Finally, let us define the differential reflection coefficient to be the fraction of the incident energy flux that is reflected into the solid angle element $d\Omega_\mathrm{s}$. In other words, by cancelling common terms in Eq. (A.17) and Eq. (A.26), then by definition

$$\frac{\partial R_{\alpha\beta}}{\partial\Omega_\mathrm{s}} := \frac{P_\text{refl}(\Omega_\mathrm{s})}{P_\text{inc}} = \frac{1}{L_1L_2}\left(\frac{\omega}{2\pi c}\right)^2 \frac{\cos^2(\theta_\mathrm{s})}{\cos(\theta_0)} \left|R_{\alpha\beta}(\mathbf{q}_\parallel|\mathbf{k}_\parallel)\right|^2 . \tag{A.27}$$

Obviously, only the reflectivity R depends on the specifics of the surface. Therefore, upon surface averaging the *mean differential reflection coefficient*, and performing the substitution $L_1L_2 \to A$ as discussed above, (MDRC) becomes

$$\left\langle \frac{\partial R_{\alpha\beta}}{\partial\Omega_\mathrm{s}} \right\rangle = \frac{1}{A}\left(\frac{\omega}{2\pi c}\right)^2 \frac{\cos^2(\theta_\mathrm{s})}{\cos(\theta_0)} \left\langle \left|R_{\alpha\beta}(\mathbf{q}_\parallel|\mathbf{k}_\parallel)\right|^2 \right\rangle . \tag{A.28}$$

Appendix B

Symmetric expansion of the second order scattering matrix

The term from Eq. (5.12) that contains $S^{(2)}_{\alpha\beta}$, let's name it S_2, looks like

$$\begin{aligned} S_2 = S^{(2)}_{\alpha\beta}(\mathbf{q}_\parallel|\mathbf{k}_\parallel) \int \frac{d^2p_\parallel}{(2\pi)^2} \frac{S^{(2)}_{\alpha\beta}(\mathbf{q}_\parallel|\mathbf{p}_\parallel|\mathbf{k}_\parallel)}{S^{(0)}_{\alpha\beta}(\mathbf{q}_\parallel|\mathbf{k}_\parallel)} \\ \times \int d^2x_\parallel \zeta(\mathbf{x}_\parallel) \exp\left[-i(\mathbf{q}_\parallel - \mathbf{p}_\parallel)\cdot\mathbf{x}_\parallel\right] \int d^2y_\parallel \zeta(\mathbf{y}_\parallel) \exp\left[-i(\mathbf{p}_\parallel - \mathbf{k}_\parallel)\cdot\mathbf{y}_\parallel\right]. \end{aligned} \tag{B.1}$$

We want to extract one of the integrals, along with one exponential factor that does not depend on $\mathbf{p}_\parallel$. The two linear variable transformations that facilitate this are

$$\mathbf{y}_\parallel = \mathbf{x}_\parallel - \mathbf{u}_\parallel \tag{B.2a}$$

$$\mathbf{x}_\parallel = \mathbf{y}_\parallel - \mathbf{v}_\parallel. \tag{B.2b}$$

The idea, following Ref. 15, is to perform each transformation on two equal components of S_2

$$S_2 = \underbrace{\frac{1}{2}S_2}_{\text{Use Eq. (B.2a)}} + \underbrace{\frac{1}{2}S_2}_{\text{Use Eq. (B.2b)}} := S_2^{[1]} + S_2^{[2]}, \tag{B.3}$$

where in the last step, the notation of square brackets have been introduced to notationally distinguish the terms. Then, we just insert

$$\begin{aligned}
S_2^{[1]} &= \frac{1}{2} S_{\alpha\beta}^{(0)}(\mathbf{q}_\| | \mathbf{k}_\|) \int \frac{d^2 p_\|}{(2\pi)^2} \frac{S_{\alpha\beta}^{(2)}(\mathbf{q}_\| | \mathbf{p}_\| | \mathbf{k}_\|)}{S_{\alpha\beta}^{(0)}(\mathbf{q}_\| | \mathbf{k}_\|)} \int d^2 x_\| \int d^2 u_\| \zeta(\mathbf{x}_\|) \zeta(\mathbf{x}_\| - \mathbf{u}_\|) \\
&\quad \times \exp\left[-i[(\mathbf{q}_\| - \mathbf{p}_\|) + (\mathbf{p}_\| - \mathbf{k}_\|)] \cdot \mathbf{x}_\|\right] \exp\left[i(\mathbf{p}_\| - \mathbf{k}_\|) \cdot \mathbf{u}_\|\right] \\
&= \frac{1}{2} S_{\alpha\beta}^{(0)}(\mathbf{q}_\| | \mathbf{k}_\|) \int d^2 x_\| \exp\left[-i(\mathbf{q}_\| - \mathbf{k}_\|) \cdot \mathbf{x}_\|\right] \int \frac{d^2 p_\|}{(2\pi)^2} \frac{S_{\alpha\beta}^{(2)}(\mathbf{q}_\| | \mathbf{p}_\| | \mathbf{k}_\|)}{S_{\alpha\beta}^{(0)}(\mathbf{q}_\| | \mathbf{k}_\|)} \\
&\quad \times \int d^2 u_\| \exp\left[i(\mathbf{p}_\| - \mathbf{k}_\|) \cdot \mathbf{u}_\|\right] \zeta(\mathbf{x}_\|) \zeta(\mathbf{x}_\| - \mathbf{u}_\|),
\end{aligned} \tag{B.4}$$

and

$$\begin{aligned}
S_2^{[2]} &= \frac{1}{2} S_{\alpha\beta}^{(0)}(\mathbf{q}_\| | \mathbf{k}_\|) \int \frac{d^2 p_\|}{(2\pi)^2} \frac{S_{\alpha\beta}^{(2)}(\mathbf{q}_\| | \mathbf{p}_\| | \mathbf{k}_\|)}{S_{\alpha\beta}^{(0)}(\mathbf{q}_\| | \mathbf{k}_\|)} \int d^2 v_\| \int d^2 y_\| \zeta(\mathbf{y}_\| - \mathbf{v}_\|) \zeta(\mathbf{y}_\|) \\
&\quad \times \exp\left[i(\mathbf{q}_\| - \mathbf{p}_\|) \cdot \mathbf{v}_\|\right] \exp\left[-i[(\mathbf{q}_\| - \mathbf{p}_\|) + (\mathbf{p}_\| - \mathbf{k}_\|)] \cdot \mathbf{y}_\|\right] \\
&= \frac{1}{2} S_{\alpha\beta}^{(0)}(\mathbf{q}_\| | \mathbf{k}_\|) \int d^2 y_\| \exp\left[-i(\mathbf{q}_\| - \mathbf{k}_\|) \cdot \mathbf{y}_\|\right] \int \frac{d^2 p_\|}{(2\pi)^2} \frac{S_{\alpha\beta}^{(2)}(\mathbf{q}_\| | \mathbf{p}_\| | \mathbf{k}_\|)}{S_{\alpha\beta}^{(0)}(\mathbf{q}_\| | \mathbf{k}_\|)} \\
&\quad \times \int d^2 v_\| \exp\left[i(\mathbf{q}_\| - \mathbf{p}_\|) \cdot \mathbf{v}_\|\right] \zeta(\mathbf{y}_\|) \zeta(\mathbf{y}_\| - \mathbf{v}_\|).
\end{aligned} \tag{B.5}$$

By changing the name of the integration variables in Eq. (B.5) by $\mathbf{y}_\| \to \mathbf{x}_\|$ and $\mathbf{v}_\| \to \mathbf{u}_\|$, we may sum up Eq. (B.4) and Eq. (B.5) to finally write

$$\begin{aligned}
S_2 &= \frac{1}{2} S_{\alpha\beta}^{(0)}(\mathbf{q}_\| | \mathbf{k}_\|) \int d^2 x_\| \exp\left[-i(\mathbf{q}_\| - \mathbf{k}_\|) \cdot \mathbf{x}_\|\right] \int \frac{d^2 p_\|}{(2\pi)^2} \frac{S_{\alpha\beta}^{(2)}(\mathbf{q}_\| | \mathbf{p}_\| | \mathbf{k}_\|)}{S_{\alpha\beta}^{(0)}(\mathbf{q}_\| | \mathbf{k}_\|)} \\
&\quad \times \int d^2 u_\| \Big\{ \exp\left[i(\mathbf{q}_\| - \mathbf{p}_\|) \cdot \mathbf{u}_\|\right] + \exp\left[i(\mathbf{p}_\| - \mathbf{k}_\|) \cdot \mathbf{u}_\|\right] \Big\} \zeta(\mathbf{x}_\|) \zeta(\mathbf{x}_\| - \mathbf{u}_\|).
\end{aligned} \tag{B.6}$$

Appendix C

Proof of expansion of the power spectrum

With the definition of the power spectrum of a isotropic correlation function W,

$$g(|\mathbf{Q}_{\|}|) = \int d^2u_{\|} W(u_{\|}) \exp\left[-i\mathbf{Q}_{\|} \cdot \mathbf{u}_{\|}\right] = \int d^2u_{\|} W(u_{\|}) \exp\left[-iQ_{\|}u_{\|}\cos(\phi_u - \phi_Q)\right], \tag{C.1}$$

and the Jacobian $d^2u_{\|} = u_{\|}du_{\|}d\phi_u$ of polar coordinates, we may write down the power spectrum as

$$\begin{aligned} g(|\mathbf{p}_{\|} - \mathbf{k}_{\|}|) &= \int d^2u_{\|} W(u_{\|}) \exp\left[-i\mathbf{p}_{\|} \cdot \mathbf{u}_{\|}\right] \exp\left[-i\mathbf{k}_{\|} \cdot \mathbf{u}_{\|}\right] \\ &= \int_0^\infty du_{\|}u_{\|}W(u_{\|}) \int_{-\pi}^{\pi} d\phi_u \exp\left[-ip_{\|}u_{\|}\cos(\phi_p - \phi_u)\right] \exp\left[ik_{\|}u_{\|}\cos(\phi_k - \phi_u)\right] \end{aligned} \tag{C.2}$$

The exponential functions of cosine-arguments may be replaced by the Jacobi-Anger-identity [52, 53]

$$\exp\left[iz\cos(\theta)\right] = \sum_{n=-\infty}^{\infty} i^n J_n(z) \exp\left[in\theta\right], \tag{C.3}$$

where $J_n(z)$ is the n-th Bessel function of the first kind with the argument z. The resulting expansion is

$$
\begin{aligned}
g(|\mathbf{p}_\| - \mathbf{k}_\||) = &\int_0^\infty du_\| u_\| W(u_\|) \int_{-\pi}^{\pi} d\phi_u \left[\sum_{m=-\infty}^{\infty} i^m J_m(-p_\| u_\|) \exp\left[im(\phi_u - \phi_p)\right]\right] \\
&\times \left[\sum_{n=-\infty}^{\infty} i^n J_n(k_\| u_\|) \exp\left[in(\phi_u - \phi_k)\right]\right] \\
= &\sum_{m=-\infty}^{\infty} \sum_{n=-\infty}^{\infty} i^{m+n} \exp\left[i(m\phi_p + n\phi_k)\right] \\
&\times \int_0^\infty du_\| u_\| W(u_\|) J_m(-p_\| u_\|) J_n(k_\| u_\|) \int_{-\pi}^{\pi} d\phi_u \exp\left[-i(m+n)\phi_u\right].
\end{aligned}
\tag{C.4}
$$

From physical considerations, we know that $\lim_{u_\| \to \infty} W(u_\|) = 0$, so the convergence properties of the integral should be sufficient to justify the switching of the sum and integral signs.

We now make use of the Bessel function property that $J_m(-z) = (-1)^m J_m(z)$ [52, 53], and the fact that

$$
\int_{-\pi}^{\pi} d\phi_u \exp\left[-i(m+n)\phi_u\right] = \frac{2}{m+n} \sin\left([m+n]\pi\right). \tag{C.5}
$$

Then,

$$
\begin{aligned}
g(|\mathbf{p}_\| - \mathbf{k}_\||) = 2\pi &\sum_{m=-\infty}^{\infty} \sum_{n=-\infty}^{\infty} (-1)^m i^{m+n} \exp\left[i(m\phi_p + n\phi_k)\right] \operatorname{sinc}(m+n) \\
&\times \int_0^\infty du_\| u_\| W(u_\|) J_m(p_\| u_\|) J_n(k_\| u_\|),
\end{aligned}
\tag{C.6}
$$

using the definition

$$
\operatorname{sinc}(x) := \frac{\sin(\pi x)}{\pi x}. \tag{C.7}
$$

Clearly, $\operatorname{sinc}(z) = 0 \; \forall z \in \mathbb{Z}$ except $z = 0$ for which it happens that $\operatorname{sinc}(0) = 1$. Therefore, only the terms where $n = -m$ contribute to the sum, and

$$
\begin{aligned}
g(|\mathbf{p}_\| - \mathbf{k}_\||) = 2\pi &\sum_{m=-\infty}^{\infty} (-1)^m i^{m+(-m)} \exp\left[im(\phi_p - \phi_k)\right] \\
&\times \int_0^\infty du_\| u_\| W(u_\|) J_m(p_\| u_\|) J_{-m}(k_\| u_\|).
\end{aligned}
\tag{C.8}
$$

By inserting another Bessel function relation, that $J_{-m}(z) = (-1)^m J_m(z)$ [52, 53], and changing the index name, we finally arrive at

$$
g(|\mathbf{p}_\| - \mathbf{k}_\||) = 2\pi \sum_{n=-\infty}^{\infty} \exp\left[in(\phi_p - \phi_k)\right] \int_0^\infty du_\| u_\| W(u_\|) J_n(p_\| u_\|) J_n(k_\| u_\|), \tag{C.9}
$$

which is the desired result. Expressed in terms L_n from Eq. (5.33) the power spectrum expansion becomes

$$g(|\mathbf{p}_\parallel - \mathbf{k}_\parallel|) = 2\pi \sum_{n=-\infty}^{\infty} \exp\left[in(\phi_p - \phi_k)\right] L_n(p_\parallel | k_\parallel). \tag{C.10}$$

Appendix D

Detailed calculation of the exponent factor of MDRC

There final expression for the incoherent MDRC consists of three parts that are multiplied. One of them is of the form $\exp\left[\tau_{\alpha\beta}(\mathbf{q}_{\|}|\mathbf{k}_{\|})\right]$ where

$$\tau_{\alpha\beta}(\mathbf{q}_{\|}|\mathbf{k}_{\|}) = \delta^2 \Re \int \frac{d^2p_{\|}}{(2\pi)^2} \left[g(\mathbf{q}_{\|}-\mathbf{p}_{\|}) + g(\mathbf{p}_{\|}-\mathbf{k}_{\|})\right] \frac{S^{(2)}_{\alpha\beta}(\mathbf{q}_{\|}|\mathbf{p}_{\|}|\mathbf{k}_{\|})}{S^{(0)}_{\alpha\beta}(\mathbf{q}_{\|}|\mathbf{k}_{\|})}, \tag{D.1}$$

where $\alpha\beta$ is the polarisation state, $g()$ is the power spectrum of the correlation function, and $S^{(n)}_{\alpha\beta}$ is the n-th order scattering matrix predicted by small-amplitude perturbation theory. In the following, it will be shown in detail how the angular part of the integral is extracted and performed, and how one arrives at the final expression for the exponent factor.

D.1 List of analytical angular integrals

For later convenience, an exhaustive list of the analytical integrals over the angular components that appear in the calculation of the exponent factor are provided. From the definitions of the exponent integral partial kernel $\sigma_{\alpha\beta}(\mathbf{q}_{\|}|\mathbf{p}_{\|}|\mathbf{k}_{\|})$ and the expansions of the power spectra $g(|\mathbf{q}_{\|}-\mathbf{p}_{\|}|)$ and $g(|\mathbf{p}_{\|}-\mathbf{k}_{\|}|)$ given in Appendix C, all possible dependencies of ϕ_p is captured by the terms

$$\begin{aligned}
[\hat{\mathbf{q}}_{\|}\cdot\hat{\mathbf{p}}_{\|}] &= \cos(\phi_p-\phi_q)\\
[\hat{\mathbf{p}}_{\|}\cdot\hat{\mathbf{k}}_{\|}] &= \cos(\phi_k-\phi_p)\\
[\hat{\mathbf{q}}_{\|}\times\hat{\mathbf{p}}_{\|}]_3 &= \sin(\phi_p-\phi_q)\\
[\hat{\mathbf{p}}_{\|}\times\hat{\mathbf{k}}_{\|}]_3 &= \sin(\phi_p-\phi_q)
\end{aligned}$$

$$\begin{aligned}
[\hat{\mathbf{q}}_{||} \cdot \hat{\mathbf{p}}_{||}][\hat{\mathbf{p}}_{||} \cdot \hat{\mathbf{k}}_{||}] &= \cos(\phi_p - \phi_q)\cos(\phi_k - \phi_p) \\
[\hat{\mathbf{q}}_{||} \cdot \hat{\mathbf{p}}_{||}][\hat{\mathbf{p}}_{||} \times \hat{\mathbf{k}}_{||}]_3 &= \cos(\phi_p - \phi_q)\sin(\phi_p - \phi_q) \\
[\hat{\mathbf{q}}_{||} \times \hat{\mathbf{p}}_{||}]_3[\hat{\mathbf{p}}_{||} \cdot \hat{\mathbf{k}}_{||}] &= \sin(\phi_p - \phi_q)\cos(\phi_k - \phi_p) \\
[\hat{\mathbf{q}}_{||} \times \hat{\mathbf{p}}_{||}]_3[\hat{\mathbf{p}}_{||} \times \hat{\mathbf{k}}_{||}]_3 &= \sin(\phi_p - \phi_q)\sin(\phi_p - \phi_q),
\end{aligned}$$

combined with the ϕ_p-dependent terms in the power spectrum expansions;

$$\begin{aligned}
\exp\left[in(\phi_q - \phi_p)\right] &= \cos(n(\phi_q - \phi_p)) + i\sin(n(\phi_q - \phi_p)) \\
\exp\left[in(\phi_p - \phi_k)\right] &= \cos(n(\phi_p - \phi_k)) + i\sin(n(\phi_p - \phi_k)),
\end{aligned}$$

where n is an integer.

All combinations of these two sets of expressions appear inside integrals over ϕ_p which may be performed analytically. All the following integrals were calculated with the wolfram language integral engine through variable substitutions $x = \phi_p - \phi_q$ or $y = \phi_p - \phi_k$. As may be verified, all the integrals vanish for most integer values of n as they depend linearly on factors such as $\sin(n\pi)$. The cases where the integrals are non-zero are distinguished by a vanishing fraction denominator for some n. Then, the expressions are evaluated by applying L'Hôpital's rule with respect to n. After some algebra, we calculate

$$\begin{aligned}
I_1[n] &= \int_{\pi}^{\pi} d\phi_p \cos(\phi_p - \phi_q) \exp\left[in(\phi_p - \phi_q)\right] \\
&= \pi \left\{\delta[n-1] + \delta[n+1]\right\} \\
I_2[n] &= \int_{-\pi}^{\pi} d\phi_p \cos(\phi_k - \phi_p) \exp\left[in(\phi_p - \phi_q)\right] \\
&= \pi \left\{\delta[n-1] \exp\left[i(\phi_k - \phi_q)\right] + \delta[n+1] \exp\left[-i(\phi_k - \phi_q)\right]\right\} \\
I_3[n] &= \int_{\pi}^{\pi} d\phi_p \sin(\phi_p - \phi_q) \exp\left[in(\phi_p - \phi_q)\right] \\
&= \pi \left\{i\delta[n-1] - i\delta[n+1]\right\} \\
I_4[n] &= \int_{-\pi}^{\pi} d\phi_p \sin(\phi_k - \phi_p) \exp\left[in(\phi_p - \phi_q)\right] \\
&= \pi \left\{-i\delta[n-1] \exp\left[i(\phi_k - \phi_q)\right] + i\delta[n+1] \exp\left[-i(\phi_k - \phi_q)\right]\right\} \\
I_5[n] &= \int_{-\pi}^{\pi} d\phi_p \cos(\phi_p - \phi_q) \cos(\phi_k - \phi_p) \exp\left[in(\phi_p - \phi_q)\right] \\
&= \pi \left\{\delta[n] \cos(\phi_k - \phi_q) + \frac{1}{2}\delta[n-2] \exp\left[i(\phi_k - \phi_q)\right] + \frac{1}{2}\delta[n+2] \exp\left[-i(\phi_k - \phi_q)\right]\right\} \\
I_6[n] &= \int_{-\pi}^{\pi} d\phi_p \cos(\phi_p - \phi_q) \sin(\phi_k - \phi_p) \exp\left[in(\phi_p - \phi_q)\right] \\
&= \pi \left\{\delta[n] \sin(\phi_k - \phi_q) - \frac{i}{2}\delta[n-2] \exp\left[i(\phi_k - \phi_q)\right] + \frac{i}{2}\delta[n+2] \exp\left[i(\phi_k - \phi_q)\right]\right\} \\
I_7[n] &= \int_{-\pi}^{\pi} d\phi_p \sin(\phi_p - \phi_q) \cos(\phi_k - \phi_p) \exp\left[in(\phi_p - \phi_q)\right] \\
&= \pi \left\{\delta[n] \sin(\phi_k - \phi_q) + \frac{i}{2}\delta[n-2] \exp\left[i(\phi_k - \phi_q)\right] - \frac{i}{2}\delta[n+2] \exp\left[-i(\phi_k - \phi_q)\right]\right\} \\
I_8[n] &= \int_{-\pi}^{\pi} d\phi_p \sin(\phi_p - \phi_q) \sin(\phi_k - \phi_p) \exp\left[in(\phi_p - \phi_q)\right] \\
&= \pi \left\{-\cos(\phi_k - \phi_q)\delta[n] + \frac{1}{2}\delta[n-2] \exp\left[i(\phi_k - \phi_q)\right] + \frac{1}{2}\delta[n+2] \exp\left[-i(\phi_k - \phi_q)\right]\right\},
\end{aligned}$$

and

$$
\begin{aligned}
I_9[n] &= \int_{-\pi}^{\pi} d\phi_p \cos(\phi_p - \phi_q) \exp\left[in(\phi_k - \phi_p)\right] \\
&= \pi \left\{ \delta[n-1] \exp\left[i(\phi_k - \phi_q)\right] + \delta[n+1] \exp\left[-i(\phi_k - \phi_q)\right] \right\} \\
I_{10}[n] &= \int_{-\pi}^{\pi} d\phi_p \cos(\phi_k - \phi_p) \exp\left[in(\phi_k - \phi_p)\right] \\
&= \pi \left\{ \delta[n-1] + \delta[n+1] \right\} \\
I_{11}[n] &= \int_{-\pi}^{\pi} d\phi_p \sin(\phi_p - \phi_q) \exp\left[in(\phi_k - \phi_p)\right] \\
&= \pi \left\{ -i\delta[n-1] \exp\left[i(\phi_k - \phi_q)\right] + i\delta[n+1] \exp\left[-i(\phi_k - \phi_q)\right] \right\} \\
I_{12}[n] &= \int_{-\pi}^{\pi} d\phi_p \sin(\phi_k - \phi_p) \exp\left[in(\phi_k - \phi_p)\right] \\
&= \pi \left\{ i\delta[n-1] - i\delta[n+1] \right\} \\
I_{13}[n] &= \int_{-\pi}^{\pi} d\phi_p \cos(\phi_p - \phi_q) \cos(\phi_k - \phi_p) \exp\left[in(\phi_k - \phi_p)\right] \\
&= \pi \left\{ \delta[n] \cos(\phi_k - \phi_q) + \frac{1}{2}\delta[n-2] \exp\left[i(\phi_k - \phi_q)\right] + \frac{1}{2}\delta[n+2] \exp\left[-i(\phi_k - \phi_q)\right] \right\} \\
I_{14}[n] &= \int_{-\pi}^{\pi} d\phi_p \cos(\phi_p - \phi_q) \sin(\phi_k - \phi_p) \exp\left[in(\phi_k - \phi_p)\right] \\
&= \pi \left\{ \delta[n] \sin(\phi_k - \phi_q) + \frac{i}{2}\delta[n-2] \exp\left[i(\phi_k - \phi_q)\right] - \frac{i}{2}\delta[n+2] \exp\left[-i(\phi_k - \phi_q)\right] \right\} \\
I_{15}[n] &= \int_{-\pi}^{\pi} d\phi_p \sin(\phi_p - \phi_q) \cos(\phi_k - \phi_p) \exp\left[in(\phi_k - \phi_p)\right] \\
&= \pi \left\{ \delta[n] \sin(\phi_k - \phi_q) - \frac{i}{2}\delta[n-2] \exp\left[i(\phi_k - \phi_q)\right] + \frac{i}{2}\delta[n+2] \exp\left[-i(\phi_k - \phi_q)\right] \right\} \\
I_{16}[n] &= \int_{-\pi}^{\pi} d\phi_p \sin(\phi_p - \phi_q) \sin(\phi_k - \phi_p) \exp\left[in(\phi_k - \phi_p)\right] \\
&= \pi \left\{ -\delta[n] \cos(\phi_k - \phi_q) + \frac{1}{2}\delta[n-2] \exp\left[i(\phi_k - \phi_q)\right] + \frac{1}{2}\delta[n+2] \exp\left[-i(\phi_k - \phi_q)\right] \right\},
\end{aligned}
$$

as well as

$$
\begin{aligned}
I_{17}[n] &= \int_{\pi}^{\pi} d\phi_p \exp\left[in(\phi_p - \phi_q)\right] = 2\pi\delta[n] \\
I_{18}[n] &= \int_{\pi}^{\pi} d\phi_p \exp\left[in(\phi_k - \phi_p)\right] = 2\pi\delta[n].
\end{aligned}
$$

In the equations above, square bracket function arguments $f[]$ has been used to indicate that the functions domain is the set of integers. As such, $\delta[n]$ is the discrete Dirac δ function defined by

$$
\delta[n] = \begin{cases} 1 & \text{if } n = 0, \\ 0 & \text{if } n \in \mathbb{Z} \neq 0. \end{cases} \tag{D.2}
$$

D.2 Calculation of the pp-component

From Eqs. (4.16) and (5.9) we have that

$$
\begin{aligned}
S_{pp}^{(2)}(\mathbf{q}_\parallel|\mathbf{p}_\parallel|\mathbf{k}_\parallel) = \sqrt{\frac{\alpha_0(q_\parallel)}{\alpha_0(k_\parallel)}} \Bigg\{ & \frac{2\alpha_0(k_\parallel)}{d_p(q_\parallel)d_p(k_\parallel)} \frac{1}{2} \Bigg(\frac{\varepsilon-1}{\varepsilon^2}[q_\parallel k_\parallel - \alpha(q_\parallel)[\hat{\mathbf{q}}_\parallel \cdot \hat{\mathbf{k}}_\parallel]\alpha(k_\parallel)][\alpha(q_\parallel)+\alpha(k_\parallel)] \\
& + 2\left(\frac{\varepsilon-1}{\varepsilon}\right)^2 \frac{1}{\varepsilon}\alpha(q_\parallel)[\hat{\mathbf{q}}_\parallel \cdot \hat{\mathbf{p}}_\parallel]\alpha(p_\parallel)[\hat{\mathbf{p}}_\parallel \cdot \hat{\mathbf{k}}_\parallel]\alpha(k_\parallel) \Bigg) \\
& - \frac{2\alpha_0(k_\parallel)}{d_p(q_\parallel)d_p(k_\parallel)} \left[\frac{\nu_{pp}(\mathbf{q}_\parallel|\mathbf{p}_\parallel)\nu_{pp}(\mathbf{p}_\parallel|\mathbf{k}_\parallel)}{d_p(p_\parallel)} + \frac{\nu_{ps}(\mathbf{q}_\parallel|\mathbf{p}_\parallel)\nu_{sp}(\mathbf{p}_\parallel|\mathbf{k}_\parallel)}{d_s(p_\parallel)} \right] \Bigg\},
\end{aligned}
$$

which gives rise to some simplifications of the desired quantity, namely

$$
\begin{aligned}
\frac{S_{pp}^{(2)}(\mathbf{q}_\parallel|\mathbf{p}_\parallel|\mathbf{k}_\parallel)}{S_{pp}^{(0)}(\mathbf{q}_\parallel|\mathbf{k}_\parallel)} = \frac{-2\sqrt{\alpha_0(q_\parallel)\alpha_0(k_\parallel)}}{\nu_{pp}(\mathbf{q}_\parallel|\mathbf{k}_\parallel)} \Bigg\{ & \frac{1}{2}\frac{\varepsilon-1}{\varepsilon^2} \Bigg(\Big[q_\parallel k_\parallel - \alpha(q_\parallel)[\hat{\mathbf{q}}_\parallel \cdot \hat{\mathbf{k}}_\parallel]\alpha(k_\parallel)\Big] \Big[\alpha(q_\parallel)+\alpha(k_\parallel)\Big] \\
& + 2\frac{\varepsilon-1}{\varepsilon}\alpha(q_\parallel)[\hat{\mathbf{q}}_\parallel \cdot \hat{\mathbf{p}}_\parallel]\alpha(p_\parallel)[\hat{\mathbf{p}}_\parallel \cdot \hat{\mathbf{k}}_\parallel]\alpha(k_\parallel) \Bigg) \\
& - \frac{1}{d_p(p_\parallel)} \left(\frac{\varepsilon-1}{\varepsilon^2}\right)^2 \Big[\varepsilon q_\parallel p_\parallel - \alpha(q_\parallel)[\hat{\mathbf{q}}_\parallel \cdot \hat{\mathbf{p}}_\parallel]\alpha(p_\parallel)\Big] \Big[\varepsilon p_\parallel k_\parallel - \alpha(p_\parallel)[\hat{\mathbf{p}}_\parallel \cdot \hat{\mathbf{k}}_\parallel]\alpha(k_\parallel)\Big] \\
& - \frac{1}{d_s(p_\parallel)} \left(-\frac{\varepsilon-1}{\varepsilon}\right)^2 \alpha(q_\parallel)[\hat{\mathbf{q}}_\parallel \times \hat{\mathbf{p}}_\parallel]_3[\hat{\mathbf{p}}_\parallel \times \hat{\mathbf{k}}_\parallel]_3\alpha(k_\parallel) \Bigg\} \\
= -2\frac{\varepsilon-1}{\varepsilon^2}\frac{\sqrt{\alpha_0(q_\parallel)\alpha_0(k_\parallel)}}{\nu_{pp}(\mathbf{q}_\parallel|\mathbf{k}_\parallel)} \Bigg\{ & \frac{1}{2}\Big[q_\parallel k_\parallel - \alpha(q_\parallel)[\hat{\mathbf{q}}_\parallel \cdot \hat{\mathbf{k}}_\parallel]\alpha(k_\parallel)\Big] \Big[\alpha(q_\parallel)+\alpha(k_\parallel)\Big] \\
& + \frac{\varepsilon-1}{\varepsilon}\alpha(q_\parallel)\alpha(p_\parallel)\alpha(k_\parallel)[\hat{\mathbf{q}}_\parallel \cdot \hat{\mathbf{p}}_\parallel][\hat{\mathbf{p}}_\parallel \cdot \hat{\mathbf{k}}_\parallel] \\
& - \frac{1}{d_p(p_\parallel)}\frac{\varepsilon-1}{\varepsilon^2}\Big[\varepsilon^2 q_\parallel p_\parallel^2 k_\parallel - \varepsilon q_\parallel p_\parallel \alpha(p_\parallel)[\hat{\mathbf{p}}_\parallel \cdot \hat{\mathbf{k}}_\parallel]\alpha(k_\parallel) \\
& - \varepsilon p_\parallel k_\parallel \alpha(q_\parallel)[\hat{\mathbf{q}}_\parallel \cdot \hat{\mathbf{p}}_\parallel]\alpha(p_\parallel) + \alpha(q_\parallel)\alpha(p_\parallel)^2\alpha(k_\parallel)[\hat{\mathbf{q}}_\parallel \cdot \hat{\mathbf{p}}_\parallel][\hat{\mathbf{p}}_\parallel \cdot \hat{\mathbf{k}}_\parallel]\Big] \\
& - \frac{\varepsilon-1}{d_s(p_\parallel)}\left(\frac{\omega}{c}\right)^2 \alpha(q_\parallel)\alpha(k_\parallel)[\hat{\mathbf{q}}_\parallel \times \hat{\mathbf{p}}_\parallel]_3[\hat{\mathbf{p}}_\parallel \times \hat{\mathbf{k}}_\parallel]_3 \Bigg\}.
\end{aligned}
$$

Inserting the power spectrum expansions from Eq. (5.32) in the full exponent integral, we find that

$$
\begin{aligned}
\tau_{pp} = \delta^2\Re - 2\frac{\varepsilon-1}{\varepsilon^2}\frac{\sqrt{\alpha_0(q_\parallel)\alpha_0(k_\parallel)}}{\nu_{pp}(\mathbf{q}_\parallel|\mathbf{k}_\parallel)}\Bigg\{ & \frac{1}{2}\Big[q_\parallel k_\parallel - \alpha(q_\parallel)[\hat{\mathbf{q}}_\parallel\cdot\hat{\mathbf{k}}_\parallel]\alpha(k_\parallel)\Big]\Big[\alpha(q_\parallel)+\alpha(k_\parallel)\Big] \\
& \times\Bigg[\underbrace{\int\frac{d^2p_\parallel}{(2\pi)^2}g(|\mathbf{q}_\parallel-\mathbf{p}_\parallel|)}_{=1}+\underbrace{\int\frac{d^2p_\parallel}{(2\pi)^2}g(|\mathbf{p}_\parallel-\mathbf{k}_\parallel|)}_{=1}\Bigg] \\
& +\int_0^\infty dp_\parallel\frac{p_\parallel}{2\pi}\int_{-\pi}^{\pi}d\phi_p\Bigg[\frac{\varepsilon-1}{\varepsilon}\alpha(q_\parallel)\alpha(p_\parallel)\alpha(k_\parallel)\left(1-\frac{\alpha(p_\parallel)}{\varepsilon d_p(p_\parallel)}\right)\cos(\phi_p-\phi_q)\cos(\phi_k-\phi_p) \\
& -\frac{\varepsilon-1}{d_p(p_\parallel)}q_\parallel p_\parallel^2 k_\parallel+\frac{\varepsilon-1}{\varepsilon}\frac{\alpha(p_\parallel)}{d_p(p_\parallel)}\alpha(k_\parallel)q_\parallel p_\parallel\cos(\phi_k-\phi_p) \\
& +\frac{\varepsilon-1}{\varepsilon}\frac{\alpha(p_\parallel)}{d_p(p_\parallel)}\alpha(q_\parallel)p_\parallel k_\parallel\cos(\phi_p-\phi_q)-\frac{\varepsilon-1}{d_s(p_\parallel)}\left(\frac{\omega}{c}\right)^2\alpha(q_\parallel)\alpha(k_\parallel)\sin(\phi_p-\phi_q)\sin(\phi_k-\phi_p)\Bigg] \\
& \times\Bigg[\sum_{n=-\infty}^{\infty}\exp\left[in(\phi_p-\phi_q)\right]L_n(q_\parallel|p_\parallel)+\sum_{m=-\infty}^{\infty}\exp\left[im(\phi_k-\phi_p)\right]L_m(p_\parallel|k_\parallel)\Bigg]\Bigg\},
\end{aligned}
$$

where $L_n(q_\parallel|k_\parallel)$ is as defined by Eq. (5.33). We insert the fact that

$$
1-\frac{\alpha(p_\parallel)}{\varepsilon d_p(p_\parallel)}=\frac{\varepsilon\left[\alpha_0(p_\parallel)+\frac{\alpha(p_\parallel)}{\varepsilon}\right]-\alpha(p_\parallel)}{\varepsilon d_p(p_\parallel)}=\frac{\alpha_0(p_\parallel)}{d_p(p_\parallel)}, \tag{D.3}
$$

and note that the exponent may be expressed in terms of the helper integrals in Appendix D.1;

$$
\begin{aligned}
\tau_{pp} = \delta^2\Re - 2\frac{\varepsilon-1}{\varepsilon^2}\frac{\sqrt{\alpha_0(q_\parallel)\alpha_0(k_\parallel)}}{\nu_{pp}(\mathbf{q}_\parallel|\mathbf{k}_\parallel)}\Bigg\{ & \Big[q_\parallel k_\parallel - \alpha(q_\parallel)[\hat{\mathbf{q}}_\parallel\cdot\hat{\mathbf{k}}_\parallel]\alpha(k_\parallel)\Big]\Big[\alpha(q_\parallel)+\alpha(k_\parallel)\Big] \\
& +\int_0^\infty dp_\parallel\frac{p_\parallel}{2\pi}\Bigg(\frac{\varepsilon-1}{\varepsilon}\alpha(q_\parallel)\alpha(p_\parallel)\alpha(k_\parallel)\frac{\alpha_0(p_\parallel)}{d_p(p_\parallel)}\Bigg[\sum_n I_5[n]L_n(q_\parallel|p_\parallel)+\sum_m I_{13}[m]L_m(p_\parallel|k_\parallel)\Bigg] \\
& -\frac{\varepsilon-1}{d_p(p_\parallel)}q_\parallel p_\parallel^2 k_\parallel\Bigg[\sum_n I_{17}[n]L_n(q_\parallel|p_\parallel)+\sum_m I_{18}[m]L_m(p_\parallel|k_\parallel)\Bigg] \\
& +\frac{\varepsilon-1}{\varepsilon}\frac{\alpha(p_\parallel)}{d_p(p_\parallel)}\alpha(k_\parallel)q_\parallel p_\parallel\Bigg[\sum_n I_2[n]L_n(q_\parallel|p_\parallel)+\sum_m I_{10}[m]L_m(p_\parallel|k_\parallel)\Bigg] \\
& +\frac{\varepsilon-1}{\varepsilon}\frac{\alpha(p_\parallel)}{d_p(p_\parallel)}\alpha(q_\parallel)p_\parallel k_\parallel\Bigg[\sum_n I_1[n]L_n(q_\parallel|p_\parallel)+\sum_m I_9[m]L_m(p_\parallel|k_\parallel)\Bigg] \\
& -\frac{\varepsilon-1}{d_s(p_\parallel)}\left(\frac{\omega}{c}\right)^2\alpha(q_\parallel)\alpha(k_\parallel)\Bigg[\sum_n I_8[n]L_n(q_\parallel|p_\parallel)+\sum_m I_{16}[m]L_m(p_\parallel|k_\parallel)\Bigg]\Bigg)\Bigg\}.
\end{aligned}
$$

The integrals $I_r[n]$ only contribute for the $n=0$, $n=\pm1$ and $n=\pm2$-terms. Because $L_n(q_\parallel|k_\parallel)=L_{-n}(q_\parallel|k_\parallel)$, we may write the exponent only in terms of the non-negative

n-terms. Then, by insertion,

$$
\begin{aligned}
\tau_{pp} = \delta^2\Re - \frac{\varepsilon-1}{\varepsilon^2}\frac{\sqrt{\alpha_0(q_\parallel)\alpha_0(k_\parallel)}}{\nu_{pp}(\mathbf{q}_\parallel|\mathbf{k}_\parallel)}\Bigg\{ & 2\Big[q_\parallel k_\parallel - \alpha(q_\parallel)[\hat{\mathbf{q}}_\parallel\cdot\hat{\mathbf{k}}_\parallel]\alpha(k_\parallel)\Big]\Big[\alpha(q_\parallel)+\alpha(k_\parallel)\Big] \\
& + \int_0^\infty dp_\parallel p_\parallel \frac{\varepsilon-1}{\varepsilon}\Bigg(\alpha(q_\parallel)\alpha(p_\parallel)\alpha(k_\parallel)\frac{\alpha_0(p_\parallel)}{d_p(p_\parallel)} \\
& \times\Bigg[\cos(\phi_k-\phi_q)L_0(q_\parallel|p_\parallel) + \frac{1}{2}\Big\{\exp\left[i(\phi_k-\phi_q)\right] + \exp\left[-i(\phi_k-\phi_q)\right]\Big\}L_2(q_\parallel|p_\parallel) \\
& + \cos(\phi_k-\phi_q)L_0(p_\parallel|k_\parallel) + \frac{1}{2}\Big\{\exp\left[i(\phi_k-\phi_q)\right] + \exp\left[-i(\phi_k-\phi_q)\right]\Big\}L_2(p_\parallel|k_\parallel)\Bigg] \\
& - \frac{\varepsilon-1}{d_p(p_\parallel)}q_\parallel p_\parallel^2 k_\parallel\Bigg[2L_0(q_\parallel|p_\parallel) + 2L_0(p_\parallel|k_\parallel)\Bigg] \\
& + \frac{\varepsilon-1}{\varepsilon}\frac{\alpha(p_\parallel)}{d_p(p_\parallel)}\alpha(k_\parallel)q_\parallel p_\parallel\Bigg[\Big\{\exp\left[i(\phi_k-\phi_q)\right] + \exp\left[-i(\phi_k-\phi_q)\right]\Big\}L_1(q_\parallel|p_\parallel) + 2L_1(p_\parallel|k_\parallel)\Bigg] \\
& + \frac{\varepsilon-1}{\varepsilon}\frac{\alpha(p_\parallel)}{d_p(p_\parallel)}\alpha(q_\parallel)p_\parallel k_\parallel\Bigg[2L_1(q_\parallel|p_\parallel) + \Big\{\exp\left[i(\phi_k-\phi_q)\right] + \exp\left[-i(\phi_k-\phi_q)\right]\Big\}L_1(p_\parallel|k_\parallel)\Bigg] \\
& + -\frac{\varepsilon-1}{d_s(p_\parallel)}\left(\frac{\omega}{c}\right)^2\alpha(q_\parallel)\alpha(k_\parallel) \\
& \times\Bigg[-\cos(\phi_k-\phi_q)L_0(q_\parallel|p_\parallel) + \frac{1}{2}\Big\{\exp\left[i(\phi_k-\phi_q)\right] + \exp\left[-i(\phi_k-\phi_q)\right]\Big\}L_2(q_\parallel|p_\parallel) \\
& - \cos(\phi_k-\phi_q)L_0(p_\parallel|k_\parallel) + \frac{1}{2}\Big\{\exp\left[i(\phi_k-\phi_q)\right] + \exp\left[-i(\phi_k-\phi_q)\right]\Big\}L_2(p_\parallel|k_\parallel)\Bigg]\Bigg)\Bigg\}.
\end{aligned}
$$

Making use of the familiar identities (the latter of which will only become useful for the later components)

$$\cos(x) = \frac{\exp\left[ix\right] + \exp\left[-ix\right]}{2} \qquad \text{(D.4)} \qquad \sin(x) = \frac{\exp\left[ix\right] - \exp\left[-ix\right]}{2i}, \qquad \text{(D.5)}$$

and re-introducing the notation

$$\cos(\phi_k-\phi_q) = [\hat{\mathbf{q}}_\parallel\cdot\hat{\mathbf{k}}_\parallel] \qquad \text{(D.6)} \qquad \sin(\phi_k-\phi_q) = [\hat{\mathbf{q}}_\parallel\times\hat{\mathbf{k}}_\parallel]_3 \qquad \text{(D.7)}$$

and simplifying the factor $\frac{\varepsilon-1}{\varepsilon^2}$ from $\nu_{pp}(\mathbf{q}_\parallel|\mathbf{k}_\parallel)$ we can finally write down

$$
\begin{aligned}
\tau_{pp} = &-\delta^2 \Re \frac{\sqrt{\alpha_0(q_\parallel)\alpha_0(k_\parallel)}}{\varepsilon q_\parallel k_\parallel - \alpha(q_\parallel)[\hat{\mathbf{q}}_\parallel \cdot \hat{\mathbf{k}}_\parallel]\alpha(k_\parallel)} \Bigg\{ 2\Big[q_\parallel k_\parallel - \alpha(q_\parallel)[\hat{\mathbf{q}}_\parallel \cdot \hat{\mathbf{k}}_\parallel]\alpha(k_\parallel)\Big]\Big[\alpha(q_\parallel)+\alpha(k_\parallel)\Big] \\
&+ \int_0^\infty dp_\parallel p_\parallel \frac{\varepsilon-1}{\varepsilon} \Bigg(\Bigg[\alpha(q_\parallel)[\hat{\mathbf{q}}_\parallel \cdot \hat{\mathbf{k}}_\parallel]\alpha(k_\parallel) \Bigg\{ \frac{\alpha_0(p_\parallel)\alpha(p_\parallel)}{d_p(p_\parallel)} + \frac{\varepsilon}{d_s(p_\parallel)}\left(\frac{\omega}{c}\right)^2 \Bigg\} - \frac{2\varepsilon}{d_p(p_\parallel)} q_\parallel p_\parallel^2 k_\parallel \Bigg] \\
&\times \Bigg[L_0(q_\parallel|p_\parallel) + L_0(p_\parallel|k_\parallel) \Bigg] \\
&+ \Bigg[2p_\parallel \frac{\alpha(p_\parallel)}{d_p(p_\parallel)} \Bigg\{ q_\parallel \alpha(k_\parallel)[\hat{\mathbf{q}}_\parallel \cdot \hat{\mathbf{k}}_\parallel] + \alpha(q_\parallel)k_\parallel \Bigg\} \Bigg] L_1(q_\parallel|p_\parallel) \\
&+ \Bigg[2p_\parallel \frac{\alpha(p_\parallel)}{d_p(p_\parallel)} \Bigg\{ q_\parallel \alpha(k_\parallel) + \alpha(q_\parallel)k_\parallel[\hat{\mathbf{q}}_\parallel \cdot \hat{\mathbf{k}}_\parallel] \Bigg\} \Bigg] L_1(p_\parallel|k_\parallel) \\
&+ \Bigg[\alpha(q_\parallel)[\hat{\mathbf{q}}_\parallel \cdot \hat{\mathbf{k}}_\parallel]\alpha(k_\parallel) \Bigg\{ \frac{\alpha_0(p_\parallel)\alpha(p_\parallel)}{d_p(p_\parallel)} - \frac{\varepsilon}{d_s(p_\parallel)}\left(\frac{\omega}{c}\right)^2 \Bigg\} \Bigg] \Bigg[L_2(q_\parallel|p_\parallel) + L_2(p_\parallel|k_\parallel) \Bigg] \Bigg) \Bigg\}.
\end{aligned}
\tag{D.8}
$$

The symbol $\Re$ signifies the real component of its (complex) argument, and the notation is assumed to operate on all of the terms and factors succeeding it, and not merely the first set of parentheses.

D.3 Calculation of the ps-component

From Eqs. (4.16) and (5.9) we have that

$$
\begin{aligned}
S_{ps}^{(2)}(\mathbf{q}_\parallel|\mathbf{p}_\parallel|\mathbf{k}_\parallel) = &\sqrt{\frac{\alpha_0(q_\parallel)}{\alpha_0(k_\parallel)}} \Bigg\{ \frac{2\alpha_0(k_\parallel)}{d_p(q_\parallel)d_s(k_\parallel)} \frac{1}{2} \Bigg(\nu_{ps}(\mathbf{q}_\parallel|\mathbf{k}_\parallel)\Big[\alpha(q_\parallel)+\alpha(k_\parallel)\Big] \\
&+ 2\left(\frac{\varepsilon-1}{\varepsilon}\right)^2 \left(\frac{\omega}{c}\right) \alpha(q_\parallel)[\hat{\mathbf{q}}_\parallel \cdot \hat{\mathbf{p}}_\parallel]\alpha(p_\parallel)[\hat{\mathbf{p}}_\parallel \times \hat{\mathbf{k}}_\parallel]_3 \Bigg) \\
&- \frac{2\alpha_0(k_\parallel)}{d_p(q_\parallel)d_s(k_\parallel)} \left[\frac{\nu_{pp}(\mathbf{q}_\parallel|\mathbf{p}_\parallel)\nu_{ps}(\mathbf{p}_\parallel|\mathbf{k}_\parallel)}{d_p(p_\parallel)} + \frac{\nu_{ps}(\mathbf{q}_\parallel|\mathbf{p}_\parallel)\nu_{ss}(\mathbf{p}_\parallel|\mathbf{k}_\parallel)}{d_s(p_\parallel)} \right] \Bigg\}.
\end{aligned}
$$

This gives rise to some simplifications in the desired quantity

$$
\begin{aligned}
\frac{S_{ps}^{(2)}(\mathbf{q}_\parallel|\mathbf{p}_\parallel|\mathbf{k}_\parallel)}{S_{ps}^{(0)}(\mathbf{q}_\parallel|\mathbf{k}_\parallel)} = &\frac{-2\sqrt{\alpha_0(q_\parallel)\alpha_0(k_\parallel)}}{\nu_{ps}(\mathbf{q}_\parallel|\mathbf{k}_\parallel)} \Bigg\{ \frac{1}{2}\nu_{ps}(\mathbf{q}_\parallel|\mathbf{k}_\parallel)\Big[\alpha(q_\parallel)+\alpha(k_\parallel)\Big] \\
&+ \left(\frac{\varepsilon-1}{\varepsilon}\right)^2 \left(\frac{\omega}{c}\right) \alpha(q_\parallel)[\hat{\mathbf{q}}_\parallel \cdot \hat{\mathbf{p}}_\parallel]\alpha(p_\parallel)[\hat{\mathbf{p}}_\parallel \times \hat{\mathbf{k}}_\parallel]_3 \\
&- \frac{1}{d_p(p_\parallel)} \left(\frac{\varepsilon-1}{\varepsilon^2}\right) \left(-\frac{\varepsilon-1}{\varepsilon}\right) \left(\frac{\omega}{c}\right) \Big[\varepsilon q_\parallel p_\parallel - \alpha(q_\parallel)[\hat{\mathbf{q}}_\parallel \cdot \hat{\mathbf{p}}_\parallel]\alpha(p_\parallel)\Big]\alpha(p_\parallel)[\hat{\mathbf{p}}_\parallel \times \hat{\mathbf{k}}_\parallel]_3 \\
&- \frac{1}{d_s(p_\parallel)} \left(\frac{\varepsilon-1}{\varepsilon}\right) \left(\frac{\omega}{c}\right) [\hat{\mathbf{q}}_\parallel \times \hat{\mathbf{p}}_\parallel]_3 \alpha(q_\parallel)(\varepsilon-1) \left(\frac{\omega}{c}\right)^2 [\hat{\mathbf{p}}_\parallel \cdot \hat{\mathbf{k}}_\parallel] \Bigg\}
\end{aligned}
$$

$$
\begin{aligned}
&= \frac{-2\sqrt{\alpha_0(q_\parallel)\alpha_0(k_\parallel)}}{\nu_{ps}(\mathbf{q}_\parallel|\mathbf{k}_\parallel)}\Bigg\{\frac{1}{2}\nu_{ps}(\mathbf{q}_\parallel|\mathbf{k}_\parallel)\Big[\alpha(q_\parallel)+\alpha(k_\parallel)\Big] + \left(-\frac{\varepsilon-1}{\varepsilon}\right)\left(\frac{\omega}{c}\right)\alpha(q_\parallel) \\
&\times \Bigg[\left(-\frac{\varepsilon-1}{\varepsilon}\right)\alpha(p_\parallel)[\hat{\mathbf{q}}_\parallel\cdot\hat{\mathbf{p}}_\parallel][\hat{\mathbf{p}}_\parallel\times\hat{\mathbf{k}}_\parallel]_3 \\
&- \frac{1}{d_p(p_\parallel)}\left(\frac{\varepsilon-1}{\varepsilon^2}\right)\varepsilon q_\parallel p_\parallel\frac{\alpha(p_\parallel)}{\alpha(q_\parallel)}[\hat{\mathbf{p}}_\parallel\times\hat{\mathbf{k}}_\parallel]_3 \\
&+ \frac{1}{d_p(p_\parallel)}\left(\frac{\varepsilon-1}{\varepsilon^2}\right)\alpha(p_\parallel)^2[\hat{\mathbf{q}}_\parallel\cdot\hat{\mathbf{p}}_\parallel][\hat{\mathbf{p}}_\parallel\times\hat{\mathbf{k}}_\parallel]_3 \\
&- \frac{\varepsilon-1}{d_s(p_\parallel)}\left(\frac{\omega}{c}\right)^2[\hat{\mathbf{q}}_\parallel\times\hat{\mathbf{p}}_\parallel]_3[\hat{\mathbf{p}}_\parallel\cdot\hat{\mathbf{k}}_\parallel]\Bigg]\Bigg\}.
\end{aligned}
$$

Inserting the power spectrum expansions from Eq. (5.32) in the full exponent integral, we find that

$$
\begin{aligned}
\tau_{ps} &= \delta^2\Re\frac{-2\sqrt{\alpha_0(q_\parallel)\alpha_0(k_\parallel)}}{\nu_{ps}(\mathbf{q}_\parallel|\mathbf{k}_\parallel)}\Bigg\{\frac{1}{2}\nu_{ps}(\mathbf{q}_\parallel|\mathbf{k}_\parallel)\Big[\alpha(q_\parallel)+\alpha(k_\parallel)\Big] \\
&\times\Bigg[\underbrace{\int\frac{d^2p_\parallel}{(2\pi)^2}g(|\mathbf{q}_\parallel-\mathbf{p}_\parallel|)}_{=1}+\underbrace{\int\frac{d^2p_\parallel}{(2\pi)^2}g(|\mathbf{p}_\parallel-\mathbf{k}_\parallel|)}_{=1}\Bigg] \\
&+\left(-\frac{\varepsilon-1}{\varepsilon}\right)\left(\frac{\omega}{c}\right)\alpha(q_\parallel)\int_0^\infty dp_\parallel\frac{p_\parallel}{2\pi}\int_{-\pi}^{\pi}d\phi_p\Bigg[\Bigg(-\frac{\varepsilon-1}{\varepsilon}\alpha(p_\parallel)+\frac{1}{d_p(p_\parallel)}\frac{\varepsilon-1}{\varepsilon^2}\alpha(p_\parallel)^2\Bigg) \\
&\times\cos(\phi_p-\phi_q)\sin(\phi_k-\phi_p)-\frac{1}{d_p(p_\parallel)}\frac{\varepsilon-1}{\varepsilon}q_\parallel p_\parallel\frac{\alpha(p_\parallel)}{\alpha(q_\parallel)}\sin(\phi_k-\phi_p) \\
&-\frac{\varepsilon-1}{d_s(p_\parallel)}\left(\frac{\omega}{c}\right)^2\sin(\phi_p-\phi_q)\cos(\phi_k-\phi_p)\Bigg] \\
&\times\Bigg[\sum_{n=-\infty}^{\infty}\exp\left[in(\phi_p-\phi_q)\right]L_n(q_\parallel|p_\parallel)+\sum_{m=-\infty}^{\infty}\exp\left[im(\phi_k-\phi_p)\right]L_m(p_\parallel|k_\parallel)\Bigg]\Bigg\},
\end{aligned}
$$

and further inserting the helper integrals from Appendix D.1 where applicable, whence

$$
\begin{aligned}
\tau_{ps} &= \delta^2\Re\frac{-2\sqrt{\alpha_0(q_\parallel)\alpha_0(k_\parallel)}}{\nu_{ps}(\mathbf{q}_\parallel|\mathbf{k}_\parallel)}\Bigg\{\nu_{ps}(\mathbf{q}_\parallel|\mathbf{k}_\parallel)\Big[\alpha(q_\parallel)+\alpha(k_\parallel)\Big]-\frac{1}{2\pi}\left(-\frac{\varepsilon-1}{\varepsilon}\right)\left(\frac{\omega}{c}\right)\alpha(q_\parallel) \\
&\times\int_0^\infty dp_\parallel p_\parallel\Bigg[\frac{\varepsilon-1}{\varepsilon}\alpha(p_\parallel)\underbrace{\left(1-\frac{\alpha(p_\parallel)}{\varepsilon d_p(p_\parallel)}\right)}_{=\alpha_0(p_\parallel)/d_p(p_\parallel)}\Bigg[\sum_n I_6[n]L_n(q_\parallel|p_\parallel)+\sum_m I_{14}[m]L_m(p_\parallel|k_\parallel)\Bigg] \\
&+\frac{1}{d_p(p_\parallel)}\frac{\varepsilon-1}{\varepsilon}q_\parallel p_\parallel\frac{\alpha(p_\parallel)}{\alpha(q_\parallel)}\Bigg[\sum_n I_4[n]L_n(q_\parallel|p_\parallel)+\sum_m I_{12}[m]L_m(p_\parallel|k_\parallel)\Bigg] \\
&+\frac{\varepsilon-1}{d_s(p_\parallel)}\left(\frac{\omega}{c}\right)^2\Bigg[\sum_n I_7[n]L_n(q_\parallel|p_\parallel)+\sum_m I_{15}[m]L_m(p_\parallel|k_\parallel)\Bigg]\Bigg]\Bigg\}
\end{aligned}
$$

$$
\begin{aligned}
&= \delta^2 \Re \frac{-2\sqrt{\alpha_0(q_\parallel)\alpha_0(k_\parallel)}}{\nu_{ps}(\mathbf{q}_\parallel|\mathbf{k}_\parallel)} \Bigg\{ \nu_{ps}(\mathbf{q}_\parallel|\mathbf{k}_\parallel)\Big[\alpha(q_\parallel)+\alpha(k_\parallel)\Big] - \frac{1}{2}\left(-\frac{\varepsilon-1}{\varepsilon}\right)\left(\frac{\omega}{c}\right)\alpha(q_\parallel)\int_0^\infty dp_\parallel p_\parallel \\
&\quad \times \Bigg[\frac{\varepsilon-1}{\varepsilon}\frac{\alpha(p_\parallel)\alpha_0(p_\parallel)}{d_p(p_\parallel)}\Bigg[\sin(\phi_k-\phi_q)L_0(q_\parallel|p_\parallel) - \frac{i}{2}\Big\{\exp\left[i(\phi_k-\phi_q)\right]-\exp\left[-i(\phi_k-\phi_q)\right]\Big\}L_2(q_\parallel|p_\parallel) \\
&\quad + \sin(\phi_k-\phi_q)L_0(p_\parallel|k_\parallel) + \frac{i}{2}\Big\{\exp\left[i(\phi_k-\phi_q)\right]-\exp\left[-i(\phi_k-\phi_q)\right]\Big\}L_2(p_\parallel|k_\parallel)\Bigg] \\
&\quad + \frac{1}{d_p(p_\parallel)}\frac{\varepsilon-1}{\varepsilon}q_\parallel p_\parallel \frac{\alpha(p_\parallel)}{\alpha(q_\parallel)}\Bigg[-i\Big\{\exp\left[i(\phi_k-\phi_q)\right]-\exp\left[-i(\phi_k-\phi_q)\right]\Big\}L_1(q_\parallel|p_\parallel)\Bigg] \\
&\quad + \frac{\varepsilon-1}{d_s(p_\parallel)}\left(\frac{\omega}{c}\right)^2\Bigg[\sin(\phi_k-\phi_q)L_0(q_\parallel|p_\parallel) + \frac{i}{2}\Big\{\exp\left[i(\phi_k-\phi_q)-\exp\left[-i(\phi_k-\phi_q)\right]\right]\Big\}L_2(q_\parallel|p_\parallel) \\
&\quad + \sin(\phi_k-\phi_q)L_0(p_\parallel|k_\parallel) - \frac{i}{2}\Big\{\exp\left[i(\phi_k-\phi_q)\right]-\exp\left[i(\phi_k-\phi_q)\right]\Big\}L_2(p_\parallel|k_\parallel)\Bigg]\Bigg]\Bigg\},
\end{aligned}
$$

where the relation $L_{-n}() = L_n()$ has been applied. Using Eqs. (D.4)–(D.7) and Eq. (5.7b) we may write

$$
\begin{aligned}
\tau_{ps} &= \delta^2 \Re \frac{-2\sqrt{\alpha_0(q_\parallel)\alpha_0(k_\parallel)}}{\nu_{ps}(\mathbf{q}_\parallel|\mathbf{k}_\parallel)} \Bigg\{ \nu_{ps}(\mathbf{q}_\parallel|\mathbf{k}_\parallel)\Big[\alpha(q_\parallel)+\alpha(k_\parallel)\Big] - \frac{1}{2}\nu_{ps}(\mathbf{q}_\parallel|\mathbf{k}_\parallel)\int_0^\infty dp_\parallel p_\parallel \\
&\quad \times \Bigg[\Bigg[\frac{\varepsilon-1}{\varepsilon}\frac{\alpha_0(p_\parallel)\alpha(p_\parallel)}{d_p(p_\parallel)} + \frac{\varepsilon-1}{d_s(p_\parallel)}\left(\frac{\omega}{c}\right)^2\Bigg]\Bigg[L_0(\mathbf{q}_\parallel|\mathbf{p}_\parallel) + L_0(\mathbf{p}_\parallel|\mathbf{k}_\parallel)\Bigg] \\
&\quad + \Bigg[\frac{\varepsilon-1}{\varepsilon}\frac{2q_\parallel p_\parallel}{d_p(p_\parallel)}\frac{\alpha(p_\parallel)}{\alpha(q_\parallel)}\Bigg]L_1(\mathbf{q}_\parallel|\mathbf{p}_\parallel) \\
&\quad + \Bigg[\frac{\varepsilon-1}{\varepsilon}\frac{\alpha_0(p_\parallel)\alpha(p_\parallel)}{d_p(p_\parallel)} - \frac{\varepsilon-1}{d_s(p_\parallel)}\left(\frac{\omega}{c}\right)^2\Bigg]\Bigg[L_2(\mathbf{q}_\parallel|\mathbf{p}_\parallel) - L_2(\mathbf{p}_\parallel|\mathbf{k}_\parallel)\Bigg]\Bigg]\Bigg\},
\end{aligned}
$$

or; finally,

$$
\begin{aligned}
\tau_{ps} &= \delta^2 \Re \sqrt{\alpha_0(q_\parallel)\alpha_0(k_\parallel)}\Bigg\{-2\Big[\alpha(q_\parallel)+\alpha(k_\parallel)\Big] + \frac{\varepsilon-1}{\varepsilon}\int_0^\infty dp_\parallel p_\parallel \\
&\quad \times \Bigg[\Bigg[\frac{\alpha_0(p_\parallel)\alpha(p_\parallel)}{d_p(p_\parallel)} + \frac{\varepsilon}{d_s(p_\parallel)}\left(\frac{\omega}{c}\right)^2\Bigg]\Bigg[L_0(\mathbf{q}_\parallel|\mathbf{p}_\parallel) + L_0(\mathbf{p}_\parallel|\mathbf{k}_\parallel)\Bigg] \\
&\quad + \Bigg[\frac{2q_\parallel p_\parallel}{d_p(p_\parallel)}\frac{\alpha(p_\parallel)}{\alpha(q_\parallel)}\Bigg]L_1(\mathbf{q}_\parallel|\mathbf{p}_\parallel) \\
&\quad + \Bigg[\frac{\alpha_0(p_\parallel)\alpha(p_\parallel)}{d_p(p_\parallel)} - \frac{\varepsilon}{d_s(p_\parallel)}\left(\frac{\omega}{c}\right)^2\Bigg]\Bigg[L_2(\mathbf{q}_\parallel|\mathbf{p}_\parallel) - L_2(\mathbf{p}_\parallel|\mathbf{k}_\parallel)\Bigg]\Bigg]\Bigg\}.
\end{aligned}
\tag{D.9}
$$

D.4 Calculation of the sp-component

From Eqs. (4.16) and (5.9) we have that

$$
\begin{aligned}
S^{(2)}_{sp}(\mathbf{q}_\parallel|\mathbf{p}_\parallel|\mathbf{k}_\parallel) = \sqrt{\frac{\alpha_0(q_\parallel)}{\alpha_0(k_\parallel)}}\Bigg\{ & \frac{2\alpha_0(k_\parallel)}{d_s(q_\parallel)d_p(k_\parallel)}\frac{1}{2}\Big(\nu_{sp}(\mathbf{q}_\parallel|\mathbf{k}_\parallel)\Big[\alpha(q_\parallel)+\alpha(k_\parallel)\Big] \\
& + 2\left(\frac{\varepsilon-1}{\varepsilon}\right)^2\left(\frac{\omega}{c}\right)[\hat{\mathbf{q}}_\parallel\times\hat{\mathbf{p}}_\parallel]_3\alpha(p_\parallel)[\hat{\mathbf{p}}_\parallel\cdot\hat{\mathbf{k}}_\parallel]\alpha(k_\parallel)\Big) \\
& - \frac{2\alpha_0(k_\parallel)}{d_s(q_\parallel)d_p(k_\parallel)}\left[\frac{\nu_{sp}(\mathbf{q}_\parallel|\mathbf{p}_\parallel)\nu_{pp}(\mathbf{p}_\parallel|\mathbf{k}_\parallel)}{d_p(p_\parallel)}+\frac{\nu_{ss}(\mathbf{q}_\parallel|\mathbf{p}_\parallel)\nu_{sp}(\mathbf{p}_\parallel|\mathbf{k}_\parallel)}{d_s(p_\parallel)}\right]\Bigg\}.
\end{aligned}
$$

This gives rise to some simplifications in the desired quantity

$$
\begin{aligned}
\frac{S^{(2)}_{sp}(\mathbf{q}_\parallel|\mathbf{p}_\parallel|\mathbf{k}_\parallel)}{S^{(0)}_{sp}(\mathbf{q}_\parallel|\mathbf{k}_\parallel)} = & \frac{-2\sqrt{\alpha_0(q_\parallel)\alpha_0(k_\parallel)}}{\nu_{sp}(\mathbf{q}_\parallel|\mathbf{k}_\parallel)}\Bigg\{\frac{1}{2}\nu_{sp}(\mathbf{q}_\parallel|\mathbf{k}_\parallel)\Big[\alpha(q_\parallel)+\alpha(k_\parallel)\Big] \\
& + \left(\frac{\varepsilon-1}{\varepsilon}\right)^2\left(\frac{\omega}{c}\right)[\hat{\mathbf{q}}_\parallel\times\hat{\mathbf{p}}_\parallel]_3\alpha(p_\parallel)[\hat{\mathbf{p}}_\parallel\cdot\hat{\mathbf{k}}_\parallel]\alpha(k_\parallel) \\
& - \frac{1}{d_p(p_\parallel)}\left(-\frac{\varepsilon-1}{\varepsilon}\right)\left(\frac{\omega}{c}\right)[\hat{\mathbf{q}}_\parallel\times\hat{\mathbf{p}}_\parallel]_3\alpha(p_\parallel)\left(\frac{\varepsilon-1}{\varepsilon^2}\right)\Big[\varepsilon p_\parallel k_\parallel-\alpha(p_\parallel)[\hat{\mathbf{p}}_\parallel\cdot\hat{\mathbf{k}}_\parallel]\alpha(k_\parallel)\Big] \\
& - \frac{1}{d_s(p_\parallel)}(\varepsilon-1)\left(\frac{\omega}{c}\right)^2[\hat{\mathbf{q}}_\parallel\cdot\hat{\mathbf{p}}_\parallel]\left(-\frac{\varepsilon-1}{\varepsilon}\right)\left(\frac{\omega}{c}\right)[\hat{\mathbf{p}}_\parallel\times\hat{\mathbf{k}}_\parallel]_3\alpha(k_\parallel)\Bigg\} \\
= & \frac{-2\sqrt{\alpha_0(q_\parallel)\alpha_0(k_\parallel)}}{\nu_{sp}(\mathbf{q}_\parallel|\mathbf{k}_\parallel)}\Bigg\{\frac{1}{2}\nu_{sp}(\mathbf{q}_\parallel|\mathbf{k}_\parallel)\Big[\alpha(q_\parallel)+\alpha(k_\parallel)\Big]+\left(-\frac{\varepsilon-1}{\varepsilon}\right)\left(\frac{\omega}{c}\right)\alpha(k_\parallel) \\
& \times\Bigg[\Bigg\{\left(-\frac{\varepsilon-1}{\varepsilon}\right)\alpha(p_\parallel)+\frac{1}{d_p(p_\parallel)}\left(\frac{\varepsilon-1}{\varepsilon^2}\right)\alpha(p_\parallel)^2\Bigg\}[\hat{\mathbf{q}}_\parallel\times\hat{\mathbf{p}}_\parallel]_3[\hat{\mathbf{p}}_\parallel\cdot\hat{\mathbf{k}}_\parallel] \\
& - \frac{1}{d_p(p_\parallel)}\left(\frac{\varepsilon-1}{\varepsilon^2}\right)\varepsilon p_\parallel k_\parallel\frac{\alpha(p_\parallel)}{\alpha(k_\parallel)}[\hat{\mathbf{q}}_\parallel\times\hat{\mathbf{p}}_\parallel]_3 \\
& - \frac{\varepsilon-1}{d_s(p_\parallel)}\left(\frac{\omega}{c}\right)^2[\hat{\mathbf{q}}_\parallel\cdot\hat{\mathbf{p}}_\parallel][\hat{\mathbf{p}}_\parallel\times\hat{\mathbf{k}}_\parallel]_3\Bigg]\Bigg\}.
\end{aligned}
$$

Inserting the power spectrum expansions from Eq. (5.32) in the full exponent integral, we find that

$$
\begin{aligned}
\tau_{sp} = \delta^2\Re\frac{-2\sqrt{\alpha_0(q_\parallel)\alpha_0(k_\parallel)}}{\nu_{sp}(\mathbf{q}_\parallel|\mathbf{k}_\parallel)}\Bigg\{ & \frac{1}{2}\nu_{sp}(\mathbf{q}_\parallel|\mathbf{k}_\parallel)\Big[\alpha(q_\parallel)+\alpha(k_\parallel)\Big] \\
\times\Bigg[& \underbrace{\int\frac{d^2p_\parallel}{(2\pi)^2}g(|\mathbf{q}_\parallel-\mathbf{p}_\parallel|)}_{=1}+\underbrace{\int\frac{d^2p_\parallel}{(2\pi)^2}g(|\mathbf{p}_\parallel-\mathbf{k}_\parallel|)}_{=1}\Bigg] \\
+ \left(-\frac{\varepsilon-1}{\varepsilon}\right)\left(\frac{\omega}{c}\right)\alpha(k_\parallel) & \int_0^\infty dp_\parallel\frac{p_\parallel}{2\pi}\int_{-\pi}^{\pi}d\phi_p\Bigg[\left(-\frac{\varepsilon-1}{\varepsilon}\right)\alpha(p_\parallel)\Bigg\{\underbrace{1-\frac{\alpha(p_\parallel)}{\varepsilon d_p(p_\parallel)}}_{=\alpha_0(p_\parallel)/d_p(p_\parallel)}\Bigg\}
\end{aligned}
$$

$$
\begin{aligned}
&\times \sin(\phi_p-\phi_q)\cos(\phi_k-\phi_p) - \frac{1}{d_p(p_\parallel)}\frac{\varepsilon-1}{\varepsilon}p_\parallel k_\parallel \frac{\alpha(p_\parallel)}{\alpha(k_\parallel)}\sin(\phi_p-\phi_q) \\
&- \frac{\varepsilon-1}{d_s(p_\parallel)}\left(\frac{\omega}{c}\right)^2 \cos(\phi_p-\phi_q)\sin(\phi_k-\phi_p)\Bigg] \\
&\times \Bigg[\sum_{n=-\infty}^{\infty}\exp\left[in(\phi_p-\phi_q)\right]L_n(q_\parallel|p_\parallel) + \sum_{m=-\infty}^{\infty}\exp\left[im(\phi_k-\phi_p)\right]L_m(p_\parallel|k_\parallel)\Bigg]\Bigg\},
\end{aligned}
$$

and further inserting the helper integrals from Appendix D.1 where applicable, whence

$$
\begin{aligned}
\tau_{sp} &= \delta^2\Re\frac{-2\sqrt{\alpha_0(q_\parallel)\alpha_0(k_\parallel)}}{\nu_{sp}(\mathbf{q}_\parallel|\mathbf{k}_\parallel)}\Bigg\{\nu_{sp}(\mathbf{q}_\parallel|\mathbf{k}_\parallel)\Big[\alpha(q_\parallel)+\alpha(k_\parallel)\Big] \\
&\quad - \frac{1}{2\pi}\left(-\frac{\varepsilon-1}{\varepsilon}\right)\left(\frac{\omega}{c}\right)\alpha(k_\parallel)\int_0^\infty dp_\parallel p_\parallel \\
&\quad \times \Bigg[\frac{\varepsilon-1}{\varepsilon}\alpha(p_\parallel)\frac{\alpha_0(p_\parallel)}{d_p(p_\parallel)}\Bigg[\sum_n I_7[n]L_n(q_\parallel|p_\parallel) + \sum_m I_{15}[m]L_m(p_\parallel|k_\parallel)\Bigg] \\
&\quad + \frac{1}{d_p(p_\parallel)}\frac{\varepsilon-1}{\varepsilon}p_\parallel k_\parallel\frac{\alpha(p_\parallel)}{\alpha(k_\parallel)}\Bigg[\sum_n I_3[n]L_n(q_\parallel|p_\parallel) + \sum_m I_{11}[m]L_m(p_\parallel|k_\parallel)\Bigg] \\
&\quad + \frac{\varepsilon-1}{d_s(p_\parallel)}\left(\frac{\omega}{c}\right)^2\Bigg[\sum_n I_7[n]L_n(q_\parallel|p_\parallel) + \sum_m I_{15}[m]L_m(p_\parallel|k_\parallel)\Bigg]\Bigg]\Bigg\} \\
&= \delta^2\Re\frac{-2\sqrt{\alpha_0(q_\parallel)\alpha_0(k_\parallel)}}{\nu_{sp}(\mathbf{q}_\parallel|\mathbf{k}_\parallel)}\Bigg\{\nu_{sp}(\mathbf{q}_\parallel|\mathbf{k}_\parallel)\Big[\alpha(q_\parallel)+\alpha(k_\parallel)\Big] \\
&\quad - \frac{1}{2}\left(-\frac{\varepsilon-1}{\varepsilon}\right)\left(\frac{\omega}{c}\right)\alpha(k_\parallel)\int_0^\infty dp_\parallel p_\parallel\Bigg[\frac{1}{d_p(p_\parallel)}\frac{\varepsilon-1}{\varepsilon}p_\parallel k_\parallel\frac{\alpha(p_\parallel)}{\alpha(k_\parallel)} \\
&\quad \times\Bigg[\sin(\phi_k-\phi_q)L_0(q_\parallel|p_\parallel) + \frac{i}{2}\Big\{\exp\left[i(\phi_k-\phi_q) - \exp\left[-i(\phi_k-\phi_q)\right]\right]\Big\}L_2(q_\parallel|p_\parallel) \\
&\quad + \sin(\phi_k-\phi_q)L_0(p_\parallel|k_\parallel) - \frac{i}{2}\Big\{\exp\left[i(\phi_k-\phi_q)\right] - \exp\left[i(\phi_k-\phi_q)\right]\Big\}L_2(p_\parallel|k_\parallel)\Bigg] \\
&\quad + \frac{1}{d_p(p_\parallel)}\frac{\varepsilon-1}{\varepsilon}p_\parallel k_\parallel\frac{\alpha(p_\parallel)}{\alpha(k_\parallel)}\Bigg[-i\Big\{\exp\left[i(\phi_k-\phi_q)\right] - \exp\left[-i(\phi_k-\phi_q)\right]\Big\}L_1(p_\parallel|k_\parallel)\Bigg] \\
&\quad + \frac{\varepsilon-1}{d_s(p_\parallel)}\left(\frac{\omega}{c}\right)^2 \\
&\quad \times\Bigg[\sin(\phi_k-\phi_q)L_0(q_\parallel|p_\parallel) - \frac{i}{2}\Big\{\exp\left[i(\phi_k-\phi_q)\right] - \exp\left[-i(\phi_k-\phi_q)\right]\Big\}L_2(q_\parallel|p_\parallel) \\
&\quad + \sin(\phi_k-\phi_q)L_0(p_\parallel|k_\parallel) + \frac{i}{2}\Big\{\exp\left[i(\phi_k-\phi_q)\right] - \exp\left[-i(\phi_k-\phi_q)\right]\Big\}L_2(p_\parallel|k_\parallel)\Bigg]\Bigg]\Bigg\},
\end{aligned}
$$

where the relation $L_{-n}() = L_n()$ has been applied. Using Eqs. (D.4)–(D.7) and the

Eq. (5.7c) we may write

$$
\begin{aligned}
\tau_{sp} = \delta^2 \Re \frac{-2\sqrt{\alpha_0(q_\parallel)\alpha_0(k_\parallel)}}{\nu_{sp}(\mathbf{q}_\parallel|\mathbf{k}_\parallel)} & \Bigg\{ \nu_{sp}(\mathbf{q}_\parallel|\mathbf{k}_\parallel)\Big[\alpha(q_\parallel)+\alpha(k_\parallel)\Big] - \frac{1}{2}\nu_{sp}(\mathbf{q}_\parallel|\mathbf{k}_\parallel)\int_0^\infty dp_\parallel p_\parallel \\
& \times \left[\left[\frac{\varepsilon-1}{\varepsilon}\alpha(p_\parallel)\frac{\alpha_0(p_\parallel)}{d_p(p_\parallel)} + \frac{\varepsilon-1}{d_s(p_\parallel)}\left(\frac{\omega}{c}\right)^2\right]\Big[L_0(\mathbf{q}_\parallel|\mathbf{p}_\parallel)+L_0(\mathbf{p}_\parallel|\mathbf{k}_\parallel)\Big]\right. \\
& + \left[\frac{2p_\parallel k_\parallel}{d_p(p_\parallel)}\frac{\varepsilon-1}{\varepsilon}\frac{\alpha(p_\parallel)}{\alpha(k_\parallel)}\right]L_1(\mathbf{p}_\parallel|\mathbf{k}_\parallel) \\
& \left. + \left[\frac{\varepsilon-1}{\varepsilon}\alpha(p_\parallel)\frac{\alpha_0(p_\parallel)}{d_p(p_\parallel)} - \frac{\varepsilon-1}{d_s(p_\parallel)}\left(\frac{\omega}{c}\right)^2\right]\Big[L_2(\mathbf{q}_\parallel|\mathbf{p}_\parallel)-L_2(\mathbf{p}_\parallel|\mathbf{k}_\parallel)\Big]\right]\Bigg\},
\end{aligned}
$$

or; finally,

$$
\begin{aligned}
\tau_{sp} = \delta^2 \Re \sqrt{\alpha_0(q_\parallel)\alpha_0(k_\parallel)} & \Bigg\{ -2\Big[\alpha(q_\parallel)+\alpha(k_\parallel)\Big] + \frac{\varepsilon-1}{\varepsilon}\int_0^\infty dp_\parallel p_\parallel \\
& \times \left[\left[\alpha(p_\parallel)\frac{\alpha_0(p_\parallel)}{d_p(p_\parallel)} + \frac{\varepsilon}{d_s(p_\parallel)}\left(\frac{\omega}{c}\right)^2\right]\Big[L_0(\mathbf{q}_\parallel|\mathbf{p}_\parallel)+L_0(\mathbf{p}_\parallel|\mathbf{k}_\parallel)\Big]\right. \\
& + \left[\frac{2p_\parallel k_\parallel}{d_p(p_\parallel)}\frac{\alpha(p_\parallel)}{\alpha(k_\parallel)}\right]L_1(\mathbf{p}_\parallel|\mathbf{k}_\parallel) \\
& \left. + \left[\alpha(p_\parallel)\frac{\alpha_0(p_\parallel)}{d_p(p_\parallel)} - \frac{\varepsilon}{d_s(p_\parallel)}\left(\frac{\omega}{c}\right)^2\right]\Big[L_2(\mathbf{q}_\parallel|\mathbf{p}_\parallel)-L_2(\mathbf{p}_\parallel|\mathbf{k}_\parallel)\Big]\right]\Bigg\}.
\end{aligned}
\tag{D.10}
$$

D.5 Calculation of the ss-component

From Eqs. (4.16) and (5.9) we have that

$$
\begin{aligned}
S_{ss}^{(2)}(\mathbf{q}_\parallel|\mathbf{p}_\parallel|\mathbf{k}_\parallel) = \sqrt{\frac{\alpha_0(q_\parallel)}{\alpha_0(k_\parallel)}} & \Bigg\{ \frac{2\alpha_0(k_\parallel)}{d_s(q_\parallel)d_s(k_\parallel)}\frac{1}{2}\bigg(\nu_{ss}(\mathbf{q}_\parallel|\mathbf{k}_\parallel)\Big[\alpha(q_\parallel)+\alpha(k_\parallel)\Big] \\
& + 2\varepsilon\left(\frac{\omega}{c}\right)^2[\hat{\mathbf{q}}_\parallel\times\hat{\mathbf{p}}_\parallel]_3\alpha(p_\parallel)[\hat{\mathbf{p}}_\parallel\times\hat{\mathbf{k}}_\parallel]_3\bigg) \\
& - \frac{2\alpha_0(k_\parallel)}{d_s(q_\parallel)d_s(k_\parallel)}\left[\frac{\nu_{sp}(\mathbf{q}_\parallel|\mathbf{p}_\parallel)\nu_{ps}(\mathbf{p}_\parallel|\mathbf{k}_\parallel)}{d_p(p_\parallel)} + \frac{\nu_{ss}(\mathbf{q}_\parallel|\mathbf{p}_\parallel)\nu_{ss}(\mathbf{p}_\parallel|\mathbf{k}_\parallel)}{d_s(p_\parallel)}\right]\Bigg\}.
\end{aligned}
$$

This gives rise to some simplifications in the desired quantity

$$\begin{aligned}\frac{S_{ss}^{(2)}(\mathbf{q}_\parallel|\mathbf{p}_\parallel|\mathbf{k}_\parallel)}{S_{ss}^{(0)}(\mathbf{q}_\parallel|\mathbf{k}_\parallel)} = \frac{-2\sqrt{\alpha_0(q_\parallel)\alpha_0(k_\parallel)}}{\nu_{ss}(\mathbf{q}_\parallel|\mathbf{k}_\parallel)}&\bigg\{\frac{1}{2}\nu_{ss}(\mathbf{q}_\parallel|\mathbf{k}_\parallel)\Big[\alpha(q_\parallel)+\alpha(k_\parallel)\Big]\\ &+\varepsilon\left(\frac{\omega}{c}\right)^2\alpha(p_\parallel)[\hat{\mathbf{q}}_\parallel\times\hat{\mathbf{p}}_\parallel]_3[\hat{\mathbf{p}}_\parallel\times\hat{\mathbf{k}}_\parallel]_3\\ &-\frac{1}{d_p(p_\parallel)}\left(-\frac{\varepsilon-1}{\varepsilon}\right)^2\left(\frac{\omega}{c}\right)^2\alpha(p_\parallel)^2[\hat{\mathbf{q}}_\parallel\times\hat{\mathbf{p}}_\parallel]_3[\hat{\mathbf{p}}_\parallel\times\hat{\mathbf{k}}_\parallel]_3\\ &-\frac{1}{d_s(p_\parallel)}(\varepsilon-1)^2\left(\frac{\omega}{c}\right)^4[\hat{\mathbf{q}}_\parallel\cdot\hat{\mathbf{p}}_\parallel][\hat{\mathbf{p}}_\parallel\cdot\hat{\mathbf{k}}_\parallel]\bigg\}.\end{aligned}$$

Inserting the power spectrum expansions from Eq. (5.32) in the full exponent integral, we find that

$$\begin{aligned}\tau_{ss} = \delta^2\Re\frac{-2\sqrt{\alpha_0(q_\parallel)\alpha_0(k_\parallel)}}{\nu_{ss}(\mathbf{q}_\parallel|\mathbf{k}_\parallel)}&\bigg\{\frac{1}{2}\nu_{ss}(\mathbf{q}_\parallel|\mathbf{k}_\parallel)\Big[\alpha(q_\parallel)+\alpha(k_\parallel)\Big]\\ &\times\Bigg[\underbrace{\int\frac{d^2p_\parallel}{(2\pi)^2}g(|\mathbf{q}_\parallel-\mathbf{p}_\parallel|)}_{=1}+\underbrace{\int\frac{d^2p_\parallel}{(2\pi)^2}g(|\mathbf{p}_\parallel-\mathbf{k}_\parallel|)}_{=1}\Bigg]\\ &+(\varepsilon-1)\left(\frac{\omega}{c}\right)^2\int_0^\infty dp_\parallel\frac{p_\parallel}{2\pi}\int_{-\pi}^{\pi}d\phi_p\Bigg[\left(\frac{\varepsilon}{\varepsilon-1}\alpha(p_\parallel)-\frac{1}{d_p(p_\parallel)}\frac{\varepsilon-1}{\varepsilon^2}\alpha(p_\parallel)^2\right)\\ &\times\sin(\phi_p-\phi_q)\sin(\phi_k-\phi_p)-\frac{\varepsilon-1}{d_s(p_\parallel)}\left(\frac{\omega}{c}\right)^2\cos(\phi_p-\phi_q)\cos(\phi_k-\phi_p)\Bigg]\\ &\times\Bigg[\sum_{n=-\infty}^{\infty}\exp\left[in(\phi_p-\phi_q)\right]L_n(q_\parallel|p_\parallel)+\sum_{m=-\infty}^{\infty}\exp\left[im(\phi_k-\phi_p)\right]L_m(p_\parallel|k_\parallel)\Bigg]\bigg\},\end{aligned}$$

and further inserting the helper integrals from Appendix D.1 where applicable, whence

$$
\begin{aligned}
\tau_{ss} &= \delta^2 \Re \frac{-2\sqrt{\alpha_0(q_\parallel)\alpha_0(k_\parallel)}}{\nu_{ss}(\mathbf{q}_\parallel|\mathbf{k}_\parallel)} \Bigg\{ \nu_{ss}(\mathbf{q}_\parallel|\mathbf{k}_\parallel)\Big[\alpha(q_\parallel)+\alpha(k_\parallel)\Big] \\
&\quad - \frac{1}{2\pi}(\varepsilon-1)\left(\frac{\omega}{c}\right)^2 \int_0^\infty dp_\parallel p_\parallel \Bigg[\left(\frac{\varepsilon}{\varepsilon-1}\alpha(p_\parallel) - \frac{1}{d_p(p_\parallel)}\frac{\varepsilon-1}{\varepsilon^2}\alpha(p_\parallel)^2\right) \\
&\quad \times \left[\sum_n I_8[n] L_n(q_\parallel|p_\parallel) + \sum_m I_{16}[m] L_m(p_\parallel|k_\parallel)\right] \\
&\quad - \frac{\varepsilon-1}{d_s(p_\parallel)}\left(\frac{\omega}{c}\right)^2 \left[\sum_n I_5[n] L_n(q_\parallel|p_\parallel) + \sum_m I_{13}[m] L_m(p_\parallel|k_\parallel)\right]\Bigg]\Bigg\} \\
&= \delta^2 \Re \frac{-2\sqrt{\alpha_0(q_\parallel)\alpha_0(k_\parallel)}}{\nu_{ss}(\mathbf{q}_\parallel|\mathbf{k}_\parallel)} \Bigg\{ \nu_{ss}(\mathbf{q}_\parallel|\mathbf{k}_\parallel)\Big[\alpha(q_\parallel)+\alpha(k_\parallel)\Big] \\
&\quad - \frac{1}{2}(\varepsilon-1)\left(\frac{\omega}{c}\right)^2 \int_0^\infty dp_\parallel p_\parallel \Bigg[\left(\frac{\varepsilon}{\varepsilon-1}\alpha(p_\parallel) - \frac{1}{d_p(p_\parallel)}\frac{\varepsilon-1}{\varepsilon^2}\alpha(p_\parallel)^2\right) \\
&\quad \times \Bigg[-\cos(\phi_k-\phi_q) L_0(q_\parallel|p_\parallel) + \frac{1}{2}\Big\{\exp\left[i(\phi_k-\phi_q)\right] + \exp\left[-i(\phi_k-\phi_q)\right]\Big\} L_2(q_\parallel|p_\parallel) \\
&\quad - \cos(\phi_k-\phi_q) L_0(p_\parallel|k_\parallel) + \frac{1}{2}\Big\{\exp\left[i(\phi_k-\phi_q)\right] + \exp\left[-i(\phi_k-\phi_q)\right]\Big\} L_2(p_\parallel|k_\parallel)\Bigg] \\
&\quad - \frac{\varepsilon-1}{d_s(p_\parallel)}\left(\frac{\omega}{c}\right)^2 \Bigg[\cos(\phi_k-\phi_q) L_0(q_\parallel|p_\parallel) + \frac{1}{2}\Big\{\exp\left[i(\phi_k-\phi_q)\right] + \exp\left[-i(\phi_k-\phi_q)\right]\Big\} L_2(q_\parallel|p_\parallel) \\
&\quad + \cos(\phi_k-\phi_q) L_0(p_\parallel|k_\parallel) + \frac{1}{2}\Big\{\exp\left[i(\phi_k-\phi_q)\right] + \exp\left[-i(\phi_k-\phi_q)\right]\Big\} L_2(p_\parallel|k_\parallel)\Bigg]\Bigg]\Bigg\}
\end{aligned}
$$

where the relation $L_{-n}() = L_n()$ has been applied. Using Eqs. (D.4)–(D.7) and Eq. (5.7d) we may write

$$
\begin{aligned}
\tau_{ss} &= \delta^2 \Re \frac{-2\sqrt{\alpha_0(q_\parallel)\alpha_0(k_\parallel)}}{\nu_{ss}(\mathbf{q}_\parallel|\mathbf{k}_\parallel)} \Bigg\{ \nu_{ss}(\mathbf{q}_\parallel|\mathbf{k}_\parallel)\Big[\alpha(q_\parallel)+\alpha(k_\parallel)\Big] + \frac{1}{2}\nu_{ss}(\mathbf{q}_\parallel|\mathbf{k}_\parallel) \int_0^\infty dp_\parallel p_\parallel \\
&\quad \times \Bigg[\left[\frac{1}{d_p(p_\parallel)}\frac{\varepsilon-1}{\varepsilon^2}\alpha(p_\parallel)^2 - \frac{\varepsilon}{\varepsilon-1}\alpha(p_\parallel) - \frac{\varepsilon-1}{d_s(p_\parallel)}\left(\frac{\omega}{c}\right)^2\right]\Big[L_0(\mathbf{q}_\parallel|\mathbf{p}_\parallel) + L_0(\mathbf{p}_\parallel|\mathbf{k}_\parallel)\Big] \\
&\quad + \left[-\frac{1}{d_p(p_\parallel)}\frac{\varepsilon-1}{\varepsilon^2}\alpha(p_\parallel)^2 + \frac{\varepsilon}{\varepsilon-1}\alpha(p_\parallel) - \frac{\varepsilon-1}{d_s(p_\parallel)}\left(\frac{\omega}{c}\right)^2\right]\Big[L_2(\mathbf{q}_\parallel|\mathbf{p}_\parallel) + L_2(\mathbf{p}_\parallel|\mathbf{k}_\parallel)\Big]\Bigg]\Bigg\},
\end{aligned}
$$

or; finally,

$$\tau_{ss} = \delta^2 \Re \sqrt{\alpha_0(q_\parallel)\alpha_0(k_\parallel)} \Bigg\{ -2\Big[\alpha(q_\parallel) + \alpha(k_\parallel)\Big] + \int_0^\infty dp_\parallel p_\parallel$$
$$\times \Bigg[\Bigg[-\frac{1}{d_p(p_\parallel)} \frac{\varepsilon - 1}{\varepsilon^2} \alpha(p_\parallel)^2 + \frac{\varepsilon}{\varepsilon - 1} \alpha(p_\parallel) + \frac{\varepsilon - 1}{d_s(p_\parallel)} \left(\frac{\omega}{c}\right)^2 \Bigg] \Big[L_0(\mathbf{q}_\parallel|\mathbf{p}_\parallel) + L_0(\mathbf{p}_\parallel|\mathbf{k}_\parallel) \Big]$$
$$+ \Bigg[\frac{1}{d_p(p_\parallel)} \frac{\varepsilon - 1}{\varepsilon^2} \alpha(p_\parallel)^2 - \frac{\varepsilon}{\varepsilon - 1} \alpha(p_\parallel) + \frac{\varepsilon - 1}{d_s(p_\parallel)} \left(\frac{\omega}{c}\right)^2 \Bigg] \Big[L_2(\mathbf{q}_\parallel|\mathbf{p}_\parallel) + L_2(\mathbf{p}_\parallel|\mathbf{k}_\parallel) \Big] \Bigg] \Bigg\}. \tag{D.11}$$

Appendix E

Extra figures

When calculating the in-plane cuts of out-of-plane incoherent MDRC for the systems in Sec. 7.3, a selection of azimuthal scattering angles was used. Only some of these inspired interesting and in-depth discussion, as the remaining was simply predictable ”intermediate” stages between the extremes. In this appendix, plots of those intermediate scattering plane incoherent MDRC are given, for the reader that wishes to examine the exact values involved.

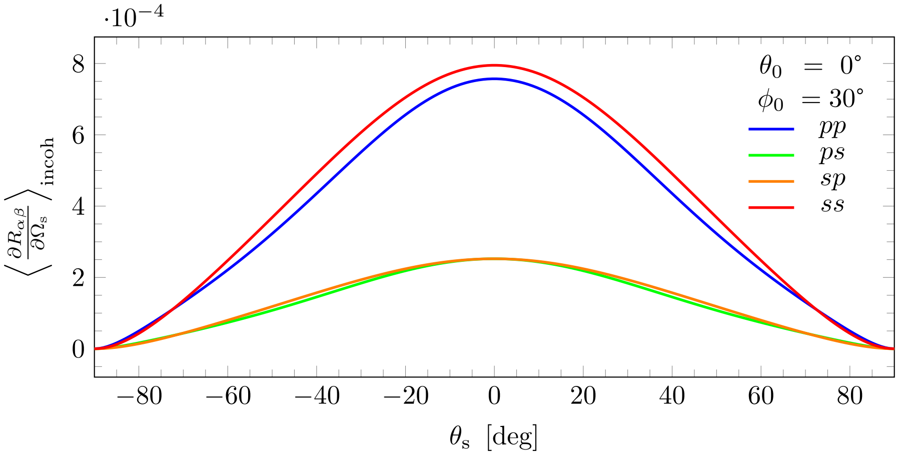

Figure E.1: Planar cut of the calculated incoherent MDRC as a function of the polar scattering angle, after light scattering from a randomly rough dielectric surface with incidence angles $\theta_0 = 0°$ and $\phi_0 = 0°$, and the azimuthal scattering angle $\phi_S = 30°$. The surface height distribution is Gaussian, with statistical parameters $\delta = 0.025\lambda$ and $a = 0.25\lambda$ taken from Ref. 16.

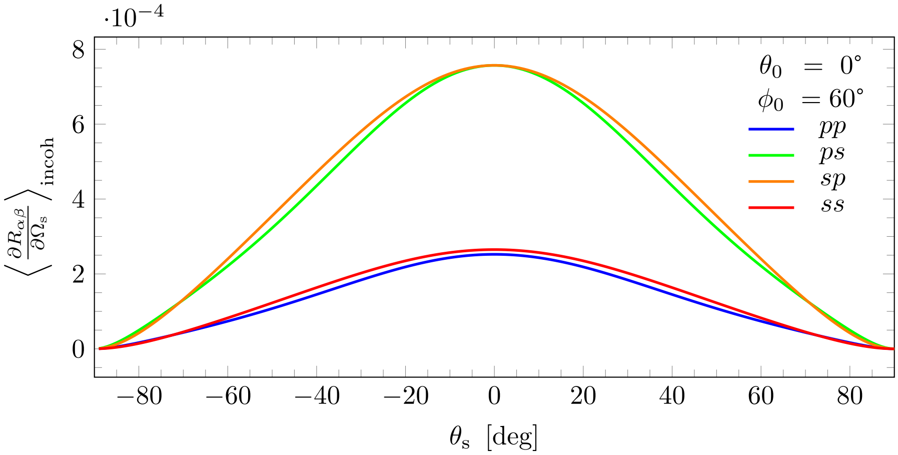

Figure E.2: Planar cut of the calculated incoherent MDRC as a function of the polar scattering angle, after light scattering from a randomly rough dielectric surface with incidence angles $\theta_0 = 0°$ and $\phi_0 = 0°$, and the azimuthal scattering angle $\phi_S = 60°$. The surface height distribution is Gaussian, with statistical parameters $\delta = 0.025\lambda$ and $a = 0.25\lambda$ taken from Ref. 16.

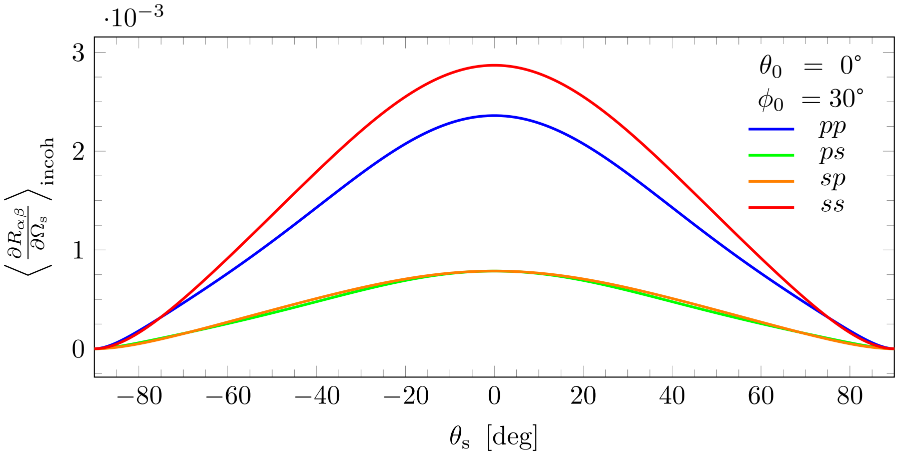

Figure E.3: Planar cut of the calculated incoherent MDRC as a function of the polar scattering angle, after light scattering from a randomly rough dielectric surface with incidence angles $\theta_0 = 0°$ and $\phi_0 = 0°$, and the azimuthal scattering angle $\phi_S = 30°$. The surface height distribution is Gaussian, with statistical parameters $\delta = 0.050\lambda$ and $a = 0.25\lambda$ taken from Ref. 16.

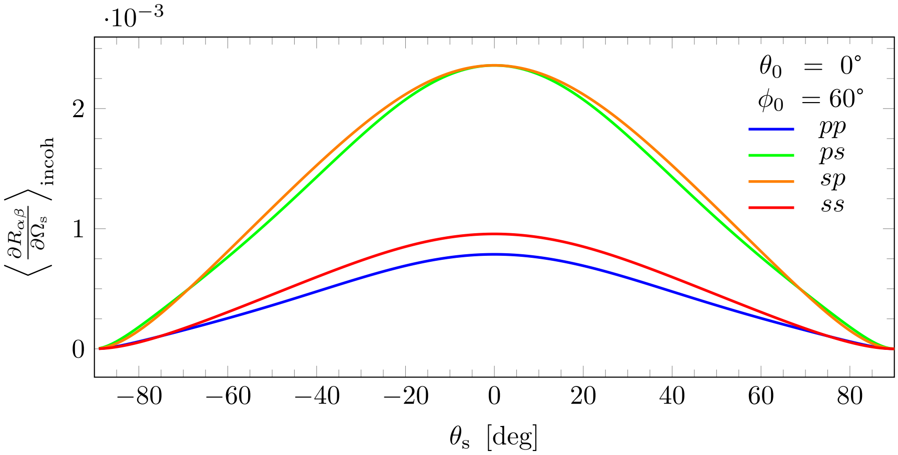

Figure E.4: Planar cut of the calculated incoherent MDRC as a function of the polar scattering angle, after light scattering from a randomly rough dielectric surface with incidence angles $\theta_0 = 0°$ and $\phi_0 = 0°$, and the azimuthal scattering angle $\phi_S = 60°$. The surface height distribution is Gaussian, with statistical parameters $\delta = 0.050\lambda$ and $a = 0.25\lambda$ taken from Ref. 16.

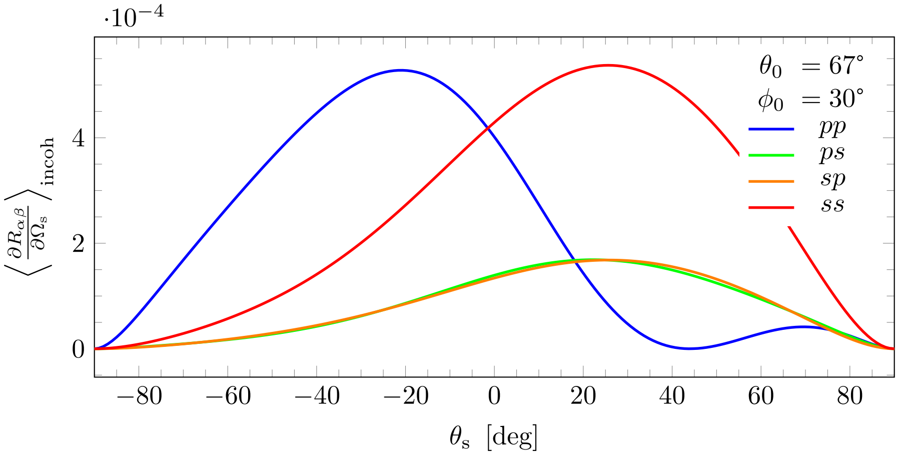

Figure E.5: Planar cut of the calculated incoherent MDRC as a function of the polar scattering angle, after light scattering from a randomly rough dielectric surface with incidence angles $\theta_0 = 67°$ and $\phi_0 = 0°$, and the azimuthal scattering angle $\phi_S = 30°$. The surface height distribution is Gaussian, with statistical parameters $\delta = 0.025\lambda$ and $a = 0.25\lambda$ taken from Ref. 16.

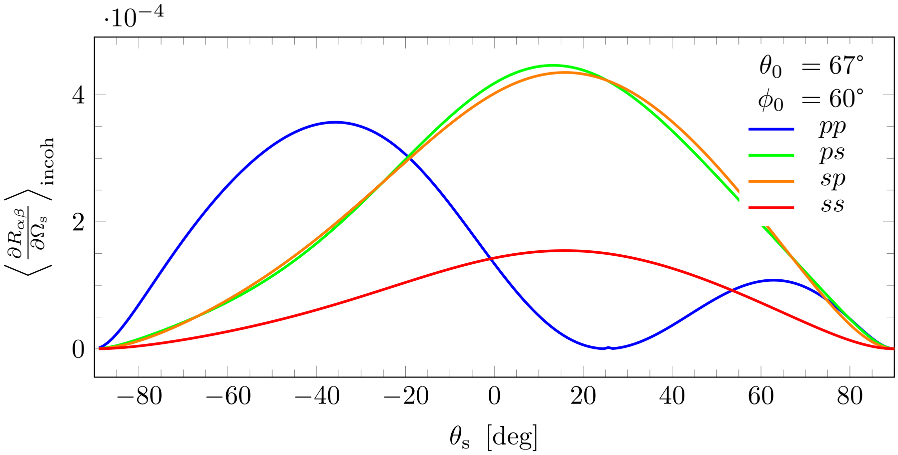

Figure E.6: Planar cut of the calculated incoherent MDRC as a function of the polar scattering angle, after light scattering from a randomly rough dielectric surface with incidence angles $\theta_0 = 67°$ and $\phi_0 = 0°$, and the azimuthal scattering angle $\phi_S = 60°$. The surface height distribution is Gaussian, with statistical parameters $\delta = 0.025\lambda$ and $a = 0.25\lambda$ taken from Ref. 16. The planar cut is defined by the azimuthal scattering angle of 60°.

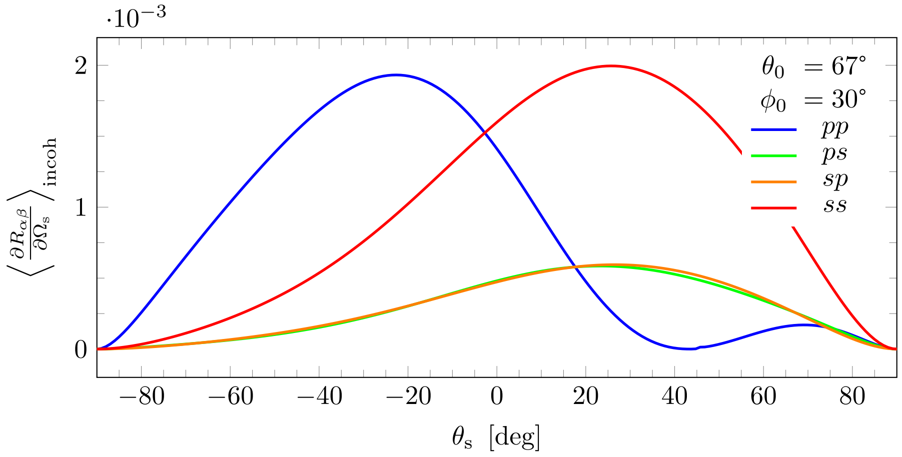

Figure E.7: Planar cut of the calculated incoherent MDRC as a function of the polar scattering angle, after light scattering from a randomly rough dielectric surface with incidence angles $\theta_0 = 67°$ and $\phi_0 = 0°$, and the azimuthal scattering angle $\phi_S = 30°$. The surface height distribution is Gaussian, with statistical parameters $\delta = 0.050\lambda$ and $a = 0.25\lambda$ taken from Ref. 16.

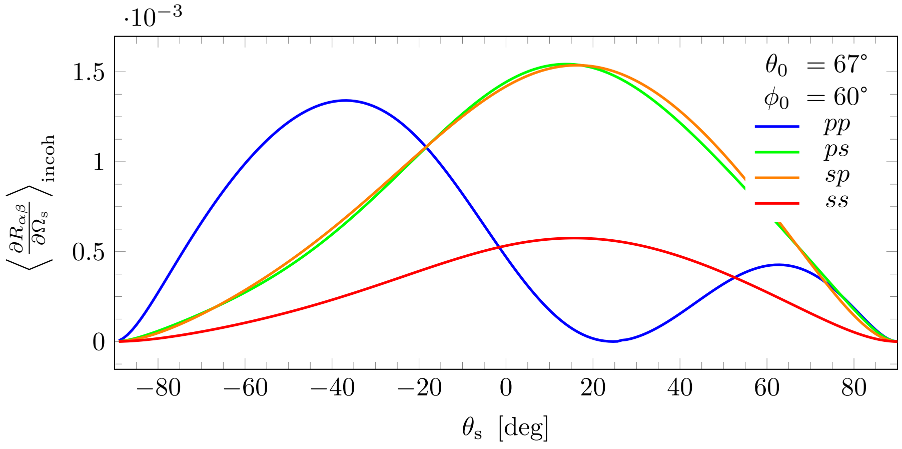

Figure E.8: Planar cut of the calculated incoherent MDRC as a function of the polar scattering angle, after light scattering from a randomly rough dielectric surface with incidence angles $\theta_0 = 67°$ and $\phi_0 = 0°$, and the azimuthal scattering angle $\phi_S = 60°$. The surface height distribution is Gaussian, with statistical parameters $\delta = 0.050\lambda$ and $a = 0.25\lambda$ taken from Ref. 16.

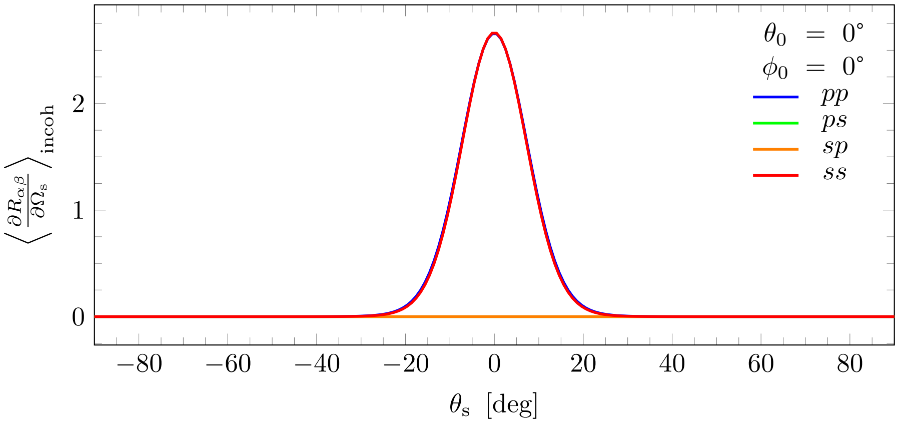

Figure E.9: Planar cut of the calculated incoherent MDRC as a function of the polar scattering angle, after light scattering from a randomly rough gold surface with incidence angles $\theta_0 = 0°$ and $\phi_0 = 0°$, and the azimuthal scattering angle $\phi_S = 0°$. The surface height distribution is Gaussian, with statistical parameters $\delta = 0.047\lambda$ and $a = 1.79\lambda$ taken from Ref. 15.

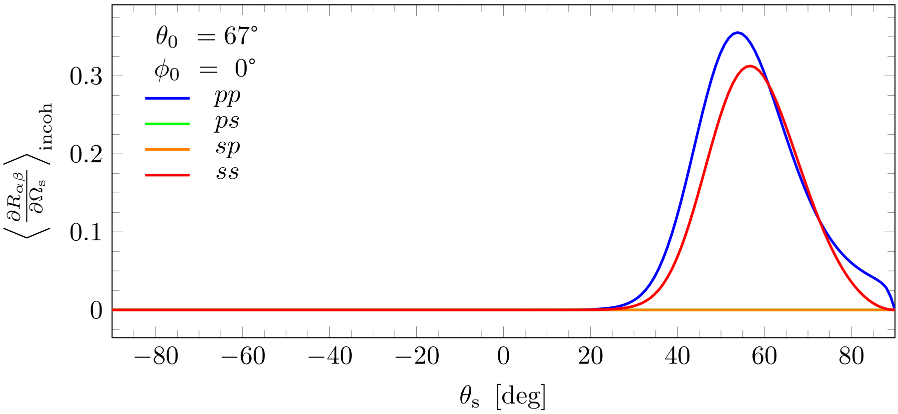

Figure E.10: Planar cut of the calculated incoherent MDRC as a function of the polar scattering angle, after light scattering from a randomly rough gold surface with incidence angles $\theta_0 = 67°$ and $\phi_0 = 0°$, and the azimuthal scattering angle $\phi_S = 0°$. The surface height distribution is Gaussian, with statistical parameters $\delta = 0.047\lambda$ and $a = 1.79\lambda$ taken from Ref. 15. The planar cut is defined by the azimuthal scattering angle of 0°.

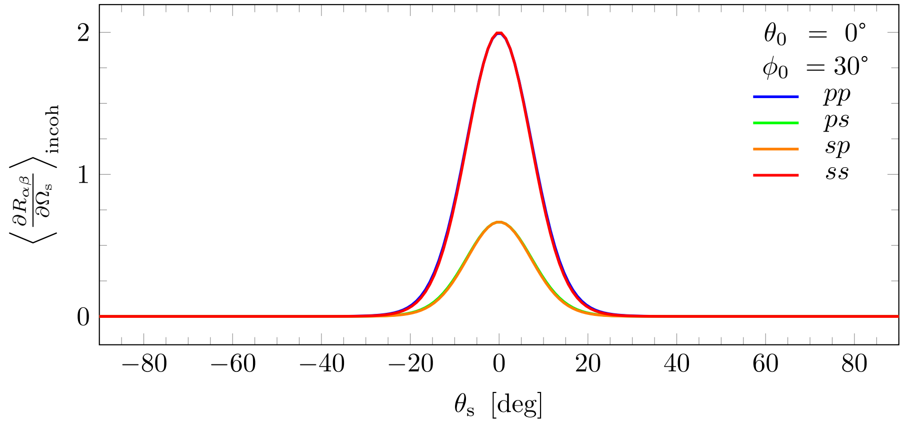

Figure E.11: Planar cut of the calculated incoherent MDRC as a function of the polar scattering angle, after light scattering from a randomly rough gold surface with incidence angles $\theta_0 = 0°$ and $\phi_0 = 0°$, and the azimuthal scattering angle $\phi_S = 30°$. The surface height distribution is Gaussian, with statistical parameters $\delta = 0.047\lambda$ and $a = 1.79\lambda$ taken from Ref. 15.

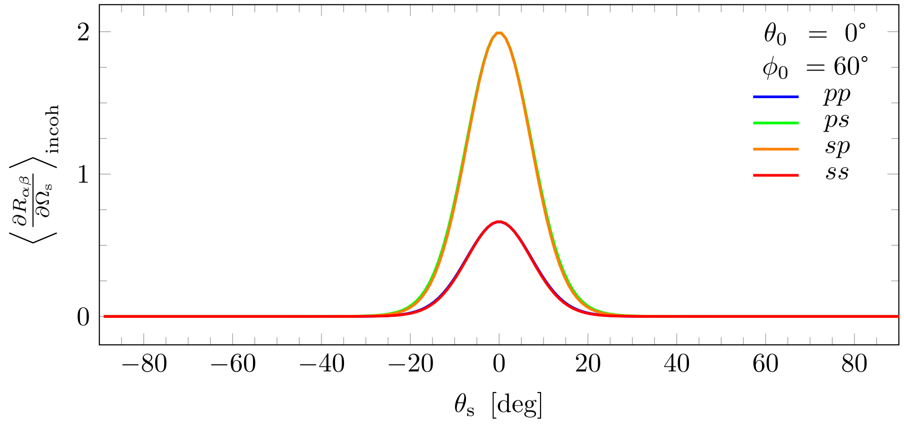

Figure E.12: Planar cut of the calculated incoherent MDRC as a function of the polar scattering angle, after light scattering from a randomly rough gold surface with incidence angles $\theta_0 = 0°$ and $\phi_0 = 0°$, and the azimuthal scattering angle $\phi_S = 60°$. The surface height distribution is Gaussian, with statistical parameters $\delta = 0.047\lambda$ and $a = 1.79\lambda$ taken from Ref. 15.

References

1. Simonsen, I. Optics of surface disordered systems. A random walk through rough surface scattering phenomena. *The European Physics Journal Special Topics* **181,** 1–103 (Jan. 2010).
2. Liang, D. *et al.* Electromagnetic Scattering by Rough Surfaces with Large Heights and Slopes with Approximation to Microwave Remote Sensing of Rough Surface Over Layered Media. *Progress in Electromagnetic Research* **95,** 199–218 (2009).
3. Tsang, L. *et al.* Electromagnetic Computation in Scattering of Electromagnetic Waves by Random Rough Surface and Dense Media in Microwave Remote Sensing of Land Surfaces. *Proceedings of the IEEE* **101,** 255–279 (2013).
4. Kemppinen, O., Nousiainen, T. & Lindqvist, H. The impact of surface roughness on scattering by realistically shaped wavelength-scale dust particles. *Journal of Quantitative Spectroscopy and Radiative Transfer* **150.** Topical issue on optical particle characterization and remote sensing of the atmosphere: Part I, 55–67 (2015).
5. Nousiainen, T. *et al.* Light scattering by large Saharan dust particles: Comparison of modeling and experimental data for two samples. *Journal of Quantitative Spectroscopy and Radiative Transfer* **112,** 420–433 (2011).
6. Riskilä, E., Lindqvist, H. & Muinonen, K. Light scattering by fractal roughness elements on ice crystal surfaces. *Journal of Quantitative Spectroscopy and Radiative Transfer* **267,** 107561 (2021).
7. Viotti, M. *Science Instrument: MARSIS.* From NASA (2013): `https://mars.nasa.gov/express/mission/sc_science_marsis01.html` and `https://mars.nasa.gov/express/mission/sc_science_marsis02.html` (accessed 2021/07/10).

8. Campbell, B. A. & Shepard, M. K. Coherent and incoherent components in near-nadir radar scattering: Applications to radar sounding of Mars. *Journal of Geophysical Research: Planets* **108** (2003).
9. Müller, J. *et al.* TCO and light trapping in silicon thin film solar cells. *Solar Energy* **77.** Thin Film PV, 917–930 (2004).
10. Kim, M. S., Lee, J. H. & Kwak, M. K. Review: Surface Texturing Methods for Solar Cell Efficiency Enhancement. *Int. J. Precis. Eng. Manuf.* **21,** 1389–1398 (2020).
11. Kanafi, M. M. & Tuononen, A. J. Application of three-dimensional printing to pavement texture effects on rubber friction. *Road Materials and Pavement Design* **18,** 865–881 (2017).
12. Simonsen, I., Kryvi, J. B. & Maradudin, A. A. *Inversion of in-plane, co-polarized light scattering data in p and s polarization to obtain the normalized surface-height autocorrelation function and the rms-roughness of a two-dimensional randomly rough metal surface* 2021. arXiv: `2104.12650 [physics.optics]`.
13. Simonsen, I. *et al.* Determination of the normalized-surface-height autocorrelation function of a two-dimensional randomly rough dielectric surface by the inversion of light-scattering data. *Phys. Rev. A* **93,** 043829 (4 Apr. 2016).
14. Simonsen, V. P., Bedeaux, D. & Simonsen, I. *Non-parametric reconstruction of the statistical properties of penetrable, isotropic randomly rough surfaces from in-plane, co-polarized light scattering data: Application to computer generated and experimental scattering data* 2021. arXiv: `2105.02745 [physics.optics]`.
15. Alcalá, A. G. N. *et al.* Specular and diffuse scattering of light from two-dimensional randomly rough metal surfaces: experimental and theoretical results. *Waves in Random and Complex Media* **19,** 600–636 (2009).
16. Hetland, Ø. S. *et al.* Numerical studies of the scattering of light from a two-dimensional randomly rough interface between two dielectric media. *Phys. Rev. A* **93,** 053819 (5 May 2016).
17. Bennett, J. M. & Mattsson, L. *Introduction to Surface Roughness and Scattering* 2nd ed. (Optical Society of America, Washington, D.C., USA, 1999).
18. Bennett, J. M. in *Light Scattering and Nanoscale Surface Roughness* (ed Maradudin, A. A.) 1–33 (Springer, Boston, MA, USA, 2007).
19. Kaupp, G. *Atomic Force Microscopy, Scanning Nearfield Optical Microscopy and Nanoscrathcing: Application to Rough and Natural Surfaces* (Springer Verlag, Berlin, Germany, 2006).
20. Feder, J. *Fractals* (Plenum Press, New York, NY, USA, 1988).
21. Avnir, D., Farin, D. & Pfeifer, P. Molecular fractal surfaces. *Nature* **308,** 261–263 (1984).
22. Oglivy, J. A. *Theory of Wave Scattering from Random Rough Surfaces* (IOP Publishing, Bristol, UK, 1991).

23. Franceschetti, G. & Riccio, D. in *Scattering, Natural Surfaces, and Fractals* (eds Franceschetti, G. & Riccio, D.) 21–59 (Academic Press, Burlington, MA, USA, 2007).
24. Jacobs, K. *Stochastic Processes for Physicists* (Cambridge University Press, Cambridge, UK, 2010).
25. Agarwal, R., Patki, G. & Basu, S. An analysis of surface profiles for stationarity and ergodicity. *Precision Engineering* **1,** 159–165 (1979).
26. Maradudun, A. A. & Michel, T. The transverse correlation length for randomly rough surfaces. *Journal of Statistical Physics* **58,** 485–501 (Feb. 1990).
27. Jackson, J. D. *Classical Electrodynamics* 3rd ed. (John Wiley & Sons, New York, NY, USA, 1999).
28. Griffiths, D. J. *Introduction to Electrodynamics* 4th ed. (Cambridge University Press, Cambridge, UK, 2017).
29. Kittel, C. *Introduction to Solid State Physics* 8th ed. (John Wiley & Sons, Hoboken, NJ, USA, 2005).
30. Römer, H. *Theoretical Optics* 2nd ed. (Wiley-WCH Verlag, Weinheim, Germany, 2009).
31. Kreyszig, E. *Advanced Engineering Mathematics - International student version* 3rd ed. (John Wiley & Sons, Hoboken, NJ, USA, 2011).
32. Boyd, R. W. in *Nonlinear Optics* (ed Boyd, R. W.) 3rd ed., 1–67 (Academic Press, Burlington, VT, USA, 2008).
33. Agulló-López, F., Cabrera, J. M. & Agulló-Rueda, F. *Electrooptics. Phenomena, Materials and Applications* (Academic Press, London, UK, 1994).
34. Born, M. & Wolf, E. *Principles of Optics* 7 ed. (expanded, reprint) (Cambridge University Press, Cambridge, UK, 2002).
35. The International Bureau of Weights and Measures (BIPM). *The International System of Units* 2019.
36. Wong, C. W. *Introduction to Mathematical Physics* 2nd ed. (Oxford University Press, Oxford, UK, 2013).
37. Nieto-Vesperinas, M. *Scattering and Diffraction in Physical Optics* 2nd ed. (World Scientific Publishing, Singapore, Singapore, 2006).
38. Voronovich, A. G. in *Light Scattering and Nanoscale Surface Roughness* (ed Maradudin, A. A.) 93–105 (Springer, Boston, MA, USA, 2007).
39. Millar, R. F. On the Rayleigh assumption in scattering by a periodic surface. *Mathematical Proceedings of the Cambridge Philosophical Society* **65,** 773–791 (1969).
40. Millar, R. F. On the Rayleigh assumption in scattering by a periodic surface. II. *Mathematical Proceedings of the Cambridge Philosophical Society* **69,** 217–225 (1971).

41. Tishchenko, A. V. Numerical demonstration of the validity of the Rayleigh hypothesis. *Opt. Express* **17,** 17102–17117 (Sept. 2009).
42. Banon, J.-P. *On the Simulation of Electromagnetic Wave Scattering by Periodic and Randomly Rough Layered Structures based on the Reduced Rayleigh Equations: Theory, numerical analysis and applications.* PhD thesis (NTNU, 2018).
43. Nordam, T., Letnes, P. A. & Simonsen, I. Validity of the Rayleigh hypothesis for two-dimensional randomly rough metal surfaces. *Journal of Physics: Conference Series* **454,** 012033 (Aug. 2013).
44. Brown, G. *et al.* Vector theory of light scattering from a rough surface: Unitary and reciprocal expansions. *Surface Science* **136,** 381–397 (1984).
45. Berginc, G. in *Light Scattering and Nanoscale Surface Roughness* (ed Maradudin, A. A.) 127–179 (Springer, Boston, MA, USA, 2007).
46. McGurn, A. R. & Maradudin, A. A. Perturbation theory results for the diffuse scattering of light from two-dimensional randomly rough metal surfaces. *Waves in Random Media* **6,** 251–267 (1996).
47. Shen, J. & Maradudin, A. A. Multiple scattering of waves from random rough surfaces. *Phys. Rev. B* **22,** 4234–4240 (9 Nov. 1980).
48. Sánchez-Gil, J. A., Maradudin, A. A. & Méndez, E. R. Limits of validity of three perturbation theories of the specular scattering of light from one-dimensional, randomly rough, dielectric surfaces. *J. Opt. Soc. Am. A* **12,** 1547–1558 (July 1995).
49. Fitzgerald, R. M. & Maradudin, A. A. A reciprocal phase-perturbation theory for rough-surface scattering. *Waves in Random Media* **4,** 275–296 (1994).
50. Kubo, R. Generalized Cumulant Expansion Method. *Journal of the Physical Society of Japan* **17,** 1100–1120 (1962).
51. O'Donnell, K. A. in *Light Scattering and Nanoscale Surface Roughness* (ed Maradudin, A. A.) 107–126 (Springer, Boston, MA, USA, 2007).
52. Weisstein, E. W. *Bessel Function of the First Kind* From *MathWorld*–A Wolfram Web Resource. URL: `https://mathworld.wolfram.com/BesselFunctionoftheFirstKind.html` (accessed 2020/10/15).
53. *Handbook of Mathematical Functions* (eds Abramowitz, M. & Stegun, I. A.) (Dover Publications Inc., New York, NY, USA, 1972).
54. Virtanen, P. *et al.* SciPy 1.0: Fundamental Algorithms for Scientific Computing in Python. *Nature Methods* **17.** [version 1.5.4], 261–272 (2020).
55. The SciPy community. *scipy.integrate.quad* – from documentation, 2021 (accessed 2021/06/23).
56. Harris, C. R. *et al.* Array programming with NumPy. *Nature* **585.** [version 1.19.4], 357–362 (2020).
57. The SciPy community. *scipy.optimize.curve_fit* – from documentation, 2021 (accessed 2021/06/29).

58. Wynn, P. On a Device for Computing the $e_m(S_n)$ Transformation. *Mathematical Tables and Other Aids to Computation* **10,** 91–96 (1956).
59. Lohr, P. J. *Implementation of Wynn's Epsilon Method For Convergence Acceleration.* [version 0.0.1] GitHub repository (2019). URL: `https://github.com/pjlohr/WynnEpsilon` (accessed 2021/02/25).
60. Simonsen, I., Maradudin, A. A. & Leskova, T. A. Scattering of electromagnetic waves from two-dimensional randomly rough perfectly conducting surfaces: The full angular intensity distribution. *Phys. Rev. A* **81,** 013806 (1 Jan. 2010).
61. Hetland, Ø. S. *et al.* Numerical studies of the transmission of light through a two-dimensional randomly rough interface. *Phys. Rev. A* **95,** 043808 (4 Apr. 2017).
62. González-Alcalde, A. K. *et al.* Experimental and numerical studies of the scattering of light from a two-dimensional randomly rough interface in the presence of total internal reflection: optical Yoneda peaks. *Opt. Express* **24,** 25995–26005 (Nov. 2016).
63. Maradudin, A. A., Méndez, E. R. & Leskova, T. A. in *Designer Surfaces* (eds Maradudin, A. A., Méndez, E. R. & Leskova, T. A.) 201–305 (Elsevier, Amsterdam, 2008).

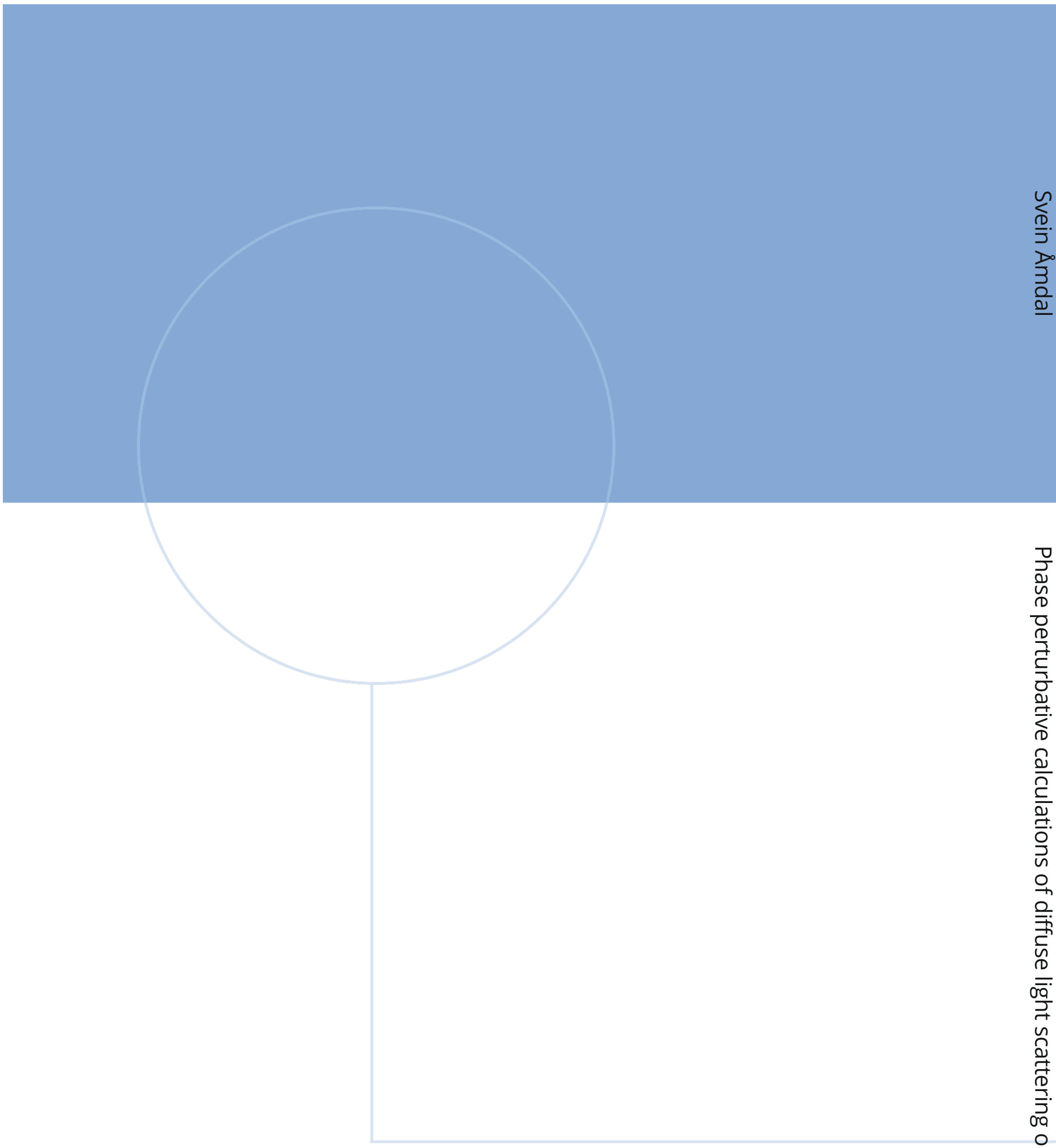

Svein Åmdal

Phase perturbative calculations of diffuse light scattering on randomly rough surfaces in and out of plane

NTNU
Norwegian University of
Science and Technology